

Sheffield Hallam University

Assessment of the long term performance of repaired reinforced concrete.

LIMBACHIYA, Mukeshchandra K.

Available from the Sheffield Hallam University Research Archive (SHURA) at:

<http://shura.shu.ac.uk/19962/>

A Sheffield Hallam University thesis

This thesis is protected by copyright which belongs to the author.

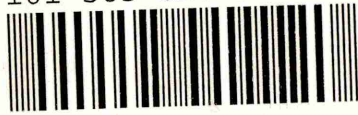
The content must not be changed in any way or sold commercially in any format or medium without the formal permission of the author.

When referring to this work, full bibliographic details including the author, title, awarding institution and date of the thesis must be given.

Please visit <http://shura.shu.ac.uk/19962/> and <http://shura.shu.ac.uk/information.html> for further details about copyright and re-use permissions.

LEARNING CENTRE
CITY CAMPUS, POND STREET,
SHEFFIELD, S1 1WB.

101 585 620 9



REFERENCE

Fines are charged at 50p per hour

10 SEP 2003

5.00

10 FEB 2005 8.04pm

ProQuest Number: 10697268

All rights reserved

INFORMATION TO ALL USERS

The quality of this reproduction is dependent upon the quality of the copy submitted.

In the unlikely event that the author did not send a complete manuscript and there are missing pages, these will be noted. Also, if material had to be removed, a note will indicate the deletion.



ProQuest 10697268

Published by ProQuest LLC (2017). Copyright of the Dissertation is held by the Author.

All rights reserved.

This work is protected against unauthorized copying under Title 17, United States Code
Microform Edition © ProQuest LLC.

ProQuest LLC.
789 East Eisenhower Parkway
P.O. Box 1346
Ann Arbor, MI 48106 – 1346

**SCHOOL OF CONSTRUCTION
SHEFFIELD HALLAM UNIVERSITY**

**ASSESSMENT OF THE LONG TERM
PERFORMANCE OF REPAIRED
REINFORCED CONCRETE**

by
MUKESHCHANDRA K. LIMBACHIYA

B.E. (Civil Eng.), M.S. University,

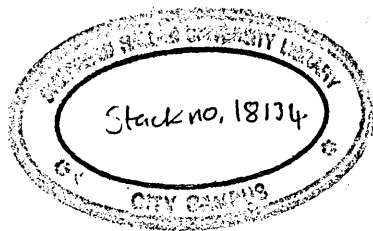
Baroda, INDIA, 1987

M.Sc. (Structural Eng.), UMIST,

Manchester, UK, 1992

**A thesis submitted in fulfilment of the requirements of
Sheffield Hallam University
for the degree of Doctor of Philosophy**

November 1995



ABSTRACT

Rational decisions about cost-effective maintenance and structural repair are hampered by the absence of comprehensive data on structural performance of generic repair materials acting compositely with deteriorated concrete elements. In the present climate of durability problems in concrete construction such information is of critical importance. In order to assess long-term structural performance of repaired elements, basic short and long-term properties of generic repair materials are required under various exposure conditions. The principle requirements to ensure satisfactory long-term performance of the repair have always been high dimensional stability and relatively high early bond strength of the repair material with the substrate concrete.

As part of a " Brite Euram " project, sponsored by E.E.C., the author has obtained considerable experimental data on properties of three commercially available generic repair materials, which are significant to the subsequent structural behaviour of repaired concrete members. A comparison is also made between the performance of these repair materials with a plain concrete mix of similar strength and stiffness. The following generic repair materials were used: a high performance non-shrinkable concrete, a mineral based cementitious material with no additives and no coarse aggregate size particles, and a cementitious mortar which contains styrene acrylic copolymer with fibre additives. The repair materials are supplied as single component systems by their manufacturers, ready for on-site mixing and use, and require only the addition of clean water.

Data on strength, stiffness, post peak-load ductility under compression, swelling, shrinkage and creep deformations under various curing conditions are presented in this thesis. In addition water permeability coefficients and chloride penetration profiles of the materials at various ages of exposure have been determined. A comprehensive compilation of chloride diffusion data is made and an empirical expression is derived for the prediction of long-term chloride penetration profiles based on data obtained at relatively early ages. Application of this prediction model to the field data of some Arabian Gulf structures is made.

The influence of repair materials on the performance of reinforced concrete compression members has been studied. A theoretical model is also derived to predict the long-term structural interaction between a repair patch and substrate concrete in short compression members of reinforced concrete. The model is based on the basic properties of materials, such as creep deformation, drying shrinkage and modulus of elasticity. The validity of the model is established on the basis of the experimental data obtained in this study.

At the end of the thesis, conclusions and recommendations for future research are made.

Declaration

I hereby declare that no portion of the work referred to in this thesis has been submitted in support of an application for another degree or qualification of this or any other university or other institution of learning. All sources of information have been duly acknowledged.

Mukeshchandra Limbachiya

November 1995

Acknowledgements

The author wishes foremost to express his sincere appreciation to Professor P.S.Mangat for his guidance, valuable suggestions and encouragement throughout the preparation of this work.

The author appreciates the assistance of the technical staff of the Department of Engineering at Aberdeen University and the technical staff of the School of Construction at Sheffield Hallam University.

The author gratefully acknowledges the advice and suggestions of Dr. F. Al-Shawi of the School of Construction at Sheffield Hallam University.

CONTENTS

| | Page |
|--|-------------|
| ABSTRACT | (i) |
| DECLARATION | (iv) |
| ACKNOWLEDGEMENTS | (v) |
| CONTENTS | (vi) |
| NOTATION | (xii) |
| LIST OF FIGURES | (xiv) |
| LIST OF TABLES | (xxvi) |
| | |
| CHAPTER 1 <u>INTRODUCTION</u> | 1 |
| 1.1 INTRODUCTION | 1 |
| 1.2 SCOPE OF RESEARCH | 1 |
| 1.3 SCOPE OF PRESENT INVESTIGATION | 2 |
| 1.4 EXPERT SYSTEM OF THE BRITE/EURAM PROJECT | 4 |
| 1.5 THESIS LAYOUT | 5 |
| | |
| CHAPTER 2 <u>EXPERIMENTAL PROGRAMME</u> | 8 |
| 2.1 INTRODUCTION | 8 |
| 2.2 OBJECTIVES OF THE INVESTIGATION | 9 |
| 2.3 DETAILS OF THE EXPERIMENTAL PROGRAMME | 9 |
| 2.3.1 Properties of repair materials which influence long-term performance of concrete structures | 9 |
| 2.3.2 Long-term deformation properties of repair materials | 10 |
| 2.3.3 Chloride diffusion into concrete and repair materials | 11 |

| | | |
|----------------------|---|-----------|
| 2.3.4 | Influence of repair materials on the structural performance of reinforced concrete compression members | 12 |
| 2.3.5 | Long-term structural interaction in repaired compression elements | 13 |
| 2.4 | MATERIALS | 14 |
| 2.4.1 | Introduction | 14 |
| 2.4.2 | Cement | 14 |
| 2.4.3 | Aggregates | 16 |
| 2.4.4 | Steel reinforcement | 17 |
| CHAPTER 3 | | |
| | <u>PROPERTIES OF REPAIR MATERIALS WHICH INFLUENCE LONG-TERM PERFORMANCE OF CONCRETE STRUCTURES</u> | 22 |
| 3.1 | INTRODUCTION | 22 |
| 3.2 | LITERATURE REVIEW | 22 |
| 3.2.1 | Introduction | 22 |
| 3.2.2 | Test methods on permeability | 24 |
| 3.2.2.1 | Initial surface absorption test | 25 |
| 3.2.2.2 | Figg method | 26 |
| 3.2.2.3 | Original work by Figg | 26 |
| 3.2.2.4 | Modified Figg methods | 27 |
| 3.2.2.5 | Pressure induced flow | 27 |
| 3.2.3 | Techniques to represent the complete stress-strain curves | 31 |
| 3.2.3.1 | Process of fracture of concrete | 35 |
| 3.2.3.2 | Crack initiation | 36 |
| 3.3 | EXPERIMENTAL PROGRAMME | 38 |
| 3.3.1 | Materials and details of mixes | 38 |
| 3.3.2 | Casting, curing and testing | 41 |
| 3.3.2.1 | Strength tests | 41 |
| 3.3.2.2 | Elastic modulus test | 43 |
| 3.3.2.3 | Coefficient of water permeability | 43 |
| 3.3.2.4 | Stress-strain curves | 47 |
| 3.4 | RESULTS AND DISCUSSION | 49 |
| 3.4.1 | Strength and elastic modulus | 49 |

| | | |
|------------------|--|------------|
| 3.4.2 | Water permeability | 54 |
| 3.4.3 | Stress-strain curves | 54 |
| 3.4.3.1 | Initiation stress | 60 |
| 3.4.3.2 | Critical stress | 64 |
| 3.4.3.3 | Ultimate strain | 64 |
| 3.4.3.4 | Strain capacity and mode of failure | 65 |
| 3.5 | FURTHER DISCUSSION | 66 |
| 3.6 | CONCLUSIONS | 70 |
| CHAPTER 4 | <u>LONG TERM DEFORMATIONS OF REPAIR MATERIALS</u> | 72 |
| 4.1 | INTRODUCTION | 72 |
| 4.2 | LITERATURE REVIEW | 73 |
| 4.2.1 | Shrinkage and swelling deformations | 73 |
| 4.2.2 | Creep of concrete | 77 |
| 4.2.2.1 | Delayed elastic strain and flow creep | 77 |
| 4.2.2.2 | Creep at high stresses | 78 |
| 4.3 | EXPERIMENTAL PROGRAMME | 82 |
| 4.3.1 | Details of mixes and materials | 82 |
| 4.3.2 | Casting and curing | 84 |
| 4.3.3 | Testing | 85 |
| 4.4 | RESULTS AND DISCUSSION | 86 |
| 4.4.1 | Free shrinkage and swelling deformation of repair materials and concrete | 86 |
| 4.4.2 | Creep of concrete and repair materials | 99 |
| 4.4.3 | Analytical expressions for shrinkage and creep deformations | 109 |
| 4.5 | CONCLUSIONS | 118 |
| CHAPTER 5 | <u>CHLORIDE DIFFUSION INTO CONCRETE AND REPAIR MATERIALS</u> | 120 |
| 5.1 | INTRODUCTION | 120 |

| | | |
|------------------|--|------------|
| 5.2 | LITERATURE REVIEW | 122 |
| 5.2.1 | A chloride "Threshold" for corrosion | 123 |
| 5.2.2 | Diffusion of chloride | 125 |
| 5.2.3 | Factors effecting diffusion | 127 |
| 5.2.4 | Prediction of chloride concentration | 128 |
| 5.3 | EXPERIMENTAL PROGRAMME | 129 |
| 5.3.1 | Objectives | 129 |
| 5.3.2 | Materials | 130 |
| 5.3.3 | Mixing and casting | 130 |
| 5.3.4 | Curing | 131 |
| 5.3.5 | Sampling | 133 |
| 5.3.6 | Chemical analysis | 134 |
| 5.4 | RESULTS AND DISCUSSION | 136 |
| 5.4.1 | Influence of initial curing | 136 |
| 5.4.1.1 | Chloride ingress after 28 days | 136 |
| 5.4.1.2 | Chloride ingress after 90 days | 144 |
| 5.4.1.3 | Chloride ingress after 180 days | 146 |
| 5.4.2 | Influence of Early Exposure to chloride solution | 153 |
| 5.4.3 | Influence of duration of exposure to chloride environment | 156 |
| 5.4.3.1 | Chloride diffusion profiles at different ages of exposure | 156 |
| 5.4.3.2 | Relationship between diffusion coefficient and duration of exposure | 164 |
| 5.5 | PREDICTION OF LONG-TERM CHLORIDE PENETRATION | 171 |
| 5.5.1 | Surface chloride concentration and diffusion coefficient | 173 |
| 5.5.2 | Theory for predicting long-term chloride diffusion | 183 |
| 5.5.3 | Application of prediction model to the field data | 188 |
| 5.6 | CONCLUSIONS | 200 |
| CHAPTER 6 | <u>INFLUENCE OF REPAIR MATERIALS ON THE STRUCTURAL PERFORMANCE OF REINFORCED CONCRETE COMPRESSION MEMBERS</u> | 202 |
| 6.1 | INTRODUCTION | 202 |

| | | |
|------------------|--|------------|
| 6.2 | LITERATURE REVIEW | 203 |
| 6.2.1 | Reinforced concrete compression members | 204 |
| 6.2.1.1 | Elastic theory | 206 |
| 6.2.1.2 | Effect of creep and shrinkage | 207 |
| 6.3 | EXPERIMENTAL WORK | 209 |
| 6.3.1 | Details of column specimens | 209 |
| 6.3.2 | Details of mix and materials | 210 |
| 6.3.3 | Casting and curing | 212 |
| 6.3.4 | Repair of columns | 215 |
| 6.3.5 | Test procedure | 216 |
| 6.4 | ANALYSIS OF VOIDED SECTION OF COMPRESSION MEMBERS | 216 |
| 6.4.1 | Elastic analysis | 216 |
| 6.4.2 | Ultimate analysis | 223 |
| 6.5 | RESULTS AND DISCUSSION | 227 |
| 6.5.1 | Mode of failure | 228 |
| 6.5.2 | Load distribution in steel, concrete and repair phases | 228 |
| 6.5.3 | Ultimate strength | 238 |
| 6.5.4 | Theoretical analysis | 246 |
| 6.6 | CONCLUSIONS | 248 |
| CHAPTER 7 | <u>LONG-TERM STRUCTURAL INTERACTION IN REPAIRED COMPRESSION ELEMENTS</u> | 250 |
| 7.1 | INTRODUCTION | 250 |
| 7.2 | LITERATURE REVIEW | 251 |
| 7.3 | EXPERIMENTAL PROGRAMME | 260 |
| 7.3.1 | Materials and Mix Proportions | 261 |
| 7.3.2 | Details of Specimens, Casting, Curing and Testing | 261 |
| 7.3.2.1 | Determination of sustained stress/strength ratio | 266 |
| 7.4 | RESULTS AND DISCUSSION | 269 |
| 7.4.1 | Influence of longitudinal steel reinforcement on the shrinkage of concrete | 269 |

| | | |
|------------------|---|------------|
| 7.4.2 | Influence of patch repair on the shrinkage of concrete | 269 |
| 7.4.3 | Load distribution in reinforced concrete column specimens under sustained axial loading | 276 |
| 7.4.3.1 | Schematic representation | 276 |
| 7.4.4 | Creep deformation | 283 |
| 7.4.4.1 | Creep curves for short reinforced concrete columns | 283 |
| 7.4.4.2 | Creep of the concrete and repair phase in reinforced columns | 287 |
| 7.5 | A THEORY FOR THE CREEP OF REPAIRED REINFORCED CONCRETE COLUMNS UNDER COMPRESSION | 294 |
| 7.5.1 | Introduction | 294 |
| 7.5.2 | Analysis of creep effects on repaired columns | 295 |
| 7.5.2.1 | Determination of modulus of elasticity and stress on loading | 300 |
| 7.5.2.2 | Comparison of experimental and predicted total strains | 301 |
| 7.6 | CONCLUSIONS | 304 |
| CHAPTER 8 | <u>CONCLUSIONS AND RECOMMENDATION FOR FUTURE RESEARCH</u> | 305 |
| 8.1 | CONCLUSIONS | 305 |
| 8.2 | RECOMMENDATION FOR FUTURE RESEARCH | 309 |
| CHAPTER 9 | <u>REFERENCES</u> | 310 |
| | <u>LIST OF PUBLICATIONS</u> | 326 |

NOTATIONS

| | |
|--------------------|---|
| K_{LD} | Coefficient of water permeability (m/s) |
| Q | Volume of flow rate |
| A | Area of flow |
| h | Water head |
| ϵ_C | Concrete strain |
| ϵ_R | Strain on repair patch |
| ϵ_{Vol} | Volumetric strain |
| E_S | Modulus of elasticity of steel reinforcement |
| A_S | Cross-sectional area of steel reinforcement |
| A_C | Cross-sectional area of concrete |
| ϵ_{sh} | Shrinkage strain |
| ϵ_{creep} | Creep strain |
| C_0 | Equilibrium chloride concentration on the surface |
| $C_{(x,t)}$ | Chloride concentration at any position x and time t |
| D_c | Diffusion coefficient in Cm^2/Sec |
| D_{ct} | Diffusion coefficient at time t in Cm^2/Sec |
| $D_{c,28}$ | Diffusion coefficient after 28 days in Cm^2/Sec |
| E_d | Dynamic modulus of elasticity in MN/m^2 |
| m | empirical constant |
| L | Sample length |
| erf | Error function |
| t | Time in seconds or minutes |
| t_m | Time in months |
| W_p | Dry weight of sample powder in grams |

| | |
|-----------------------|---|
| P | Axial load |
| P_u | Ultimate loading |
| f_{cu} | Compressive cube strength |
| f_y | Yield stress of the steel reinforcement |
| σ_c | Stress in concrete |
| β | modular ratio |
| Φ | Creep function |
| φ | Creep coefficient |
| σ₀ | Initial stress on the application of load |
| E_R | Modulus of elasticity of repair material |

LIST OF FIGURES

| Figure No. | | Page |
|------------|--|------|
| 2.1 | Grading curve for fine aggregates used in experimental work presented in chapters 3, 6 and 7 | 18 |
| 2.2 | Grading curve for coarse aggregates used in experimental work presented in chapters 3, 6 and 7 | 18 |
| 2.3 | Grading curves for fine aggregates used in experimental work presented in chapters 4 and 5 | 19 |
| 2.4 | Grading curves for coarse aggregates used in experimental work presented in chapters 4 and 5 | 19 |
| 2.5 | Stress-strain curve for 12mm diameter reinforcement | 21 |
| 3.1 | Initial surface absorption test equipment, after BSI[14] | 28 |
| 3.2 | Apparatus for determining the water permeability of concrete, after Figg [16] | 28 |
| 3.3 | Apparatus for determining the air permeability of concrete, after Figg [16] | 28 |
| 3.4 | Water permeability test rig, after Bamforth[23] | 30 |
| 3.5 | Stress-strain curves of aggregate, hardened cement paste and concrete [45] | 37 |
| 3.6 | The stages of cracking in concrete under compression | 39 |
| 3.7 | Grading curves for repair materials | 42 |
| 3.8 | General layout of the permeability instrument | 46 |
| 3.9 | Test arrangement for stress-strain curves | 50 |
| 3.10 | Strain gauge locations on the two opposite faces of concrete and repair materials specimens | 52 |
| 3.11 | Development of compressive strength | 53 |
| 3.12 | Load versus longitudinal strain measured on test sample (material A) and steel tube | 59 |

| | | |
|------|---|----|
| 3.13 | Stress-strain curves for Material A | 61 |
| 3.14 | Stress-strain curves for Material B | 61 |
| 3.15 | Stress-strain curves for Material C | 62 |
| 3.16 | Stress-strain curve for concrete | 62 |
| 3.17 | Relationship between stress-strength ratio and poisson's ratio | 67 |
| 3.18 | Stress-strain curves of repair materials and concrete mix | 67 |
| 3.19 | Stress-strain curves for plain concrete obtained in this study and by others [33,38] | 68 |
| 3.20 | Relationship between repair materials and longitudinal strain at a post-peak stress / strength ratio of 0.4 | 69 |
| 4.1 | Results of long-term shrinkage deformation for materials; (a) A; (b) D; (c) F and (d) G, after Emberson and Mays [13] | 76 |
| 4.2 | Typical strain profile for concrete under sustained stress | 79 |
| 4.3 | Effect of time under load on the delayed elastic and flow strain components: age at loading 10 days [72] | 80 |
| 4.4 | Deformation of repair materials | 89 |
| 4.5 | Influence of relative humidity on shrinkage of Material A | 90 |
| 4.6 | Influence of relative humidity on shrinkage of Material B | 91 |
| 4.7 | Influence of relative humidity on shrinkage of Material C | 92 |
| 4.8 | Influence of relative humidity on shrinkage of concrete mix | 93 |
| 4.9 | Relative shrinkage of repair materials under curing condition of 20°C, 30% R.H. | 94 |
| 4.10 | Relative shrinkage of repair materials under curing condition of 20°C, 45% R.H. | 95 |
| 4.11 | Relative shrinkage of repair materials under curing condition of 20°C, 55% R.H. | 96 |
| 4.12 | Relative shrinkage of repair materials, water cured at 20°C for first 28 days followed by 20°C, 55% R.H. curing | 97 |

| | | |
|------|---|-----|
| 4.13 | Compression creep curves at applied stress/strength ratios of 30%, 45% and 55% for Material A | 101 |
| 4.14 | Compression creep curves at applied stress/strength ratios of 30%, 45% and 55% for Material B | 102 |
| 4.15 | Compression creep curves at applied stress/strength ratios of 30%, 45% and 55% for Material C | 103 |
| 4.16 | Compression creep curves at applied stress/strength ratios of 30%, 45% and 55% for concrete mix | 104 |
| 4.17 | Compression creep test results at 30% stress/strength ratio | 106 |
| 4.18 | Compression creep test results at 45% stress/strength ratio | 107 |
| 4.19 | Compression creep test results at 55% stress/strength ratio | 108 |
| 4.20 | Comparison between the experimental and theoretical shrinkage curves based on the hyperbolic expression | 112 |
| 4.21 | Comparison between the experimental and theoretical shrinkage curves based on the logarithmic expression | 113 |
| 4.22 | Comparison between the experimental and theoretical creep curves based on hyperbolic expression [30% stress / strength ratio] | 114 |
| 4.23 | Comparison between the experimental and theoretical creep curves based on logarithmic expression [30% stress / strength ratio] | 115 |
| 4.24 | Comparison between the experimental and theoretical creep curves based on hyperbolic expression [45% stress / strength ratio] | 116 |
| 4.25 | Comparison between the experimental and theoretical creep curves based on logarithmic expression [55% stress / strength ratio] | 117 |
| 5.2 | Three different forms of chloride, after Tuuti [98] | 125 |
| 5.3 | Sealing of a specimen on five faces | 133 |
| 5.4 | Cutting the specimen into two halves | 134 |
| 5.5 | Sample locations for chloride analysis | 134 |

| | | |
|------|---|-----|
| 5.6 | Influence of initial curing conditions on chloride diffusion for Material A (at 28 days) | 139 |
| 5.7 | Influence of initial curing conditions on chloride diffusion for Material B (at 28 days) | 139 |
| 5.8 | Influence of initial curing conditions on chloride diffusion for Material C (at 28 days) | 140 |
| 5.9 | Influence of initial curing conditions on chloride diffusion for concrete (at 28 days) | 140 |
| 5.10 | Chloride diffusion for repair materials at 28 days, water cured at 20°C | 142 |
| 5.11 | Chloride diffusion for repair materials at 28 days, air cured at 20°C & 55% R.H. | 142 |
| 5.12 | Chloride diffusion for repair materials at 28 days, wet/air cured at 20°C | 143 |
| 5.13 | Chloride diffusion for repair materials at 28 days, cured under ambient conditions | 143 |
| 5.14 | Influence of initial curing conditions on chloride diffusion for Material A (at 90 days) | 147 |
| 5.15 | Influence of initial curing conditions on chloride diffusion for Material B (at 90 days) | 147 |
| 5.16 | Influence of initial curing conditions on chloride diffusion for Material C (at 90 days) | 148 |
| 5.17 | Influence of initial curing conditions on chloride diffusion for concrete (at 90 days) | 148 |
| 5.18 | Chloride diffusion for repair materials at 90 days, water cured at 20°C | 149 |
| 5.19 | Chloride diffusion for repair materials at 90 days, air cured at 20°C & 55% R.H. | 149 |
| 5.20 | Influence of initial curing conditions on chloride diffusion for Material A (at 180 days) | 150 |
| 5.21 | Influence of initial curing conditions on chloride diffusion for Material B (at 180 days) | 150 |

| | | |
|------|--|-----|
| 5.22 | Influence of initial curing conditions on chloride diffusion for Material C (at 180 days) | 151 |
| 5.23 | Influence of initial curing conditions on chloride diffusion for concrete (at 180 days) | 151 |
| 5.24 | Chloride diffusion for repair materials at 180 days, water cured at 20°C | 152 |
| 5.25 | Chloride diffusion for repair materials at 180 days, air cured at 20°C and 55% R.H. | 152 |
| 5.26 | Influence of early exposure on chloride diffusion after 28 days | 154 |
| 5.27 | Influence of early exposure on chloride diffusion after 90 days | 154 |
| 5.28 | Influence of early exposure on chloride diffusion after 180 days | 155 |
| 5.29 | Chloride diffusion profiles for repair Material A at various periods of exposure to chloride (initial water cured at 20°C for the first 28 days) | 158 |
| 5.30 | Chloride diffusion profiles for repair Material B at various periods of exposure to chloride (initial water cured at 20°C for the first 28 days) | 158 |
| 5.31 | Chloride diffusion profiles for repair Material C at various periods of exposure to chloride (initial water cured at 20°C for the first 28 days) | 159 |
| 5.32 | Chloride diffusion profiles for concrete mix at various periods of exposure to chloride (initial water cured at 20°C for first 28 days) | 159 |
| 5.33 | Chloride diffusion profiles for repair Material A at various periods of exposure to chloride (initial air cured at 20°C, 55% R.H. for the first 28 days) | 160 |
| 5.34 | Chloride diffusion profiles for repair Material B at various periods of exposure to chloride (initial air cured at 20°C, 55% R.H. for the first 28 days) | 160 |
| 5.35 | Chloride diffusion profiles for repair Material C at various periods of exposure to chloride (initial air cured at 20°C, 55% R.H. for the first 28 days) | 161 |

| | | |
|------|--|-----|
| 5.36 | Chloride diffusion profiles for concrete mix at various periods of exposure to chloride (initial air cured at 20°C, 55% R.H. for the first 28 days) | 161 |
| 5.37 | Chloride diffusion profiles for Material A at various periods of exposure to chloride (early exposure - 24 hours after casting) | 162 |
| 5.38 | Chloride diffusion profiles for Material B at various periods of exposure to chloride (early exposure - 24 hours after casting) | 162 |
| 5.39 | Chloride diffusion profiles for Material C at various periods of exposure to chloride (early exposure - 24 hours after casting) | 163 |
| 5.40 | Chloride diffusion profiles for concrete at various periods of exposure to chloride (early exposure - 24 hours after casting) | 163 |
| 5.41 | Diffusion coefficient versus exposure time for repair materials and concrete (initial curing for 28 days 20°C, 55% R.H.) | 165 |
| 5.42 | Diffusion coefficient versus exposure time for repair materials and concrete (initial water curing for 28 days at 20°C) | 165 |
| 5.43 | Diffusion coefficient versus exposure time for repair materials and concrete (early exposure - 24 hours after casting) | 166 |
| 5.44 | Diffusion coefficient versus time for mixes A1, B1, C1 and D1, after El-Khatib [125] | 170 |
| 5.45 | Diffusion coefficient versus time for mixes A3, B3, C3, D3, E3 and F3, after Molloy [126] | 170 |
| 5.46 | Relation between effective diffusion and time for repair materials and concrete mix exposed to chloride solution (initially air cured for the first 28 days at 20°C, 55% R.H.) | 174 |
| 5.47 | Relation between effective diffusion and time for repair materials and concrete mix exposed to chloride solution (initially water cured for first 28 days at 20°C) | 174 |
| 5.48 | Relation between effective diffusion coefficient and time for repair materials and concrete mix exposed to chloride solution (24 hours after casting) | 175 |

| | | |
|------|--|-----|
| 5.49 | Relationship between diffusion coefficient and time for initial water cured specimens, using m and D_1 values from Table 5.5 | 177 |
| 5.50 | Relationship between diffusion coefficient and time for initial air cured specimens, using m and D_1 values from Table 5.5 | 177 |
| 5.51 | Relationship between diffusion coefficient and time for early exposed (24 hours after casting) specimens, using m and D_1 values from table 5.6 | 178 |
| 5.52 | Equilibrium chloride concentration with time for repair materials and concrete mix (for initial water cured at 20°C) | 179 |
| 5.53 | Equilibrium chloride concentration with time for repair materials and concrete mix (for initial air curing at 20°C, 55% R.H.) | 179 |
| 5.54 | Equilibrium chloride concentration with time for repair materials and concrete mix (for specimens immersed in the chloride solution at 24 hours after casting) | 180 |
| 5.55 | Relationship between C_o and D_c for repair materials and concrete mix | 181 |
| 5.56 | Relationship between C_o and D_c values for mixes used by El-Khatib [125] | 181 |
| 5.57 | Relationship between C_o and D_c for mixes used by different researchers | 182 |
| 5.58 | Predicted chloride diffusion profiles for Material A (initially air cured at 20°C, 55% R.H. - after 180 days) | 189 |
| 5.59 | Predicted chloride diffusion profile for Material C (initially water cured at 20°C, after 180 days) | 189 |
| 5.60 | Predicted chloride profile for concrete mix (initially air cured at 20°C, 55% R.H.- after 180 days) | 190 |
| 5.61 | Predicted chloride profile for concrete mix (initially water cured at 20°C - after 180 days) | 190 |

| | | |
|------|--|-----|
| 5.62 | Prediction of chloride concentration after 20 years exposure, Port Rashid (control - splash zone) | 194 |
| 5.63 | Prediction of chloride concentration after 20 years exposure, Port Rashid (control - top of dock) | 194 |
| 5.64 | Prediction of chloride concentration after 20 years exposure, Port Rashid (zamdrain - tidal zone) | 195 |
| 5.65 | Prediction of chloride concentration after 20 years exposure, Port Rashid (zamdrain - splash zone) | 195 |
| 5.66 | Prediction of chloride concentration after 20 years exposure, Jebel Ali Port (control - tidal zone) | 196 |
| 5.67 | Prediction of chloride concentration after 20 years exposure, Jebel Ali Port (control - splash zone) | 196 |
| 5.68 | Prediction of chloride concentration after 20 years exposure, Jebel Ali Port (zamdrain - splash zone) | 197 |
| 5.69 | Prediction of chloride concentration after 20 years exposure, Jebel Ali Port (control - splash zone) | 197 |
| 5.70 | Prediction of chloride concentration after 20 years exposure, Jebel Ali Port (control - top of dock) | 198 |
| 5.71 | Prediction of chloride concentration after 20 years exposure, Jebel Ali Port (zamdrain - tidal zone) | 198 |
| 5.72 | Prediction of chloride concentration after 20 years exposure, Jebel Ali Port (zamdrain - splash zone) | 199 |
| 5.73 | Prediction of chloride concentration after 20 years exposure, Jebel Ali Port (zamdrain - top of dock) | 199 |
| 6.1 | Reinforcement details | 213 |
| 6.2 | Void dimensions for (a) batch I, and (b) batch II specimens | 214 |
| 6.3 | Location of demec points on reinforced concrete columns (control) | 217 |
| 6.4 | Location of demec points on voided column specimens; (a) void on one face (batch I), and (b) void on two opposite faces (batch II) | 218 |

| | | |
|------|--|-----|
| 6.5 | Location of demec points on repaired column specimens; (a) void on one face (batch I), and (b) void on two opposite faces (batch II) | 219 |
| 6.6 | Axially loaded voided column | 221 |
| 6.7 | Voided cross-section | 221 |
| 6.8 | Strain distribution on voided portion of column | 222 |
| 6.9 | Strain distribution on voided cross-section at point of failure | 225 |
| 6.10 | Stress distribution for the single void specimen | 226 |
| 6.11 | Simplified stress distribution as suggested in BS 8110 [92] | 226 |
| 6.12 | Design stress-strain curves, after BS 8110 [92] | 226 |
| 6.13 | Load-strain relationship for columns I (batch I), repaired with Material A | 233 |
| 6.14 | Load-strain relationship for columns II (batch I), repaired with Material B | 233 |
| 6.15 | Load-strain relationship for columns III (batch I), repaired with Material C | 234 |
| 6.16 | Load-strain relationship for voided columns (batch I) | 234 |
| 6.17 | Stress-strain curve for the longitudinal steel reinforcement | 235 |
| 6.18 | Stress-strain relationship for (a) Material A, (b) Material B, (c) Material C and (d) Concrete | 236 |
| 6.19 | Load distribution in concrete, repair and steel phases of column specimens (repaired with Material A), Batch I | 237 |
| 6.20 | Load distribution in concrete, repair and steel phases of column specimens (repaired with Material B), Batch I | 237 |
| 6.21 | Load distribution in concrete, repair and steel phases of column specimens (repaired with Material C), Batch I | 237 |
| 6.22 | Load distribution in concrete and steel phases of voided column specimens, Batch I | 237 |

| | | |
|------|---|-----|
| 6.23 | Load distribution in concrete and steel phases of control column specimens, Batch I | 239 |
| 6.24 | Strain distribution for columns I (batch II), repaired with Material A | 240 |
| 6.25 | Strain distribution for columns II (batch II), repaired with Material B | 240 |
| 6.26 | Strain distribution for columns III (batch II), repaired with Material C | 240 |
| 6.27 | Strain distribution for voided columns (batch II) | 240 |
| 6.28 | Load distribution in the concrete, repair and steel phases of column specimens (repaired with Material A), Batch II | 241 |
| 6.29 | Load distribution in the concrete, repair and steel phases of column specimens (repaired with Material B), Batch II | 241 |
| 6.30 | Load distribution in the concrete, repair and steel phases of column specimens (repaired with Material C), Batch II | 241 |
| 6.31 | Load distribution in the concrete and steel phases of voided column specimens, Batch II | 241 |
| 6.32 | Load distribution in the concrete and steel phases of control column specimens, Batch II | 242 |
| 6.33 | Comparison of theoretical and experimental load distribution for control column specimens, Batch I | 243 |
| 6.34 | Comparison of theoretical and experimental load distribution for voided column specimens, Batch I | 243 |
| 6.35 | The residual compressive strength of repaired column, compared to control columns (batch I) | 245 |
| 6.36 | The residual compressive strength of repaired column, compared to control columns (batch II) | 245 |
| 7.1 | Details of creep and shrinkage rectangular plain, symmetrically reinforced and unsymmetrically reinforced concrete prisms, after Brooks et al [152] | 255 |
| 7.2 | Measured total deformation of symmetrically reinforced concrete prisms, (a) under stress of 5 Mpa, and (b) shrinkage, after Brooks et al [152] | 256 |

| | | |
|------|--|-----|
| 7.3 | Measured total deformation of unsymmetrically reinforced concrete prisms, (a) under stress of 5 Mpa, and (b) shrinkage, after Brooks et al [152] | 257 |
| 7.4 | Reinforcement details | 262 |
| 7.5 | Column specimen showing the voids before patch repair | 264 |
| 7.6 | Location of demec points on reinforced concrete column (control) | 267 |
| 7.7 | Location of demec points on repaired column specimens | 267 |
| 7.8 | Influence of reinforcing steel on the shrinkage of concrete | 272 |
| 7.9 | Influence of repair material A on the shrinkage of reinforced concrete column | 273 |
| 7.10 | Influence of repair material B on the shrinkage of reinforced concrete column | 274 |
| 7.11 | Influence of repair material C on the shrinkage of reinforced concrete column | 275 |
| 7.12 | Schematic load distribution in reinforced concrete compression members under sustained load | 277 |
| 7.13 | Strain in steel reinforcement of control column (batch I) specimen under sustained loading | 280 |
| 7.14 | Stress-strain curve for the longitudinal steel reinforcement | 281 |
| 7.15 | Experimental load distribution under sustained load | 282 |
| 7.16 | Creep curves of short reinforced concrete column specimens and unreinforced prisms | 285 |
| 7.17 | Comparison of measured stress decrement in concrete with predicted using creep model suggested by Samra [144] | 286 |
| 7.18 | Influence of repair material A on the creep of reinforced concrete | 289 |
| 7.19 | Influence of repair material B on the creep of reinforced concrete | 290 |
| 7.20 | Influence of repair material C on the creep of reinforced concrete | 291 |

| | | |
|------|---|-----|
| 7.21 | Load distribution in steel, repair and concrete phases of repaired reinforced concrete columns (average of three) under sustained load (repaired with Material A) | 292 |
| 7.22 | Load distribution in steel, repair and concrete phases of repaired reinforced concrete columns (average of three) under sustained load (repaired with Material B) | 292 |
| 7.23 | Load distribution in steel, repair and concrete phases of repaired reinforced concrete columns (average of three) under sustained load (repaired with Material C) | 293 |
| 7.24 | Load distribution in steel and concrete phases of reinforced concrete columns (average of three) under sustained load | 293 |
| 7.25 | Relation between strain and time for a unit stress applied during the period t_0 to t | 296 |
| 7.26 | Comparison between the experimental and theoretical total strain ratio from the proposed expression for reinforced columns repaired with Material A | 302 |
| 7.27 | Comparison between the experimental and theoretical total strain ratio from the proposed expression for reinforced columns repaired with Material B | 302 |
| 7.28 | Comparison between the experimental and theoretical total strain ratio from the proposed expression for reinforced columns repaired with Material C | 303 |
| 7.29 | Comparison of total strain ratio for the reinforced concrete columns repaired with three different repair materials | 303 |

LIST OF TABLES

| Table No. | | Page |
|-----------|--|------|
| 2.1 | Chemical composition of the OPC used in the manufacture of the concrete specimens in chapters 3, 6 and 7 | 15 |
| 2.2 | Chemical composition of the OPC used in the manufacture of the concrete specimens in chapters 4 and 5 | 16 |
| 2.3 | The chemical composition of 12 mm diameter high yield steel reinforcement | 20 |
| 3.1 | General requirements of patch repair materials for structural compatibility | 24 |
| 3.2 | Expression for complete stress-strain curves available in literature | 33 |
| 3.3 | Some typical properties of repair materials | 53 |
| 3.4 | Water permeability results | 55 |
| 3.5 | Experimental results for repair materials and concrete mix | 63 |
| 4.1 | Categories of patch repair systems used by Emberson and Mays [13] | 75 |
| 4.2 | Shrinkage strains (microstrain) | 75 |
| 4.3 | Relationship between stress-strength ratio and ϵ_{od}/ϵ_E [73] | 80 |
| 4.4 | Experimental programme | 83 |
| 4.5 | Details of mixes and materials | 83 |
| 4.6 | Shrinkage and swelling deformation strains at 90 days (microstrain) | 88 |
| 4.7 | Creep strains at 90 days, instantaneous elastic strain on loading and cube strength prior to loading | 105 |
| 4.8 | Details of hyperbolic expression for shrinkage and creep (at 30% stress / strength ratio) | 110 |
| 4.9 | Details of logarithmic expression for shrinkage and creep (at 30% stress / strength ratio) | 110 |
| 4.10 | Maximum percentage error for both expressions | 111 |

| | | |
|--------|--|-----|
| 5.1 | Chloride threshold levels for initiation of corrosion in reinforced concrete | 124 |
| 5.2 | Equilibrium chloride concentration on the surface, C_0 , (% by weight of material) under different initial curing conditions (after 28 days) | 137 |
| 5.3 | Details of mixes used by El-Khatib [125] | 167 |
| 5.4 | Details of mixes used by Molly [126] | 169 |
| 5.5 | D1 and m values for the various materials for initially either water cured or air cured for 28 days | 173 |
| 5.6 | D1 and m values for the various materials for early exposed (24 hours after casting) specimens | 173 |
| 5.6(a) | The values of constant K_s | 184 |
| 5.7 | Percentage of chloride (by weight of cement) at given depth and location of Port Rashid | 191 |
| 5.8 | Percentage of chloride (by weight of cement) at given depth and location of Jebel Ali Port | 192 |
| 5.9 | D_c and C_0 values used in the analysis of Port Rashid | 193 |
| 5.10 | D_c and C_0 values used in the analysis of Jebel Ali Port | 193 |
| 6.1 | Details of mixes and materials | 211 |
| 6.2 | Details of column specimens | 215 |
| 6.3 | Results of a failure load and residual strength of batches I and II tests | 244 |
| 6.4 | Comparison between the experimental and theoretical failure load of defective reinforced concrete columns of batch I | 248 |
| 7.1 | Parameters of deformation reduction factors for the various methods of predicting deformation of reinforced concrete | 253 |
| 7.2 | Experimental programme | 264 |
| 7.3 | Comparison between the instantaneous loads in concrete and steel as determined by two procedures | 279 |

CHAPTER 1

INTRODUCTION

1.1 INTRODUCTION

The durability of a material or structure refers to its ability to withstand the environmental conditions to which it is exposed. Although concrete structures have mostly performed satisfactorily during their service life, there are nevertheless significant problems which occur in many structures and the causes are often related to durability of the composite material. As a result, in recent years, repair, refurbishment and maintenance of reinforced concrete structures has become a significant part of the total cost of construction worldwide.

Under current practice, there are no standard procedures for the design of patch repairs. Design is usually based on the experience of specialist contractors and when selection of repair materials is made, emphasis is normally given to their relatively short term properties such as strength, bond and early age plastic shrinkage/expansion etc. Although these properties indicate the immediate performance of the repair they give little information on its long-term performance with respect to cracking and efficient composite action with the substrate materials to carry applied loads and deformations. Therefore, there is an important need for recognising and understanding the properties of generic repair materials, which are of significance to the subsequent structural behaviour of repaired concrete members.

1.2 SCOPE OF RESEARCH

A patch repair is an effective restoration technique when an element or a whole structure shows signs of distress, especially spalling and delamination. Most of the research carried out on generic repair materials in the past has focused on the basic short-term

strength and bond properties of repair materials which are of immediate concern when repair is applied. However, long-term deformation properties, such as creep and shrinkage, which can affect internal stresses of the repaired members have received little attention. Also relatively little information is available on the chloride diffusion characteristics of these generic repair materials and mathematical models which can be used to predict long-term chloride concentration in repair are not available.

In this context, therefore, long-term deformation properties together with the chloride diffusion characteristics of generic repair materials deserve attention. Furthermore, a more fundamental investigation of the structural interaction between repair patch and substrate concrete needs to be undertaken, and the potential importance of property mismatch needs to be quantified. Information on complete stress-strain characteristics and long-term deformations of the repair and substrate material will be required for such an investigation. Data on permeability and chloride diffusion characteristics together with prediction models for long-term chloride concentration will be valuable for assessment of durability of repair.

1.3 SCOPE OF PRESENT INVESTIGATION

There is a growing need for valid expressions for the evaluation of structural interaction between the repair patch and substrate concrete to allow for the design of effective and economical remedial work. In addition procedures for predicting the long-term durability of repair patches need to be developed. Although several studies have been carried out on concrete repair materials in recent years, the important aspects outlined above have been largely neglected.

The overall aims of this thesis therefore, were:-

- to investigate strength and deformation properties of three generic repair materials, which are of significance to the subsequent structural behaviour of repaired members, and also to compare their performance relative to plain concrete mixes which may also be suitable for repair in their own right.
- to establish chloride diffusion and water permeability properties of these generic repair materials, together with the derivation of a theoretical model which can be used to predict long-term chloride diffusion for a given exposure condition.
- to study experimentally and theoretically the short and long term structural interaction between a repair patch and the substrate concrete in short compression members of reinforced concrete. Relate the long-term interaction to basic materials properties, such as stiffness, creep and shrinkage, of the repair materials and substrate concrete.

Based on the results obtained from the experiments, mathematical models for predicting the chloride concentrations as well as the long-term structural performance of repaired columns have been proposed. These models and proposals formed an important input to a research project entitled "*Assessment of Performance and Optimal Strategies for Inspection and Maintenance of Concrete Structures Using Reliability-Based Expert Systems*" sponsored by CEC within the **BRITE/EURAM** research programme. The objective of this project was to optimise strategies for inspection, maintenance and repair of reinforced concrete bridges by developing improved methods for modelling the deterioration of existing as well as future structures using reliability-based expert system. A general description of the expert system is given in the following section.

1.4 GENERAL DESCRIPTION OF THE EXPERT SYSTEM OF THE BRITE/EURAM PROJECT

The expert system consists of two main modules: **BRIDGE 1** and **BRIDGE 2** and a number of databases (structural data, service data, inspection data, repair data, inspection procedures, repair techniques, list of defects and list of causes) and **FORTRAN** programmes (**FORTRAN** programmes for reliability analysis, updating analysis, structural analysis and inspection procedures) and also **INPUT** and **OUTPUT** modules.

The expert system can be used in two different ways:

1. The **BRIDGE 1** module of the expert system may be used in-situ during the inspection of a bridge to supply information on the causes of observed defects, related defects and appropriate diagnosis methods, and may be used also to record the inspection data to be used in later assessments of the reliability of the bridge.
2. The **BRIDGE 2** module of the expert system may be used in the office to perform detailed analysis of the inspection data and laboratory results. The output of the analysis includes updated assessment of the reliability of the bridge and recommendations on the appropriate actions to be taken; the options are no action, detailed structural assessment or repair work with recommendations on the relevant repair procedures, usually presented in that order as the calculated reliability of the bridge decreases.

The reliability of the bridge is determined by using the reliability index β for a single failure element or for the whole bridge. The reliability of the bridge is assumed to decrease with time due to deterioration, and failure is considered to occur when the expected

reliability index falls below a minimum value. Updating of stochastic variables, such as material properties and diffusion coefficients, is performed according to Bayesian statistical theory on measured samples of the stochastic variables.

The role of the author in this project was to develop procedures for assessing the influence of spalling (due to corrosion) and different generic repair materials on the structural performance of repaired reinforced compression members, in the form of simple models to be used in the expert systems. Along with the structural study, information on the short and long-term properties of the repair materials were also provided.

1.5 THESIS LAYOUT

In this thesis the author has attempted to bring together the latest information from the field of reinforced concrete repair work, to provide researchers and engineers with convenient compilation of information. Such information is of great importance in the design of inspection and maintenance strategies for reinforced concrete structures where repair work is carried out.

This thesis is divided into nine chapters, the introduction and eight other chapters.

Details of the experimental programme are outlined in chapter 2. Information on the materials used throughout the investigation is also given. These include the chemical compositions of the cement, grading curves of aggregates etc.

Properties of repair materials which are significant to the subsequent structural performance of the reinforced concrete structures are reported in chapter 3. The first part of the chapter deals with the typical properties of generic repair materials, and compares their performance with plain concrete of similar grade. These properties include compressive

strength, modulus of elasticity, water permeability, together with the complete compressive stress-strain characteristics including the post-cracking branches. Full description of repair materials and grading curves for the aggregates used in these materials are also given in this chapter.

Chapter 4 is devoted to the study of the long-term deformation of repair materials. The effect of varying curing environment on shrinkage deformation was examined using five different curing regimes. Expansion characteristics of the generic repair materials under saturated condition were also determined. The sustained stress-strength ratio for the long-term creep tests, of 90 days duration, ranged between 0.3 to 0.55 of the 28 days cube strength.

In chapter 5, a study of the chloride diffusion characteristics into concrete and repair materials is presented. Based on relatively early age diffusion coefficients obtained from the measurements of chloride concentration profiles for these materials at various test ages, a method for predicting chloride concentrations in repair materials exposed to long-term chloride contaminated environment is proposed.

Short compression members simulating deterioration due to reinforcement corrosion on one face and two faces were considered in chapter 6. The influence of three generic repair materials on such defective members has been studied. These include, mode of failure, compressive strength, load distribution in the repair patch and substrate concrete, stiffness and fracture process of the materials.

In chapter 7, the long-term structural performance of short reinforced concrete columns has been studied experimentally using test elements incorporating repair patches which were symmetrically positioned at the middle of the columns. The structural interaction between the repair patch and substrate concrete after repair work was investigated and was related to the basic material properties. A mathematical model is derived to describe the

long-term stress distribution in repaired short compression members.

Conclusions and proposals for future research are presented in chapter 8, while chapter 9 lists sources of information that are referred in this thesis.

The current list of publications resulting from this research programme are given at the end of the thesis.

CHAPTER 2

EXPERIMENTAL PROGRAMME

2.1 INTRODUCTION

Different repair methods and generic materials are currently used to overcome damage in deteriorated structures. The basic mechanical and physical interactions of such available products and the substrate on which they are used need to be established before assessment can be made and suitable repair materials chosen. Research has shown the potential importance of property mismatch between patch repair materials and the reinforced concrete substrate.

During service life, incompatibilities in the form of differing strengths and stiffness between repair and substrate concrete can create difficulties, while drying shrinkage of repair materials may reduce longer-term structural efficiency by either initial tensile strains induced in the repair, or due to cracking at the repair/substrate interface. Also, creep of the repair material under sustained stress render the load sharing capacity of the repair less effective with time. A beneficial effect of creep can be to reduce the differential tensile strains induced by shrinkage of the repair material. Permeability of repair materials influences the rate of ingress of aggressive substances such as chlorides and sulphates into them, and consequently has a major effect on the durability of the repair in the long-term.

The overall aim of the experimental programme was, therefore, to investigate short and long-term properties of specially formulated generic repair materials, and the structural performance of short reinforced concrete columns after repair to simulate corrosion damage had been carried out.

2.2 OBJECTIVES OF THE INVESTIGATION

The principal objectives of the experimental work were:-

1. To establish typical properties of repair materials, which influence long-term structural performance of repaired reinforced concrete elements.
2. To study long-term deformation properties of these repair materials, such as shrinkage, swelling and creep, under different conditions of exposure.
3. To investigate the chloride diffusion characteristics in concrete and repair materials.
4. To derive a method for prediction of long-term chloride ion concentration in repair materials exposed to a chloride contaminated environment, based on early age data.
5. To study the influence of different generic repair materials on the structural performance of reinforced concrete short compression members.
6. To relate the long-term structural interaction between repair patch and the substrate concrete to basic material properties such as stiffness, creep and shrinkage.
7. To derive a mathematical model for predicting long-term structural performance of repaired reinforced concrete short columns.

2.3 DETAILS OF THE EXPERIMENTAL PROGRAMME

2.3.1 Properties of repair materials which influence long-term performance of concrete structures

This series of tests was carried out in order to study the strength, stiffness, post peak-load behaviour under compression and water permeability characteristics of three commercially available generic repair materials, together with a plain concrete mix of similar strength, which was used to provide control specimens for comparison. The stress-strain tests

of specimens were conducted using a steel tube to absorb the pressure release during the test, when the repair material attained its maximum load. This prevented a sudden failure of the repair material and allowed the determination of the descending portion of the stress-strain curve of the material. The strains from the specimens and tube were measured by means of electrical resistance strain gauges.

The generic repair materials are labelled as A, B and C, where Material A is a blend of portland cement, graded aggregates of maximum size of 5mm and additives, Material B is a mineral based cementitious material with no coarse aggregate size particles or additives, and Material C is a single component cementitious mortar which contains styrene acrylic copolymer and fibre. They are supplied as single component systems by their manufacturers, ready for on-site mixing and requiring only the addition of clean water. The mix proportions (by weight) of the concrete mix were 1 : 2.24 : 3.22; with a water to cement ratio of 0.56. The cement content was 343 kg/m³. This mix was used as a control for comparison of the properties of repair materials.

A majority of the specimens were tested at the age of 28 days. The development of compressive strength with age, for each repair material was also established. A high-performance, non-shrinkage repair material A, develops strength rapidly and reaches a high compressive strength at 28 days age.

Details of this series of experiments are given in chapter 3.

2.3.2 Long-term deformation properties of materials

An experimental investigation was carried out in order to establish the shrinkage, swelling and creep deformations of materials. The effects of varying the curing environment on shrinkage deformation were examined by using five different curing regimes incorporating

different relative humidities and temperatures. Free shrinkage and swelling measurements were made on four faces of each specimen. The first shrinkage measurement was taken after 24 hours after casting.

For creep tests, all the specimens were cured in water at 20°C for 28 days prior to loading. All the prism specimens for creep tests were accompanied by identical prisms for free shrinkage data. In the creep tests two prisms of each mix were loaded together in a standard creep rig. The concentricity of the applied load was ensured by achieving reasonably similar strains on the four tie rods of the creep rigs. The duration of the creep tests was 90 days followed by creep recovery for a further period of 60 days. The sustained stress-strength ratios applied to the specimens were 0.30, 0.45 and 0.55 of the 28 day cube strength. Creep strains under load and creep recovery were measured at regular intervals on two opposite faces of each specimen by means of a Demec extensometer over a gauge length of 200mm.

The results show that shrinkage of the repair materials is significantly greater than shrinkage of concrete. Also the shrinkage of these specially formulated repair mortars, especially those modified with a polymer admixture, is very sensitive to relative humidity of exposure compared with normal concrete.

Details of this series of experiments are given in chapter 4.

2.3.3 Chloride diffusion into concrete and repair materials

This study was carried out in order to investigate the chloride diffusion characteristics into plain concrete and repair materials of various constituents. The influence of initial curing conditions on diffusion was also investigated.

The investigation of chloride diffusion was carried out in two parts;

- In the first part four initial curing conditions were employed for the first 28 days after casting, before any exposure of the specimens to a chloride solution. Air curing at 20°C, 55 % RH, wet/air curing at 20°C, 55 % RH, air curing under ambient conditions and relatively uncontrolled conditions of the laboratory air and water curing at 20°C,
- in the second part, specimens were exposed to a chloride environment at 24 hours after casting in order to simulate some practical conditions where the repair patches cannot be protected from chloride exposure for a long period after application.

After the initial curing period of 28 days in part one and 24 hours in part two, specimens were immersed in a sodium chloride solution (175 gm of NaCl per litre) and analysis of chloride ingress into specimens took place after 28, 90 and 180 days of immersion.

Diffusion coefficients of the various mixes were calculated from the chloride concentration data. An empirical expression to predict long-term chloride concentration is derived. A comprehensive review of current data on chloride diffusion coefficients for concrete and repair materials has been made for use with the long-term prediction models. Application of this prediction model to the field data of some Arabian Gulf structures is made. This series of experiments are reported in chapter 5.

2.3.4 Influence of repair materials on the structural performance of reinforced concrete compression members

This series of tests were carried out in order to study the influence of three generic repair materials on the structural performance of reinforced concrete compression members

and load-strain characteristics of the repaired members.

A total of twenty reinforced concrete column specimens of size 150 X 150 X 750mm were employed in this investigation. All the column specimens were reinforced longitudinally with four 12mm diameter high yield steel bars, the centroid of each bar being located at 26mm from the face of a specimen. Mild steel bar of 6mm diameter was used for stirrup reinforcement in each column specimen. In order to facilitate strain measurement in the longitudinal steel, studs of 10mm diameter were welded to the longitudinal bars in the reinforcing cage over a gauge length of 200mm.

The concrete mix from which the column specimens were manufactured had the same proportions as described in section 2.3.1. Some columns were cast with centrally positioned voids of depth 55mm and length 200mm, to represent the spalling and corrosion damage found in practice. The load deformation behaviour across voided and repaired column specimens was studied upto failure loads.

Uniaxial compression tests were performed on the column specimens under a constant stress rate of loading. At regular load increments, longitudinal strains in the concrete substrate and the repaired zone were measured by means of Demec extensometer over a gauge length of 200mm.

Details of this series of experiments are given in chapter 6.

2.3.5 Long-term structural interaction in repaired compression elements

This investigation was carried out in order to quantify the structural interaction between a repair patch and substrate concrete as a function of basic material properties such as shrinkage, creep and modulus of elasticity. Experimental studies were carried out using three generic repair materials and a control concrete mix to simulate repairs in short

compression members. Details of the reinforced concrete specimens are as described in section 2.3.4.

All the specimens were cured in a temperature and humidity controlled room for 28 days prior to testing. A total of twenty four column specimens were cast in three series. From the eight columns of each series, four were used for the uniaxial creep test and four for measuring shrinkage strain. All the specimens were tested for a period of 120 days. Then voids on two opposite faces were made to simulate spalling of concrete in real life and then repair work was carried out using generic repair materials A, B and C.

The redistribution of stresses caused by the repair materials was monitored. A mathematical model was derived to describe the long-term stress distribution in repaired short compression members.

Details of this series of experiments are given in Chapter 7.

2.4 MATERIALS

2.4.1 Introduction

This section presents details of materials used throughout the experimental programme. Two different sources of cement and aggregates were used as indicated in sections 2.4.2 and 2.4.3. Details of generic repair materials are given in chapter 3.

2.4.2 Cement

Two different sources of cement were used in the course of the experimental investigation. For the experimental work described in sections 2.3.1, 2.3.4 and 2.3.5 and presented in chapters 3, 6 and 7, ordinary portland cement was supplied by Caledonian Ltd, Aberdeen, Grampian. The chemical composition of batches of the cement used is shown in

Table 2.1. The analysis was carried out at the laboratories of the Chemistry Department, UMIST, Manchester, in accordance with the relevant British Standards [1].

Table 2.1

Chemical composition of the ordinary portland cement used in the manufacture of the concrete specimens of chapters 3, 6 and 7

| | |
|---|---------|
| CaO | 64.20 % |
| SiO ₂ | 20.22 % |
| Al ₂ O ₃ | 4.80 % |
| Fe ₂ O ₃ | 3.27 % |
| SO ₃ | 2.81 % |
| MgO | 2.60 % |
| K ₂ O | 0.53 % |
| Na ₂ O | 0.07 % |
| Tricalcium Silicate (C ₃ S) | 47.82 % |
| Dicalcium Silicate (C ₂ S) | 23.14 % |
| Tetracalcium Aluminoferrite (C ₄ AF) | 8.74 % |
| Tricalcium Aluminate (C ₃ A) | 8.51 % |

For the experimental investigations described in sections 2.3.2, 2.3.3 and presented in chapters 4 and 5, ordinary portland cement was supplied by Castle Cement Limited,

Stamford, Lincolnshire. The chemical composition of batches of the cement used is shown in Table 2.2. The analysis was provided by the supplier.

Table 2.2

Chemical composition of the ordinary portland cement used in the manufacture of the concrete specimens of chapters 4 and 5.

| | |
|---|---------|
| CaO | 64.80 % |
| SiO ₂ | 20.80 % |
| Al ₂ O ₃ | 4.90 % |
| Fe ₂ O ₃ | 2.90 % |
| SO ₃ | 3.10 % |
| MgO | 1.00 % |
| K ₂ O | 0.67 % |
| Na ₂ O | 0.13 % |
| Tricalcium Silicate (C ₃ S) | 56.1 % |
| Dicalcium Silicate (C ₂ S) | 17.4 % |
| Tetracalcium Aluminoferrite (C ₄ AF) | 8.80 % |
| Tricalcium Aluminate (C ₃ A) | 8.10 % |

2.4.3 Aggregates

Two different combinations of fine and coarse aggregates were used in the course of the experimental investigation. For the experimental work described in sections 2.3.1, 2.3.4

and 2.3.5 and presented in chapters 3, 6 and 7, fine aggregate was supplied by Lochhills Quarry, Dyce, Grampian Region. This was a coarse sand conforming to the medium zone limits of BS 882; 1965 [2], as shown in figure 2.1. Coarse aggregate used for the above experimental investigation was 10mm maximum size crushed grey granite from Lochhills Quarry, Dyce, Grampian Region. Its grading conformed to the limits defined by BS 882: 1965 [2] for 10mm coarse aggregate, as shown in figure 2.2. For the experimental investigations described in sections 2.3.2, 2.3.3 and presented in chapters 4 and 5, coarse aggregate and fine aggregate were supplied by Tarmac Road Stone, East Midlands. The grading curve for the fine aggregate, which was a natural sand, conformed to the medium zone limits of BS 882 [2] as shown in figure 2.3. Coarse aggregate was washed, crushed granite which conformed to the grading for 10mm maximum size coarse aggregate defined by BS 882: 1965[2] as shown in figure 2.4.

2.4.4 Steel reinforcement

Reinforcing bars used in the manufacture of specimens for the experimental investigation presented in chapters 6 and 7 were standard 12mm diameter high-yield bars, with a herring-bone deformation pattern of twin longitudinal projections and transverse ribs. The chemical composition of the steel is shown in Table 2.3. The analysis of samples of the steel used in the investigation was carried out at the laboratories of the Department of Materials Science, UMIST, Manchester [3].

The stress-strain curve for the 12mm diameter steel reinforcement is presented in figure 2.5.

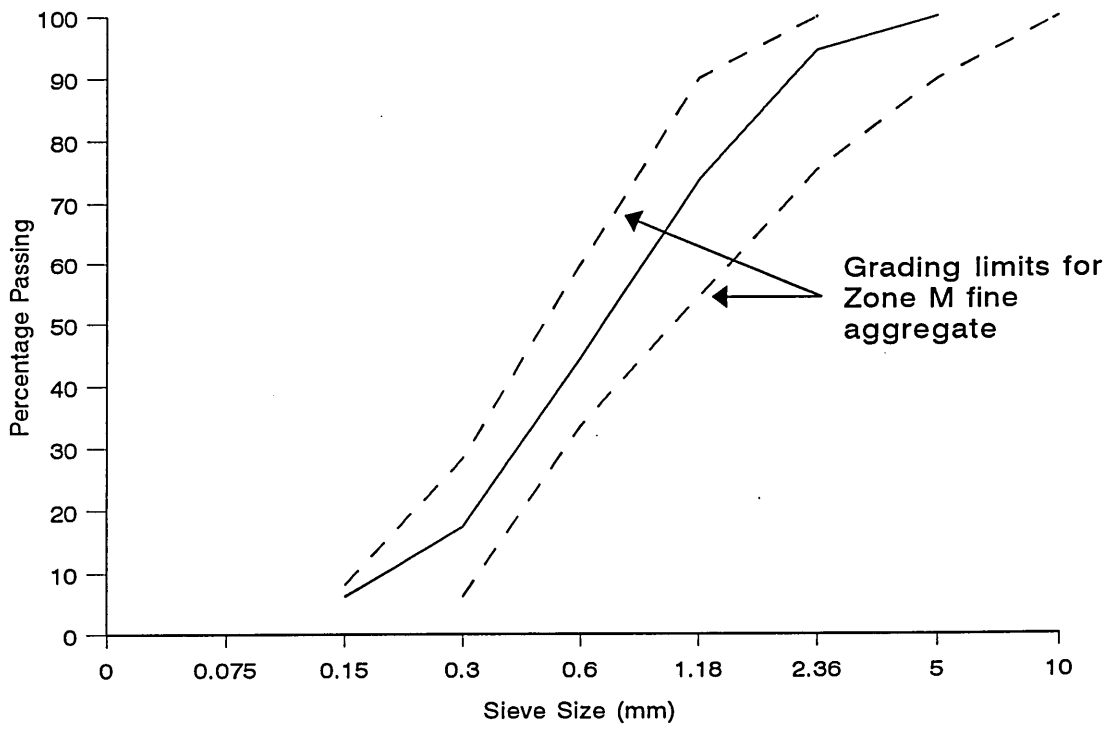


Figure 2.1
Grading curves for Fine Aggregates used in Experimental work presented in Chapters 3, 6 and 7

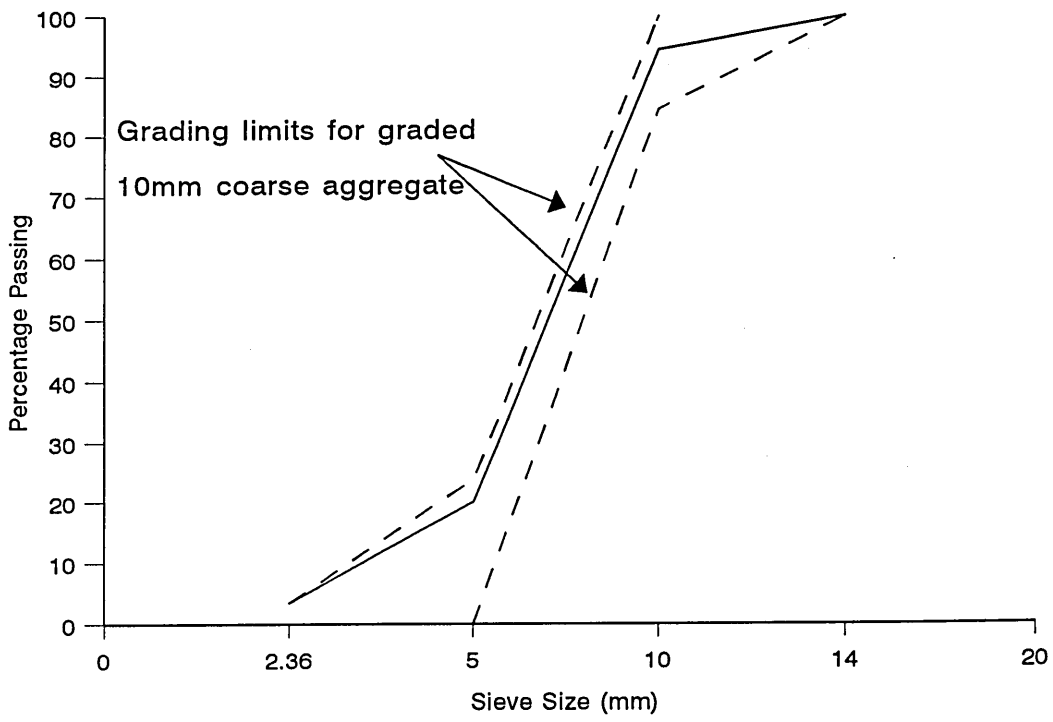


Figure 2.2
Grading curves for Coarse Aggregates used in experimental work presented in Chapters 3, 6 and 7

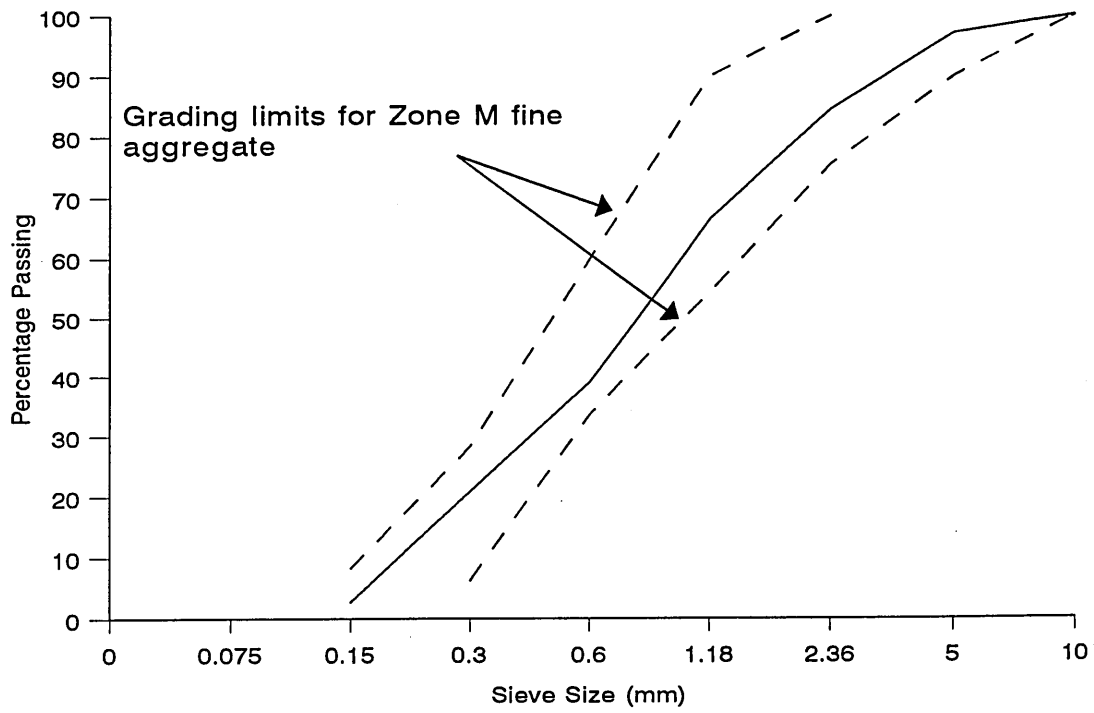


Figure 2.3
Grading curves for Fine Aggregates used in Experimental work presented in Chapters 4 and 5

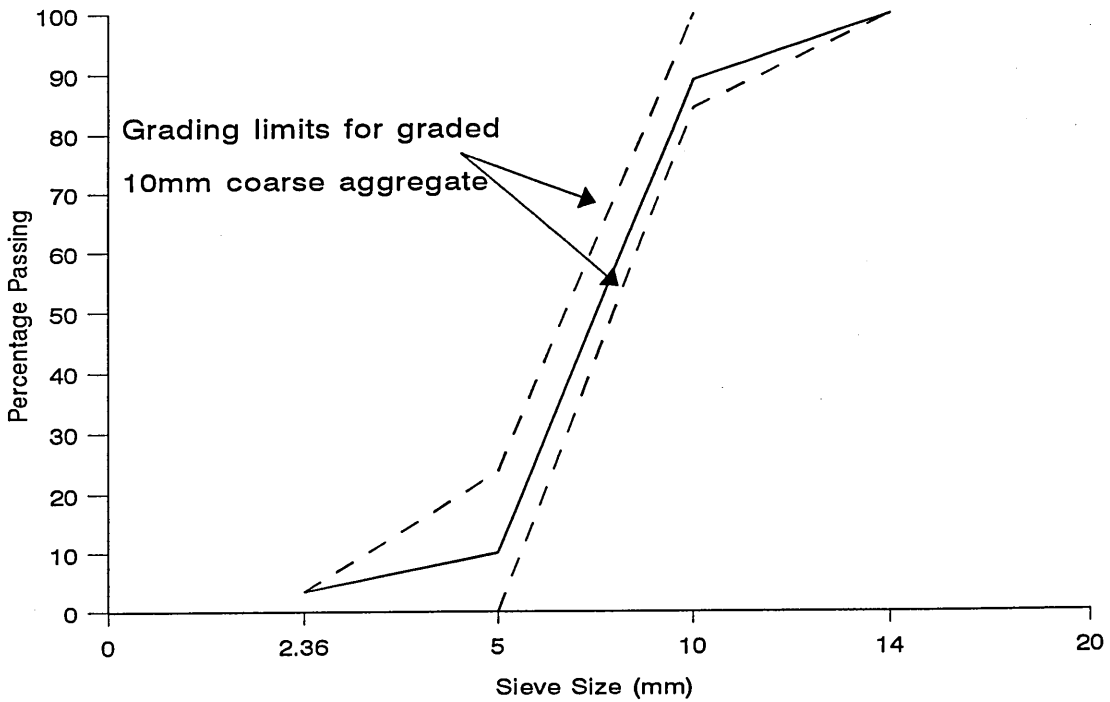


Figure 2.4
Grading curves for Coarse Aggregates used in experimental work presented in Chapters 4 and 5

Table 2.3**The chemical composition of 12mm diameter high yield steel reinforcement**

| | | |
|----|---|--------|
| Fe | % | 99.321 |
| C | % | 0.052 |
| Si | % | 0.030 |
| Mn | % | 0.290 |
| P | % | 0.012 |
| S | % | 0.008 |
| Cr | % | 0.020 |
| Mo | % | 0.020 |
| Ni | % | 0.030 |
| Al | % | 0.098 |
| B | % | 0.001 |
| Co | % | 0.005 |
| Ca | % | 0.030 |
| Nb | % | 0.008 |
| Pb | % | 0.010 |
| Sn | % | 0.010 |
| Ti | % | 0.005 |
| V | % | 0.040 |
| W | % | 0.010 |

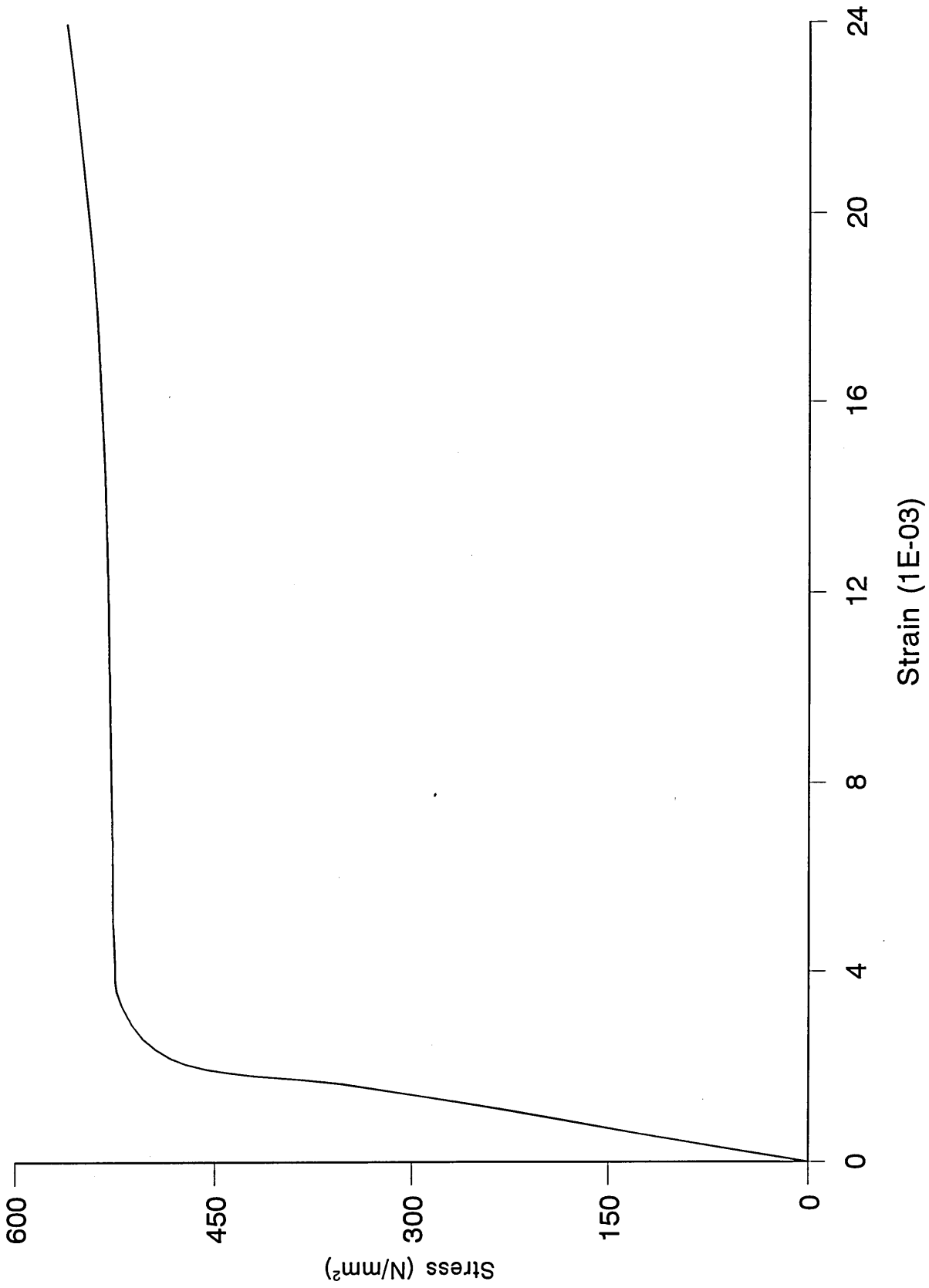


Figure 2.5
Stress-Strain curve for the longitudinal steel reinforcement

CHAPTER 3

PROPERTIES OF REPAIR MATERIALS WHICH INFLUENCE LONG-TERM PERFORMANCE OF CONCRETE STRUCTURES

3.1 INTRODUCTION

Results of an experimental investigation on the basic properties of three generic repair materials which influence long-term performance of repaired concrete structures are given in this chapter. The chapter deals with the typical mechanical properties of repair materials, and compares their performance with plain concrete. Also experimental data on the complete compressive stress-strain characteristics of repair materials and plain concrete are presented. A detailed discussion of the stress-strain behaviour of the materials under uniaxial compression is made on the basis of the experimental data. A comprehensive literature review of relevant topics precedes the results of the experimental investigation.

3.2 LITERATURE REVIEW

3.2.1 Introduction

In recent years, repair, refurbishment and maintenance of existing reinforced concrete structures have become a significant part of the total cost of construction in the U.K. and elsewhere in the world [4]. A patch repair is an effective restoration technique when an element or a whole structure shows signs of distress, especially spalling and delamination [5]. Several studies have been carried out to investigate the long-term durability of repaired concrete members in aggressive environments [6-8]. However, the basic properties of repair materials which influence long-term performance of concrete structures have received little attention.

Different repair methods and generic materials are currently in use to overcome damage in deteriorated structures. The basic mechanical and physical characteristics of such available products and the substrate on which they are used need to be established before assessment can be made and a suitable repair material is chosen, Several researchers [9-12] have highlighted the potential importance of property mismatch between patch repair materials and the substrate concrete.

During service life, incompatibilities in the form of differing strength and modulus of elasticity between repair and substrate concrete can create difficulties, while drying shrinkage of repair materials may reduce long-term structural efficiency by either initial tensile strains induced in the repair or due to cracking at the repair/substrate interface. Also, creep of the repair materials under sustained stress may render the load sharing capacity of the repair less effective with time. Permeability of repair materials influences the rate of ingress of aggressive substances such as chlorides and sulphates into them, and consequently has a major effect on the durability of the repair in the long-term. Table 3.1 shows general requirements of repair materials for efficient structural repair, as suggested by Emberson and Mays [13].

In recent years considerable effort has been directed towards establishing a relationship for both the ascending and descending branches of the stress-strain relationship of concrete. Even though the ascending branch has been fairly well characterised over the past years, there is, however, limited information available on the descending part of the curve due to the various difficulties of testing.

TABLE 3.1 General requirements of patch repair materials for structural compatibility [13]

| Property | Relationship of repair mortar (R) to concrete substrate (C) |
|---|---|
| Strength in compression, tension and flexure | $R \geq C$ |
| Elastic Modulus in compression, tension and flexure | $R \approx C$ |
| Poisson's ratio | Dependent on modulus and type of repair |
| Coefficient of thermal expansion | $R \approx C$ |
| Adhesion in tension and shear | $R \geq C$ |
| Curing and long-term shrinkage | $R \leq C$ |
| Strain capacity | $R \geq C$ |
| Creep | Dependence on whether creep causes desirable or undesirable effects |
| Fatigue performance | $R \geq C$ |

3.2.2 Test methods on permeability

The permeability of concrete can be measured in situ or in the laboratory on samples moved from site. The various test methods available have been classified under these two headings and within these classifications three main processes are identified, absorption and capillary effects, pressure differential permeability, and ionic and gas diffusion. Some of the test methods may involve more than one mechanism.

Concrete is considered to be a porous material, so water can penetrate via the pores into the concrete matrix. The movement of water through the pores of concrete has many important consequences in determining the properties and durability of such concrete. Permeability is a flow property and is defined as the ease with which a fluid will pass through a material under the action of a pressure differential.

Where the performance of structural reinforced concrete is in question, it is primarily that portion of concrete within 50mm of the outside surface that is of interest, since the outer steel bars will almost invariably be located within that region. The main function of the outer layer concrete (or repair material in case of a repaired structure) is to protect the steel from corrosion by maintaining a highly alkaline and impermeable cover to prevent the ingress of air and moisture. If the alkalinity of the cover is reduced through carbonation or if chlorides are present in the cement matrix, rusting of the steel can occur if oxygen and water are available at the corrosion site. So measurement of the permeability should, provide an indication of the durability of the concrete and repaired structure.

3.2.2.1 Initial surface absorption test (ISAT)

The test allows measuring the rate at which water is absorbed into a concrete surface. This is not a test to measure the bulk permeability of concrete. However, the measurement of the properties of the concrete surface is of particular importance for determining durability of the embedded steel, frost resistance and weathering.

BS 1881 part 5 [14] describes the methods by which the ISAT is conducted. It consists of a cap with a minimum surface area of 5000mm² which is sealed to the concrete surface and filled with water as shown in figure 3.1. The rate at which water absorbed into

the concrete under a pressure head of 200mm is measured by movement along a capillary tube attached to the cap at time intervals 10 min, 30 min, 1 hour and 2 hours, as specified by the current standard. The results are normally quoted in ml/m²/s.

ISAT can be used to measure the effect of curing and formwork stripping times on surface permeability. There are, however, some practical difficulties with carrying out this test on site but these are usually overcome with practice. The major difficulties are in achieving a satisfactory water-tight seal between the cap and the concrete surface and in securing the cap in place without the use of clamps. The preferred material for use as a seal is modelling clay, modified to appropriate softness by vaseline. Some new sealing techniques have been carried out to improve the site use capability of the ISAT equipment [15], but no suitable alternative sealing material has been developed.

3.2.2.2 Figg method

This method is intended to provide a measurement of the properties of the surface skin (cover) of concrete in a relatively non-destructive way. The results are quoted as the number of seconds for a given, but arbitrary, air pressure or water volume change. The method is considered to be a permeability method and it is possible that true permeability may be calculated from the results obtained from the Figg method.

3.2.2.3 Original work by Figg

The test is conducted by drilling a hole of 5.5mm diameter and 30mm depth into the concrete [16]. After thorough cleaning, the hole is plugged for part of the depth by polyether foam and then sealed with a catalysed silicone rubber. Measurements of concrete properties using either air or water can then be made with slight variation in the equipment as shown

in figures 3.2 and 3.3 [16].

In case of water , a head of water of 100mm was used as shown in figure 3.2 and the time for the meniscus to travel 50mm is recorded. It is considered that the measurements are relatively insensitive to the actual head of water used, as capillary suction is dominant.

In this test, it should be noted that the aggregate type affects the absolute value of the result.

3.2.2.4 Modified Figg methods

Some workers have used Figg's original method [17], others conducted similar work but with modified equipment or methods. These modified methods by Pihlajavaara and Paroll [18], Richards [19], Building Research Establishment [20], Cather et al [21] and Kasai et al. [22] were derived for a number of reasons. One of these reasons is that the original published paper did not give full details of the equipment used by Figg and, therefore, some other workers have used equipment which was available in their own laboratories.

Comparison of results between the different workers has been difficult to achieve, although the techniques used are similar. This is due to the difference in the total volume of the test system. The measurement is the time for a pressure change in a given volume of air as a result of air movement into the drilled hole. Different times are obtained as the total "dead" volume of the system differs. The volume includes the hole, the manometer and any part of the equipment open to these at the time of test.

3.2.2.5 Pressure induced flow (liquids or gas)

True permeability can be measured by using these tests. Specimens (a core or a cube) should be sealed from all faces except the two opposite parallel faces between which the flow

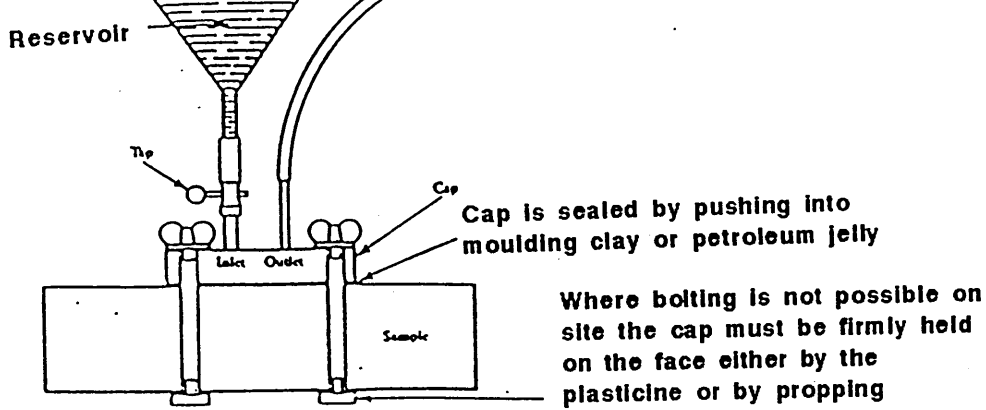
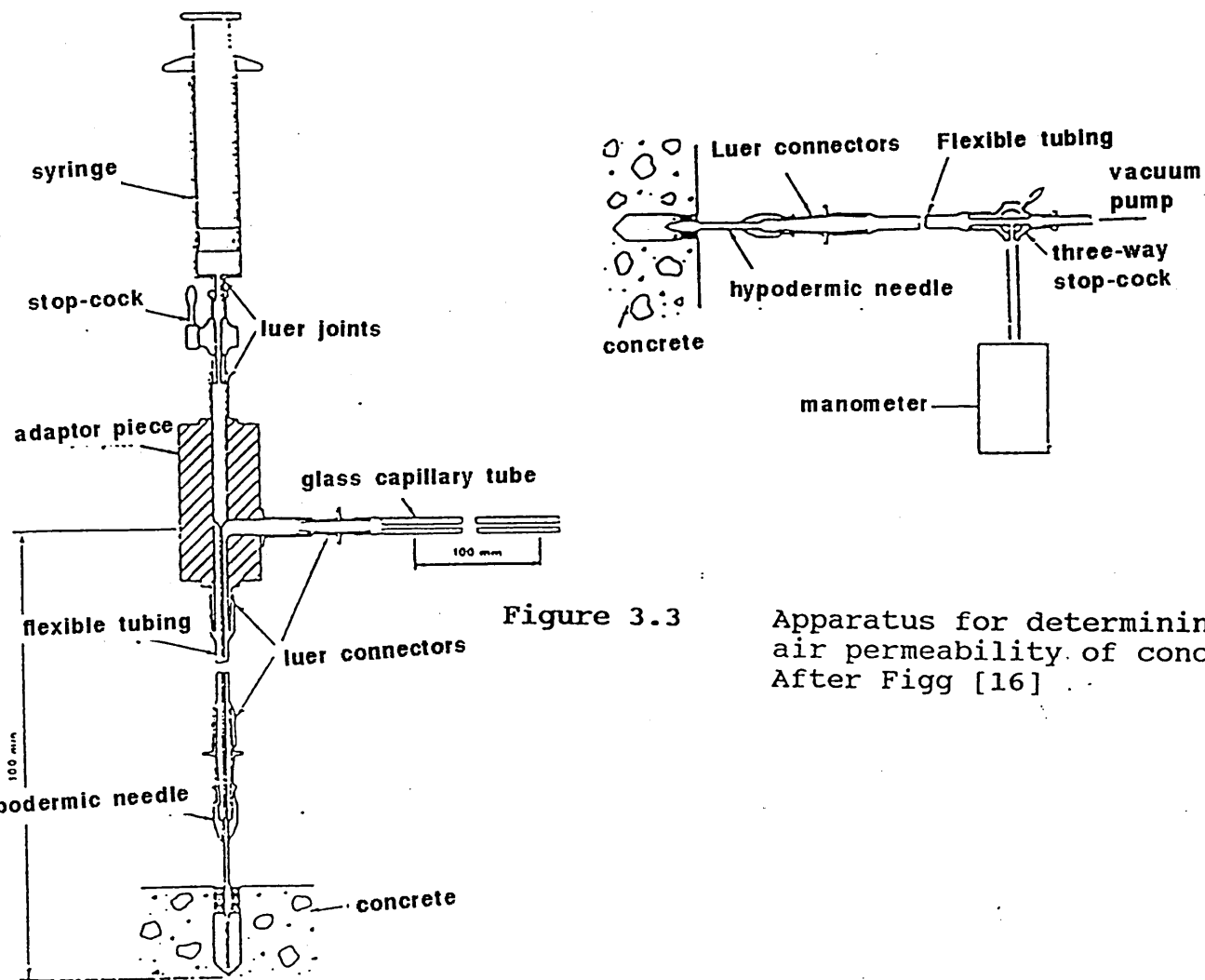


Figure 3.1 Initial surface absorption test equipment, After BSI [14]



Apparatus for determining the air permeability of concrete, After Figg [16]

Figure 3.2 Apparatus for determining the water permeability of concrete, After Figg [16]

of a liquid or a gas can be promoted by an applied pressure. This test can be impractical, especially on low permeability concrete using a liquid because of the length of time taken to conduct each test. In such cases other tests may be performed based on the measurement of the depth of penetration of liquid as observed on subsequent splitting of the test sample.

A typical cell arrangement is shown in figure 3.4 [23]. The test specimens are discs, 50 mm thick and 100 mm diameter, cut from cylinders of 100mm diameter X 200 mm long. The test specimen is cast into a resin sleeve with a similar taper. Flow past the specimen is prevented by an O-ring seal between the other surface of the resin sleeve and the inner face of the brass sleeve.

Specimen preparation involves masking the top and bottom faces of the discs, and placing them in a brass mould identical to that used in the test rig. The annular space is then filled with epoxy resin to form the tapered resin sleeve. After the resin has cured for 24 hours the specimen is removed from the mould and weighed before being installed in the permeability rig. After completion of the test, the specimen is again weighed, to determine the increase in moisture content during test.

The cell is designed to operate at working pressures up to $10.3 \times 10^5 \text{ N/m}^2$ (150 psi). Flow is normally measured by observing the rate of flow of water through a calibrated glass tube. Water pressure is applied from a pneumatic reservoir, the pressure being controlled from a standard gas cylinder and valve. For concretes with very low permeability coefficients (less than 10^{-12} m/s or 10^{-19} m^2) complete penetration of the specimen may take several days or more. In such cases the specimens are removed from the test rig after about two weeks and split, and the permeability coefficient calculated from the measured depth of water penetration.

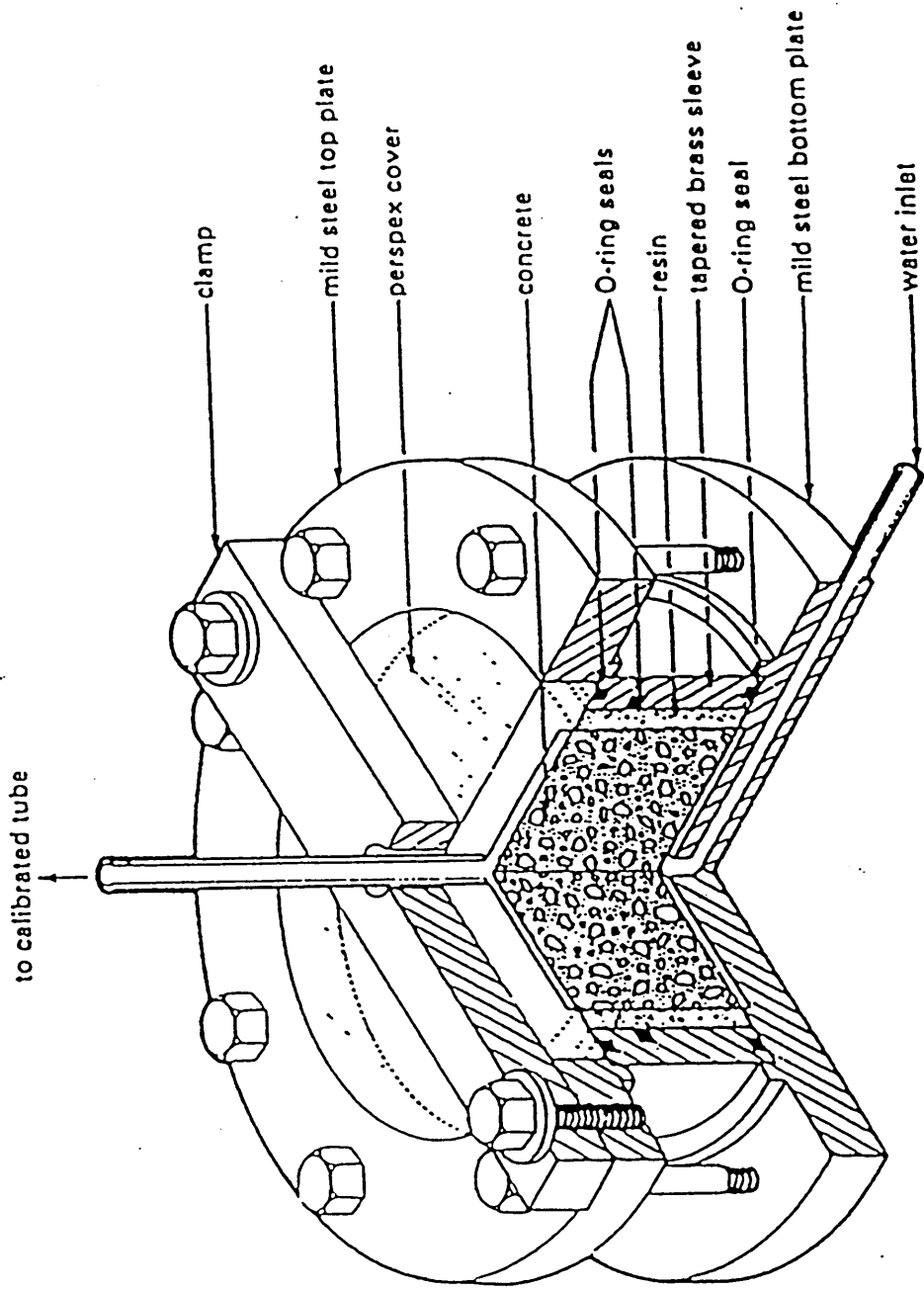


Figure 3.4 Water permeability test rig, after Bamforth [23].

3.2.3 Techniques to represent the complete stress-strain curves

Various techniques have been proposed in an attempt to represent the complete stress-strain curve of concrete. As a result of these techniques various stress-strain functions have been produced as summarised in Table 3.2. Most of these equations, developed by different researchers, are rather complex [24] or require more than one function [25] to cover the full range of concrete strengths commonly obtained with ordinary concrete.

Carrerira and Chu [26] have developed an equation to represent the ascending and descending branches of the concrete, as follows :-

$$\frac{f_c}{f'_c} = \frac{\beta(\epsilon/\epsilon'_c)}{\beta - 1 + (\epsilon/\epsilon'_c)^\beta} \quad (3.1)$$

$$\beta = \frac{1}{1 - \frac{f'_c}{\epsilon'_c E_{it}}} \quad (3.2)$$

Where

- f'_c = the maximum stress usually considered as the concrete compressive strength of cylindrical specimens
- E_{it} = the initial tangent modulus
- ϵ'_c = the strain corresponding to the maximum stress
- ϵ = concrete strain

Other researchers [27-30] have developed techniques to represent the complete stress-strain curves; some of these techniques are very expensive due to the fact that these

techniques require non-standard testing machines which are not available in most laboratories. For example, Barnard [29] used a testing machine which applies strain to a specimen at a constant rate and is stiff enough to allow the load to fall off in a failing specimen.

Kosaka et al [31] proposed a mathematical expression for complete stress-strain curves of concrete under uniaxial compression based on experimental data obtained from reference [32]. The expression requires some information about properties of concrete, curing method and compressive strength of concrete. These mathematical expressions are in agreement with the experimental stress-strain curves for the ascending branch but are in disagreement with the descending part [33].

Desayi and Krishnan [34] have proposed a simple equation for the ascending and descending curves of concrete, thus avoiding the use of two separate equations. The only limitation of their equation is that it does not take into account the effect of the rate of stressing or straining on the stress-strain relationship.

Many other investigators [35-37] have proposed equations for the complete stress-strain curve based on the properties of the ascending part. Wang et al [38,39] have adopted a relatively simple experimental technique to obtain the stress-strain curve including the descending branch up to 0.006 strains. The stress-strain curves were obtained by testing ordinary concrete cylinders. The cylinders were loaded in parallel with a steel tube designed specifically for that purpose. The steel used for the tube was such that it remained linear elastic up to a strain of 0.006. The thickness of the tube was designed in such a way that the sum of the load carried by the cylinder and the tube was always increasing up to the strain of 0.006.

TABLE -3.2 Expression for complete stress-strain curves available in literature

| Authors | Ref. | Stress-Strain equation | Remarks |
|------------------------|-----------|--|---|
| Saenz | 35 | $E_c[1+(3E_0/E-2)(\epsilon/\epsilon_0) + (1-2E_0/E)(\epsilon/\epsilon_0)^2]$ | |
| " | " | $\frac{E\epsilon}{1+(E/E_0-2)(\epsilon/\epsilon_0)+(\epsilon/\epsilon_0)^2}$ | |
| Desay and Krishnan | 34 | $\frac{E\epsilon}{1+(\epsilon/\epsilon_0)^2}$ | Implies $E/E_0 = 2$ |
| Smith and Young | 36, 37 | $E_{\epsilon}^{-\epsilon/\epsilon_0}$ | Implies $E/E_0 = e$ |
| Wang et al | 39 | $\frac{AX+BX^2}{1+CX+DX^2}$ | Implies $y = f/f_0, x = \epsilon/\epsilon_0,$ $E_0 = f_0/\epsilon_0$ A,B,C,D Constant |
| Carreira and Chu | 26 | $f/f'_c = \frac{\beta(\epsilon/\epsilon'_c)}{\beta-1+(\epsilon/\epsilon'_c)\beta}$ | Implies $\beta = \frac{1}{1 - \frac{f'_c}{\epsilon'_c E_{st}}}$ |
| Popovics | 32 | $f = f\epsilon \frac{n-1}{n-1+(\epsilon/\epsilon_0)^n}$ | Considering $\epsilon = \epsilon_0$ $E = \{(f_0/\epsilon_0) / (n/n-1)\}$ |
| Smith G.M Young L.E | 36 | $f = f'_c \epsilon \frac{e^{1-(\epsilon/\epsilon_0)}}{\epsilon_0}$ | f'_c = Comp strength ϵ_0 = concrete strain ϵ = variable strain in compression block e = natural logarithm base = 2.718 |

Table 3.2 : continued

| Authors | Ref | Stress-Strain equation | Remarks |
|---------|-----|---|--|
| Tsai | 41 | $Y = \frac{mX}{1 + (m - \frac{n}{n-1})X + \frac{X^n}{n-1}}$ | $Y = f_c / f'_c$, $X = \epsilon / \epsilon_c$ at $Y = 1$, $m = E_0 / E_c$, n is a factor to control the steepness of descending portion, m is a factor for ascending portion. |

The purpose of using the tube was to absorb any release of energy from the testing machine when concrete load capacity began decreasing after it reached its maximum stress.

Liu et al [40] have developed a general stress-strain relationship for concrete under uniaxial and biaxial compression. The aim of their study was to look closely at concrete prior to failure and to develop a practically useful relationship between stress and strain, then to establish failure criteria for concrete under combined stress. The proposed stress-strain relation was in good agreement with experimental and analytical results.

Tsai [41], along with various other researchers, has recognised that the descending portion of the stress-strain curve is as important as the ascending part especially if the ductility of the concrete member is desired. For that purpose he proposed a new equation to represent the uniaxial compressive stress-strain relationship. The equation generated was based on Popovics [32] then Saenz [35], which consists of two parameters, one for the ascending part and the other to control the ascending part.

Shah et al [42] used a servo-controlled closed-looped testing machine to obtain the complete stress-strain curve. They claimed that the testing specimen interaction plays an important role in determining the post peak behaviour of concrete specimens subjected to uniaxial compression. As a result of their tests they concluded that when the specimens were loaded so as to control the rate of axial strain increase, unstable failure occurred when the

diameter or the length of specimen or the strain rate was increased.

The shape of the stress-strain curve can be related to the failure of concrete under load, which takes place through progressive internal cracking [43]. The curve starts off with a linear portion up to about 30 percent of the ultimate load, and beyond that point, the curve deviates gradually towards the horizontal to reach a certain stress which is called the "critical load". Beyond that the stress-strain curve begins to bend more sharply to the horizontal and then, having reached the peak, it begins to descend and ends up with a descending tail.

Gilkey and Murphy [44] reported that the curvature of stress-strain curve increases with the amount of aggregates in the concrete. They have also reported that variances in water/cement ratio, curing and age may introduce differences in the relative deformations as well as the effect these factors have on strength.

3.2.3.1 Process of fracture of concrete

Concrete may be regarded as a composite material consisting of two phases, namely, aggregates and cement paste. This consideration yields valuable information concerning some physical and mechanical properties of concrete.

The stress-strain diagram of the hardened cement paste, aggregate and concrete, based on reference [45] are shown in figure 3.5. It is evident that the aggregate as well as the hardened cement paste exhibit a brittle behaviour. The stress-strain curve of concrete deviates from linearity even at low loads and has a descending slope after ultimate load [30,38]. It was recognised at early stages that the marked difference between the deformation of concrete and that of its constituents is mostly due to crack formation [30,38]. Normally when specimens are loaded under compression, the cracks that may occur are vertical cracks due

to tensile stresses induced in the matrix perpendicular to the direction of applied compressive stress and inclined cracks which occur at the coarse aggregate interface due to the relative movement between aggregate and matrix. The various stages of crack formation as related to the applied compressive stress and the process of fracture are discussed in the following section.

3.2.3.2 Crack initiation

In materials like concrete, internal micro cracks are present even before the application of any load due to settlement of fresh concrete [46,47]. This stage of micro-cracking is referred to as the "initial condition" [48].

The micro-cracks at the "initial condition" are concentrated at the interface of aggregate particles and cement paste [45,46 and 49,50]. These micro cracks constitute a major proportion of the crack phase in a concrete specimen at each stage of loading until failure occurs [51,52].

It is generally known that when concrete is subjected to a uniaxial compressive loading, internal micro cracking will occur from a certain stress level. This stage of fracture is called "stable crack initiation" which occurs usually at low stress levels approximately up to 40 percent of the ultimate compressive strength of concrete [51], as shown in figure 3.6. This stable crack initiation continues to a stress level beyond which a stage of stable crack propagation commences in the material [52] as shown in figure 3.6. Further considerable micro cracking occurs at a stress level during the transition phase between the state crack initiation and stable crack propagation zones.

Several researchers [52,53] have pointed out that at this stress level, which is about 40-55 percent of the ultimate strength of concrete, its poisson's ratio begins to increase. This point known as the crack "initiation stress" [52,54] which is indicated in figure 3.6.

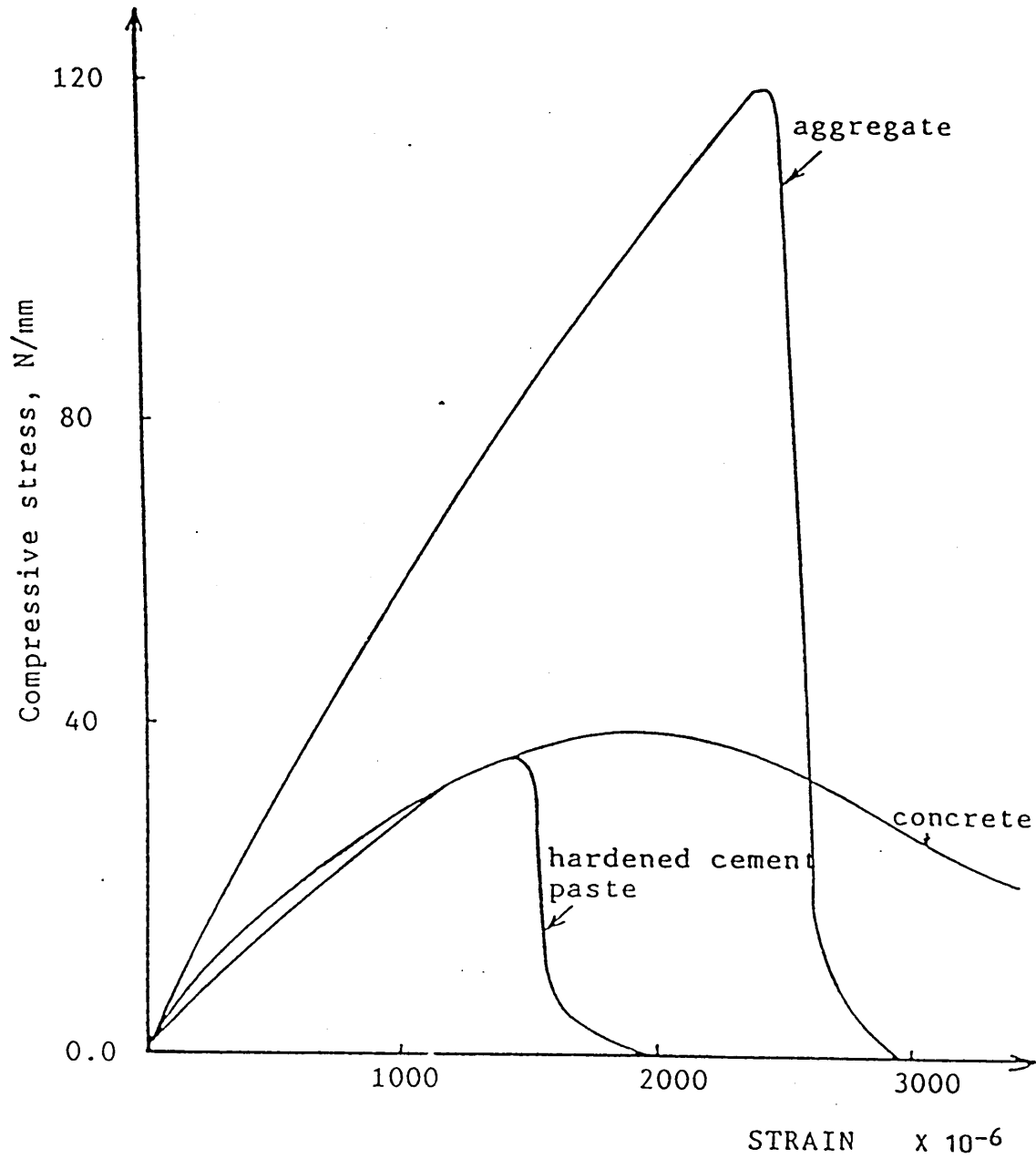


Figure 3.5 Stress-strain curves of aggregate, hardened cement paste and concrete [45].

Newman K, and Newman B. [49] have also observed an inflection point on the stress-volumetric strain curve at 50 to 60 percent of the ultimate strength as shown in figure 3.6, called as "discontinuity point". Again from the figure, an unstable propagation zone follows the stable propagation stage. This point between the two zones is called the "critical stress" level [55]. The critical stress level occurs at 70 to 90 percent of the ultimate compressive strength [49,50] and is reflected by the dilation of the matrix structure. Newman et al [49] concluded that at this point there is a reversal of the volumetric strain on the stress-strain curves.

Unstable crack propagation takes place beyond the critical stress due to excessive development of internal microcracks in the concrete. At this stage the concrete becomes unstable and the sudden release of strain energy makes cracking self-propagating until complete failure takes place. The presence of aggregate and bond cracks at the aggregate-matrix interface, impact post-cracking ductility and hence enable concrete to sustain deformation beyond the maximum stress. This gives rise to the descending branch of the stress-strain curve as shown in figure 3.6.

3.3 EXPERIMENTAL PROGRAMME

In this investigation experimental work was carried out in order to generate information on the typical properties and complete stress-strain curve of concrete and the three different repair materials under uniaxial compression.

3.3.1 Materials and details of mixes

Three commercially available generic repair materials which are labelled A, B and C were used in this study, together with a plain concrete mix of similar strength, which was used to provide control specimens for comparison. The repair materials A, B and C are

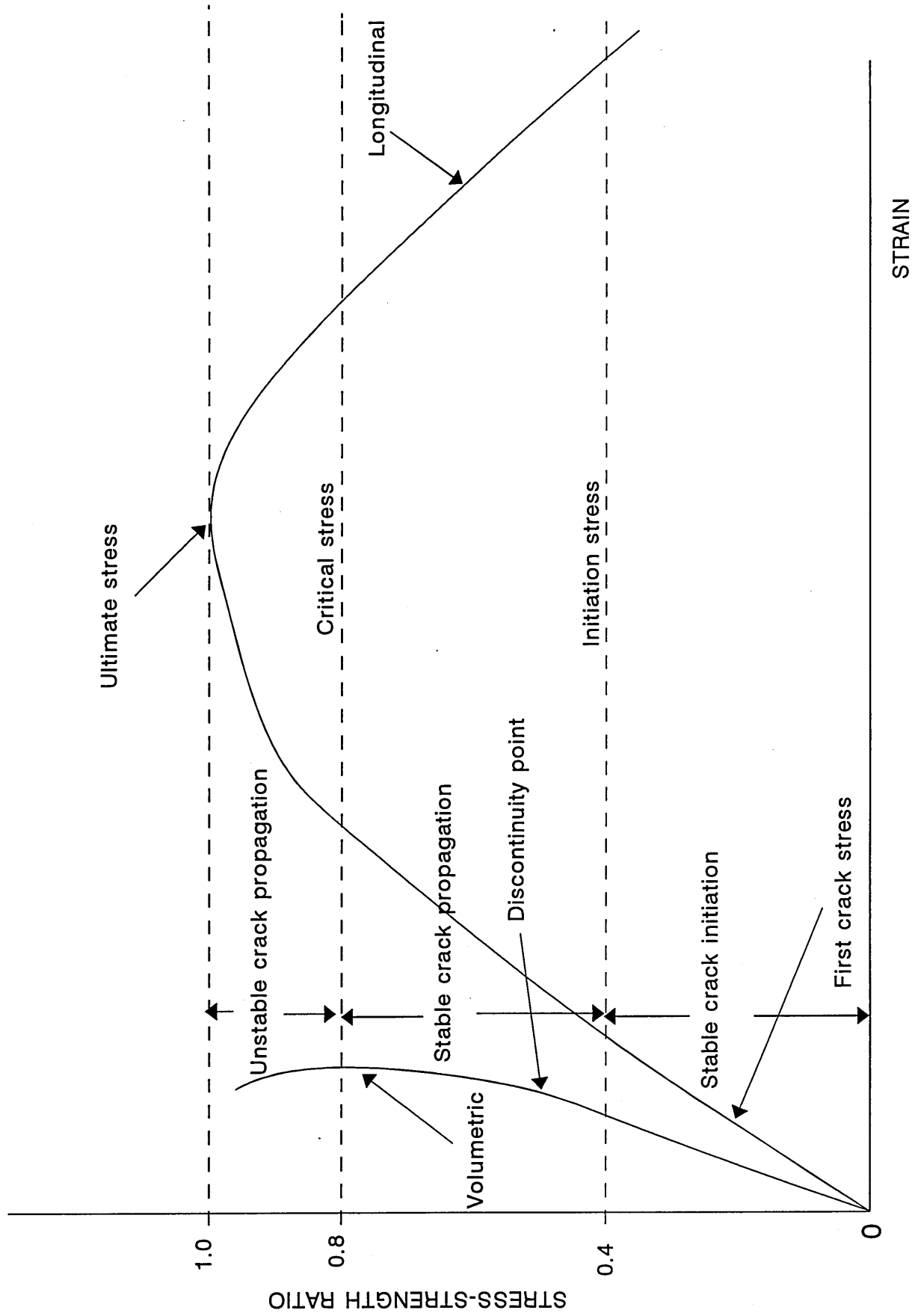


Figure 3.6 The stages of cracking in concrete under compression.

supplied as single component systems by their manufactures, ready for on-site mixing and use and requiring only the addition of clean water. Details of the repair materials are as follows :-

Material A is a blend of portland cement, graded aggregates of maximum size 5mm and additives which impart controlled expansion in both the plastic and hardened state whilst minimising water demand. The material is supplied by FOSROC (UK) Ltd. This high performance, non-shrinkable concrete is used for the reinstatement of concrete by partial or total replacement. The material conforms with the requirements of the Department of Transport Standard (BD 27/86, Clause 4) " The repair of concrete Highway Structures ", and has also been formulated to comply with the requirements of the DTp specification for Highway works, Clause 1704.6 control of alkali-silica reaction.

Water addition:- 4 litres per 30 kg pack to give typical density of the fresh material 2069 kg/m³.

Material B is a mineral cementitious material with no additives, supplied by JAHN (Netherlands). It is relatively porous to allow leaching of salts to continue from contaminated concrete after its repair.

Water addition:- 3 litres per 20 kg pack to give typical density of the fresh material 1575 kg/m³.

Material C is supplied by FLEXCRETE (UK) Ltd. It is a single component cementitious mortar which incorporates most advanced cement chemistry, microsilica, fibre and styrene acrylic copolymer technology. This results in a rapid hardening, low density, high strength

mortar with enhanced polymer properties. The thixotropic nature of the product enhances easy trowel application in structural repair of voids, rendering and in reprofiling of both vertical and horizontal surfaces.

For normal application use from 2.5 to 3.0 litres of clean water per 20 kg pack depending upon desired consistency and it gives fresh density ranges between 1650 and 1750 kg/m³.

Plain concrete mix used for comparison with the repair materials had constituents of Ordinary Portland cement, fine aggregate conforming to Zone 'M' of BS 882, and coarse aggregates of maximum size 10 mm. The mix proportions (by weight) were 1 : 2.24 : 3.22, with a water/cement ratio of 0.56. The cement content was 343 kg/m³.

The grading curves for the generic repair materials are shown in figure 3.7. It is quite apparent from figure 3.7 that, material A is much coarser than materials B and C. For example, in material A there is a significant amount of aggregates of particle size 1.18mm or greater, whereas in the case of materials B and C all particle sizes are much less than 1.18mm. Also, the grading of materials B and C are quite similar. In the case of the concrete mix, grading is much coarser, comprising of medium zone sand and 10mm maximum size coarse aggregate.

3.3.2 Casting, curing and testing

Concrete mixing was carried out in a pan type mixer. Mixing of each repair material was carried out according to the manufacturer's literature.

3.3.2.1 Strength tests

Eight 100mm cube specimens and two prism specimens of dimensions 100 x 100 x 500mm were prepared in cast iron moulds for each of the three repair materials and for plain

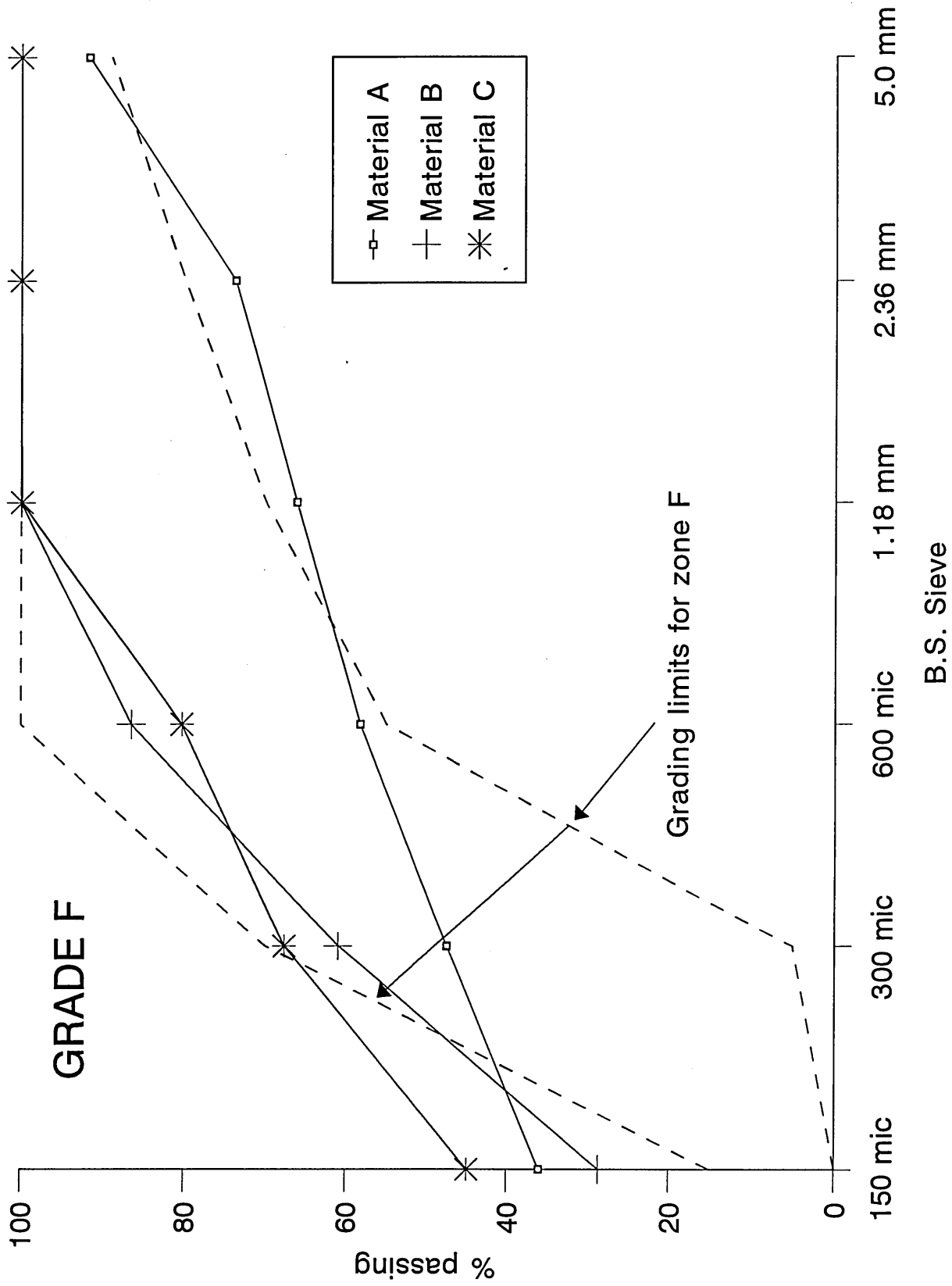


Figure 3.7 Grading curves for repair materials

concrete. The specimens were demoulded twenty four hours after casting and subsequently cured in water at 20°C by immersion in a plastic tank filled with water, which was kept under controlled temperature conditions in the laboratory. The compressive strength tests were carried out at 3, 7, 14 and 28 days in accordance with BS 1881 : part 116 [56]. The flexural strength of prism specimens was determined under four point bending in accordance with BS 1881 : part 118 [57], at the age of 28 days.

3.3.2.2 Elastic modulus test

Two 100 x 100 x 500mm prism specimens of each mix were tested to determine the static modulus of elasticity at 28 days. Specimens were cured in water at 20°C. Strain readings were taken at regular load increments on opposite longitudinal faces of a prism. A demec extensometer of gauge length 200mm was used for the purpose.

3.3.2.3 Coefficient of water permeability

Five 100mm diameter X 200mm high cylinder specimens were cast for each repair material. The specimens were demoulded after 24 hours of casting and were left to cure in a water tank at 20°C until the day of the permeability test. The specimens were taken out of the water tank after 28 days, and each cylinder was segmented into three slices. The slices were cut by a masonry saw, parallel to the top cast face of the cylinder. A circular disc of diameter 100mm and thickness 40mm \pm 1mm was obtained from the middle portion of a cylinder to provide a test specimen for the permeability apparatus. The remaining parts of the cylinders were discarded.

A "liquid Permeameter" apparatus was used to determine the coefficient of permeability of water through the disc specimen which was held in a hydrostatic cell within the permeameter. A constant flow of water was established through the sample during the test and the pressure across the sample and flow rate were monitored. A knowledge of the

viscosity of the fluid used (water) and the dimensions of the specimen was used to determine the coefficient of permeability using Darcy's law [58]. The following equation was used to calculate the coefficient of water permeability [58] :-

$$K_{LD} = \frac{Qx}{Ah} \quad (3.3)$$

Where,

| | | |
|----------|---|---|
| K_{LD} | = | coefficient of water permeability (m/s) |
| Q | = | volume flow rate (m ³ /s) |
| x | = | specimen thickness in the direction of flow (m) |
| A | = | area of flow (m ²) |
| h | = | head of water (m) |

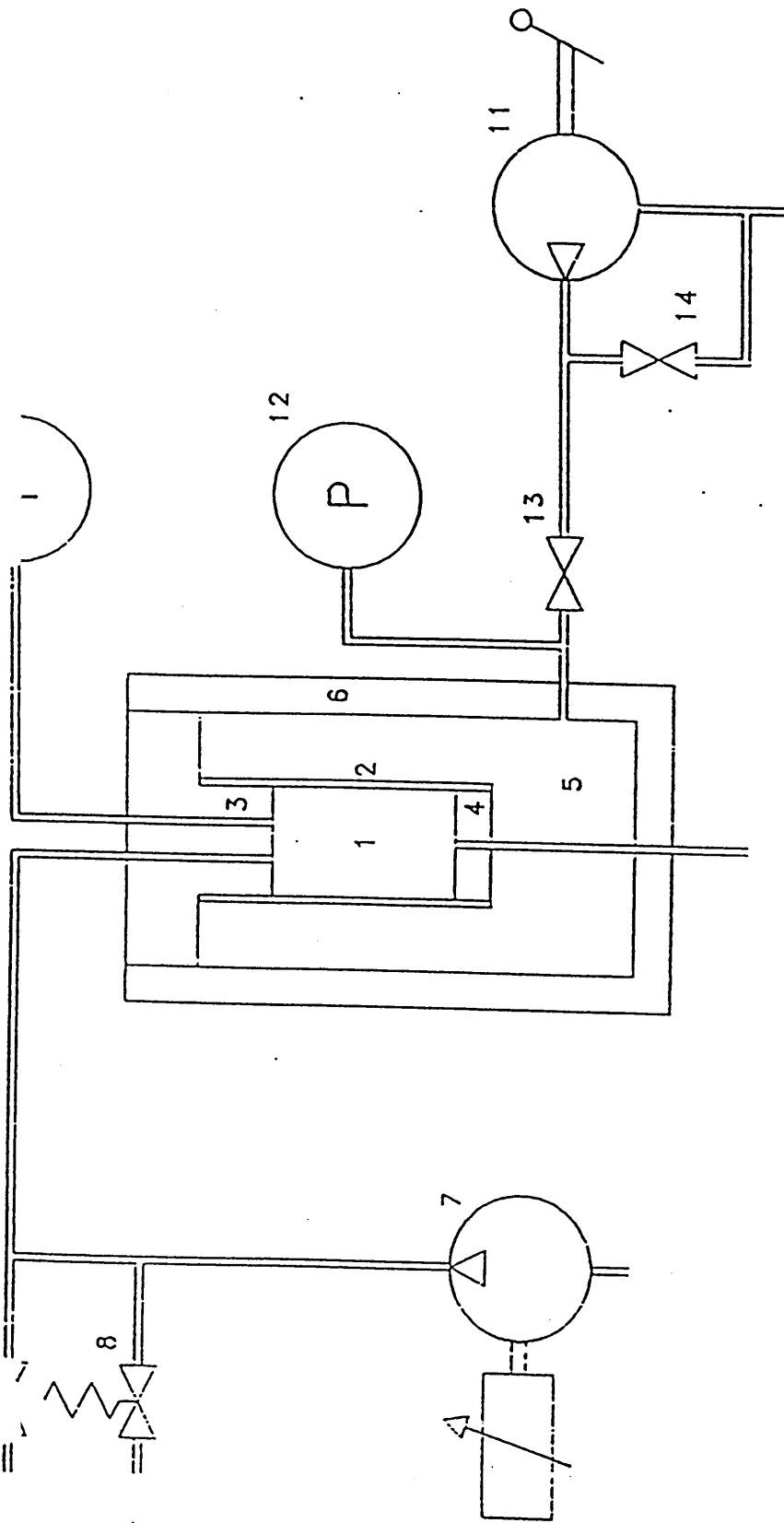
A constant flow of fluid is established through the sample, which is held in hydrostatic type cell, and the pressure across the sample is known (cross-section and length), as well as the viscosity of the fluid used, Darcy's law will provide the permeability.

General layout of the instrument is shown in figure 3.8. All system components are mounted in or on a rugged steel housing. The system comprises (as shown in figure 3.8) the sample holder, the confining pressure sensor and readout unit. The reservoir for the hydraulic fluid used in confining pressure system is placed internally, but the reservoirs for sample flooding fluid and piston rinsing (metering pump) will be external.

The sample holder is a hydrostatic cell, manufactured from stainless steel and rated for use with pressures up to 100 Bar. The cell consists of a cylindrical shell and two endplates. The end plates are held in position with a threaded retained ring. The top plate is also the fixed platen for the sample, and has fluid distribution rings machined on its inside. The sample holder is fitted with two sets of platens: one for samples with a diameter of 100mm, and one for samples with a diameter of 42mm. The maximum sample length accepted is 200mm. To enable easy loading and unloading of samples, the top plate connections are fitted with Quick-Connects.

The sample is held in its position, and effectively sealed along its circumference, by applying a confining pressure on the outside of the core sleeve. The confining pressure can be read from a gauge which is always connected to the sample holder. The cell is filled and pressurized with a handpump, which is separated from the cell by a needle valve marked "LOAD/HOLD CP". When emptying the cell the valve marked "RELEASE CP" connects the cell with the hydraulic fluid reservoir. To prevent too large pressure build-up, a pressure relief valve has been mounted in the circuit, which cracks at 50 bar approximately. A needle valve is also fitted to release pressure when the test is stopped. Both the needle valve and the pressure relief valve vent to a 1/4" fitting on the left hand side of the instrument, to allow connection to a drain or waste reservoir.

Pressure is measured directly at the core face, through a separate port in the fixed platen. The pressure sensor has a range of 0-35 Bar gauge and a digital readout is fitted with a buffered analogue output of 2 V full scale, which can be connected to any computer with a suitable A/D interface card. This tests were carried out at the University of Aberdeen.



- 1 Sample
- 2 Rubber sleeve
- 3 Fixed platen with flow and pressure parts
- 4 Floating platen with drainage part
- 5 Hydraulic oil
- 6 Pressure vessel
- 7 Constant flow pump

- 8 Safety valve
- 9 Pressure unloading valve
- 10 Pressure indicator
- 11 Handpump for application of confining pressure
- 12 Confining pressure gauge
- 13 Confining pressure retaining valve
- 14 Pump unloading valve

Figure 3.8 General layout of the Permeability Instrument

3.3.2.4 Stress-strain curve

From each mix three 75 X 75 X 300mm prism specimens and twelve cubes of 100 X 100 X 100mm were cast. The prism and cube specimens were demoulded after one day of casting and were left to cure in a water tank, under uncontrolled conditions of laboratory temperature until the day of test. The specimens were taken from the water tank after 28 days and left to dry in air, under uncontrolled conditions of laboratory temperature and humidity. That was in order to attach electrical resistance strain gauges to the prismatic specimens.

Little information is available on the complete stress-strain curve of generic repair materials. The reason for this lack of information is due to the difficulties associated with testing machines and measuring the descending portions of the curve. Most of the testing machines used by researchers are standard compression machines. Unfortunately these machines are constant stress machines rather than constant strain machines, which are controlled by a load rate instead of a constant strain rate. In addition the rigidity of the machines is limited so that sudden failure of specimens occurs soon after reaching the peak stress due to the sudden release of the energy stored in the machine. Many research workers [29,59-62] have developed different techniques to tackle this problem and to compensate for sudden energy release by acquiring new machines or modifications to the existing ones to get the post-peak behaviour of concrete. Unfortunately, most of these new techniques tend to be very costly.

In this research programme a simple method has been developed to obtain the descending portion of the stress-strain curve up to a strain of 0.007, as shown in figure 3.9. This technique is similar to those used by other researchers [37,59] and was developed in a previous research project [33].

Concrete and repair material prisms of 75 X 75 X 300mm dimensions were loaded in parallel with the steel tube by means of a constant stress loading type of testing machine as illustrated in plate 3.1. The steel tube was of thickness 3.5mm and had been designed in such a way that the load kept on increasing even when the concrete had failed inside the tube. The steel tube was made of mild steel conforming to BS 4360-43A, which was heat treated to behave elastically up to strains of 0.007.

During a test, to ensure the specimen and the tube were in direct contact with the loading platen simultaneously, brass shims were used as capping (figure 3.9), the thickness of the brass shims was varied for different specimens to between 0.002 to 0.2mm. The strain readings from the tube were taken by means of electrical resistance strain gauges of 30mm gauge length which were attached longitudinally at mid-height of the cylinder on two opposite positions as shown in plate 3.1 and figure 3.9. Electrical resistance strain gauges were also attached at the centre of two opposite faces of the test specimens as shown in figure 3.10. The gauge length was 30mm and the gauges were attached both longitudinally and laterally in order to measure strains in these directions. These strain gauges were connected to two strain meters, one for the tube strain readings and the other for test specimen readings. The strains recorded were in micro-strains (Plate 3.1).

The strains recorded from the two opposite faces of the tube were averaged. The strain readings were recorded at regular increments of load (approximately 50 kN) right up to the end of the test. Concrete and repair material strain measurements were stopped when the specimens started cracking and strain became erratic whereas the strain readings from the tube were recorded right up to the end of the test. The strains obtained from the opposite

locations were combined to obtain average values. From these results, longitudinal strains were plotted against applied stress as described in section 3.4. Volumetric strains were also calculated from these data using the following relationship :-

$$\epsilon_{vol} = \epsilon_{long} - 2\epsilon_{lat} \quad (3.4)$$

Where:-

- ϵ_{vol} = the volumetric strain
- ϵ_{long} = the strain measured in the longitudinal direction
- ϵ_{lat} = the strain measured in the lateral direction.

The cubes representative of each stress-strain curve test specimen were tested on the same day for the cube strength.

3.4 RESULTS AND DISCUSSION

3.4.1 Strength and elastic modulus

Table 3.3 gives the results of the strength (compressive and flexural) and elastic modulus tests on each repair material and figure 3.11 represents the development of compressive strength with age, for each repair material. Figure 3.11 shows that the high-performance, non shrinkable repair material A, develops strength rapidly and reaches a high compressive strength at 28 days age. Similarly the elastic modulus and modulus of rupture of material A is much greater than the other materials (Table 3.3). Repair materials B and C and the plain concrete mix have similar elastic moduli and flexural strengths. Their compressive strength is in the range of 33 - 44 N/mm² (Table 3.3).

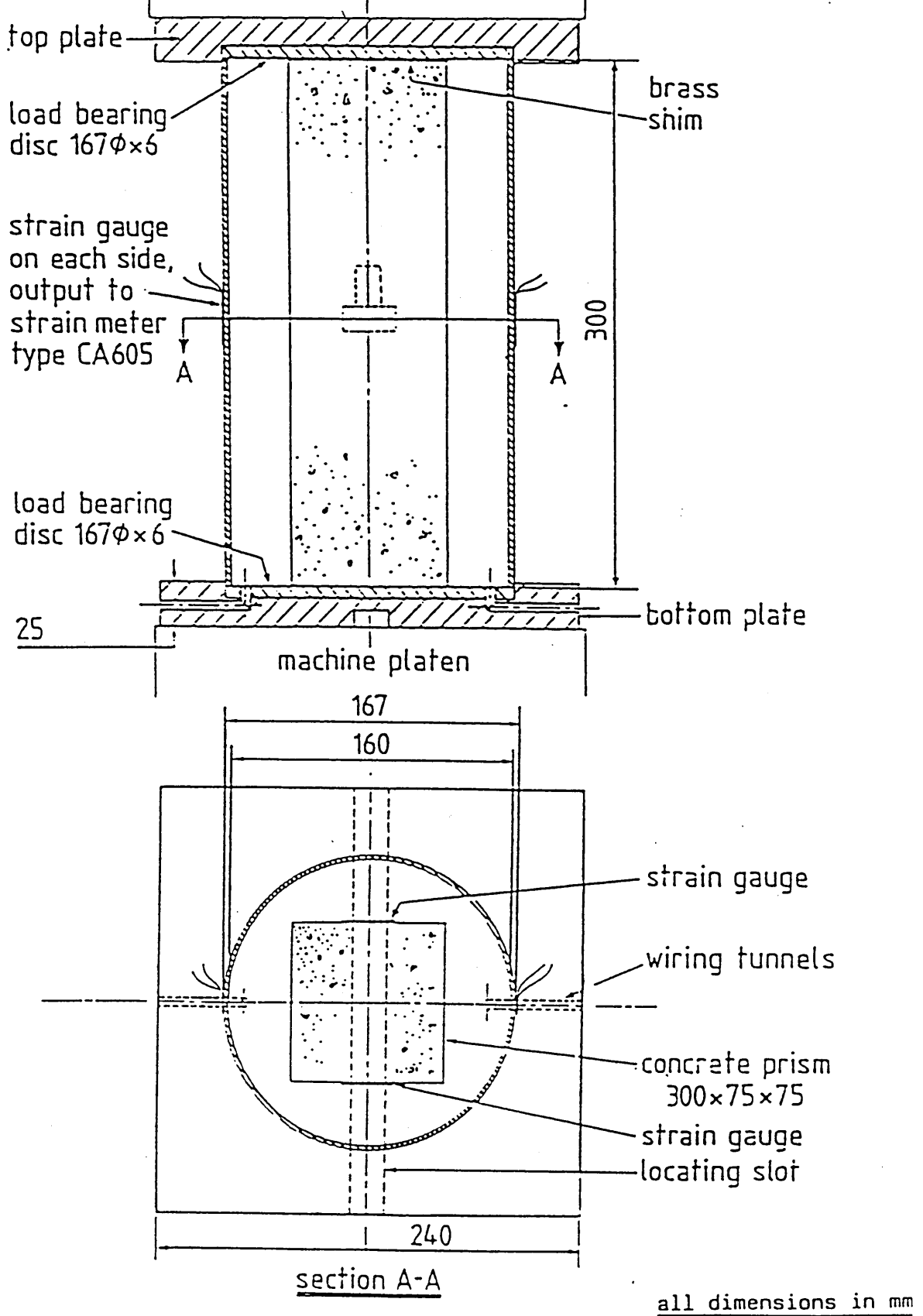


Figure 3.9 Test Arrangement for Stress-strain Curves

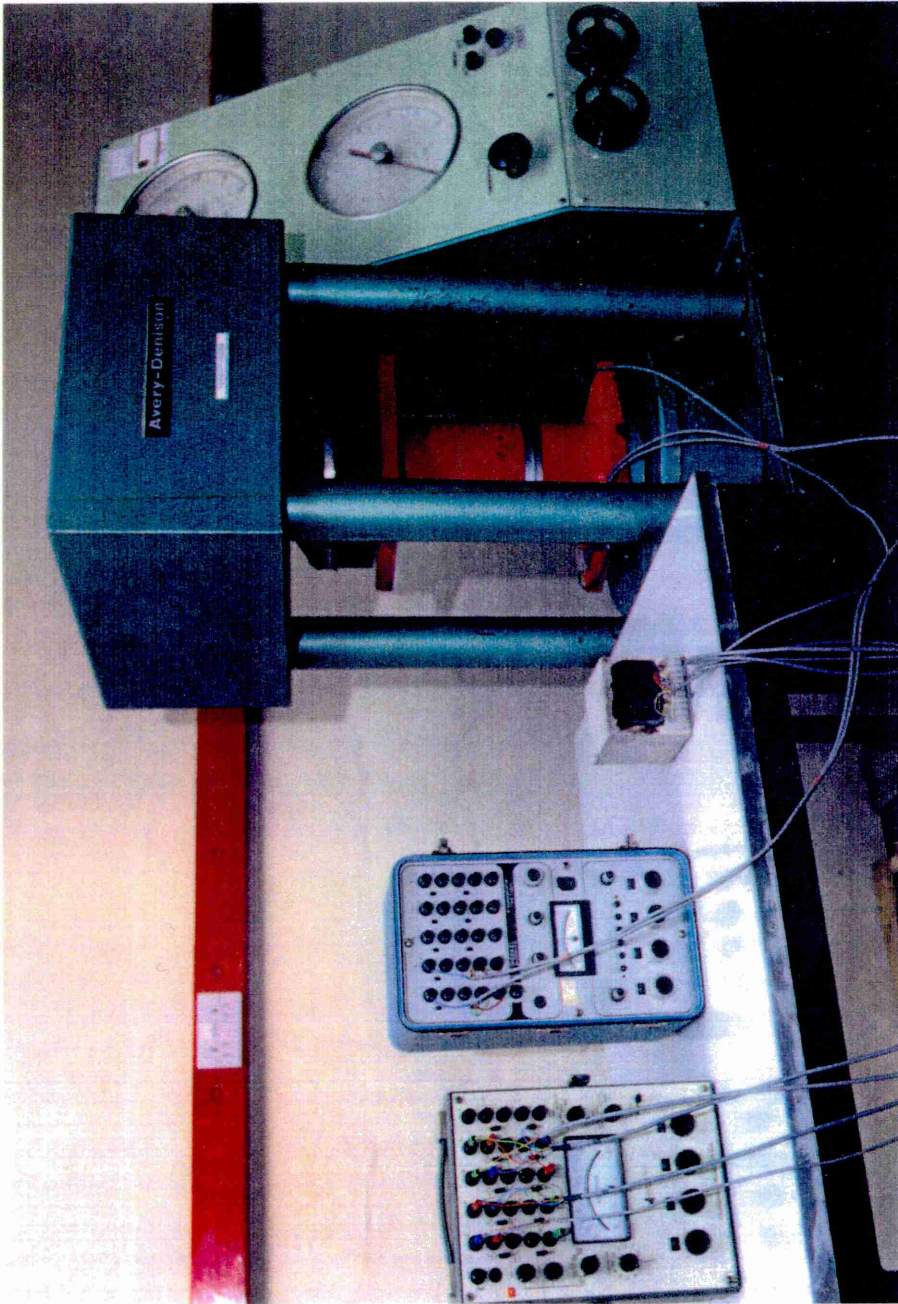


Plate 3.1 Test setup.

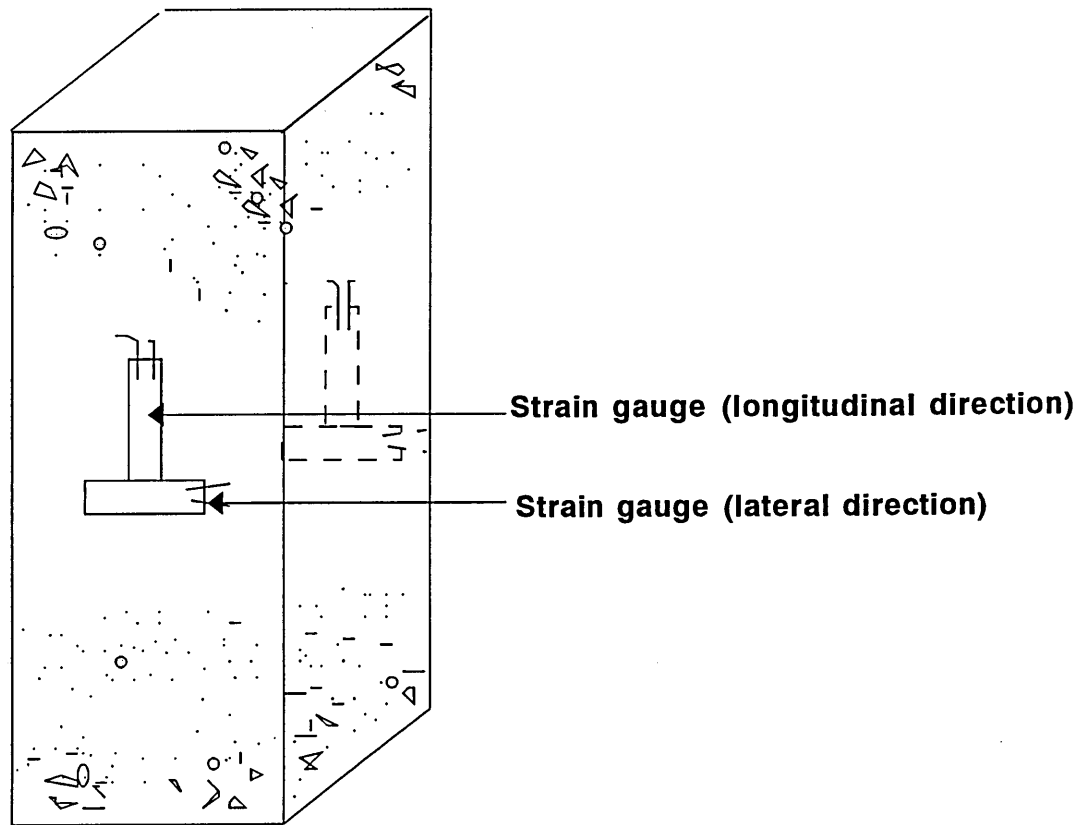


Figure 3.10 Strain gauge locations on the two opposite faces of concrete and repair materials specimens

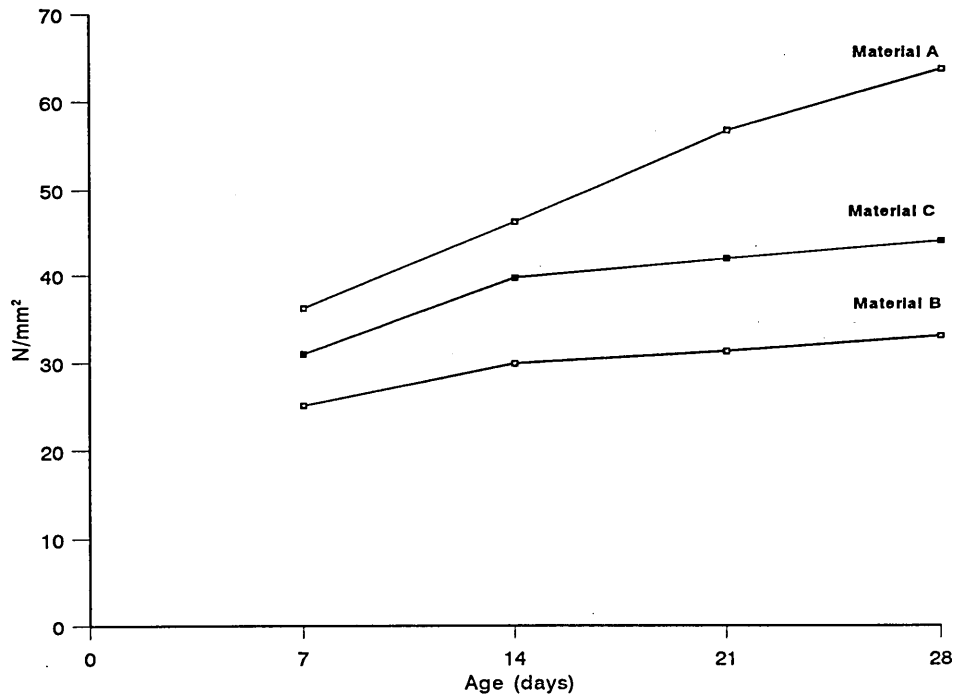


Figure 3.11 Development of Compressive Strength.

TABLE - 3.3 Some Typical Properties of repair materials.

| Material | Compressive strength (N/mm ²) | | Flexural Strength (N/mm ²) (at 28 days) | Elastic Modulus (KN/mm ²) (at 28 days) |
|----------|---|-------|---|--|
| | Age | | | |
| A | - 3 days | 36.20 | 7.74 | 31.98 |
| | - 7 days | 46.30 | | |
| | - 14 days | 56.75 | | |
| | - 28 days | 63.70 | | |
| B | - 3 days | 25.10 | 4.21 | 19.10 |
| | - 7 days | 29.90 | | |
| | - 14 days | 31.30 | | |
| | - 28 days | 33.00 | | |
| C | - 3 days | 31.00 | 3.69 | 18.30 |
| | - 7 days | 39.70 | | |
| | - 14 days | 41.95 | | |
| | - 28 days | 44.00 | | |
| Concrete | -28 days | 40.60 | 4.40 | 19.81 |

3.4.2 Water permeability

The water permeability results for each of the three repair materials and concrete are given in Table 3.4. All the permeability coefficients were derived from flow measurements using Darcy's equation (3.3). Measured values of flow rate and the calculated permeability in terms of Darcy coefficient K_{LD} in m/s are given.

The performance of the four materials tested varied significantly, the highest water permeability coefficients being recorded for the porous mineral based material B. For example, mean value of permeability coefficient K_{LD} (m/s) for materials A and C are 2.53×10^{-13} and 1.33×10^{-13} respectively, while for material B it is 5.62×10^{-11} , which shows more than an order of magnitude increase in permeability relative to the other materials.

The data in Table 3.4 show that the plain concrete repair mix has similar permeability coefficients as the repair materials A and C while its strength is similar to mix C and lower than mix A (Table 3.4). This indicates that the special formulations used for repair materials A and C do not significantly improve their impermeability.

3.4.3 Stress-strain curves

Tests were conducted on prisms of dimensions 75 X 75 X 300mm. Details of the test procedure are given in section 3.3.2. During testing, the strains were measured in longitudinal and lateral direction on the two opposite faces of the prism (figure 3.10) at each load increment. The strain readings taken from two opposite sides were compared and

TABLE - 3.4

WATER PERMEABILITY RESULTS

| MIX | SPE No. | FLOW RATE (ml/min) | | WATER HEAD (h) | | PERMEABILITY COEFFICIENT* |
|-----|------------|-----------------------|----------------------|-------------------|---------------|------------------------------|
| | | From Machine | Measured (Actual) | (m) | Time (min) | K_{LD} (m/s) |
| A | 1 | 0.001 | 0.0018 | 656.61 | 815 | 2.33×10^{-13} |
| | 2 | 0.001 | 0.0009 | 833.18 | 1440 | 0.92×10^{-13} |
| | 3 | 0.001 | 0.0024 | 534.91 | 560 | 3.81×10^{-13} |
| | 4 | 0.001 | 0.0021 | 586.78 | 1430 | 3.04×10^{-13} |
| B | 1 | 0.050 | 0.092 | 144.86 | 710 | 5.39×10^{-11} |
| | 2 | 0.050 | 0.046 | 68.05 | 810 | 5.74×10^{-11} |
| | 3 | 0.050 | 0.046 | 68.05 | 695 | 5.74×10^{-11} |
| C | 1 | 0.001 | 0.0011 | 651.62 | 445 | 1.43×10^{-13} |
| | 2 | 0.001 | 0.0007 | 707.48 | 590 | 0.84×10^{-13} |
| | 3 | 0.001 | 0.0013 | 637.66 | 960 | 1.73×10^{-13} |
| C | 1 | 0.005 | 0.0044 | 714.47 | 1545 | 5.23×10^{-13} |
| O | 2 | 0.005 | 0.0031 | 520.94 | 795 | 5.05×10^{-13} |
| N | 3 | 0.005 | 0.0055 | 265.57 | 855 | 17.5×10^{-13} |
| C. | 4 | 0.005 | 0.0060 | 331.41 | 1555 | 15.4×10^{-13} |

(* Calculated from Equation (3.3), by using actual Flow rate)

averaged. The longitudinal steel tube strains on two opposite sides were also taken to establish the full behaviour of the concrete specimen inside the tube. All strains were measured by means of electrical resistance gauges of gauge length 30mm as shown in figure 3.9 and plate 3.1.

Figure 3.12 shows a typical load versus the averaged recorded strains graph taken from the repair material A and the steel tube in the longitudinal direction. It is clear from figure 3.12, that the repair material (A) specimen and the tube are not both in direct contact with the platen of the testing machine at early stages of loading. This is shown by the difference in the two graphs (a) and (b) of figure 3.12 which are not matching each other and, therefore, indicate different strains in material A and the steel tube. Therefore, due to this difference in the two averaged longitudinal strain readings (from tube and repair material A), the reading considered for the stress-strain curves of repair material A are the average longitudinal strains recorded directly from the material A specimen at early stages of loading. After a certain applied load both the test specimen and the tube come in complete contact with the platen and start to deform together with load increments. This occurs at 375kN load in figure 3.12 when the initial slope of the load-strain graphs of both repair material A and the steel tube changes. From this point onward, each further increment of loading leads to an equal increase in strain of both the test specimen and the steel tube. Hence monitoring the steel tube strains and from the knowledge of the total applied load, the repair material A stress-strain behaviour can be evaluated. At high loads and during the descending branch of the stress-strain curve, therefore, strains of repair material (A) were determined from the strain plot of the tube such as the one given in figure 3.12, as follows :-

In figure 3.12, the strain in repair material (A) at 375kN load is

$$\epsilon_{R375} = 1460.5 \text{ microstrain}$$

The corresponding strain in the tube, $\epsilon_{s375} = 89$ microstrain.

The low value of the tube strain indicates that the repair material specimen was slightly longer than the tube and came in contact with the platen first. (This was purposely ensured during the tests.)

The difference in strain = $\epsilon_{R375} - \epsilon_{s375} = 1371.5$ microstrain.

Therefore, at any general load greater than 375 kN, say at 900 kN, the strain in the repair specimen will be :-

$$\epsilon_R = (\epsilon_{tubc} + 1371.5) \text{ microstrain.}$$

At 900 kN, this will be:-

$$\epsilon_{R900} = 2328 + 1371.5 = 3699.5 \text{ microstrain.}$$

The load taken by the steel tube is calculated from the relationship :-

$$P_s = A.\epsilon.E \quad (3.5)$$

Where :-

- P_s = the load taken by the steel tube
- ϵ = the strain measured in the longitudinal direction on steel tube
- A = the cross-sectional area of the tube
- E = the Young's Modulus which is calculated from the calibration graph of the tube before the test (figure 3.12)

Hence,

$$P_{\text{tot}} = P_R + P_S \quad (3.6)$$

Where:-

- P_{tot} = total load carried by test specimen and tube
i.e machine applied load.
- P_R = the load taken by repair material test specimen alone.

Therefore, the stress carried by repair material specimen is evaluated as :-

$$\sigma_R = \frac{P_{\text{tot}} - P_S}{A_{\text{repair}}} \quad (3.7)$$

Where:-

- σ_R = stress in test specimen.
- A_{repair} = the cross-sectional area of specimen tested.

Hence stress-strain curves are obtained by this technique.

Typical examples are shown in figures 3.13 to 3.15 for three different repair material specimens and in figure 3.16 for control concrete specimen. Each stress-strain curve presented in this chapter is an average of three prism specimens.

Together with the longitudinal strain, the lateral strains in specimens were monitored and the lateral stress-strain behaviour is plotted in figures 3.13 to 3.16. The experimental data for repair materials and the concrete are recorded in Table 3.5. These include strain

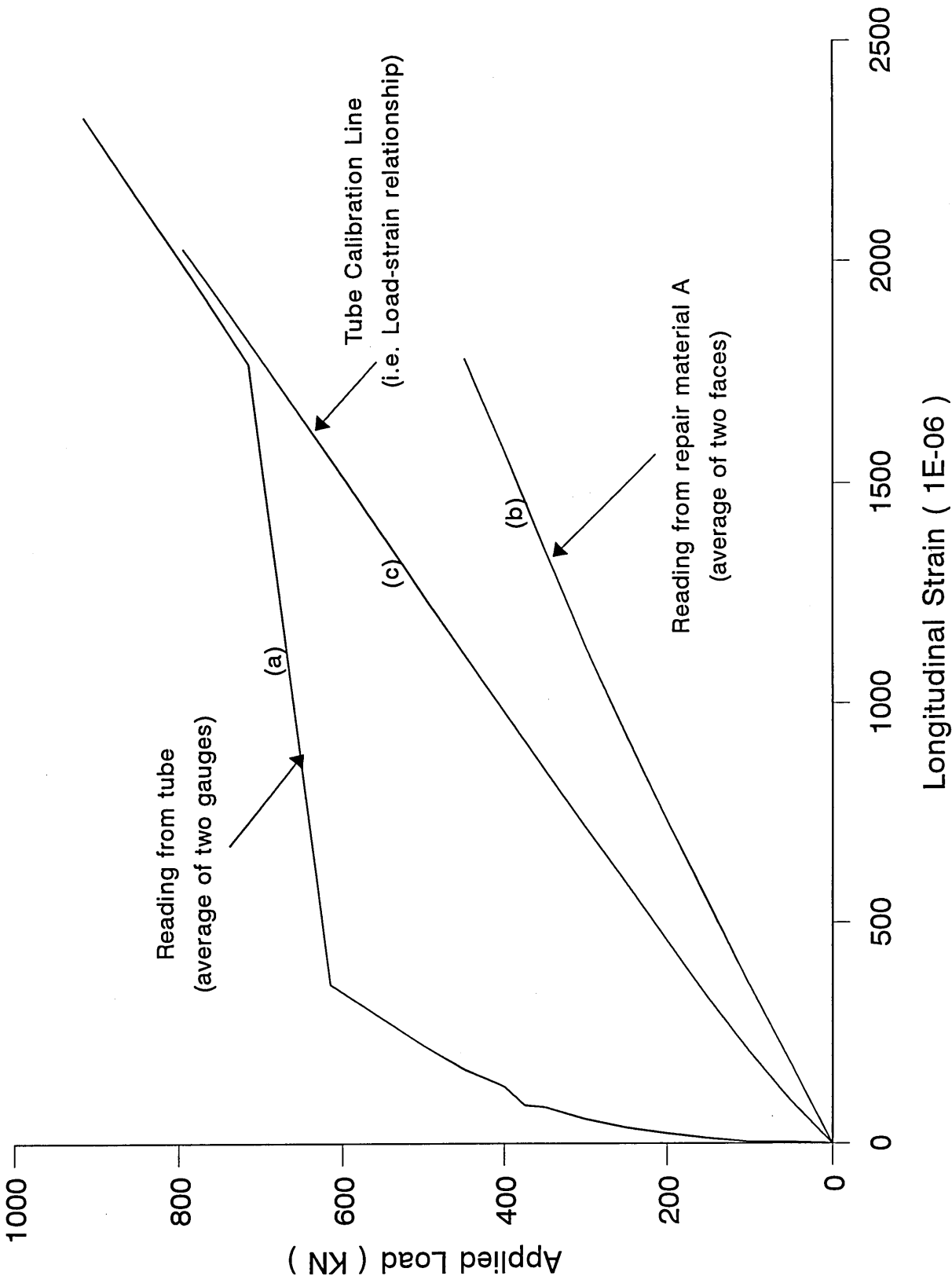


Figure 3.12 Load versus longitudinal strain measured on test sample (material A) and steel tube

capacity (longitudinal, lateral and volumetric) at initiation stress and critical stress. One of the most interesting aspects of these tests was the similarity in the ascending portion between the repair materials and concrete specimens while the descending portions of some repair materials were very different. The existence of the descending branch means that material has a capacity to withstand some load after the maximum load has been passed because the linking of microcracks is delayed before complete break-down. From figures 3.13 to 3.16, in high-strength repair material A both ascending and descending parts of the curve are steeper compared to other two repair materials (B and C) and this implies a more brittle type of behaviour.

3.4.3.1 Initiation stress

As stated previously in section 3.2.3.1, the boundary between stable crack initiation and propagation zones in figure 3.6 is referred to as the crack " Initiation Stress " [52,54]. This crack initiation stress corresponds to the point when poisson's ratio of the material starts to increase and the volumetric strain curve deviates from linearity [52,54]. The relationship between poisson's ratio and applied stress for the plain concrete and three different repair material specimens tested is shown in figure 3.17. A close examination of figure 3.17 shows a distinct reduction in the stress-strength ratio at the initiation point for repair materials B and C. For example, in plain concrete specimen of figure 3.17, the initiation stress-strength ratio is 0.58 which is in agreement with the range of values found by other researchers [33,45,49,52]. The corresponding values for the repair materials B and C is 0.3.

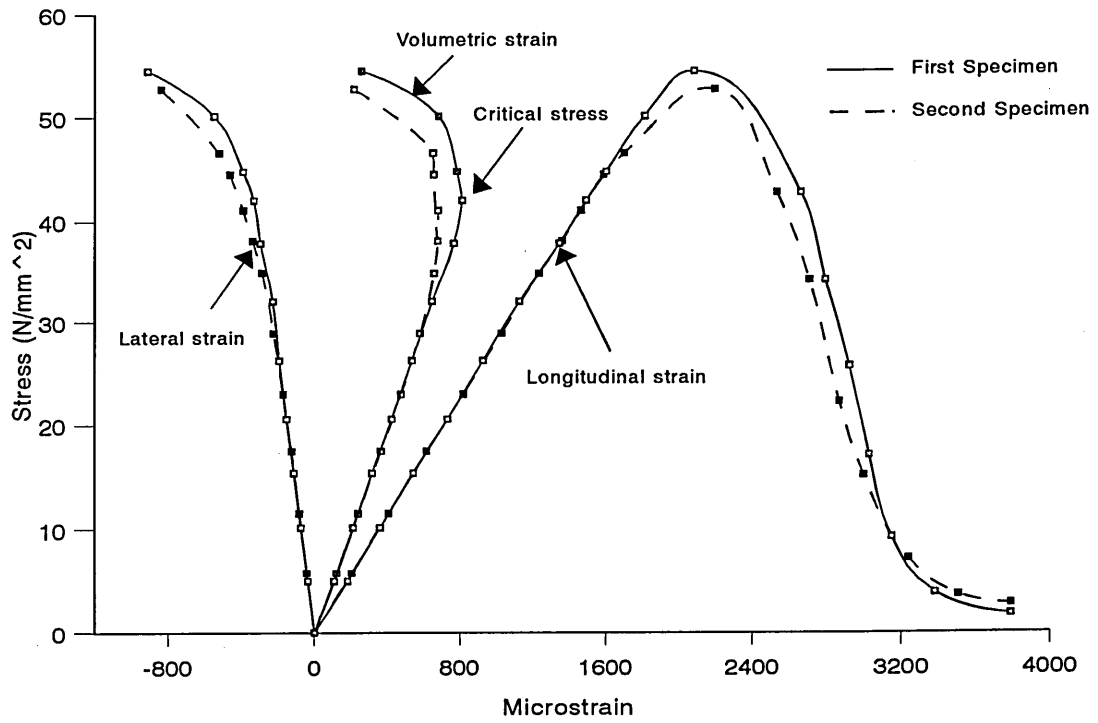


Figure 3.13 Stress-strain curves for Material A

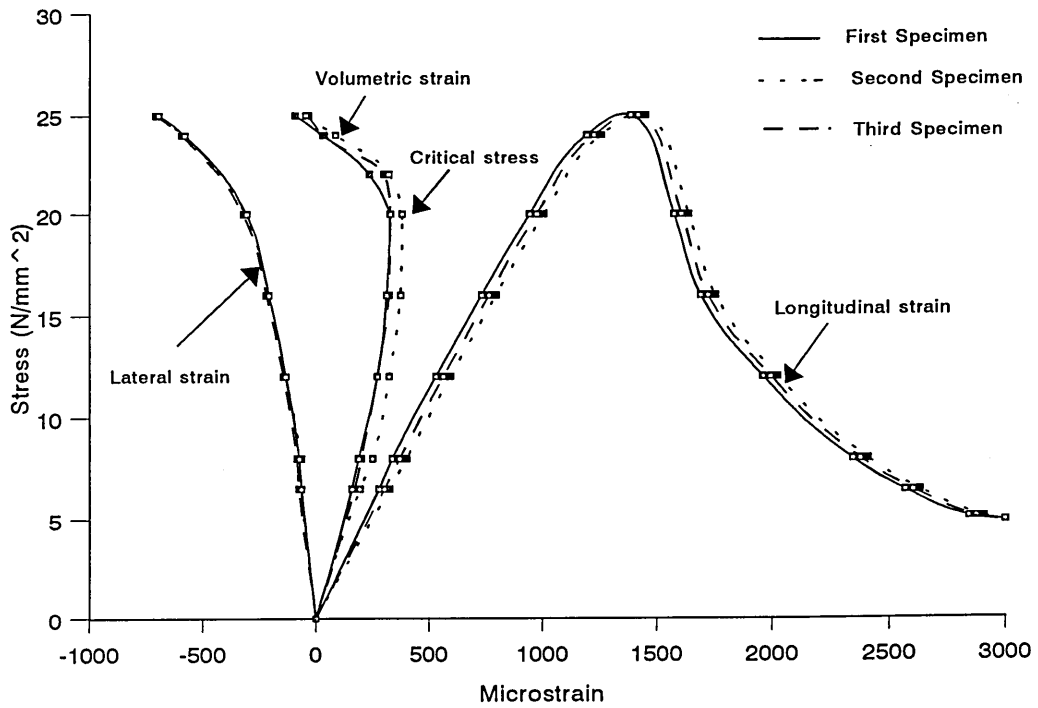


Figure 3.14 Stress-strain curves for Material B

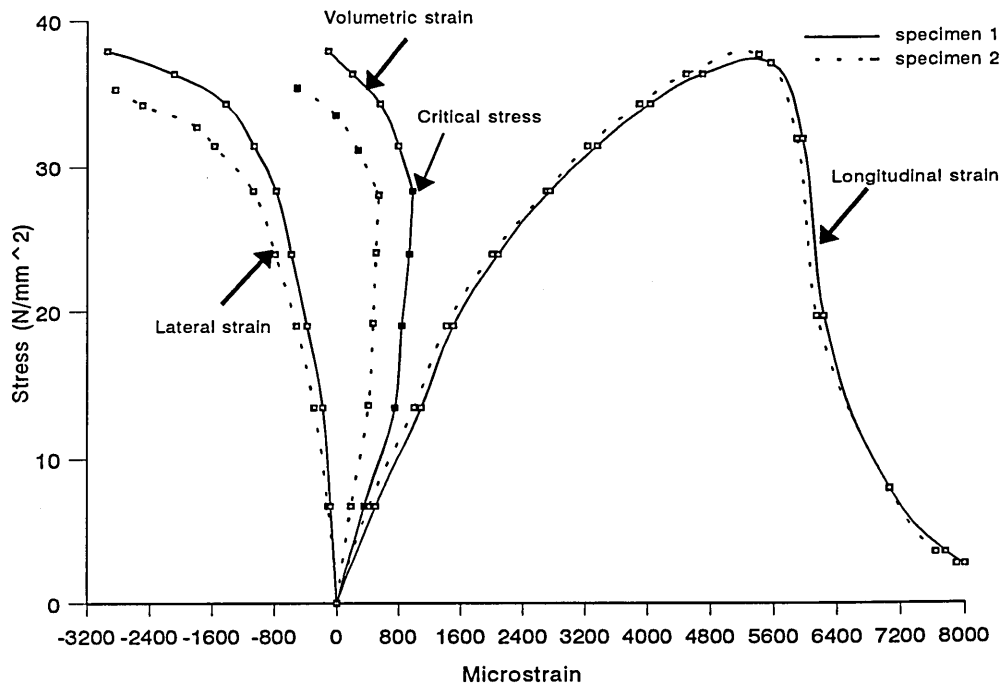


Figure 3.15 Stress-strain curves for Material C

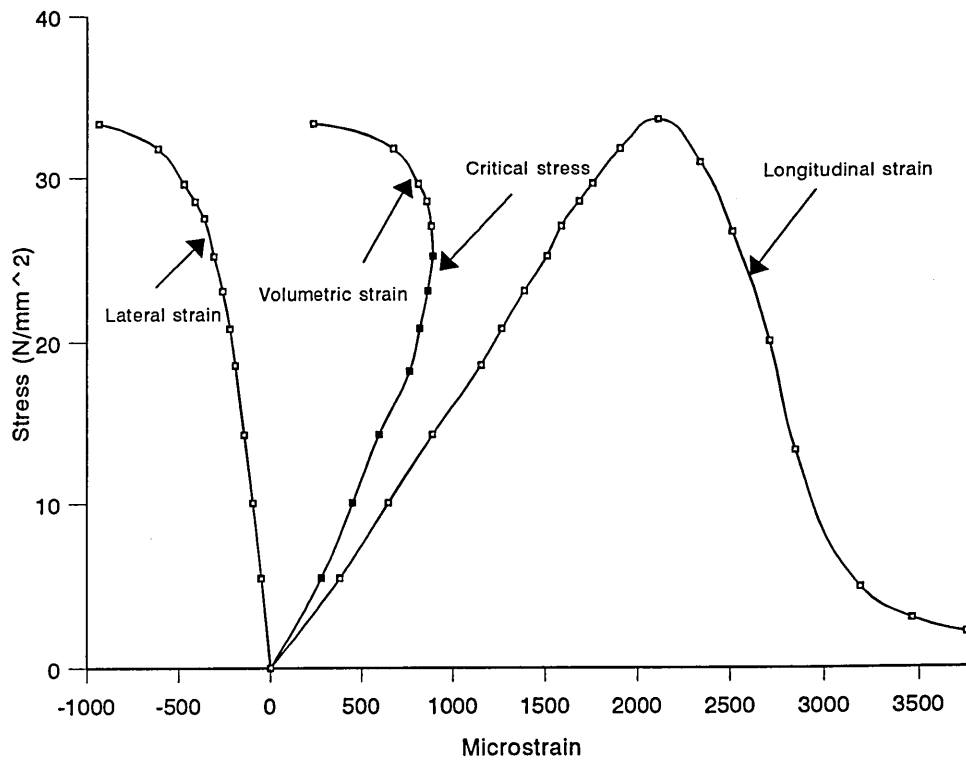


Figure 3.16 Stress-strain curve for Concrete

Table 3.5 Experimental results for repair materials and concrete specimens

| Specimen | Cube Strength (N/mm ²) | Initiation Stress | | | | | Critical Stress | | |
|------------|------------------------------------|-------------------|----------------------------|---------|------------|-------------------|----------------------------|---------|------------|
| | | Stress / Strength | Strain (10 ⁻⁶) | | | Stress / Strength | Strain (10 ⁻⁶) | | |
| | | | longitudinal | lateral | volumetric | | longitudinal | lateral | volumetric |
| Material A | 63.7 | 0.22 | 486 | 83 | 320 | 0.83 | 1587 | 395 | 797 |
| Material B | 33.0 | 0.33 | 520 | 90 | 340 | 0.80 | 1417 | 650 | 117 |
| Material C | 44.05 | 0.22 | 499 | 94 | 311 | 0.78 | 2740 | 789 | 1162 |
| Concrete | 41.0 | 0.55 | 885 | 154 | 577 | 0.80 | 1270 | 240 | 790 |

The cause of this reduction in the crack initiation stress-strength ratio of material C is most likely to be the greater interfacial surface area between the matrix and inclusions, which is generated due to polymers and fibres addition.

3.4.3.2 Critical stress

In Figure 3.6 of section 3.2.3.1, the " Critical Stress " has been defined as the boundary between the stable and unstable crack propagation zones [33] and this stress level is reflected by the dilation of the matrix structure. Hence, this level corresponds to the point on the stress-strain curve where a reversal of volumetric strain occurs. The critical stresses of the specimens investigated in this study were determined from the stress-strain curves and are recorded in Table 3.5. These are also indicated on the typical stress-strain graphs in figures 3.13 to 3.16.

Table 3.5 and figures 3.13 to 3.16 show that the range of critical stress-strength ratios is between 0.78 to 0.83 for repair materials and 0.80 for plain concrete specimens.

3.4.3.3 Ultimate strain

The results in figure 3.18 show the comparison of stress-strain curves of concrete with repair materials, which were obtained in this investigation. Each curve in figure 3.18 represents the average values obtained from three prism specimens. It is clear from this figure that the ultimate stress level and the post yield characteristics are influenced by the material constituents. For example, material A which has high strength and subsequent high elastic modulus shows the highest ultimate stress level.

The ultimate strains (at maximum stress) of concrete and repair material specimens tested in this investigation varied between 1300 microstrain to nearly 6200 microstrain as can

be seen from figure 3.18. Typical examples of stress-strain curves obtained in this investigation and by others [33,38,39] using the same experimental method are plotted in figure 3.19. The ultimate strains (at maximum stress) obtained in specimens of this investigation and reference [33] show similar values in figure 3.19 but the ultimate strains determined in references [38,39] are much greater, ranging between 3000 to 3800 microstrains. The strains at failure from references [38,39] are around 6000 microstrains whereas failure strains measured in this investigation and by Halabi [33] are found to be around 3800 microstrains. The possible reason for the higher (concrete) ultimate strains in references [38,38] is due to their assumption that the tube and concrete strains are the same at the initial stages of loading and, therefore, taking the strains directly from the tube rather than concrete specimen itself.

3.4.3.4 Strain capacity and mode of failure

The ductility of a repair patch is its ability to sustain significant inelastic deformation without any considerable variation in load resisting capacity prior to failure. Ductility can be measured by the property of toughness and the strain capacity of the material at post-peak level.

In this investigation, the post yield strain capacity of generic repair materials and concrete mix is assessed by considering the longitudinal strains at a stress-strength ratio of 0.4 on the falling branch of the stress-strain curves in figure 3.18. Figure 3.20 represents the relationship between repair materials and strain at this stress-strength ratio. These results indicate that polymer additives in repair material C cause a substantial increase in the longitudinal strain capacity. Similarly a high strength and subsequent high elastic modulus of the repair material also have influence on ultimate stress level. For example, the

longitudinal strain capacity were 3011, 2141 and 6541 microstrains for repair materials A, B and C respectively, and for plain concrete 3059 microstrain.

All the specimens tested (concrete and repair materials), failed in a gradual manner. Concrete and Repair material A specimens tested were characterised by extensive splitting cracks running longitudinally from the top of the prism to the bottom, but in the case of repair materials B & C some lateral cracks also occurred. When the steel tube was removed after the tests, the specimens were found to be extensively damaged. High-strength repair material A specimens failed in a brittle manner within the steel tube despite its ability to absorb the energy release associated with failure. The result was total collapse of repair material (A).

3.5 FURTHER DISCUSSION

The elastic modulus of repair materials is an important property - a high strength and consequently high elastic modulus of the repair material will increase the load sharing capacity of the repair patch. A mismatch in elastic modulus between the repair patch and substrate concrete can result in a redistribution of stress within the repaired member, but stress levels will depend on the proportion of load which is carried by the repair.

It is well established that it is economical to use aggregates in concrete mixes, which also lead to a technically superior material due to its dimensional stability, ductility and stiffness provided by aggregate to the cement paste matrix [26]. Similar benefits can be achieved by using fine and coarse aggregate size particles in the repair mixes.

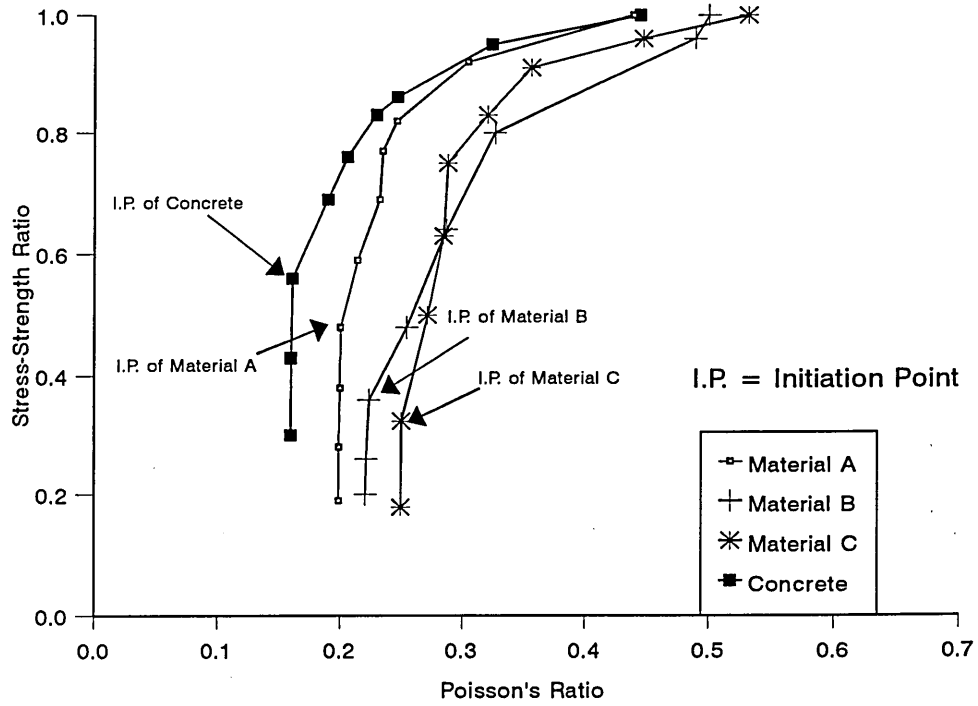


Figure 3.17 Relationship between stress-strength ratio and poisson's ratio

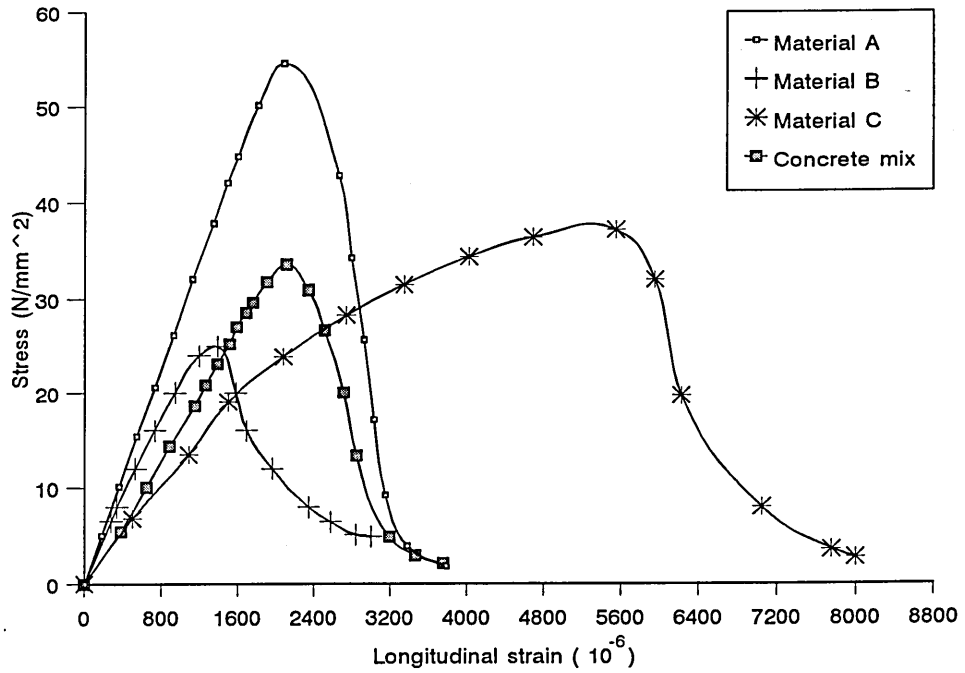


Figure 3.18 Stress-strain curves of repair materials and concrete mix

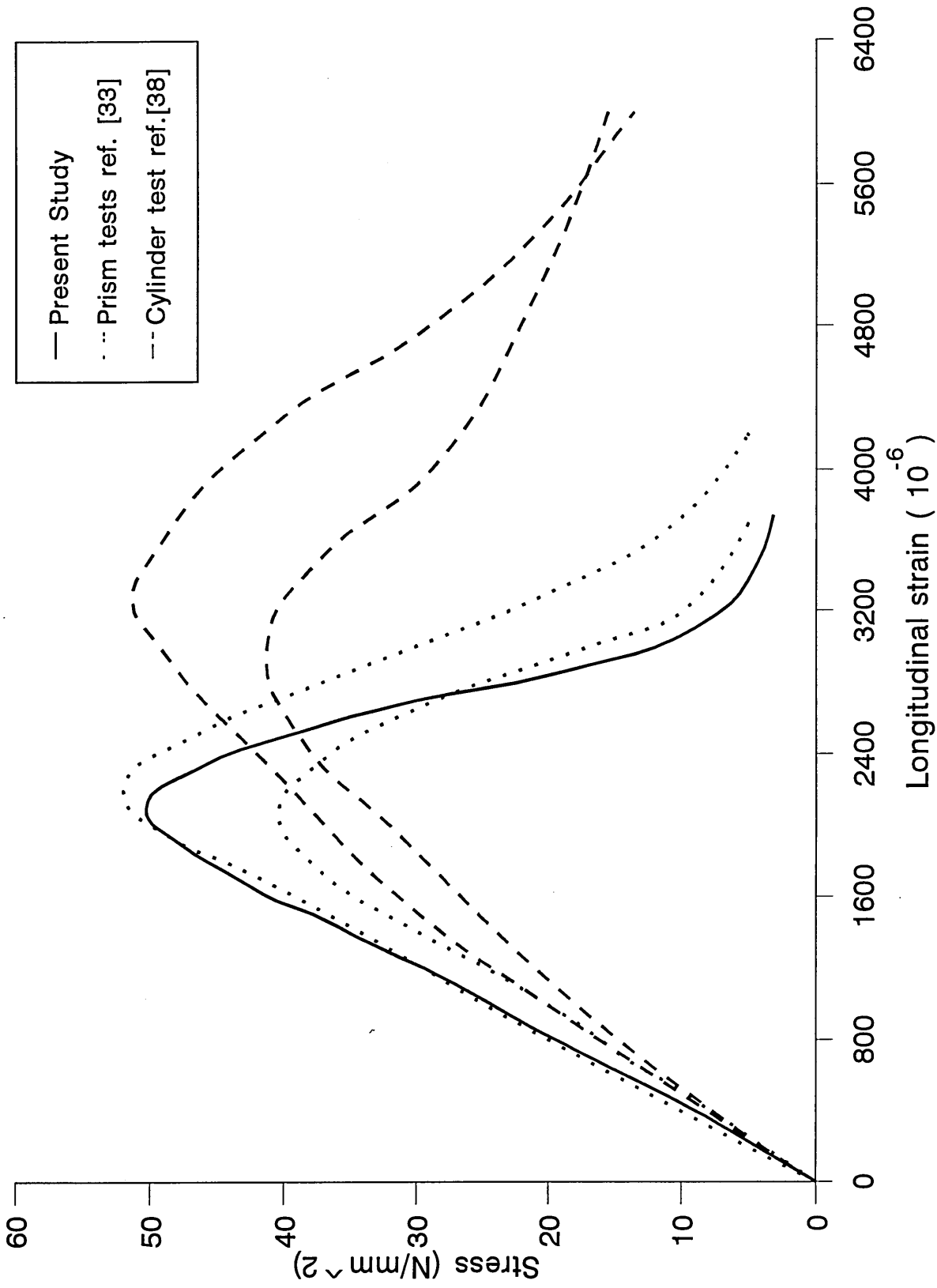


Figure 3.19 Stress-strain curves for plain concrete obtained in this study and by others [33,38]

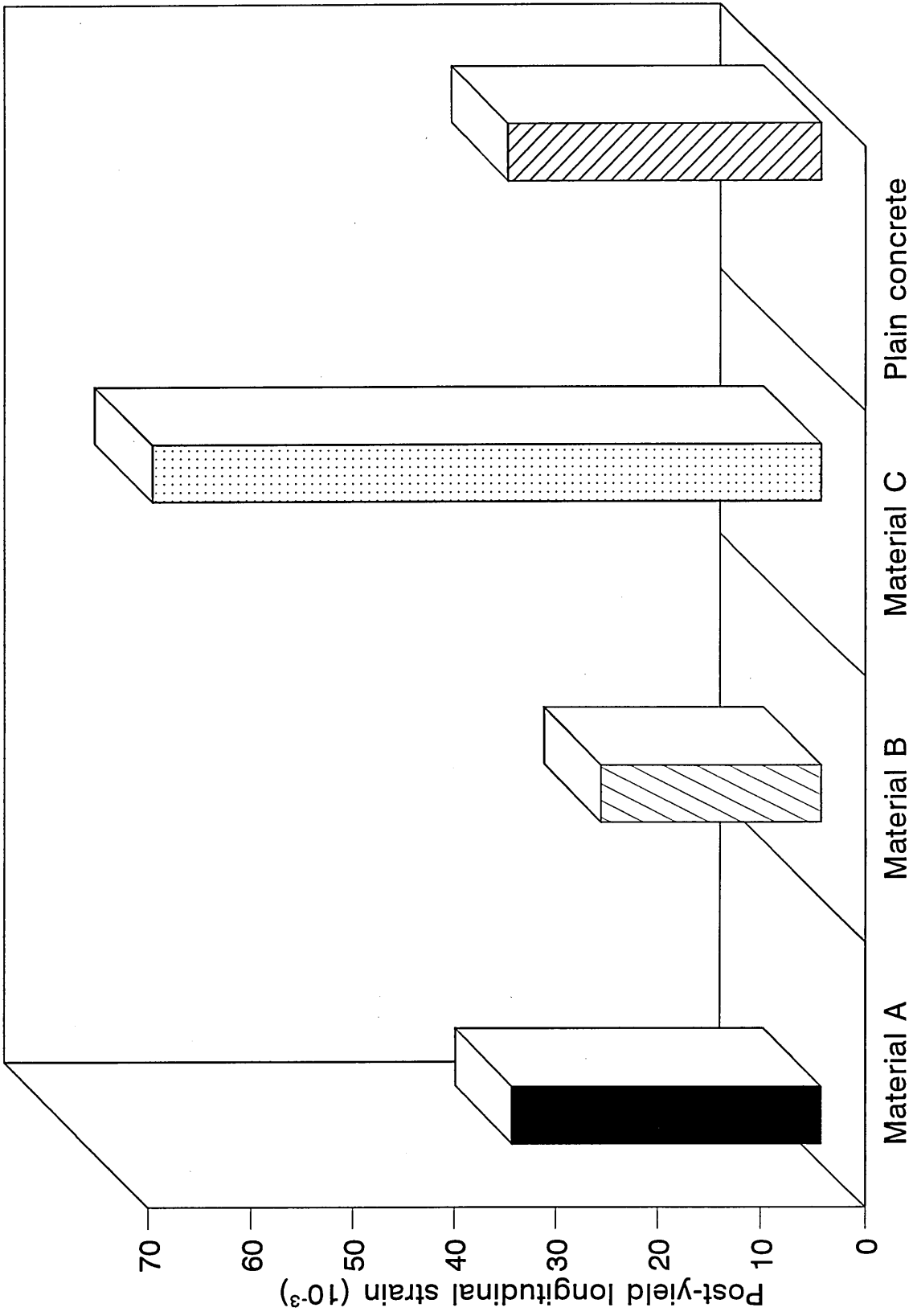


Figure 3.20 Relationship between repair materials and longitudinal strain at a post-peak stress-strength ratio of 0.4

It is generally accepted that deterioration processes in concrete structures, such as reinforcement corrosion, can be determined largely by the ability of the cover zone material to resist the ingress of deleterious agents from the environment. Therefore, the permeability of repair materials should provide an indicator of durability against reinforcement corrosion of repaired element. Polymer additives in repair materials show a small decrease in the water permeability. For example, from the results of material C it is clear that its compressive strength, stiffness and permeability are similar to a good quality concrete. If the excessively high elastic modulus material A is used for repair on a normal grade concrete substrate, excessive redistribution of stress to the patch would result.

3.6 CONCLUSIONS

The following conclusions are based on the experimental results reported in this chapter on the repair material properties which influence long-term performance of repaired concrete structures:

1. Compressive strength and modulus of elasticity are greatest for the generic repair material A which contains small aggregate particles and has a low water/powder ratio.
2. Presence of a polymer additive in the repair material reduces its water permeability. For example, the water permeability coefficients, K_{LD} (m/s), for the cementitious material with polymer additives is 1.33×10^{-13} compared to 5.62×10^{-11} for the repair mortar which is based on a mineral cement binder. The permeability coefficient of a plain concrete mix of similar strength was in the range $(5 \text{ to } 15) \times 10^{-13}$ m/s.

3. The ultimate stress level (at maximum load) of specially formulated repair materials varies significantly, the lowest ultimate stress being recorded for the porous mineral based material B. For example, average value of ultimate stress for materials A, C and control concrete were 62, 47 and 50 N/mm² respectively, while for material B it was 25 N/mm².
4. The post-peak strain capacity of the material modified with a polymer admixture is markedly improved leading to a more pronounced falling branch of stress-strain curve.
5. Test specimens of high-strength repair material A fail in a brittle manner whereas the specimens of other two repair material (B and C) tended to fail in a ductile manner.

CHAPTER 4

LONG-TERM DEFORMATIONS OF REPAIR MATERIALS

4.1 INTRODUCTION

During service life, incompatibilities in the form of creep and shrinkage deformations between repair and substrate concrete can create difficulties. Drying shrinkage of repair materials may reduce long-term structural efficiency by either initial tensile strains induced in the repair, or due to cracking at the repair/ substrate interface. Also, creep of the repair materials under sustained stress may render the load sharing capacity of the repair less effective with time.

A patch repair is an effective restoration technique when an element of or a whole structure shows signs of distress, especially spalling and delamination [5]. However, shrinkage of a repair material in a repaired element is restrained by substrate concrete and reinforcement during setting, curing and aging. Thus, although shrinkage (or swelling) can be categorized as independent of stress, the real life situation is not so simple. Shrinkage can theoretically induce enormous strains in the repair, leading to tensile and adhesion failure.

Knowledge of shrinkage deformation of repair materials is important to avoid shrinkage cracks between the recast section and the rest of the original structure, because they impair durability and structural integrity, and are also aesthetically undesirable.

Most repairs are made to older concrete which is dimensionally stable. The main requirement for successful repair is to provide a good bond between the new material and the old concrete substrate. Often bond failure is not caused by the failure of a repair material

to adhere to a properly prepared substrate, but rather by its drying or curing shrinkage. For this reason it is often desirable for repair materials to be shrinkage free or slightly expansive to avoid shrinkage cracking and /or debonding. It is also necessary to ensure tight contact and good bond with the surrounding parent materials. However, materials should not have such a high expansion as to disrupt the parent material.

The magnitude of shrinkage and swelling deformation depends largely on the material constituents. Due to differences in material constituents for different repair materials, the mechanism of restraint on the free shrinkage of matrices is not the same.

All cement-based materials, when kept under sustained load, deform slowly with time the movement being commonly known as creep. The magnitude of creep depends largely on the applied stress and the material constituents. Hardened cement paste undergoes very high creep whereas concrete shows relatively less creep under the same sustained load. This is primarily due to the restraint provided by the rigidity of coarse aggregate particles.

Prior to presenting the results of this investigation, however, a brief literature review is made of the current information available on the free shrinkage, swelling and creep deformation properties of concrete and repair materials.

4.2 LITERATURE REVIEW

4.2.1 Shrinkage and Swelling deformations

Information on the shrinkage and swelling deformation of repair materials, as affected by the materials constituents, is very limited if not non-existent. In the case of plain concrete, research [67,68] has revealed that shrinkage deformation can be estimated with sufficient knowledge of mix composition (e.g. cementitious content of OPC, pfa, slag etc., water/cement ratio, aggregate/cement ratio, aggregate type). It can also be estimated for well

defined cementitious repair materials free of polymer and unusual admixtures. Unfortunately, formulators of commercial products are reluctant to give complete details of their materials, and only general descriptions are normally available.

There seems to be little doubt that the material constituents have a large effect on the free shrinkage of repair materials. However, this effect seems to vary for different curing conditions and age of curing. At present, due to the limited nature of the available data, it is difficult to describe the shrinkage mechanism of repair materials. There is a need for a detailed investigation on different repair materials and curing conditions on the free shrinkage deformation.

Table 4.1 shows nine generic categories of repair materials, which were selected by Emberson and Mays [13], for a study of the property mismatch in patch repair of concrete. Unrestrained prism specimens of size 40mm X 40mm X 160mm long were used to measure shrinkage from an age of 24 hours. Shrinkage strains were monitored using a vibrating wire gauge. A datum reading was taken at an age of 24 hours. The specimens were stored in a temperature and humidity controlled room, in which the temperature varied from 12 to 22°C and the relative humidity from 55 to 95 percent.

Figure 4.1 shows the variation in shrinkage strain with time from the age of 24 hours to 16 months for four different repair materials as obtained by Emberson and Mays [13]. It is apparent from the results of figure 4.1 and Table 4.2 that the free shrinkage is a function of the materials constituents. The total shrinkage strains are greatest for the polyester resin mortar and the vinyl acetate modified system. The epoxy and acrylic resin systems have shown low values of total shrinkage; the magnesium phosphate system showed expansion.

Table 4.1 Categories of patch repair systems used by Emberson and Mays [13].

| Resinous materials | Polymer modified cementitious | Cementitious materials |
|---------------------|---------------------------------|------------------------|
| A: Epoxy mortar | D: SBR modified | G: OPC / sand mortar |
| B: Polyester mortar | E: Vinyl acetate modified | H: HAC mortar |
| C: Acrylic mortar | F: Magnesium phosphate modified | I: Flowing concrete |

Table 4.2 Shrinkage strains ($\mu\epsilon$)

| Repair Material | Shrinkage (24 hr to 16 months) |
|-----------------|---------------------------------|
| A | -50 |
| B | -280 |
| C | -360 |
| D | -740 |
| E | -1060 |
| F | +700 |
| G | -1140 |
| H | -760 |
| I | -650 |

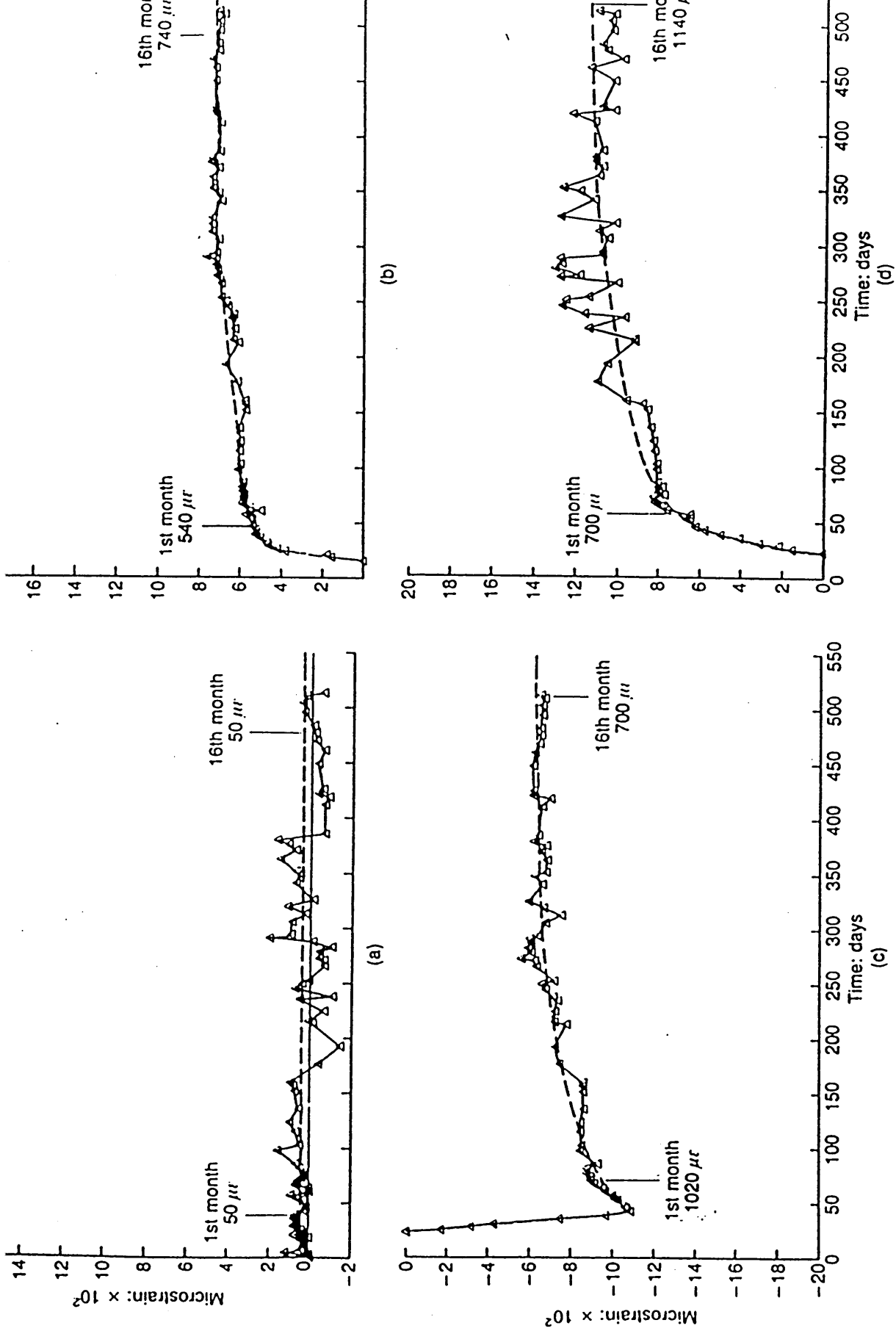


Figure 4.1 Results of long-term shrinkage deformation for materials; (a)A; (b)D; (c)F and (d)G, after Emberson and Mays [13]

4.2.2 Creep of concrete

When stress is applied to a concrete specimen and sustained for a period of time the specimen shows an immediate strain followed by a further deformation which progresses at a diminishing rate with time, as shown in figure 4.2. The immediate strain is often referred to as the elastic strain and the subsequent time dependant strain is referred to as the creep strain. The part of the strain which is immediately recoverable upon removal of the stress is called as the elastic recovery. The creep recovery which occurs over a period of time after the removal of stress is termed as delayed elastic recovery.

An analytical description of creep, as well as the understanding of the physical process that causes creep in concrete, are made considerably simple by breaking down the total creep strain in two components, namely, delayed elastic strain and the flow component of creep. These two components which comprise the overall creep of concrete are discussed more fully in the following sections.

4.2.2.1 Delayed elastic strain and flow creep

It was realised early on that the concept of "creep" of concrete lacks precise definition because it consists not only of a reversible (delayed elastic) component but also an irreversible (flow) strain component. If a test piece that has been subjected to a sustained load is relieved of the load, a noticeable creep recovery, ϵ_{od} , is observed over a period of time (figure 4.2); it has been confirmed by research [71] that the delayed elastic component of creep under load equals the creep recovery strain, ϵ_{od} , after unloading as shown in figure 4.2. The irreversible flow component of creep has been shown to be equal to the residual strain, ϵ_{op} , which remains upon removal of stress [71]. Hence, by disregarding the small effects of change in elastic modulus with time, it can be seen that the total creep strain of concrete,

ϵ_{oc} , in figure 4.2, is the sum of delayed elastic strain, ϵ_{od} , and flow creep, ϵ_{op} .

According to Illston [72], the delayed elastic strain component of creep reaches a limiting value a few days after the application of the sustained load as shown in figure 4.3. Therefore, for most practical purposes, the flow component of creep can be calculated by subtracting the limiting value of the delayed elastic strain from the total creep of concrete. The magnitude of the limiting value of the delayed elastic strain depends largely on the applied sustained stress [72,73]. The results in Table 4.3, which have been obtained by Roll [73], show the effect of applied stress on the limiting value of the delayed elastic strain, ϵ_{od} , as a ratio of the 28 days elastic strain values, ϵ_E . It is evident from these values that the delayed elastic strain increases with an increase in the sustained stress-strength ratio.

After the first few days under load, the magnitude of the delayed elastic strain of concrete can be considered to remain constant at its limiting value (figure 4.3). It follows, therefore, that the flow creep versus age under load curve for concrete is of a similar shape to the total creep curve shown in figure 4.2. The rate of creep is rapid at early ages under load followed by a more gradual creep rate. The flow component of creep can be further subdivided into two components, basic flow and drying flow. Basic flow occurs under sealed conditions of curing and depends primarily on the cement paste content and moisture content of concrete. Drying flow is closely related to shrinkage and is therefore mainly affected by the moisture gradient of the specimen.

4.2.2.2 Creep at high stresses

At stress levels below working stresses, a linear relationship exists between applied stress-strength ratio and creep strain of concrete. This conclusion is based on a wide range of data produced by various researchers [71]. Within this range of stress, creep consists

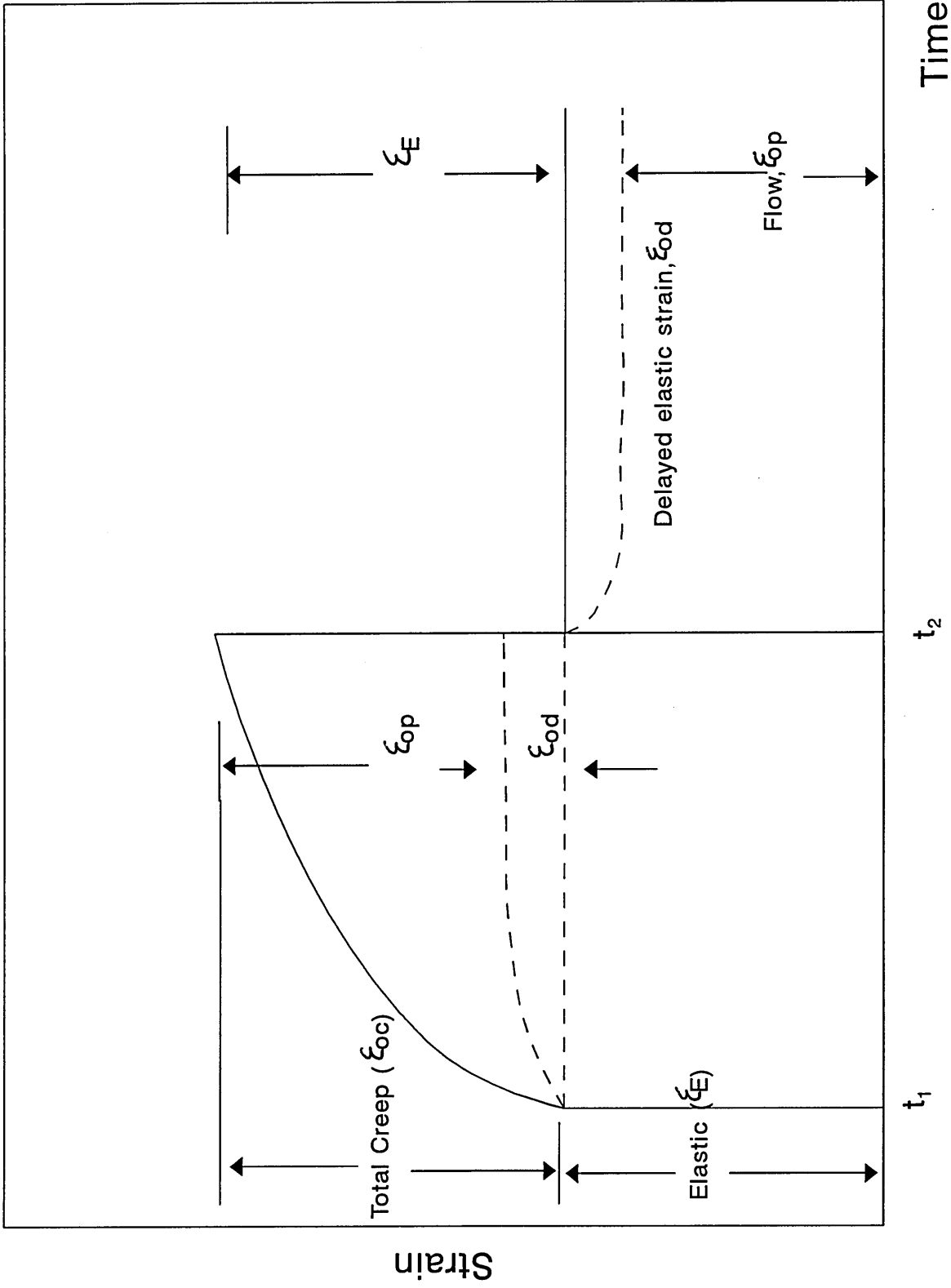


Figure 4.2 Typical strain profile for concrete under sustained stress

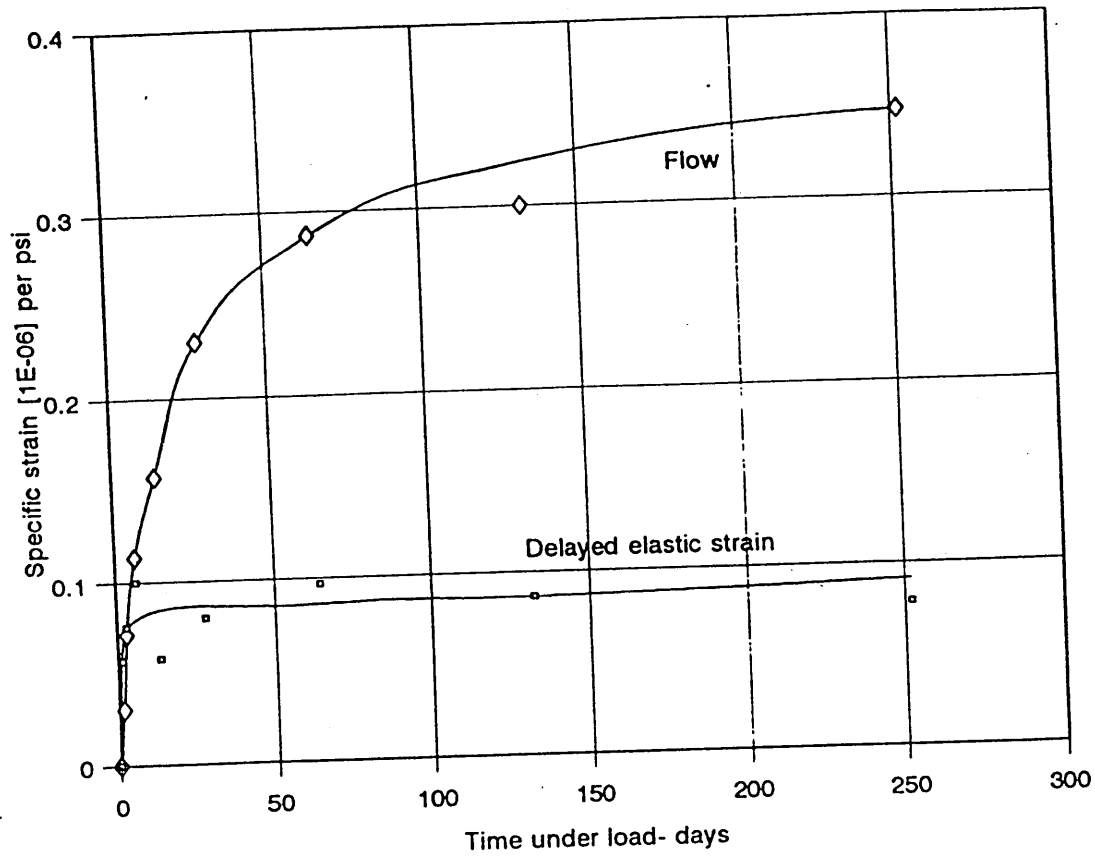


Figure 4.3 Effect of time under load on the delayed elastic and flow strain components: age at loading 10 days [72]

Table 4.3 Relationship between stress-strength ratio and ϵ_{od}/ϵ_E [73]

| | | | | |
|--------------------------------|------|------|------|------|
| Stress-Strength ratio → | 0.20 | 0.35 | 0.50 | 0.65 |
| $\epsilon_{od} / \epsilon_E$ → | 0.24 | 0.28 | 0.31 | 0.44 |

mainly of delayed elastic deformation and flow. However, there exists an upper limit of stress beyond which creep is no longer proportional to the applied stress but increases with stress at an increasing rate. At these high stress levels micro-cracking plays a major role in the development of the time-dependent deformation of concrete. In fact, a sufficiently high sustained stress may produce extensive micro-cracking, leading to eventual failure. The stress at which the advent of micro-cracking causes failure has been reported to be in excess of 0.7 of the short term strength of concrete [71].

The stress-strength ratio at which micro-cracking develops extensively is not constant and depends on the degree of heterogeneity of the concrete. For instance, mortars are less grossly heterogeneous than concrete containing large-size aggregates and, therefore, exhibit proportionality between creep and stress-strength ratio up to a high limit stress. From Hsu's work [74], it appears that the upper limit of proportionality between creep and stress is probably in the region where bond cracks begin to increase. Beyond this stress level, strains due to bond micro-cracking tend to increase creep at a higher rate.

Results of an experimental investigation on the long-term deformation characteristics of three generic repair materials and plain concrete are given in this chapter. The chapter comprises of two parts - the first part deals with the shrinkage and swelling deformation properties (independent of load) of repair materials. The effect of varying the curing environment on the shrinkage deformation is also examined. The second part of the chapter is concerned with a study of the long-term creep deformation under uniaxial compression.

4.3 EXPERIMENTAL PROGRAMME

An experimental study was carried out to establish the free shrinkage, swelling and creep deformation properties of plain concrete and three generic repair materials (namely A, B and C). These materials are commercially available, and in most cases are in widespread use in construction. Experimental programme is given in Table 4.4.

4.3.1 Details of mixes and materials

Details of repair materials and concrete mixes are given in Table 4.5. The mix proportions of concrete (by weight) were 1 : 2.24 : 3.22, with a water/cement ratio of 0.56. The cement content was 343 kg/m³. The chosen mix proportions are designed to give a 28 days cube strength of 40 N/mm² (± 1 N/mm²), and a slump of 10 - 20 mm. Ordinary portland cement, fine aggregate conforming to zone 'M' of BS 882 and coarse aggregate of 10mm nominal size were used for the control concrete.

Three different types of repair materials were used, namely high performance non-shrinkable concrete, Cement-based repair mortar and Cementitious mortar which incorporates the most advanced cement chemistry, microsilica, fibre and styrene acrylic copolymer technology. Detailed description of these repair materials are given in section 3.3.1 of chapter 3.

TABLE - 4.4 Experimental Programme

| TEST | AGE AT START OF TEST |
|---|----------------------|
| - Shrinkage | |
| * at 20°C & 55% R.H. | 1 day |
| * at 20°C & 30% R.H. | 1 day |
| * at 20°C & 45% R.H. | 1 day |
| * cured in water for 28 days, then stored in air at 20°C and 55% R.H. | 28 days |
| - Swelling | 1 day |
| - Creep | 28 days |

TABLE - 4.5 Details of Mixes and Materials.

| MIX | MATERIALS AND DESCRIPTION | QUANTITY (kg/m ³) | W/C RATIO |
|----------|---------------------------|-----------------------------------|--------------|
| CONCRETE | Ordinary Portland Cement | 342.54 | 0.56 |
| | Fine aggregate | 767.04 | |
| | 10mm Coarse aggregate | 1102.04 | |

REPAIR MATERIALS

| | | Mixed Density | Water Addition |
|---|---|------------------|---------------------------|
| A | High performance, non-shrink concrete | 2069 | 4 litres per 30 kg pack |
| B | Mineral based cementitious mortar with no additives | 1575 | 3 litres per 20 kg pack |
| C | Single component cementitious material with polymer additives | 1725 | 2.5 litres per 20 kg pack |

4.3.2 Casting and Curing

100 X 100 X 500mm size prism specimens were used in this study. This size conformed to the sizes recommended for testing concrete (to BS 1881) instead of the relatively smaller sizes permissible for repair materials (to BS 6319). This was done for the following reasons:

- * among the repair materials considered in the study was plain concrete with coarse aggregates and, therefore, the larger specimen size was considered appropriate for comparison of properties of the different materials.
- * the research is concerned with mismatch of properties between the substrate and repair material. The specification and design procedures of substrate concrete are established on the basis of properties determined from standard size of test specimens of concrete. It is therefore appropriate to use the same size of specimens for repair materials in this investigation.

Mixing the constituents of each repair material was carried out according to the manufacturer's literature. Twenty four 100 X 100 X 500mm prism specimens and twelve 100 X 100 X 100mm cube specimens were cast for plain concrete and for each of the three generic repair materials. The specimens were cast horizontally in three layers, each layer being compacted on a vibrating table for a few seconds. The fresh material was covered with polythene sheets and the specimens were demoulded after 24 hours. Subsequently, drying shrinkage specimens were transferred to four different curing conditions and demec points were attached to the four longitudinal faces of each specimen. The curing regimes adopted were:-

- (a) 20°C and 30 percent R.H.

- (b) 20°C and 45 percent R.H.
- (c) 20°C and 55 percent R.H.
- (d) cured in water for the first 28 days after casting, then stored in air at 20°C and 55 percent R.H.

The swelling deformation of the materials was determined under total immersion in water.

Prism specimens for creep were cured in water at 20°C for the first 28 days prior to loading. All the prism specimens for creep tests were accompanied by identical prism specimens for free shrinkage measurement.

4.3.3 Testing

Free shrinkage and swelling deformation measurements were made by means of a Demec Extensometer over a gauge length of 200mm. Measurements were made on the four longitudinal faces of each specimen. Consequently, each shrinkage and swelling value presented in this chapter is an average of twelve faces of three prism specimens. The datum strain reading was taken at an age of 1 day after casting and changes of length were monitored every 3 days for the first 60 days and once a week thereafter. The cube specimens of all the mixes were tested in compression at 28 days age. The 28 day compressive strength, f_{cu} , was determined primarily to maintain a check on the quality control of the mixes.

The creep tests in this investigation were conducted in accordance with standard recommendations [64]. In each of these tests, two prisms of a mix were loaded together in a standard creep rig as shown in plate 4.1. Each creep rig comprised of steel end platens supported by nuts on four 36mm diameter tie rods of high yield steel. The axial sustained load on the specimens was applied by means of a hydraulic jack via the top platens of the

creep rig. This load was maintained at a constant level by regular loading and tightening of the nuts against the end platens. The concentricity of the applied load was ensured by achieving reasonably similar strains on the four steel tie rods of a creep rig. During sustained loading, the specimens in the creep rigs were stored in a temperature and humidity controlled environment where the temperature was maintained at 20°C and the relative humidity was 55%. Three creep tests were carried out for each material at a sustained stress of 30, 45 and 55 percent of the 28 days cube strength. The initial strain on loading and subsequent increases of strain were monitored across a 200mm gauge length, across two opposite faces of each prism specimen by means of a demec extensometer.

In order to calculate the net creep strain, shrinkage was measured on separate specimens and deducted from the total strain measured on specimens in the creep rigs.

4.4 RESULTS AND DISCUSSION

4.4.1 Free shrinkage and swelling deformation of repair materials and concrete

Figure 4.4 shows the variation in shrinkage and swelling deformations with time for repair materials A, B, C and plain concrete. Comparison with the curves of plain concrete shows that all repair materials shrink more. The shrinkage curves for repair materials A and B have a general shape which is similar to concrete [65,66,69,70]. The curve for material C shows very rapid shrinkage for the first 20 days followed by similar rate of shrinkage as the other repair materials.

Figures 4.5 to 4.8 show the influence of relative humidity on the shrinkage of each material. Relative shrinkage results of the different repair materials and concrete under various curing conditions are shown in figures 4.9 to 4.12.



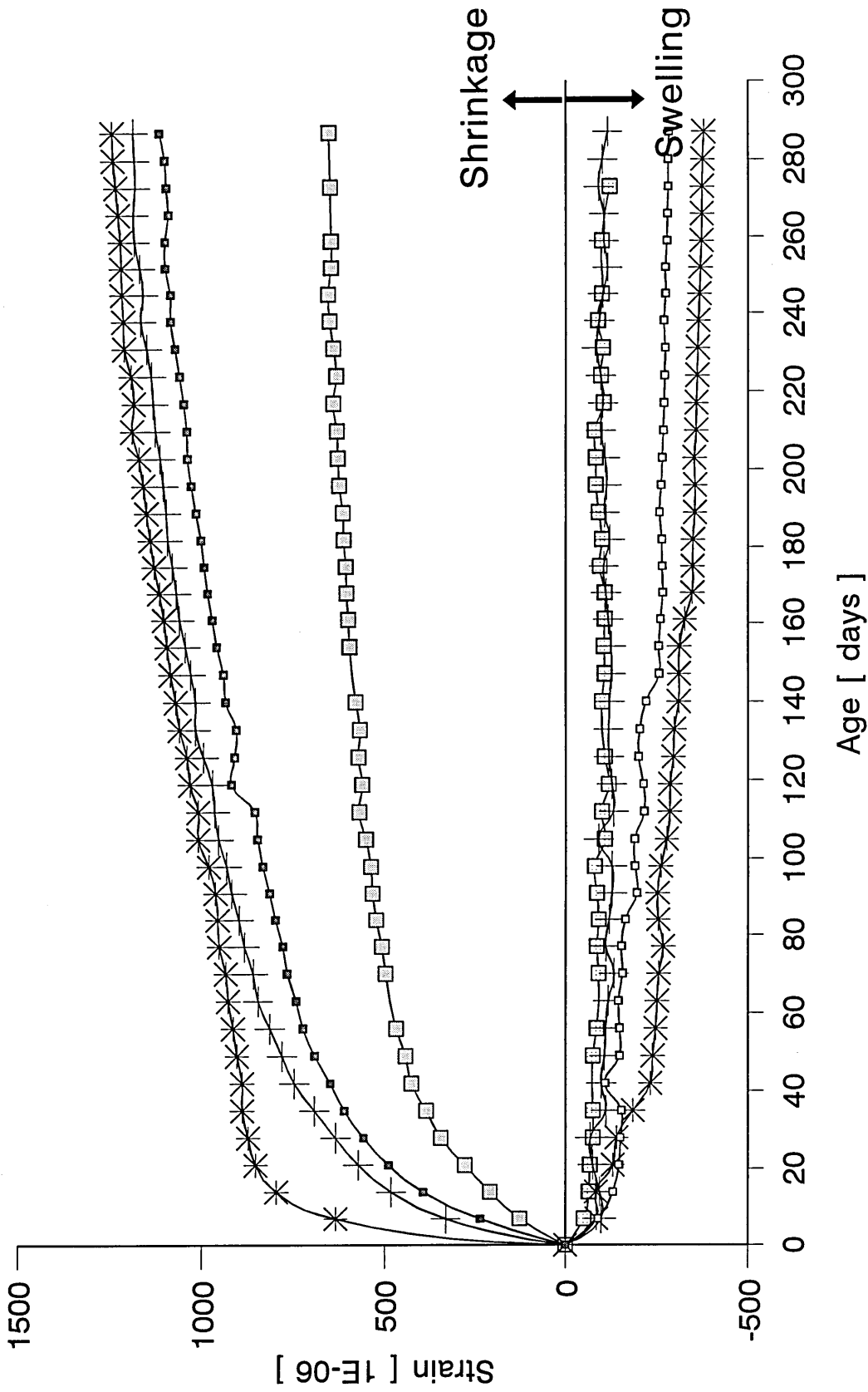
Plate 4.1 Experimental set up for the creep test.

The results plotted in figures 4.4, 4.9 to 4.12 show that the styrene acrylic latex modified repair material C has much higher values of shrinkage and swelling compared to other materials. Similar results were found by Emberson and Mays [13] for SBR and vinyl acetate polymer modified cementitious materials (Table 4.2).

The 90 days results for shrinkage (under different conditions) and swelling deformation are listed in Table 4.6. The larger magnitude of shrinkage and swelling strains of the repair materials (especially material C) relative to plain concrete is clearly evident.

Table 4.6 Shrinkage and Swelling deformation strains at 90 days(microstrain)

| Repair Material | Shrinkage (at 20°C and Relative humidity of) | | | Swelling |
|-----------------|---|------|------|----------|
| | 55% | 45% | 30% | |
| A | 814 | 891 | 931 | 197 |
| B | 918 | 1033 | 1098 | 128 |
| C | 962 | 1230 | 1474 | 254 |
| Concrete | 450 | 559 | 702 | 87 |



+ Material A * Material B □ Concrete

Figure 4.4
 Deformation of Repair Materials
 Shrinkage at 20 C & 55% R.H. and Swelling at 20 C & 100% R.H. (in water)

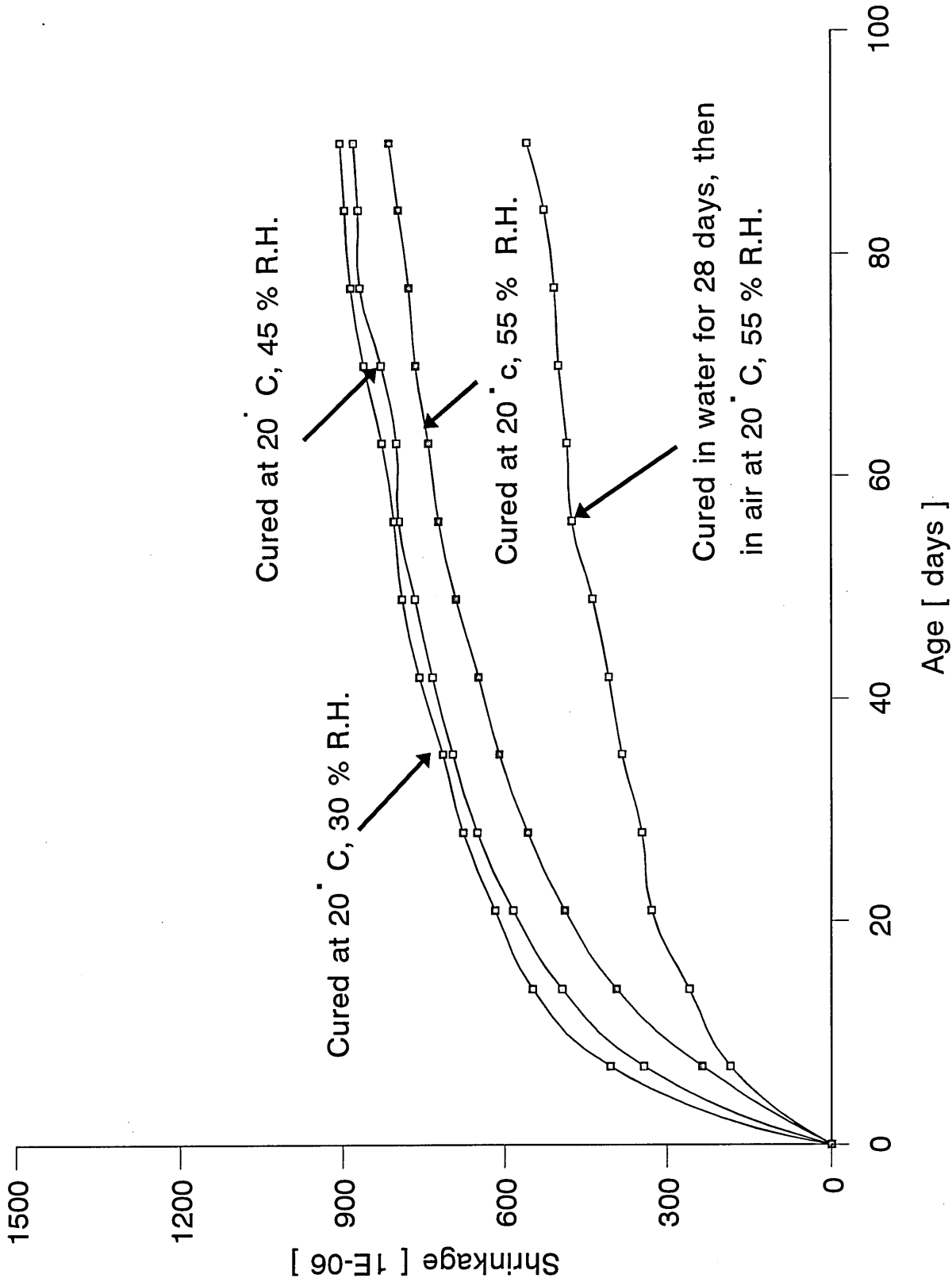


Figure 4.5
Influence of relative humidity on shrinkage of Material A

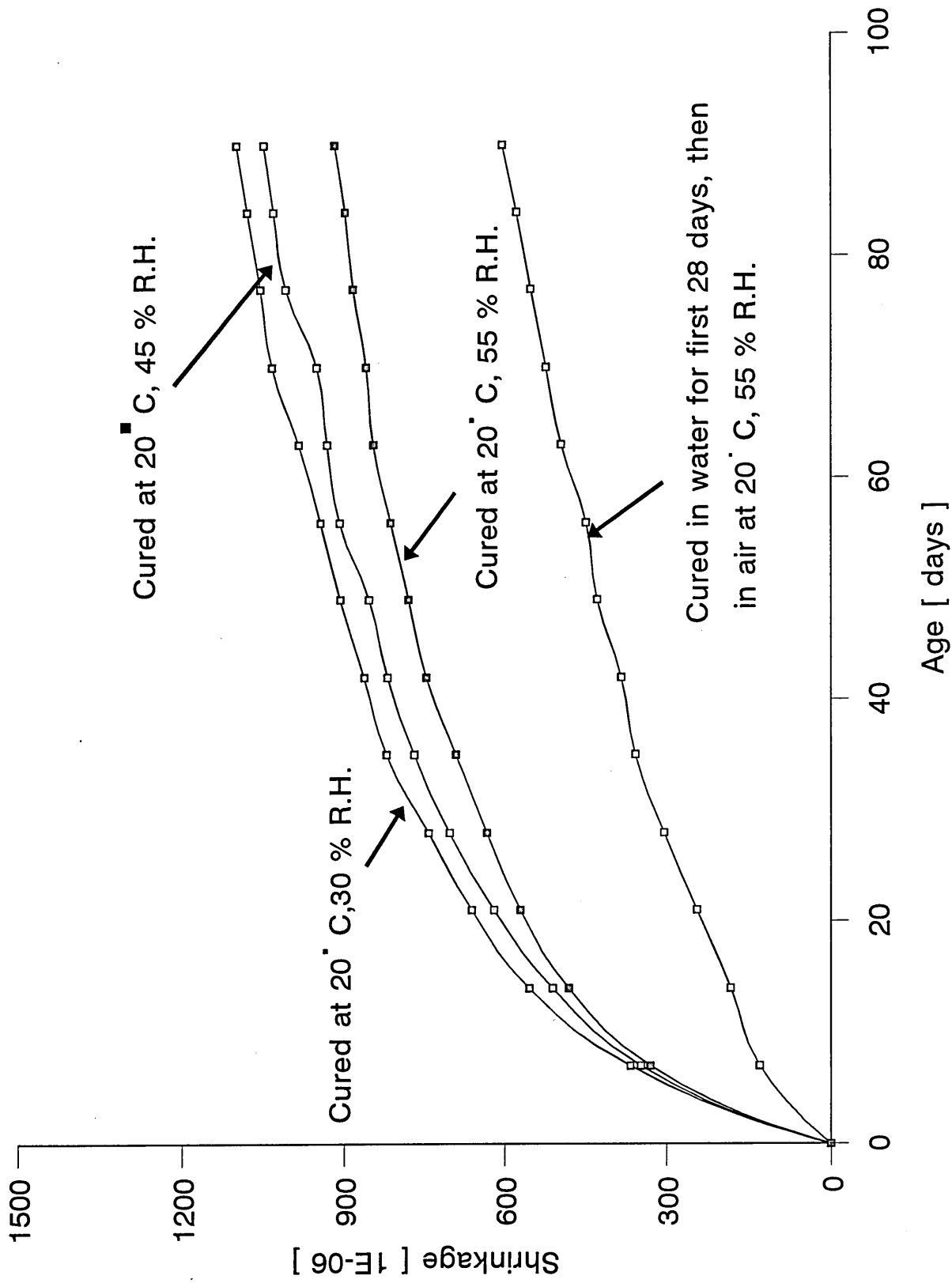


Figure 4.6
Influence of relative humidity on shrinkage of Material B

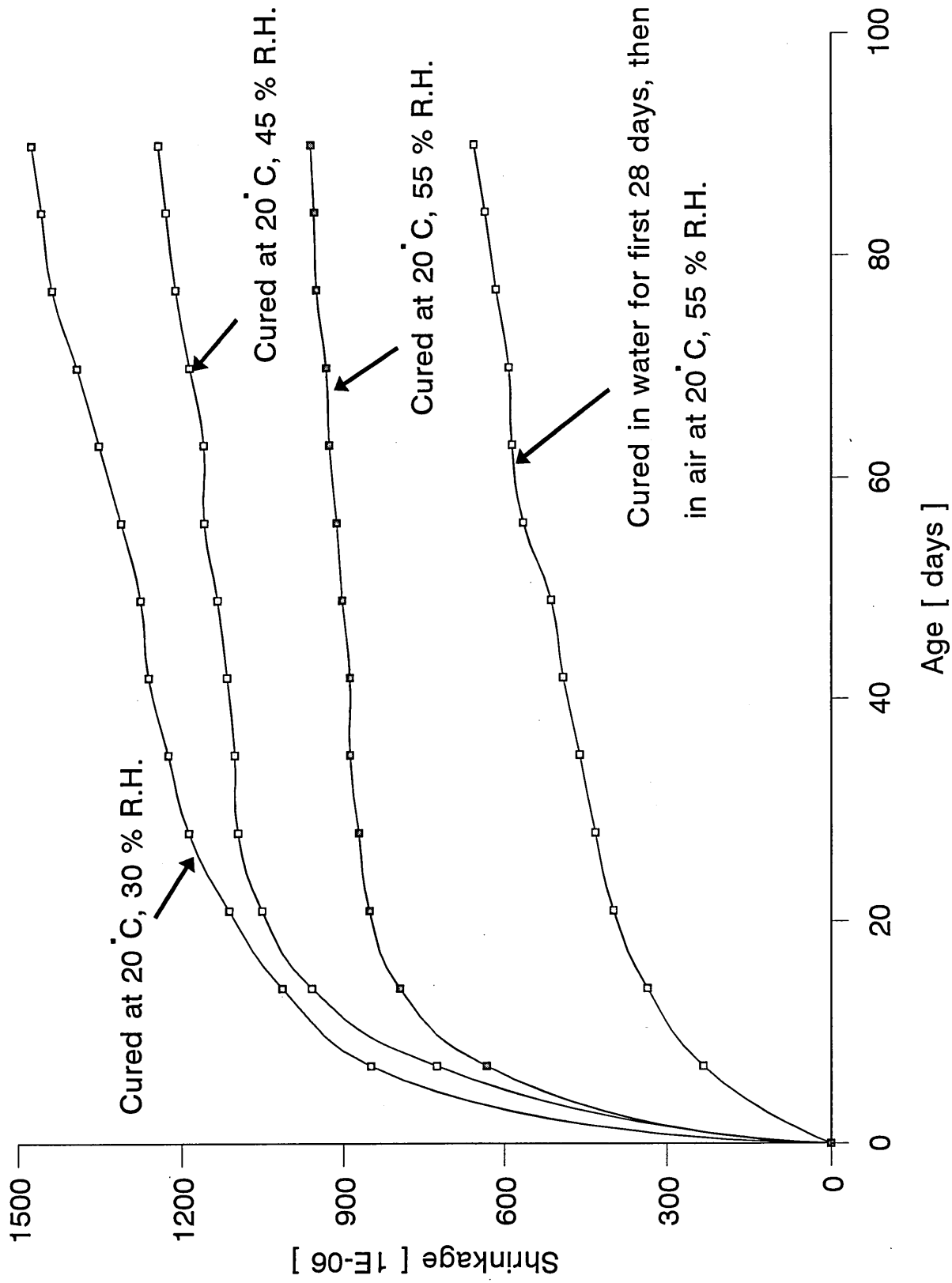


Figure 4.7
Influence of relative humidity on shrinkage of Material C

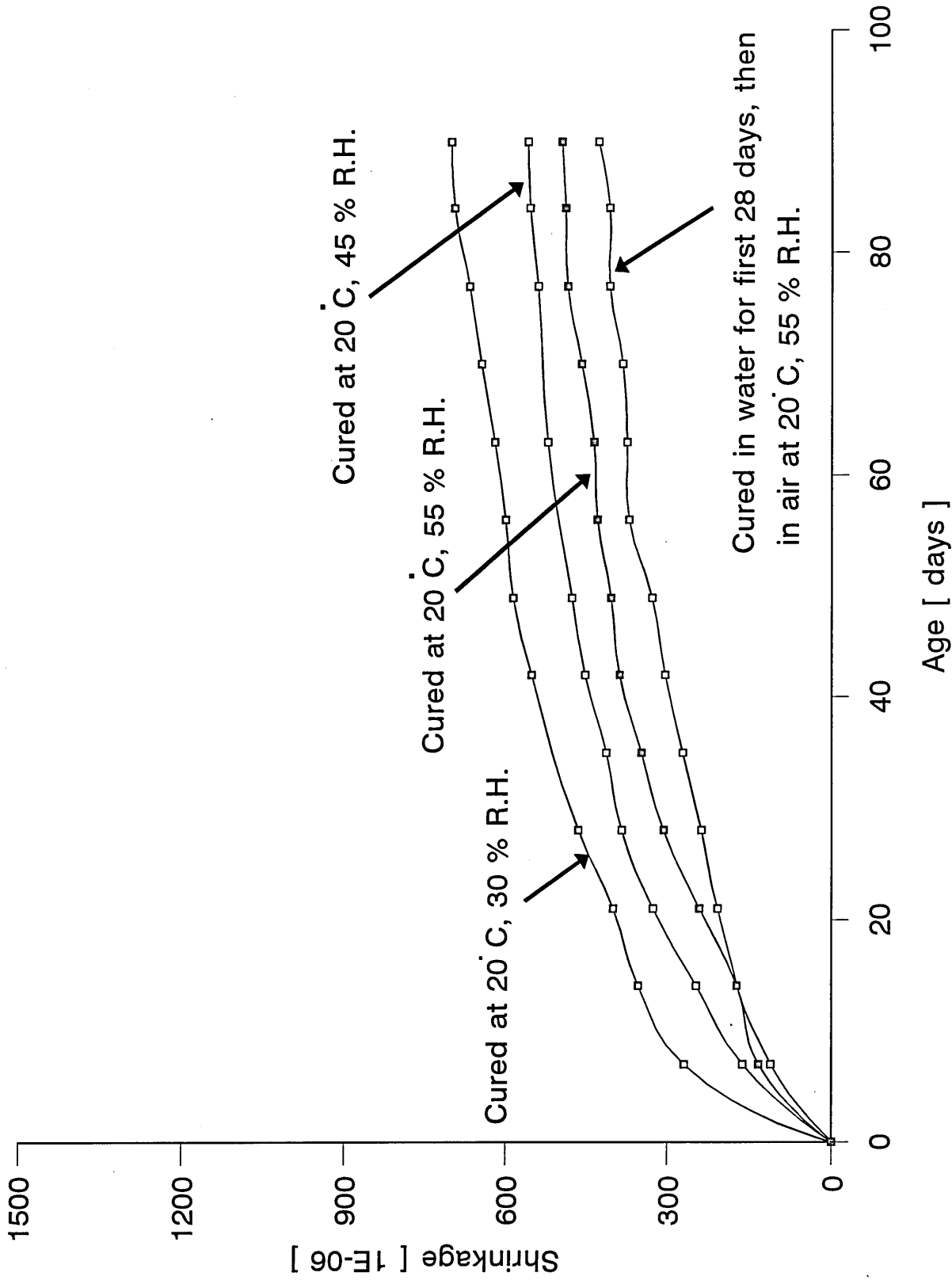


Figure 4.8
Influence of relative humidity on shrinkage of Concrete mix

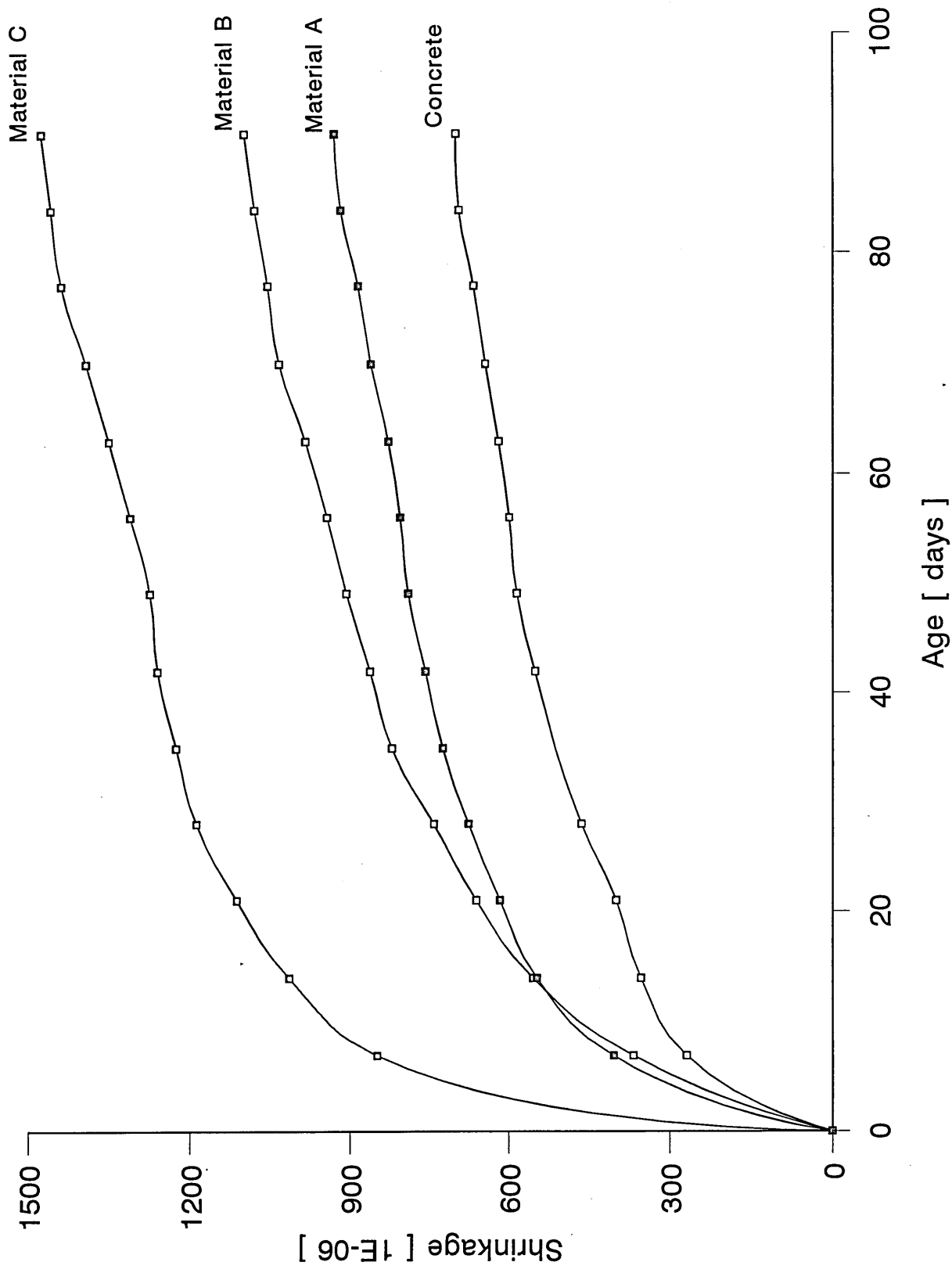


Figure 4.9
Relative shrinkage of repair materials under curing condition of 20 C, 30% R.H.

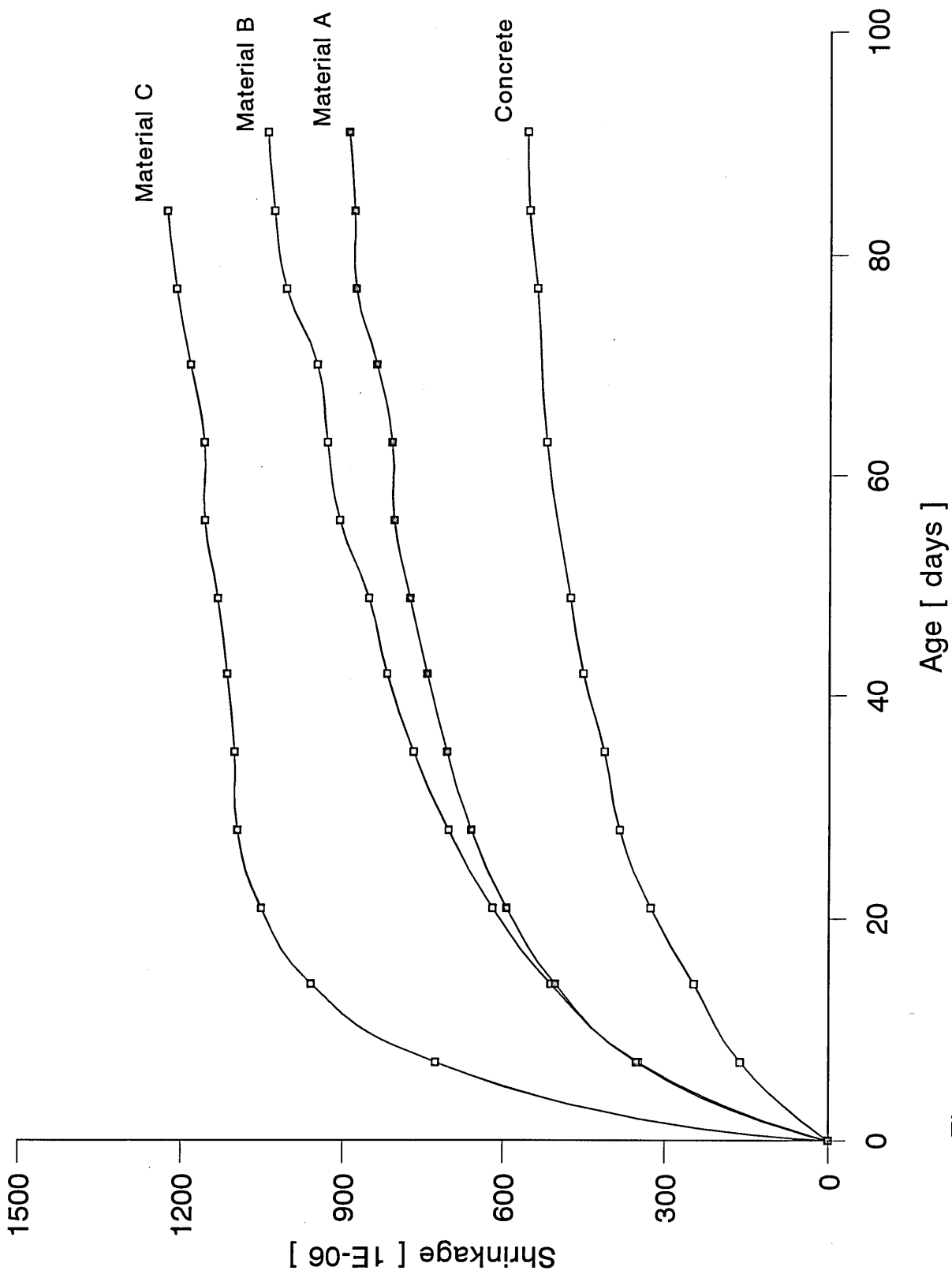


Figure 4.10
Relative shrinkage of repair materials under curing condition of 20°C, 45% R.H.

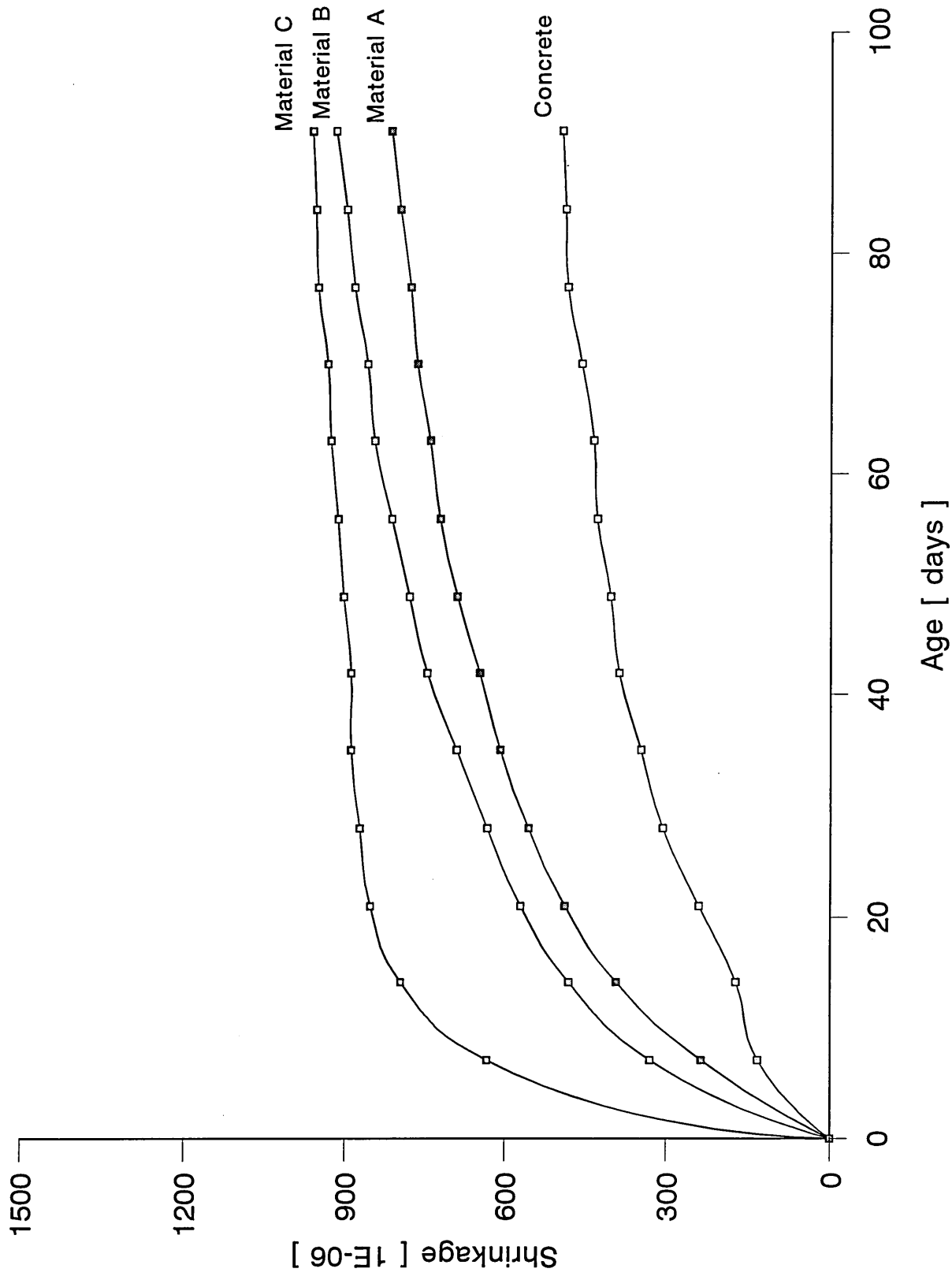


Figure 4.11
Relative shrinkage of repair materials under curing condition of 20°C, 55% R.H.

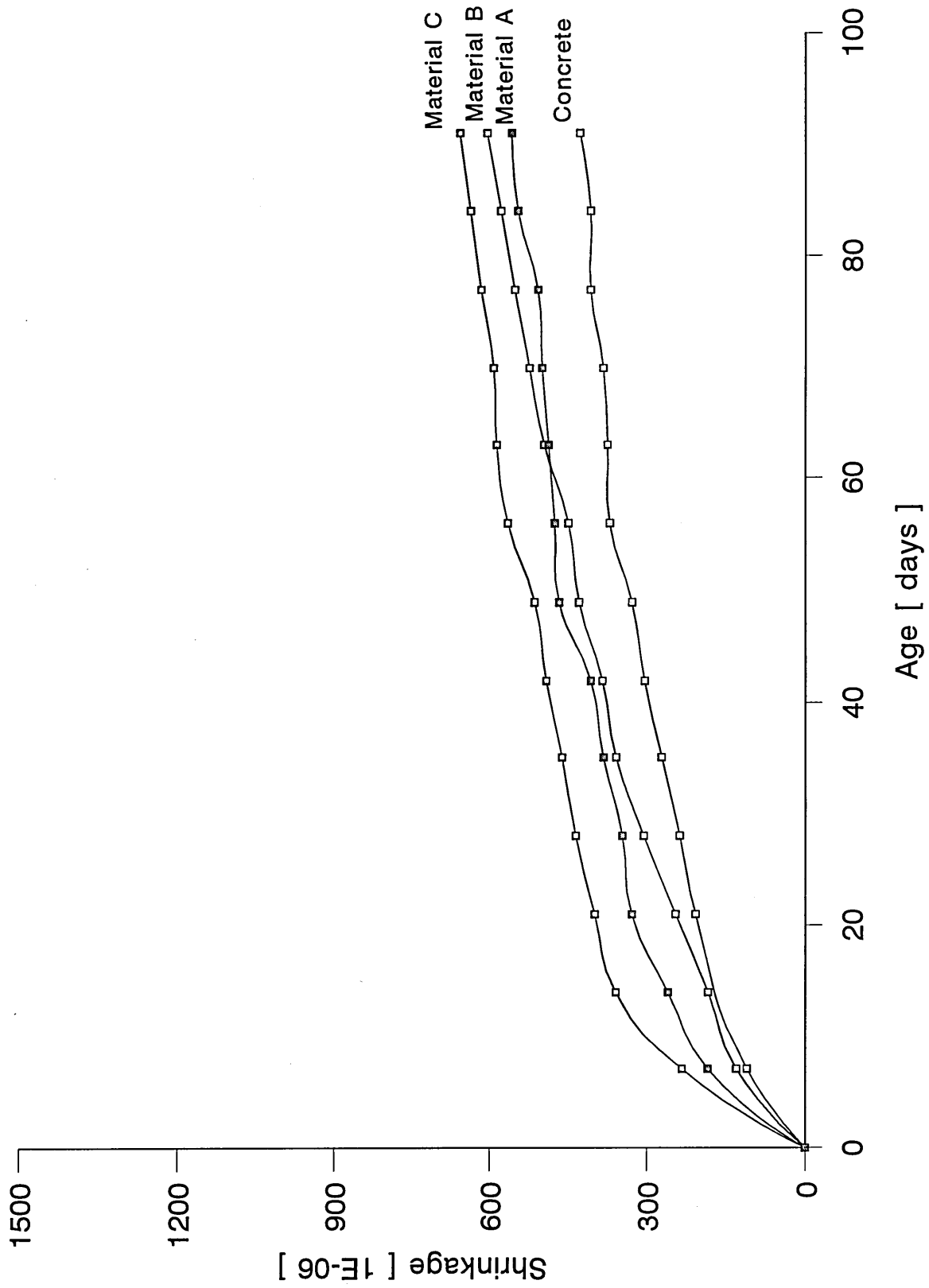


Figure 4.12
 Relative shrinkage of repair materials, water cured at 20°C for first 28 days followed by 20°C, 55% R.H. curing

In figure 4.4, for 20°C, 55% RH curing, material C leads to an 88 percent increase in shrinkage relative to the control concrete mix at 210 days age. The corresponding increase for materials A and B is 64 and 78 percent. The presence of aggregate size particle in repair material A influences shrinkage deformation. It is quite clear from the grading curves of repair materials (section 3.3.1, chapter 3) that, material A is much coarser than materials B and C. Also the grading of materials B and C are quite similar. Hence, the presence of small aggregates in material A has a higher influence on the shrinkage deformation compared to the other two materials. This is similar to the influence of aggregates on shrinkage of concrete [65,66]. For example, shrinkage (at 20°C and 55% R.H.) of the repair mortar A after 280 days is 1099.58 microstrain whereas the corresponding values for the other two repair materials B and C are 1181 and 1239.30 microstrain respectively, thus indicating increase of 8 and 13 percent.

Results of this investigation show the marked influence of moisture conditions of storage on length changes. The repair mortar modified with a polymer addition shows high shrinkage and swelling deformations compared with the other two repair materials and concrete. The relative humidity of the air surrounding the materials greatly affects the magnitude of shrinkage for materials A, B, C and concrete, as shown in Table 4.5 and figures 4.5 to 4.8. Also, these figures show that the shrinkage of specimens cured in water for the first 28 days, then stored in air at 20°C and 55 percent relative humidity, is lower than for specimens continuously cured at 20°C, 55% relative humidity after demoulding (24 hours after casting). This difference is much greater in repair materials A, B and C (figures 4.5 to 4.7) compared with plain concrete (figure 4.8). These figures also show that shrinkage of repair materials is much more sensitive to relative humidity of exposure compared to plain concrete. This is especially the case for material C (figure 4.7). For example, the increase

in shrinkage under curing at 30% relative humidity relative to 55% relative humidity curing is much greater in this repair material compared with plain concrete. The difference is even more pronounced when shrinkage at 30% relative humidity is compared with specimens cured in water for the first 28 days, then in air at 55% relative humidity. It is clear from these figures that all the repair materials used in this investigation shrink more in comparison with normal grade substrate concrete. The risk of shrinkage cracking with use of these repair materials in practical situation is, therefore, greater.

The shrinkage of repair materials A, B and C at 70 days (from figures 4.5 to 4.7) increase by 12, 17 and 37 percent respectively as relative humidity decreases from 55 percent to 30 percent (at constant temperature 20°C). The corresponding increment for concrete is 18 percent.

4.4.2 Creep of concrete and repair materials

In this study, the specimens were kept under sustained stress level ranging from 0.3 to 0.55 of the cube strength, for a period of 90 days. All creep strains are an average of four specimens. Some typical creep curves of the four materials at stress/strength ratios of 30, 45 and 55 percent are plotted in figures 4.13 to 4.16, showing the instantaneous elastic strain upon loading and the rate at which creep strains increase with time and the recovery upon unloading. The shape of the curves for each material is similar thus indicating that the creep phenomenon in each case is basically the same. The instantaneous elastic strains and the 90 days creep strains are given in Table 4.7.

From figures 4.14 and 4.15, the creep (at stress/strength ratio 0.30) of mineral based cementitious material B is 1212 microstrain whereas the corresponding value for repair material C is 1871 microstrain, thus indicating an increase of 52%. Similarly in the case of

45% stress/strength ratio, creep of repair material B is 2161 microstrain, whereas the corresponding value for repair material C is 2552 microstrain, thus indicating an increase of 17 percent.

The creep strains with time for the various materials are plotted in figure 4.17 to 4.19 which show creep strains of the repair materials relative to the plain concrete. The porous mineral based repair material B, with no additives, shows comparatively low creep strains, as does the high strength and high stiffness repair material A. The creep of the control plain concrete after 90 days under load, at stress/strength ratio of 30%, is 1446 microstrain (Table 4.7) whereas for repair materials A and B creep strains are 1217 and 1212 microstrain respectively, thus indicating decreases of 16 and 18 percent respectively relative to plain concrete.

Repair material C shows the greatest creep strains (e.g. 1871, 2552 and 3137 microstrain at stress/strength ratio of 30%, 45% and 55% respectively) due to the addition of latex modifiers in its preparation. Similar evidence of high creep strain for vinyl acetate polymer modified cementitious material is given by data from Emberson and Mays [13].

It can be seen from figures 4.13 to 4.16 and Table 4.7 that the creep of repair materials is more sensitive to stress/ strength ratio than plain concrete. For example, the results in figure 4.16 show that in the case of concrete, the difference in creep strain at 30%, 45% and 55% stress/strength ratios is smaller than the repair materials A, B, and C (figures 4.13 to 4.15). Similarly, Table 4.6 shows that at stress/strength ratio of 0.30, the creep of concrete is significantly greater than that of repair materials A and B. At 45% and 55% stress/strength ratio, however, the creep strain of materials A and B are quite similar or greater than that of concrete.

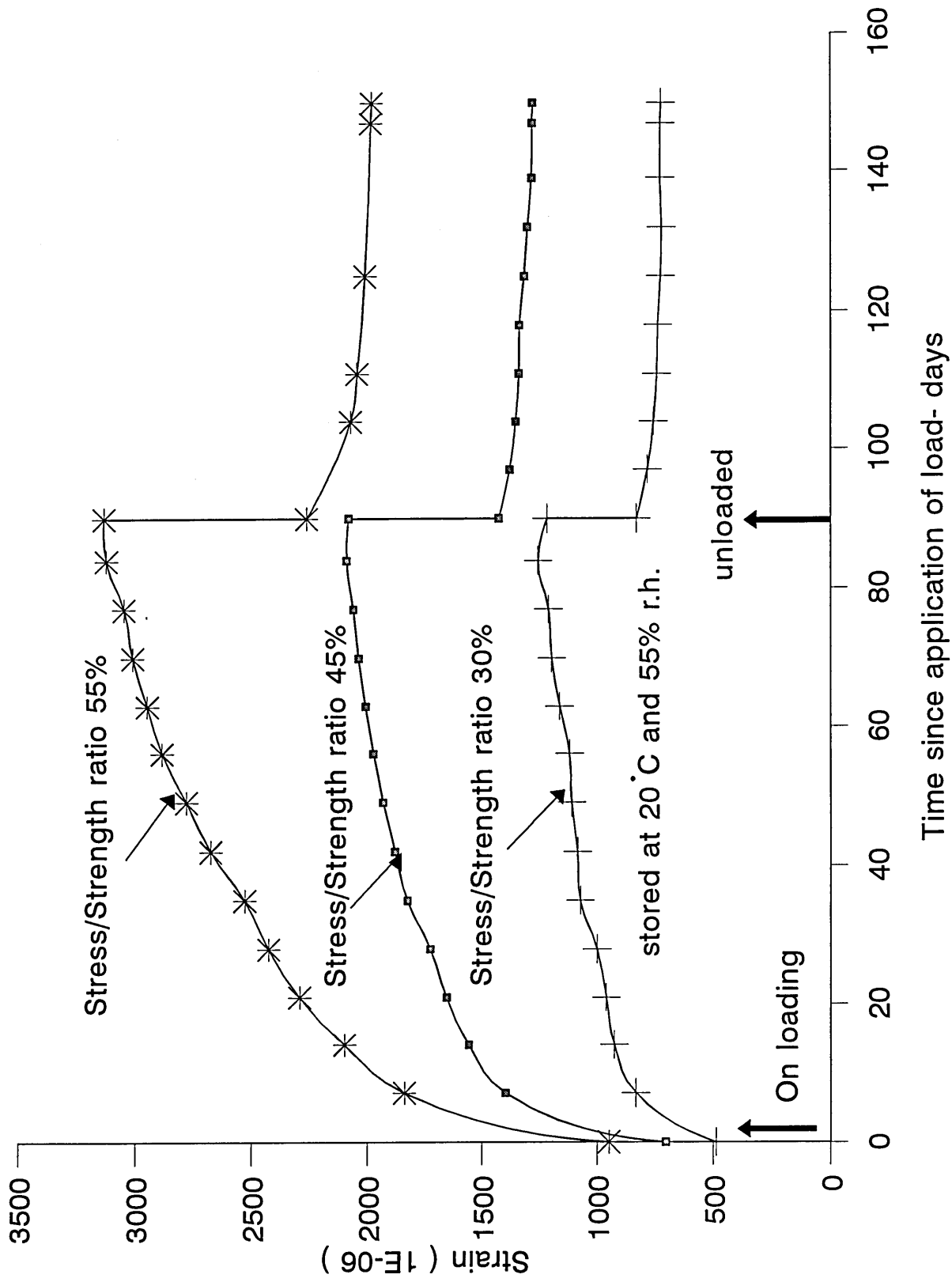


Figure 4.13
 Compression creep curves at applied stress/strength ratios of 30%, 45% and 55% for Material A

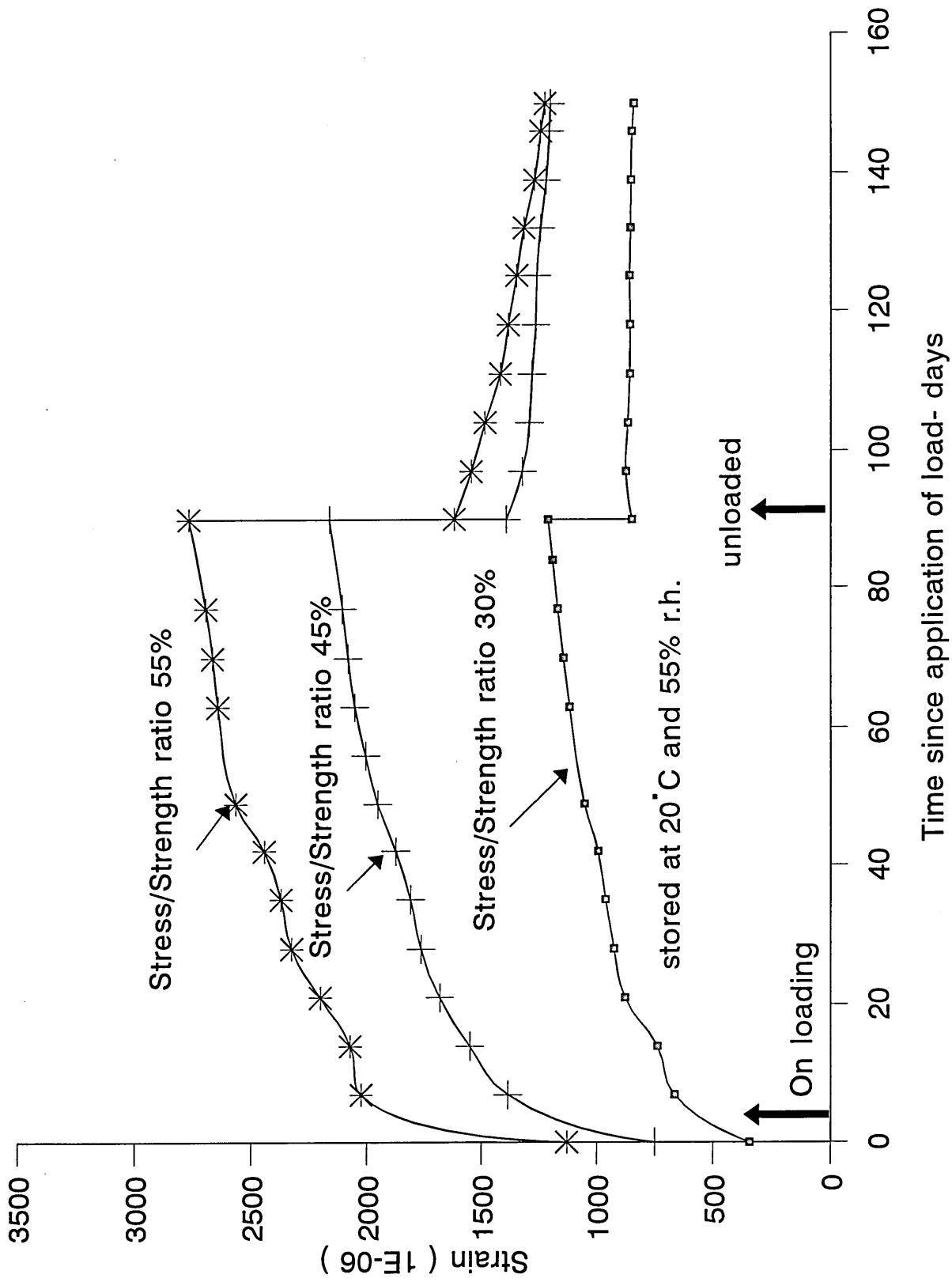


Figure 4.14
 Compression creep curves at applied stress/strength ratios of 30%, 45% and 55% for Material B

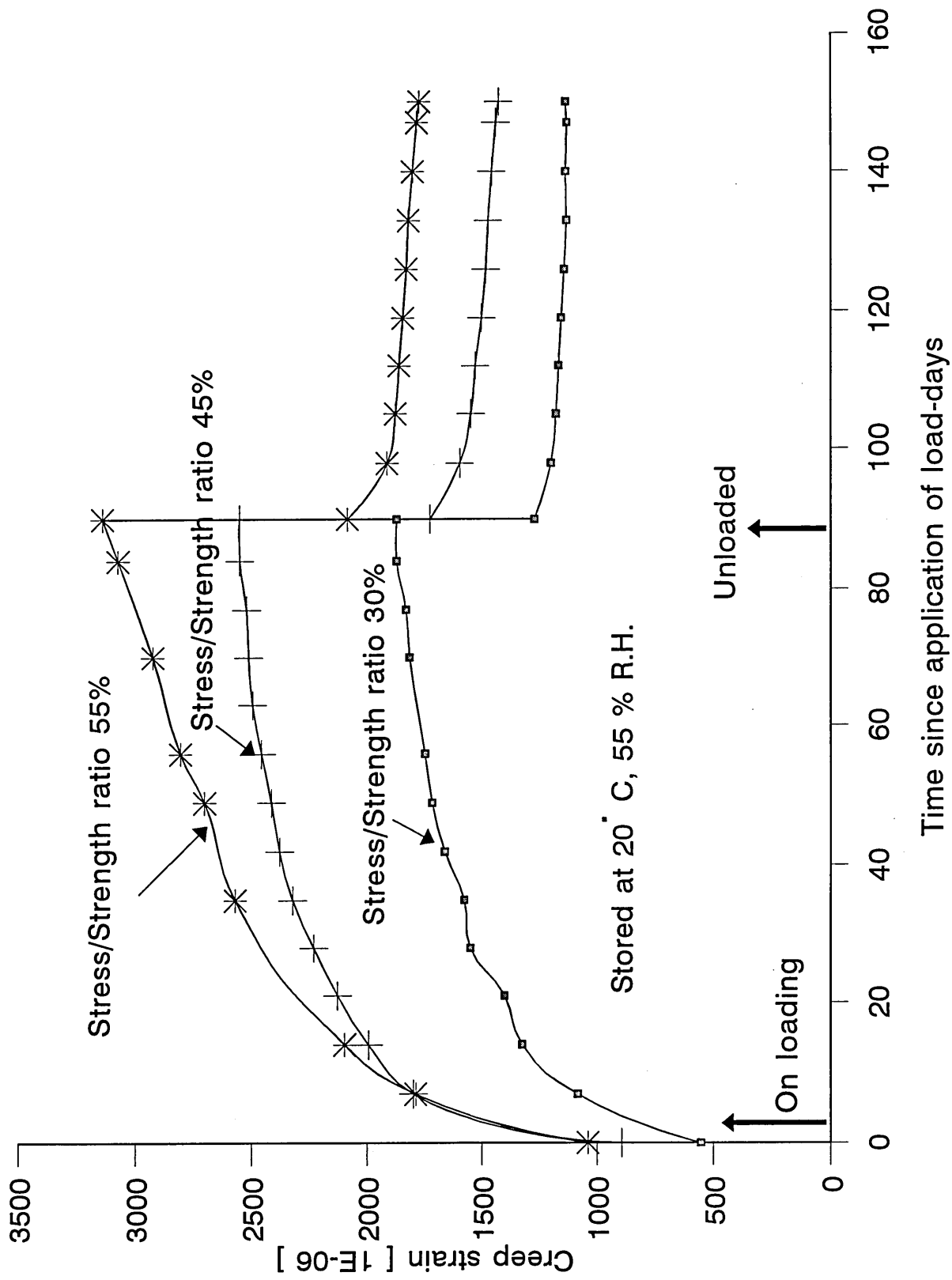


Figure 4.15
Compression creep curves at applied stress/strength ratios of 30%, 45% and 55% for Material C

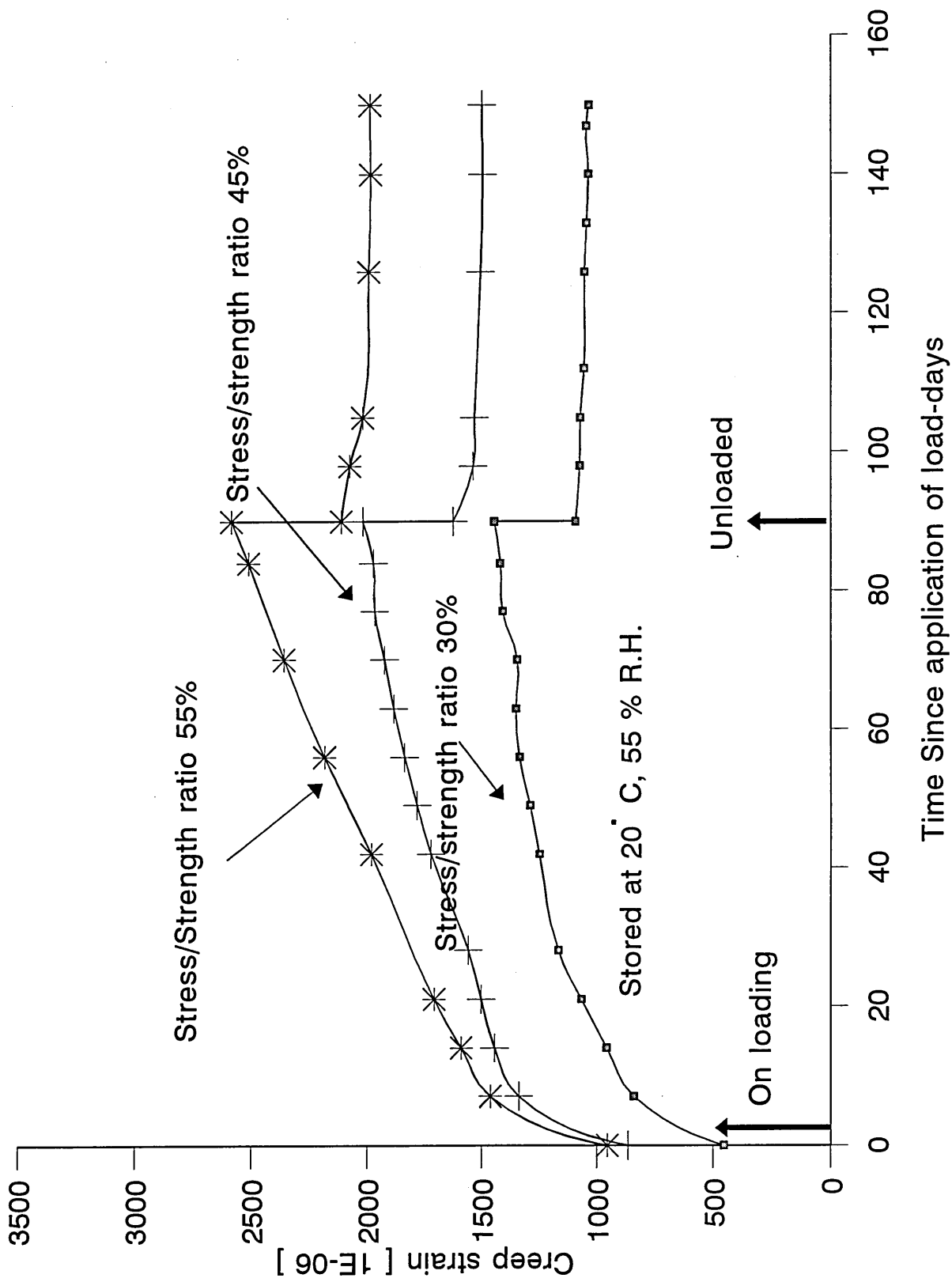


Figure 4.16
 Compression creep curves at applied stress/strength ratios of 30%, 45% and 55% for Concrete mix

Table 4.7

Creep strains at 90 days, instantaneous elastic strains on loading (microstrain) and cube strength prior to loading.

| Repair Materials → | | A | B | C | Conc. |
|----------------------------|--|------|------|------|-------|
| 30% stress/ strength | Cube strength (N / mm ²) | 60 | 33 | 40 | 38 |
| | Instantaneous elastic strain | 488 | 442 | 553 | 454 |
| | creep strain | 1217 | 1212 | 1871 | 1446 |
| 45% stress/ strength | Cube strength (N / mm ²) | 60 | 37 | 43 | 40 |
| | Instantaneous elastic strain | 704 | 749 | 893 | 866 |
| | creep strain | 2078 | 2161 | 2552 | 2148 |
| 55% stress/ strength | Cube strength (N / mm ²) | 63 | 36 | 38 | 35 |
| | Instantaneous elastic strain | 949 | 1129 | 1039 | 954 |
| | creep strain | 3129 | 2767 | 3137 | 2732 |

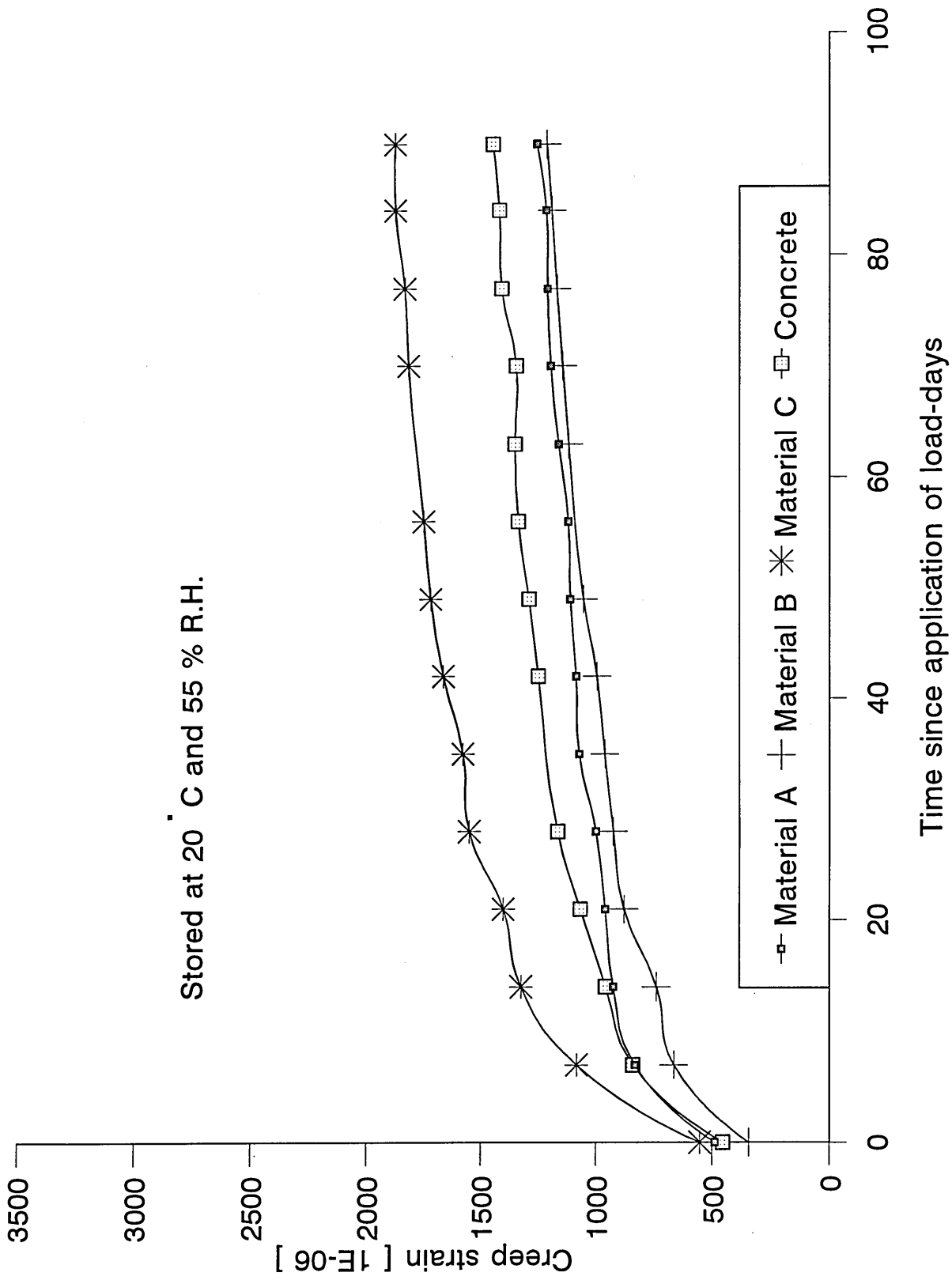


Figure 4.17
 Compression creep test results at 30% stress/strength ratio

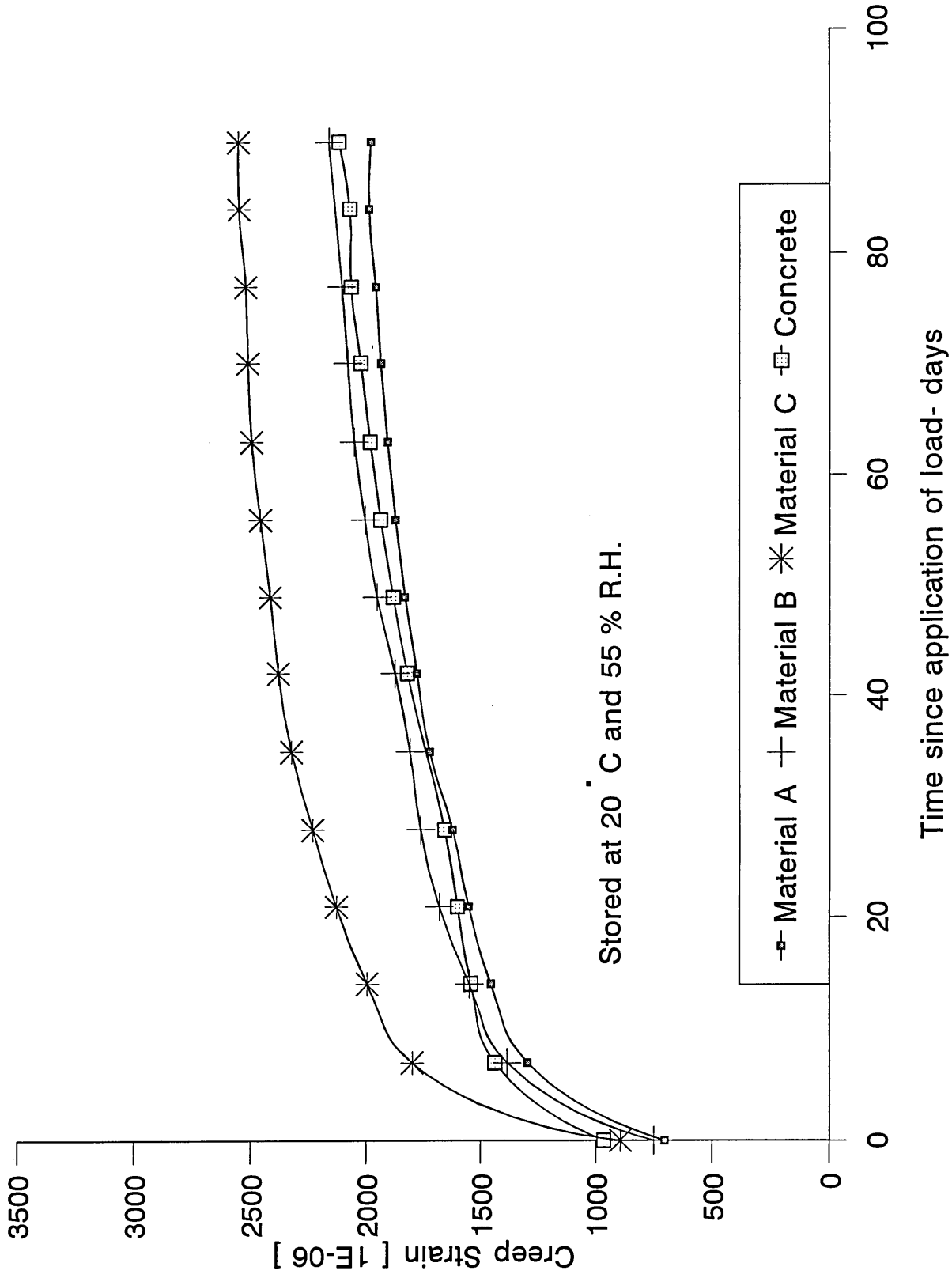


Figure 4.18
 Compression creep test results at 45% stress/strength ratio

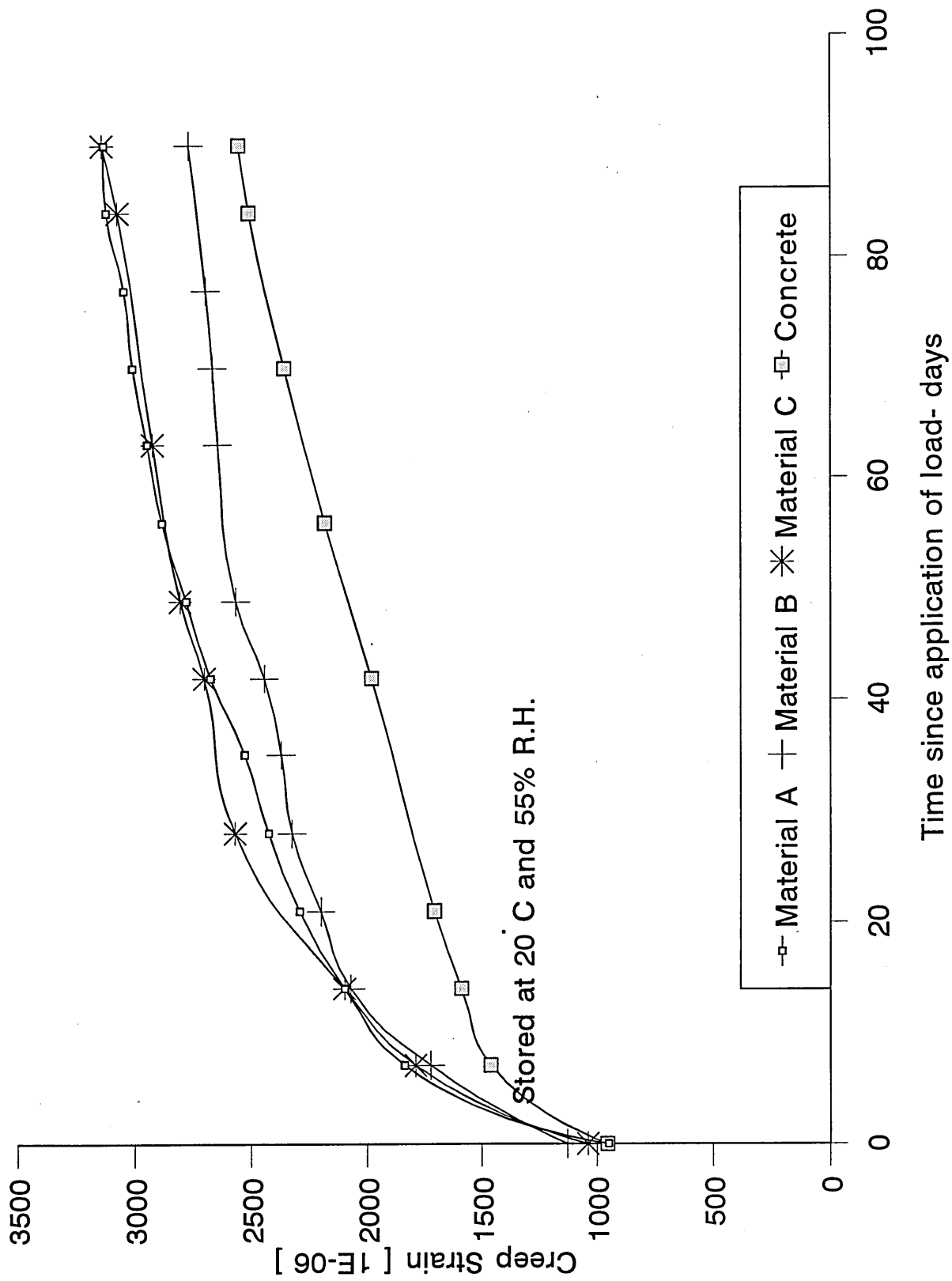


Figure 4.19
 Compression creep test results at 55% stress/strength ratio.

4.4.3 Analytical expressions for shrinkage and creep deformations

Various analytical expressions have been reported for the shrinkage and creep of cement-based materials [26,75,76] which enable the prediction of long-term strains from relatively short term experimental data. Hyperbolic and logarithmic expressions reported in literature have been found to fit experimental results generally very well and are commonly used. In this investigation, the hyperbolic and logarithmic expressions recommended by Illston and Pomeroy [26], are used to investigate their correlation with the experimental data on repair materials.

Hyperbolic Expression :

$$\epsilon = \frac{t}{a+bt} \quad (4.1)$$

Logarithmic Expression :

$$\epsilon = a' + b' \log(1+t) \quad (4.2)$$

Where,

ϵ = Free shrinkage (ϵ_s) or creep Strain (ϵ_c)(microstrain)

t = Age (days) for shrinkage data, and

Age under load (days) for creep deformation

a , b , a' and b' are constants.

By plotting the experimental data for (t/ϵ_s) and (t/ϵ_c) against t for the expression in equation 4.1 (hyperbolic) and (ϵ_s) or (ϵ_c) against $\log(1+t)$ for the expression in equation 4.2 (logarithmic), constants a , b , a' and b' are determined for the experimental shrinkage and creep curves. The results in Table 4.8 and 4.9 gives the values of these constants.

Table 4.8 Details of hyperbolic expression for shrinkage and creep

(at 30% stress/strength ratio)

| Repair Materials | Constants | | | |
|---------------------|-----------|---------|--------|---------|
| | Shrinkage | | Creep | |
| | a_s | b_s | a_c | b_c |
| A | 22,714 | 1035.90 | 18,820 | 1085.83 |
| B | 17,143 | 864.51 | 20,950 | 974.01 |
| C | 4,400 | 1030.76 | 12,630 | 814.89 |
| Concrete | 53,210 | 1429.69 | 14,286 | 855.53 |

Table 4.9 Details of logarithmic expression for shrinkage and creep

(at 30% stress/strength ratio)

| Repair Materials | Constants (X 10 ⁻⁶) | | | |
|---------------------|----------------------------------|--------|---------|--------|
| | Shrinkage | | Creep | |
| | a'_s | b'_s | a'_c | b'_c |
| A | -244.45 | 535.19 | -39.67 | 360.81 |
| B | -177.93 | 552.76 | -300.0 | 550.93 |
| C | -456.69 | 269.87 | -105.26 | 546.43 |
| Concrete | -237.50 | 377.80 | -155.68 | 555.40 |

The graphs in figures 4.20 to 4.23 show the comparison between the experimental and predicted shrinkage and creep values (at 30% stress/strength ratio) from the hyperbolic expression (equation 4.1) and logarithmic expression (equation 4.2) for the three repair materials and the concrete mix. Also some typical comparison for higher stress/strength ratios (45% and 55%) are shown in figures 4.24 and 4.25. It is evident from these results that both these expressions are in good agreement with the experimental results. The maximum percentage error between the experimental and calculated deformations at ages beyond 14 days are listed in Table 4.10.

Table 4.10 Maximum percentage error for both expressions

| Repair Materials | Maximum % error | | | | | |
|---------------------|-------------------------------------|-------|-----|-------------------------------------|-------|-----|
| | Hyperbolic expression | | | Logarithmic expression | | |
| | Shrinkage (20°C and 55% r.h.) | Creep | | Shrinkage (20°C and 55% r.h.) | Creep | |
| | | 30% | 55% | | 30% | 55% |
| A | 4 | 5 | 4 | 3 | 7 | 8 |
| B | 7 | 3 | 2 | 2 | 4 | 6 |
| C | 5 | 8 | 7 | 2 | 10 | 10 |
| Concrete | 4 | 3 | 2 | 1 | 4 | 5 |

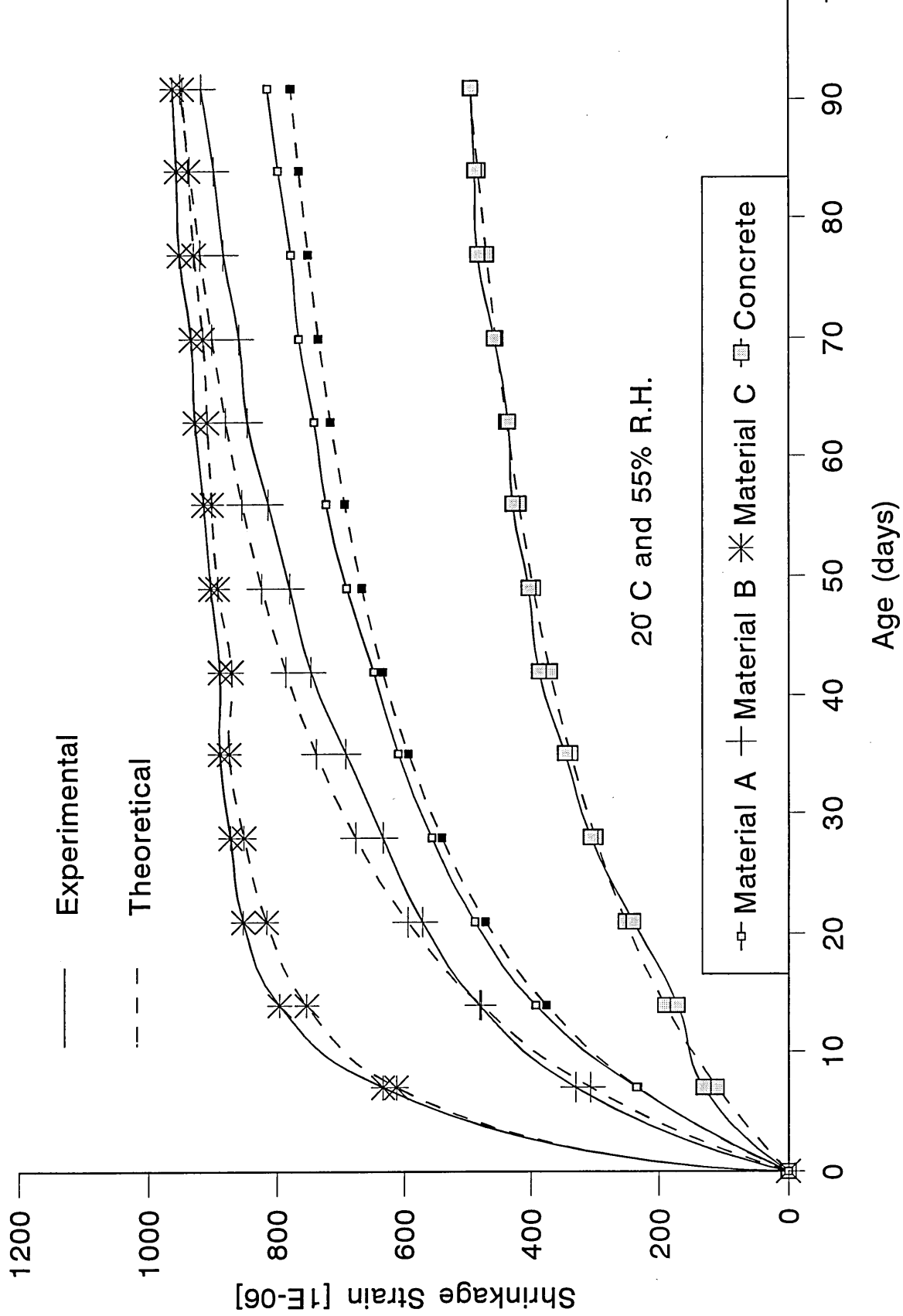


Figure 4.20 Comparison between the experimental and theoretical shrinkage curves based on the hyperbolic expression

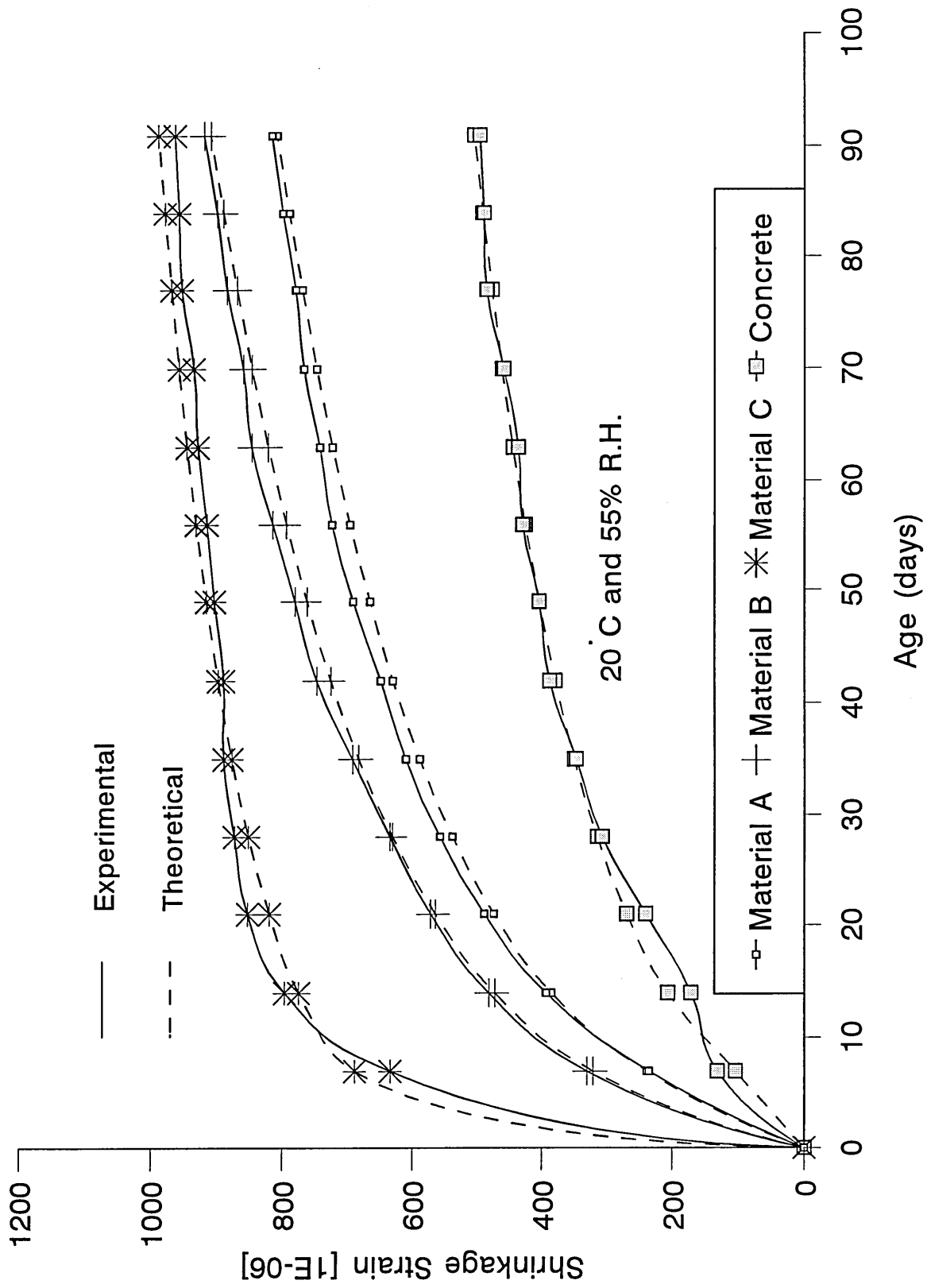


Figure 4.21 Comparison between the experimental and theoretical shrinkage curves based on the logarithmic expression

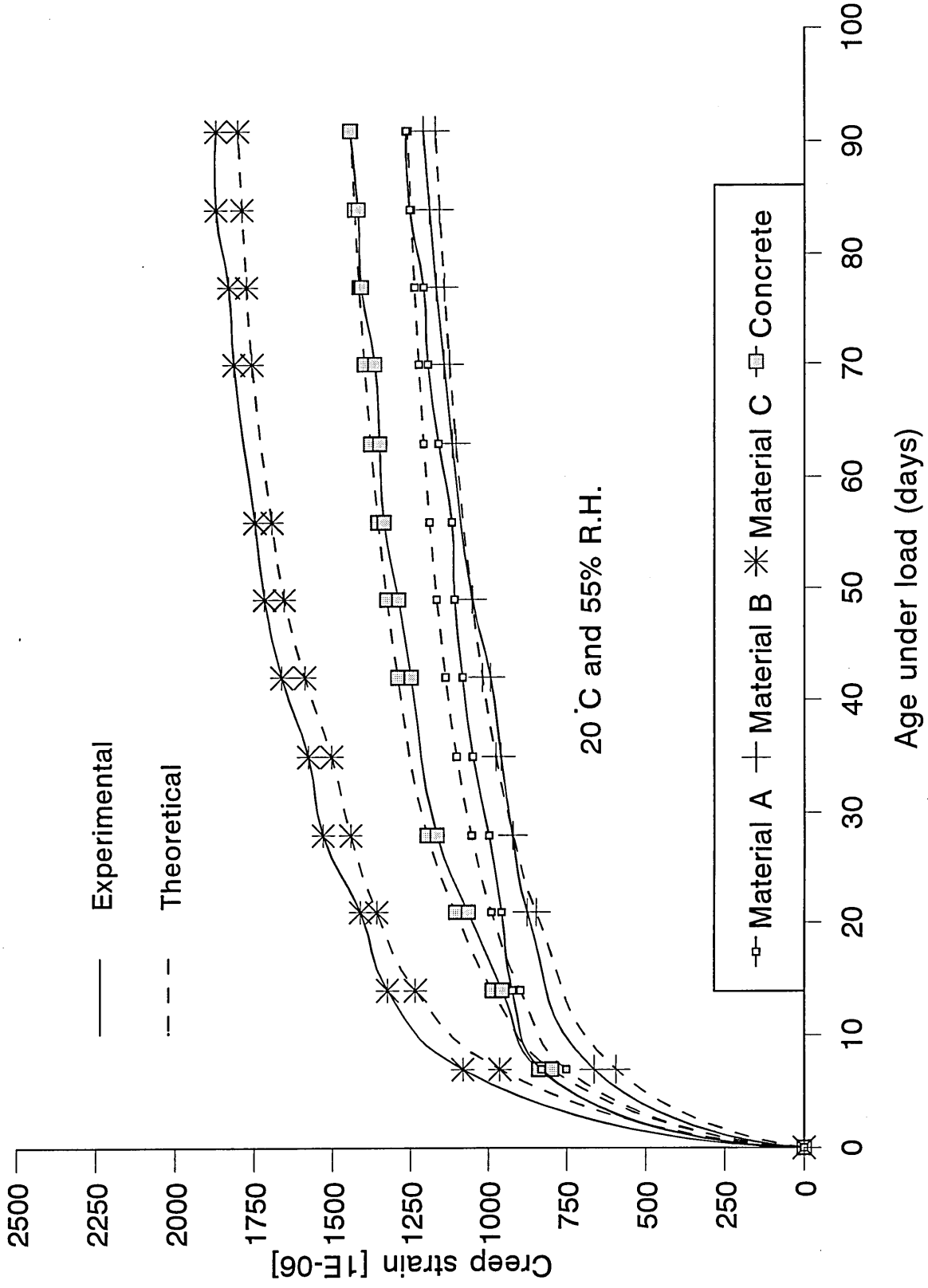


Figure 4.22 Comparison between the experimental and theoretical creep curves based on the hyperbolic expression [30% stress/strength ratio]

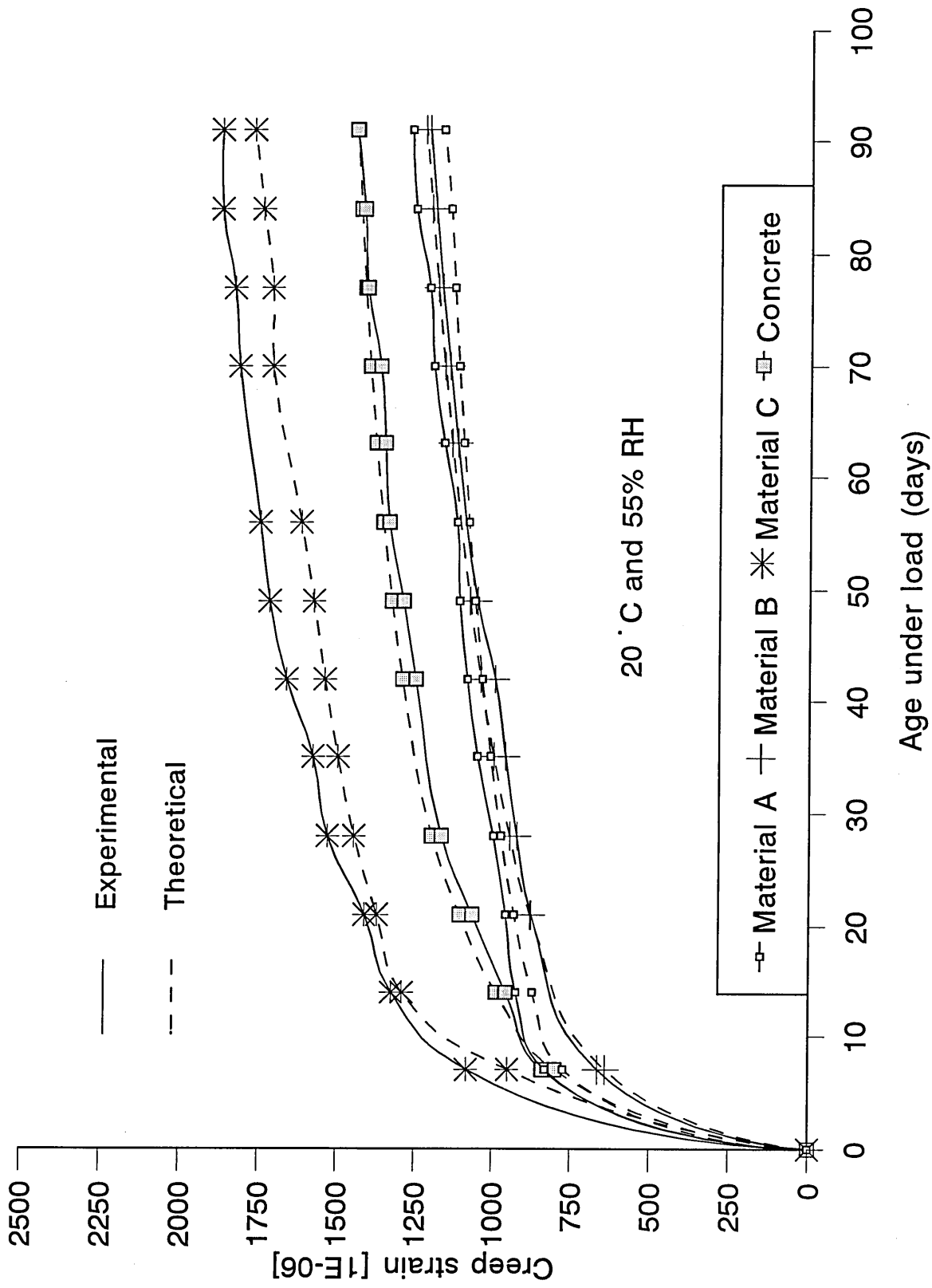


Figure 4.23 Comparison between the experimental and theoretical creep curves based on the logarithmic expression [30% stress/strength ratio]

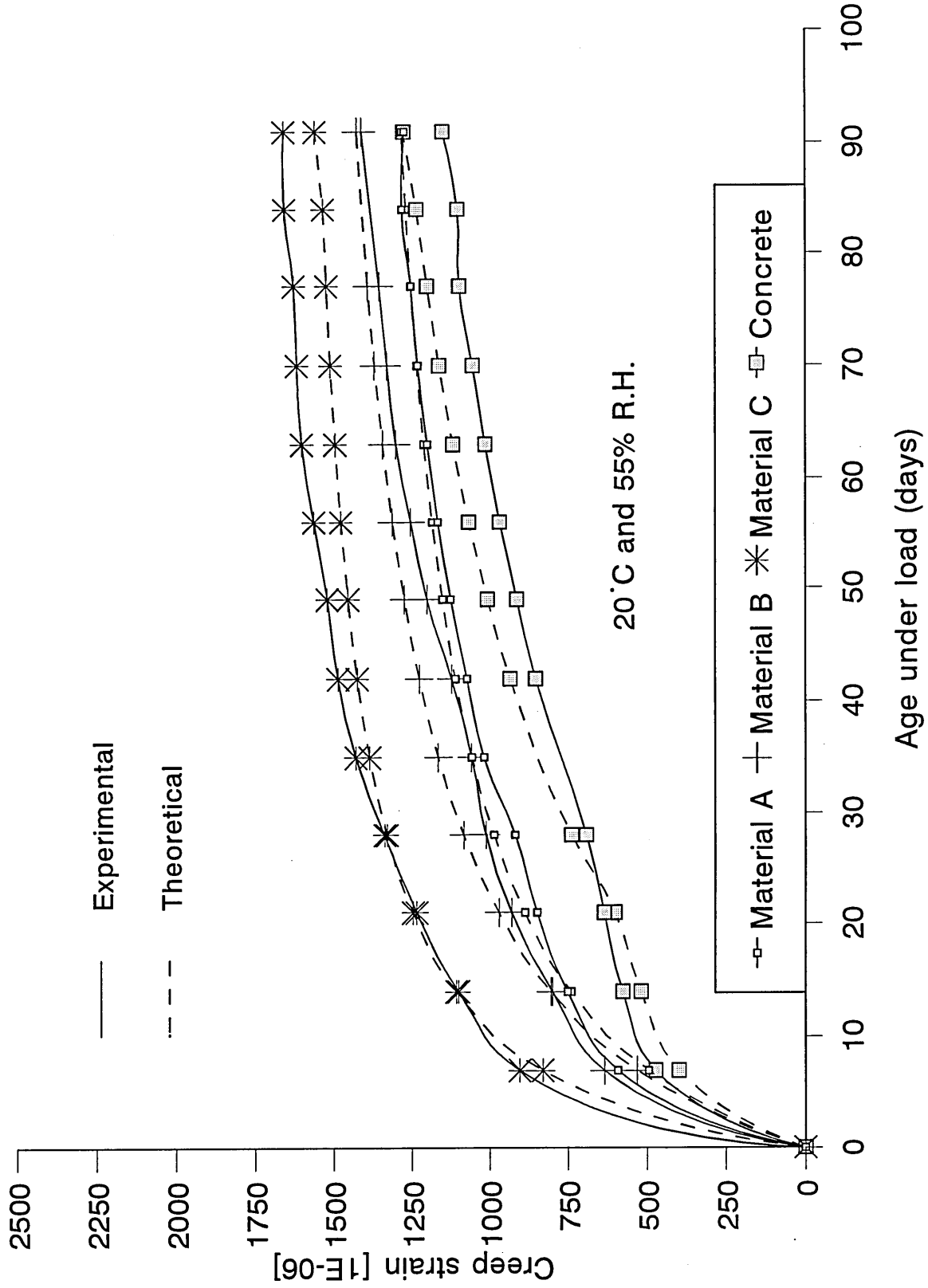


Figure 4.24 Comparison between the experimental and theoretical creep curves based on the hyperbolic expression [45% stress/strength ratio]

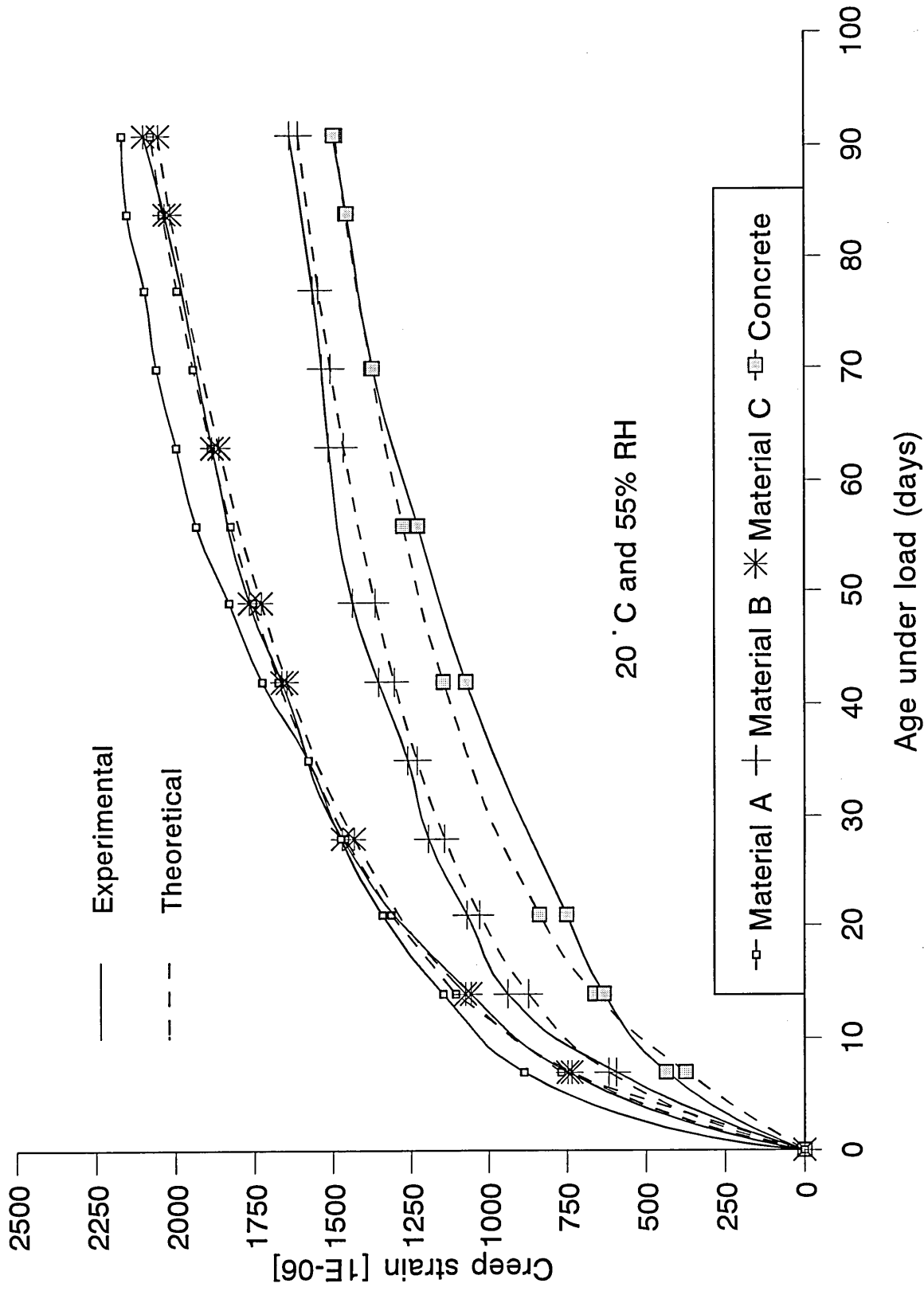


Figure 4.25 Comparison between the experimental and theoretical creep curves based on the logarithmic expression [55% stress/strength ratio]

For efficient long-term structural interaction, shrinkage and creep properties of repair material should not differ significantly from those of the substrate concrete. For example, from the results of material C it is clear that the shrinkage deformation of this material is extremely high. This would lead to unacceptably high tensile strains at the interface with the substrate with the consequent danger of cracking and adhesion failure. The high creep strains of material C relative to concrete, on the other hand, would help in reducing the tensile strains at the interface.

4.5 CONCLUSIONS

The following conclusions are based on the experimental results reported in this chapter:

1. Drying shrinkage is greatest in the cementitious repair mortar which contains a styrene acrylic copolymer despite the presence of some fibre additives in this material. In all repair materials, most of the shrinkage occurs within the first 21 days and remains relatively stable beyond that age.
2. The shrinkage of specially formulated repair mortars, especially those modified with a polymer admixture, is much more sensitive to relative humidity of curing than plain concrete. As a consequence such repairs will be much more prone to shrinkage cracking in a dry environment compared with plain concrete.
3. Compressive creep strains are also greatest for the generic repair mortar which contains styrene acrylic copolymer.

4. High performance repair material A which contains aggregates of a relatively coarser particle size has less shrinkage and creep deformations than other repair mortars.

5. The relationship between shrinkage, creep and age (under load in case of creep) can be represented by the following hyperbolic and logarithmic expressions which are normally used for plain concrete:

Hyperbolic Expression :

$$\epsilon = \frac{t}{a+bt}$$

Logarithmic Expression :

$$\epsilon = a' + b'\log(1+t)$$

CHAPTER 5

CHLORIDE DIFFUSION INTO CONCRETE AND REPAIR MATERIALS

5.1 INTRODUCTION

Although most reinforced concrete structures have shown good durability over long periods of time, the problem of corrosion of reinforcement exists in many structures. Chloride induced corrosion of reinforcement is one of the major causes of deterioration in reinforced concrete structures. Structural members damaged as a result of reinforcement corrosion are often reinstated by applying repair materials. However, this is usually successful in the long-term only if the cause of the original damage has been eliminated, and appropriate materials have been selected and properly applied.

There are a number of potential sources of chloride ions to which concrete may be exposed while in service. Many reinforced concrete structures exposed to marine or other chloride bearing environments show the typical cracking and spalling caused by corrosion of reinforcing steel near the concrete surface, even after a few years of service. Field observations and tests confirm that high chloride-ion concentrations in the vicinity of the reinforcing steel near the concrete surface are the main cause for the early onset of corrosion. So the presence and concentration of chloride ions in the vicinity of the steel determine the rate at which corrosion takes place. The concrete (or repair in case of repaired member) cover to reinforcement should therefore have the properties required to form a physical and chemical barrier against the penetration of deleterious substances such as chloride and carbon dioxide. The penetration of chloride depends on the permeability of material used as a cover to the reinforcement.

The financial implications of deterioration caused by corrosion in new and repaired concrete construction demand that careful methods of maintenance and assessment of these structures should be available. Information obtained from regular inspection surveys should enable the prediction of long-term initiation and propagation rates of corrosion in the reinforcement.

In this chapter an investigation is reported which studies chloride diffusion characteristics into plain concrete and repair materials of various constituents, and it is part of a multistage research programme dealing with corrosion of repaired reinforced concrete. The first part of this chapter deals with the chloride diffusion property of specimens initially cured in one of the four curing condition for 28 days prior to exposure to chloride environment. The second part of this investigation is concerned with specimens exposed to chloride environment at 24 hours after casting. A standard computer package [88] was used to perform a non-linear regression analysis of the experimental data on chloride concentration in order to generate the material parameters diffusion coefficient (D_c) and surface chloride concentration (C_0).

An analysis of chloride concentration profiles obtained for the three generic repair materials and plain concrete at various ages revealed the time dependency of the effective diffusion coefficient of chloride ions in to the materials. This is discussed in relation to Fick's second law of diffusion and an enhanced model is derived for the prediction of acid soluble chloride concentration in the repair materials. Prior to reporting results of this investigation, a literature review has been made on the chloride penetration into concrete.

It is generally agreed that the ingress of chloride ions into concrete leads, in many instances, to long-term deterioration of concrete structures. This is a major problem in highway bridges in the UK due to the use of de-icing salts for winter maintenance [77-79]. The findings of the Wallbank report [80] on bridges suggest that almost 75% of motorway and trunk road bridges are suffering from chloride contamination involving chloride levels greater than 0.2% (by weight of cement). Many of these bridges are less than 20 years old.

There are a number of potential sources of chloride ions to which concrete may be exposed while in service. Offshore structures are continually exposed to sea water and this is particularly hazardous in the splash zone where the wetting and drying cycles can result in very high concentrations of surface chloride. Some parts of the offshore structure are usually totally submerged in sea water, some parts are situated in the tidal zone which is subjected to wetting and drying and other parts are located in the atmospheric splash zone. Chlorides can penetrate to all different parts of the structure regardless of the zone but the rate of diffusion will be different. A more insidious source of chloride in concrete is calcium chloride which was often mixed with concrete to accelerate its setting time. This practice, however, is now strongly discouraged following the 1977 amendment to the code of practice [91]. Although many concrete structures erected prior to this amendment contain calcium chloride, the main sources of chloride in the future are likely to be the marine environment and deicing salts. Diffusion of chloride ions into hardened concrete (or repair patch) from these sources would thus pose the main durability concern for steel reinforcement. Furthermore, it has been suggested that when mixed with concrete, chloride combines chemically with the matrix to a greater extent than the chloride ions which diffuse through hardened material from an external environment [81,82]]. So, it is the free chloride ions

which are responsible for initiation of corrosion [83,84].

5.2.1 A chloride "Threshold" for corrosion

The service life of a concrete structure, with regard to corrosion of reinforcement in marine environment, can be considered as the sum of two stages [85,86]; the initiation period, during which the steel remains passive while chloride ions diffuse into the concrete surface, and the propagation period. The work by Hausmann [87] showed that there is a threshold concentration of chloride ion which must be exceeded before corrosion of steel is initiated. He suggested a threshold ratio of chloride ion activity to hydroxyl ion activity $[Cl^-]/[OH^-]$ of 0.6 in solution at the iron-matrix interface. The amount of chloride required for initiating corrosion is thus, in part, dependent upon the pH value of the liquid within the pore system of concrete. At a pH of less than 11.5, corrosion may occur without the presence of Cl^- while at a concrete pH greater than 11.5, a measurable amount of chloride is required to initiate corrosion. The amount of Cl^- required to induce corrosion increases as the pH at the iron - liquid interface increases. Table 5.1 shows a wide range of the "threshold" values suggested by various investigators [87,89-97]. It is difficult to establish a universal threshold level for chloride concentration, because of its dependence on many factors. These include pH, cement content, proportion of chloride present as chloride ions in pore fluid of concrete and the availability of oxygen. In the marine environment, the initiation period depends mainly on the amount of airborne chloride ion accumulation on the surface and on the rate at which they diffuse into the surface, until a threshold concentration has been reached that may cause depassivation and corrosion onset. Chloride in concrete, however, occurs in three forms namely free chloride ions, chloride bonded to calcium silicate hydrates (physically absorbed) and chloride combined in definite compounds such as calcium chloro-aluminate

| Source | Acid-soluble chloride (% by wt. of cement) | Water soluble chloride (% by wt. of cement) | Free Cl ⁻ (ppm) | Remarks |
|--|--|---|----------------------------|--|
| 1. ACI committee 222 on corrosion of metals in concrete [82] | 0.20 | | | |
| 2. ACI 318 (quoted in ref. [89]) | 1) 0.15 2) 1.00 3) 0.30 | | | 1) If exposed to chloride in service 2) If dry/protected from moisture 3) All other r.c.c construction |
| 3. Norwegian code NS 3474 (quoted in [82]) | 0.60 | | | |
| 4. Hausmann [87] | | | 1) 710 2) 8900 | 1) at pH 12.5 (laboratory test in Ca(OH) ₂ solution) 2) at pH 13.2 |
| 5. BRE, Everett and Kendall [90] | 1) 0.4 2) 0.4-1.0 3) > 1.0 | | | 1) Low risk of corrosion 2) Intermediate risk of corrosion 3) High risk of corrosion (strictly for chloride added at the time of mixing) |
| 6. CP 110, 1972 (revised in 1977 [91]) | 1) 0.35 2) 0.50 | | | 1) Not to be exceeded by 55% of results 2) Upper limit (strictly for chloride added at the time of mixing) |
| 7. BS 8110 [92] | 0.40 | | | |
| 8. ACI committee 201, Guide to durable concrete [93] | 1) 0.30 2) 0.40 | 0.15 | | 1) Moist environment not exposed to Cl ⁻ 2) Moist environment exposed to Cl ⁻ |
| 9. Brown and Geoghehan [94] | 1) 0.30 2) 0.40 | | | 1) Chloride added at mixing 2) Cl ⁻ penetration into hardened conc. |
| 10. Stratful et al [95] | 0.15 | | | |
| 11. Clear (FHWA) [96] | 0.20 | 0.15 | | Extensive survey of federal highways subjected to deicing salts. |
| 12. Sorensen and Maahn [97] | 0.06 (% by wt. of concrete) | | 4260 | Survey of 15-20 year old concrete structures in the Danish Shore Baelte area |

Table 5.1 Chloride threshold levels for initiation of corrosion in reinforced concrete.

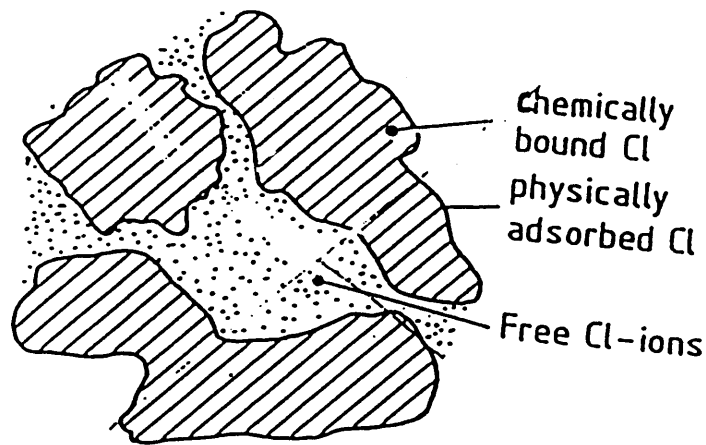


Figure 5.2 Three different forms of chloride, after Tuuti [98]

(chemically bound) [98], as shown in figure 5.2. In some cases chloride is simply referred to as chloride bound which combines both chemically bound and physical absorbed, and chloride unbound which represents the chloride in the pore solution of concrete or paste [99].

In this investigation, acid soluble chloride has been dealt with, which is the chloride soluble in nitric acid and is quoted as "per cent chloride by weight of concrete or of material". The acid soluble chloride is sometimes referred to as total chloride which comprises the bound and unbound chloride.

5.2.2 Diffusion of chloride

Mangat and Gurusamy [101-103], Brown [104], Gourley and Bieniak [105], Berke [106], Decter et al. [107] and others [108-112] indicated that the rate of chloride penetration into concrete as a function of depth from the concrete surface and time can reasonably be represented by Fick's law of diffusion [113], which is given by the following expression;

$$\frac{\partial C}{\partial t} = D_c \frac{\partial^2 C}{\partial x^2} \quad (5.1)$$

Where C is the chloride ion concentration at a distance x from the concrete surface after time t of exposure to chloride, and D_c is the chloride diffusion coefficient.

A standard solution to this partial differential equation [113,114] gives :-

$$C(x, t) = C_0 \left[1 - \operatorname{erf} \frac{x}{2\sqrt{D_c t}} \right] \quad (5.2)$$

Where,

- x = the distance from the concrete surface in cm
- t = the time in seconds
- D_c = the diffusion coefficient in cm^2/sec
- C_0 = the equilibrium chloride concentration on the concrete surface
- $C(x,t)$ = the chloride concentration at any position x at time t
- erf = the error function.

OR

$$C(x, t) = C_0 [1 - \operatorname{erf} (Z)]$$

$$\text{Where } Z = \left(\frac{x}{2\sqrt{D_c t}} \right)$$

The error function has the following properties,

$$\operatorname{erf} (-Z) = -\operatorname{erf} Z,$$

$$\operatorname{erf} (0) = 0 \quad \text{and}$$

$$\operatorname{erf} (\infty) = 1.$$

When $x = 0$ at time t , $Z = 0$ and $C(x,t) = C_0$ and when $x = \infty$ at time t , $Z = \infty$ and $C(x,t) = 0$. The above solution is, thus, correct for a semi-finite solid ($0 < x < \infty$) and is true for an isotropic medium whose structure and diffusing properties at any point are the same relative to all directions.

In a real structure if $C(x,t)$ is assumed to be the threshold chloride ion concentration for initiation of corrosion, and the depth of the reinforcement x is known, then time t to initiate corrosion can be calculated, based on a knowledge of the parameters C_0 and D_c for the particular mix.

5.2.3 Factors effecting diffusion

Initial curing to which a concrete or a repair material is subjected prior to exposure to a chloride environment, plays an important role in determining the chloride penetration rates into the materials, especially at an early age of exposure to the chloride environment [114]. The durability of repair and concrete depends largely on the extent to which the hydration products in the paste fill the space originally occupied by water [115]. Drying of the materials particularly at the surface, caused by poor curing leads to restricted hydration in the surface layers and thus to higher porosities and permeabilities [116]. Therefore, keeping the concrete and repair materials moist during the early days of curing has a far reaching effect on producing a good quality material which has a low porosity and a low permeability. This hinders the movement of harmful substances such as chloride ions and, therefore, the length of time taken to initiate corrosion will be longer.

On the other hand, rapid drying of concrete after an initial period of moist curing may lead to cracking of the concrete surface [117]. If cracks are present in the cover zone, they will form major flow paths for chloride into the concrete and towards the reinforcing steel

[118]. In cracked and uncracked sections alike, chloride ions will diffuse through the capillaries and voids within the matrix and along any cracks or voids in the aggregate particles [105] and at the interface of coarse aggregates. Mangat and Gurusamy [102,103] carried out a study on precracked specimens and concluded that chloride concentrations in the vicinity of cracks increases with increasing crack width, the effect being significant at crack width larger than 0.5mm and marginal at crack widths less than 0.2mm. The work was conducted on 100 X 100 X 500 mm prism specimens which were initially cured in laboratory air for 14 days. Specimens were then transferred either to a sea water spray chamber in the laboratory or to the tidal zone in the North Sea.

Ost and Monfore [119] determined the penetration rate of chloride into immersed concrete by exposing samples of varying permeability, as defined by their water/cement ratio, to 1% and 4% chloride solutions (10,000 ppm and 40,000 ppm). Their results indicated that the penetration rate of chloride depended on the permeability of concrete as defined by the water/cement ratio. Using their results, Browne and Geoghegan [120] predicted that a chloride level of 0.4% by weight of cement, which represents the activation level for initiating corrosion, could penetrate a 50mm cover of high quality concrete in around two years.

5.2.4 Prediction of chloride concentration

Methods for predicting long-term chloride concentration on the basis of relatively early age chloride concentration data obtained from routine inspection are needed so that the time taken for corrosion to initiate can be estimated. Also, such techniques would allow optimisation of maintenance cycles, timely application of preventive measures and provide a basis for recommending the extent and methods of repair required for the structure. Since

the availability of critical threshold levels of chloride concentrations at the reinforcement surface are required for corrosion initiation, the need to predict the time required for such chloride levels reaching the reinforcement is essential in any assessment procedure.

Molloy [126] carried out a study on durability characteristics of concrete under long-term marine curing and concluded that the chloride diffusion coefficient, D_c , is strongly dependent on the period of exposure of concrete to a chloride environment. Consequently long-term prediction of chloride concentrations on the basis of Fick's Second Law of Diffusion which inherently assumes a constant value of D_c is not an accurate procedure [133]. For accurate prediction of chloride diffusion in concrete, a modified differential equation derived based on the law of diffusion, which takes into account the time variation of D_c is required. Also the apparent surface chloride concentration (C_0) does not change clearly and significantly with time. For concrete structures exposed to a marine environment, C_0 can be assumed as 1.5 per cent by weight of cementitious materials [126,133].

5.3 EXPERIMENTAL PROGRAMME

5.3.1 Objectives

The experimental programme was carried out in order to study the chloride diffusion profiles for the three repair materials and plain concrete. Various curing regimes were adopted and their effect was also investigated. The influence of different durations of exposure to a chloride environment on chloride diffusion were also studied. Also, an empirical expression for the prediction of long-term chloride penetration profiles based on data obtained at relatively early ages was derived.

5.3.2 Materials

Three different repair materials and a plain concrete mix were used. Ordinary portland cement, fine aggregate conforming to zone 'M' of BS 882 and coarse aggregate of 10mm nominal size were used throughout. Further details of these materials are given in Section 3.3.1 of Chapter 3.

5.3.3 Mixing and casting

Cementitious repair materials A, B and C were mixed thoroughly. Mixing was conducted without addition of water, until a uniform colour and consistency was attained. Then water (of required quantity) was added slowly and mixing was continued until uniformity of the mix was achieved.

At least twelve 100 X 100 X 300 mm size prism specimens were cast in steel moulds for each of the mixes considered in this investigation, in batch I. Casting was performed in three layers, each layer being compacted on a vibrating table for a few seconds. These specimens were used for chloride diffusion tests after pre-curing them for 28 days before exposure to a chloride environment. In order to ensure that chloride penetration was allowed to occur only from one longitudinal face of the specimens, the remaining faces were sealed by means of a bituminous paint as shown in figure 5.3(a).

In batch II, six 100 X 100 X 500 mm prism specimens were cast for each material to investigate the effect of early exposure (24 hours after casting) on chloride diffusion characteristics. Since sealing of the specimen faces with a bituminous paint was impractical in this case due to the early age of exposure to a chloride environment, prior to casting in batch II, pieces of a polythene sheet of dimensions 100 X 500 mm were carefully cut to provide a barrier against chloride penetration from two (long) opposite faces of the prism

specimens, as shown in figure 5.3(b). During casting this polythene sheet was placed at 20mm from the bottom and top (trowelled) face so that under exposure chloride penetration would occur from the side faces only. Casting was performed in three layers, each layer being compacted on a vibrating table for a few seconds.

5.3.4 Curing

The prism specimens were demoulded after 24 hours. Subsequently, all specimens of batch I were exposed to either one of the initial curing conditions described below.

- a) Specimens were continuously cured in an environmental chamber at temperature of 20°C and relative humidity of 55%. Specimens were called AIR CURED AT 20°C, 55%RH.
- b) After demoulding, the specimens were covered with a wet burlap and plastic sheeting for 14 days and stored in the curing chamber at a temperature of 20°C and relative humidity of 55% for further 14 days. The covers were then removed and specimens were exposed to air under the same conditions of temperature and humidity (20°C, 55% RH), for a further 14 days. specimens were called WET/AIR CURED AT 20°C, 55% RH.
- c) Specimens were continuously cured in air at ambient conditions in the laboratory, where the temperature was fairly controlled at 20°C, but the humidity was uncontrolled and generally ranged between 30-40%. Specimens were called AIR CURED AT AMBIENT CONDITIONS.
- d) After demoulding, specimens were continuously cured at a temperature of 20°C and 100% relative humidity (in water). Specimens were called WET CURED.

All specimens of batch I were initially cured for 28 days after demoulding by one of the above curing methods. Specimens were then sealed on five faces by coating with layers of a bituminous paint in order to ensure that chloride penetrated through one longitudinal face only as shown in figure 5.3. The coated specimens were left in the laboratory air for two days to let the paint harden fully. Specimens were then immersed in a sodium chloride solution. The strength of the solution was 175 gm of sodium chloride in one litre of water (3.0M).

The specimens which were cured initially at 20°C were immersed in the sodium chloride solution which was maintained at the same temperature of 20°C. The specimens which were cured at ambient conditions were immersed in a chloride solution which was also at the ambient temperature (~ 20°C). This was achieved by storing plastic tanks containing the chloride solutions in curing rooms where the temperature was kept at these levels.

In order to study the effect of early exposure to a chloride environment on the diffusion characteristics of the different repair materials, six prism specimens were cast for each material. The specimens were covered with a polythene sheet for 24 hours after casting. The specimens were then demoulded and exposed to a chloride environment at 24 hours after casting in order to simulate some practical conditions where the repair patches cannot be protected from chloride exposure for long period after the application of repair. For example, in marine applications where the repair cannot be protected from the tide for long periods.

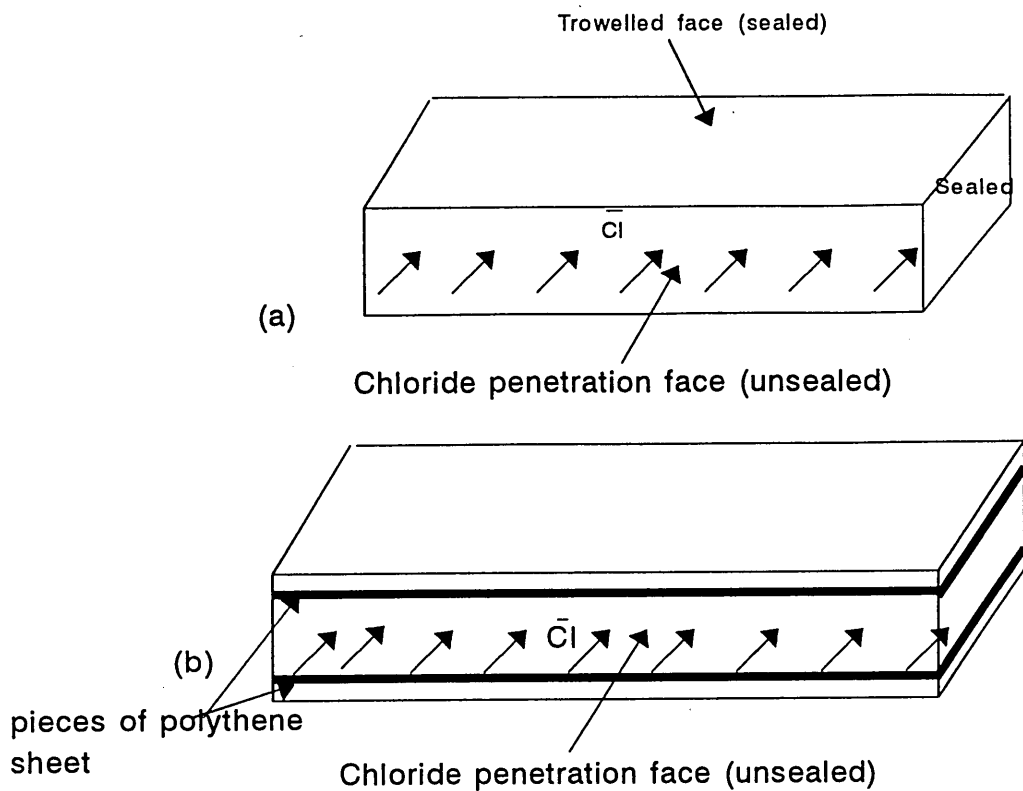


Figure 5.3 Sealing of a specimen (a) Batch I and (b) Batch II.

5.3.5 Sampling

After the required period of immersion in the chloride solution, a specimen was taken out of the tank. It was cut into two halves by a masonry saw as shown in figure 5.4. Powder samples for chloride analysis were drilled from each of the sawn faces of the prisms at various depths from the unsealed face. Drilling into each half of a specimen was performed by means of a rotary percussion drill at a distance of 10, 20, 30, 40 and 50mm from the unsealed face to the centre-line of the holes drilled as shown in figure 5.5. At 10mm distance from the unsealed face, five holes of 4 mm diameter were dry drilled, whereas at other positions three holes of 6 mm diameter were dry drilled. The powder samples drilled at each position (common distance from the unsealed face) of the sawn faces were combined to give an adequate weight of a test sample representing a given distance from the unsealed surface.

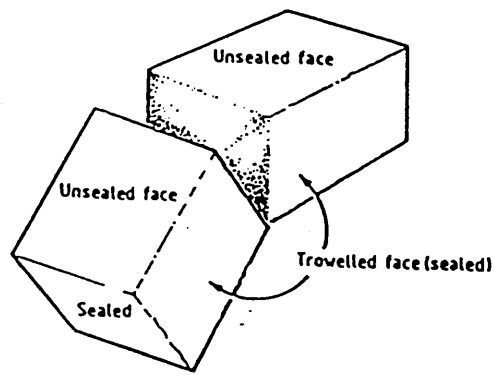


Figure 5.4 Cutting the specimen into two halves

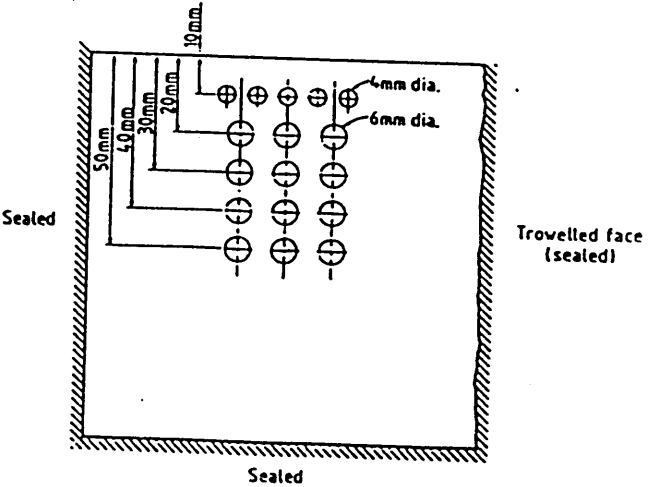


Figure 5.5 Sample locations for chloride analysis

5.3.6 Chemical analysis

The powder sample of concrete or repair material was sieved on a 200 μm sieve. Care was taken not to force any particle through the mesh. The powder passing the 200 μm size sieve was collected, from which a weight of 2 grams was measured accurately to the nearest 0.01 g. This weight was used for chemical analysis. 25ml of 0.1 molar Nitric Acid solution was added to the sample and the mixture was heated on a hot plate. The solution was boiled for one minute while stirring continuously. This process ensured the extraction of chloride from the powder. The solution was left to cool down. On cooling this solution was neutralised with Calcium carbonate and filtered into a conical flask. The solution was then ready for titration and the Mohr titration method was used to determine the concentration of chloride in the solution [121]. The procedure involved the use of 1.0 ml of indicator in the test solution. The yellow indicator solution was made by combining 4.2 g of

potassium chromate and 0.7 g of potassium dichromate in 100 ml of distilled water. After adding 1.0 ml of indicator to the test solution, silver nitrate (AgNO_3) (0.02 N) was added in small quantities, while swirling the conical flask continuously, until the yellow indicator changed into a distinct reddish colour. The volume of silver nitrate (AgNO_3) used until the colour change occurred was recorded. The change in colour was the end point of the titration when all the chloride ions (Cl^-) were neutralised. The volume of AgNO_3 used was converted to percent chloride by weight of the concrete or repair material from the following formula [122] :-

$$\% \text{Cl}^- = \frac{35.453 V_s N_s}{10 w_p} \quad (5.4)$$

Where,

V_s is the volume of AgNO_3 used in ml to neutralise Cl^-

N_s is the normality of AgNO_3 which is 0.02 N

w_p is the weight of the powder sample in grams.

Chloride analysis of the different mixes were carried out after 28 days, 90 days and 180 days of immersion of specimens in the chloride solution. The chloride concentration determined by the above analysis is termed as acid soluble chloride which includes chemically bound chloride in the matrix.

In this investigation, a BMDP computer programme [88] was employed to determine the best fit diffusion curves through a set of chloride diffusion experimental data at various depths from the concrete and repair materials surface. To run the computer programme, limits for C_0 and D_c had to be fed in. The limits fed in for C_0 were between 0 to 10% by weight of material and for D_c the range was between 10^{-10} to 10^{-4} cm^2/sec . By feeding into the computer programme the chloride penetration data at different depths and the limits for

values of C_0 and D_c , best fit chloride diffusion curves together with values of C_0 and D_c were calculated.

5.4 RESULTS AND DISCUSSION

A wide range of results are presented to determine the influence of initial curing methods and duration of exposure to chloride environment on the chloride diffusion characteristics. These are the chloride diffusion profiles, diffusion coefficients and the equilibrium chloride concentrations on the concrete surface. The chloride diffusion profiles and diffusion coefficients are also reported for the specimens exposed to chloride environment at 24 hours after casting.

In the following sections of this chapter, wherever figures presenting chloride concentration profiles are drawn, the symbols represent the experimental data (average of two specimens) points of chloride concentration at each location (depth). The full line drawn through these points is the best-fit curve representing Fick's Second Law of Diffusion given in equation (5.1).

5.4.1 Influence of initial curing

5.4.1.1 Chloride ingress after 28 days

Acid soluble chloride concentration profiles of the three different repair materials and plain concrete exposed for 28 days to chloride solution are presented in figures 5.6 to 5.9. Each figure represents chloride diffusion profiles for the different initial curing methods adopted in this investigation.

Figure 5.6 shows chloride diffusion profiles for the repair material A for the four different curing conditions adopted in this investigation. Initially air cured specimens under

ambient conditions showed higher chloride uptake than the other curing methods, and the lowest chloride uptake was found for water cured specimens. This was because in water cured specimens, the hydration would proceed at a higher rate compared to that of other curing conditions. For example, values of chloride concentration at a depth of 10mm from the unsealed face for water cured specimens at 20°C, wet/air cured at 20°C, air cured at 20°C, 55% RH and specimens cured at ambient conditions are 0.077, 0.10, 0.18 and 0.32 by weight of material respectively. A similar trend of chloride uptake as affected by initial curing conditions was found at all the other depths.

In figure 5.7, the chloride diffusion profiles for cementitious repair material B are presented for the three of the four initial curing conditions employed in this investigation. The effect of initial curing conditions on chloride levels for first 20mm depth were quite high and beyond 30mm the curing methods employed show a constant difference in diffusion profiles. The highest permeability coefficients for the porous mineral based material B, as discussed in the section 3.4.2 of chapter 3, is the reason for the higher chloride concentration values at all the depths compared with other materials.

The effect of initial curing conditions on material C is shown in figure 5.8, while figure 5.9 represents chloride diffusion profiles for control concrete mix, under various initial curing conditions. Contrary to the results of material A and material B, the air cured specimens (at 20°C & 55% RH) of concrete showed the highest values of chloride levels at all the depths. This is most likely to be due to the cracks (crazing) which appeared to have taken place on the concrete surface when drying of the specimens started. The cracks caused a rapid ingress of chloride at the surface and yielded higher values of chloride concentration at the concrete surface. However, it is important to note that the effect of this crazing (cracking) on chloride ingress in the surface zone is not significantly pronounced [103,125]

and it can be concluded that such fine cracks have little deleterious effect on chloride penetration.

The equilibrium chloride concentrations on the surface, C_0 , which were determined by applying Fick's 2nd law of diffusion to the experimental data as described in section 5.2.2, are given in the Table 5.2. It is clear from table 5.2 that the equilibrium chloride concentration on the surface, C_0 , are similarly affected by the initial curing conditions as the chloride levels in the figures 5.6 to 5.9. It is also clear that the repair materials and plain concrete behave differently under different curing conditions.

Table 5.2 Equilibrium chloride concentration on the surface, C_0 , (% by weight of material) under different initial curing conditions (after 28 days)

| Materials → | A | B | C | CONCRETE |
|----------------------------|--------|--------|--------|----------|
| Curing methods ↓ | | | | |
| Water cured at 20°C | 0.0815 | ----- | 0.3702 | 0.2931 |
| Air cured at 20°C, 55% RH | 0.2099 | 0.8985 | 0.4514 | 0.6630 |
| Cured at ambient condition | 0.3950 | 0.9347 | -- | 0.6437 |
| Wet/Air cured at 20°C | 0.1244 | 0.7241 | 0.4132 | 0.3975 |

The values obtained for the equilibrium chloride concentration on the air cured specimens of materials A, C and concrete mix were 0.21, 0.45 and 0.66% respectively. The corresponding values at a depth of 20mm were 0.12, 0.37 and 0.47%. However at depths beyond 30mm from the unsealed surface, chloride ingress profiles of materials were in relatively closer band.

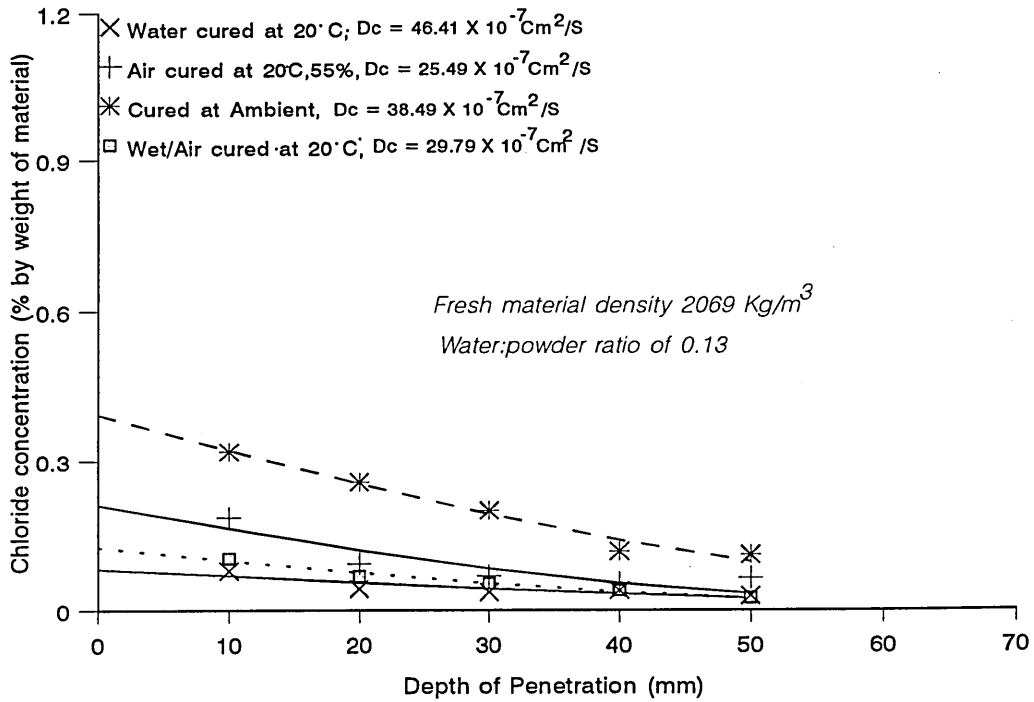


Figure 5.6
Influence of initial curing conditions on chloride diffusion for Material A (at 28 days)

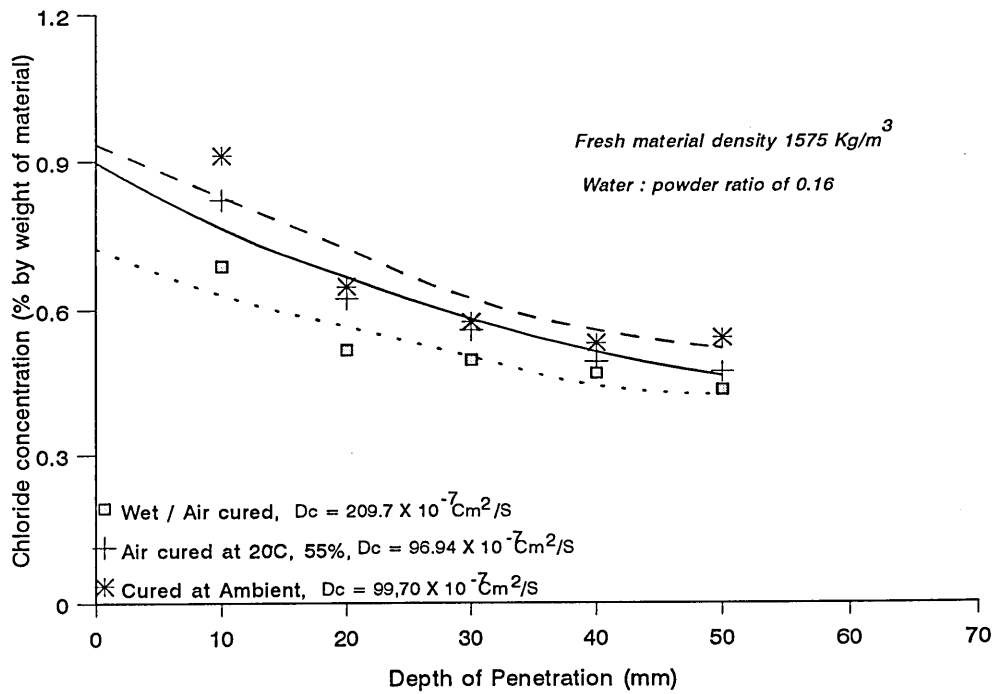


Figure 5.7
Influence of initial curing conditions on chloride diffusion for Material B (at 28 days)

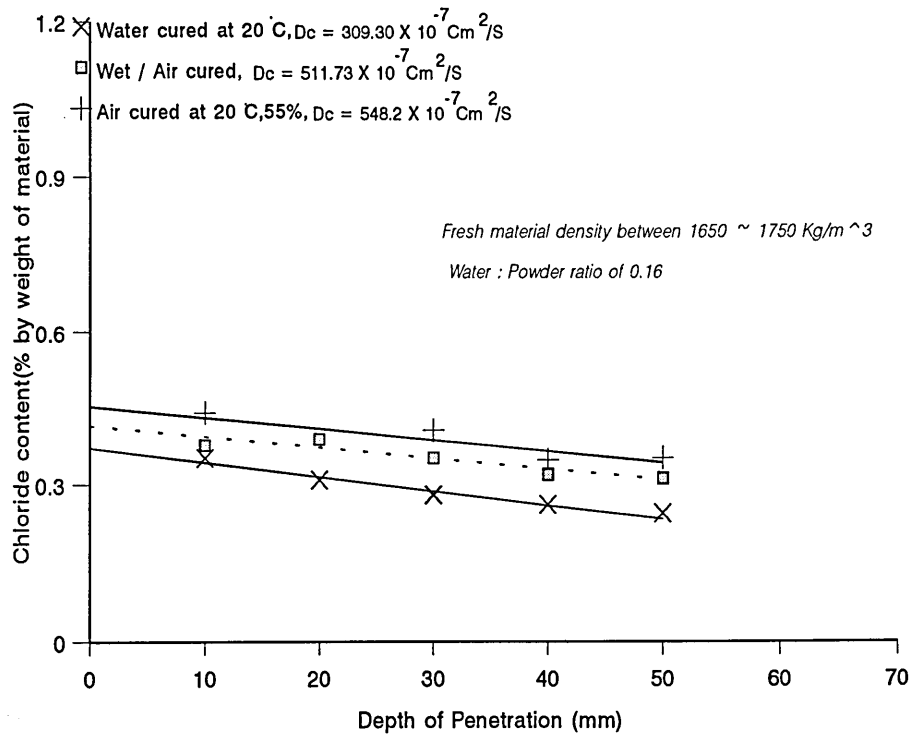


Figure 5.8
Influence of initial curing conditions on chloride diffusion for Material C (at 28 days)

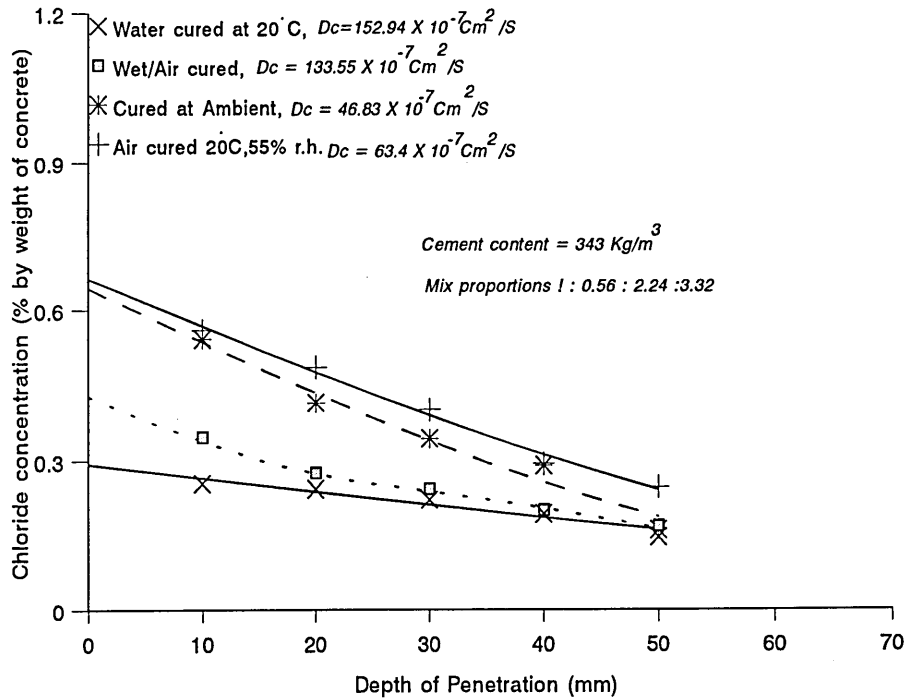


Figure 5.9
Influence of initial curing conditions on chloride diffusion for control concrete mix (at 28 days)

The diffusion coefficients, D_c , varied from $25 \times 10^{-7} \text{ Cm}^2/\text{Sec}$ to $47 \times 10^{-7} \text{ Cm}^2/\text{Sec}$ in case of high strength non-shrink repair material A. The values of D_c varied considerably with the initial curing conditions adopted prior to exposure to chloride solution. Also the chloride diffusion coefficients of the cementitious material C (with polymer additive) were considerably higher than those for other materials. Seemingly, this is true regardless of the initial curing conditions.

The results in figures 5.10 to 5.13, represent the 28 days chloride diffusion profiles for the repair materials (namely A, B and C) and concrete mix under one of the four curing conditions. It is clear from these figures that the repair mortar which is based on a mineral cement binder (material B) possesses higher diffusion characteristics than the other materials under all the curing conditions. High chloride concentration in material B is compatible with the high water permeability coefficient of the material compared to other materials as mentioned in chapter 3. For example, mean value of permeability coefficient, K_{LD} (m/s), for materials A and C are 2.53×10^{-13} and 1.33×10^{-13} respectively, while for material B it is 5.62×10^{-11} , which shows more than an order of magnitude increase in permeability relative to the other materials.

Consider figure 5.10 for example, which shows chloride diffusion profiles for the four different mixes after 28 days of immersion in chloride solution, for initially water cured specimens at 20°C. The equilibrium chloride concentration on the material surfaces were 0.08, 0.86, 0.43 and 0.29% by weight of material for the repair materials A, B, C and concrete mix respectively.

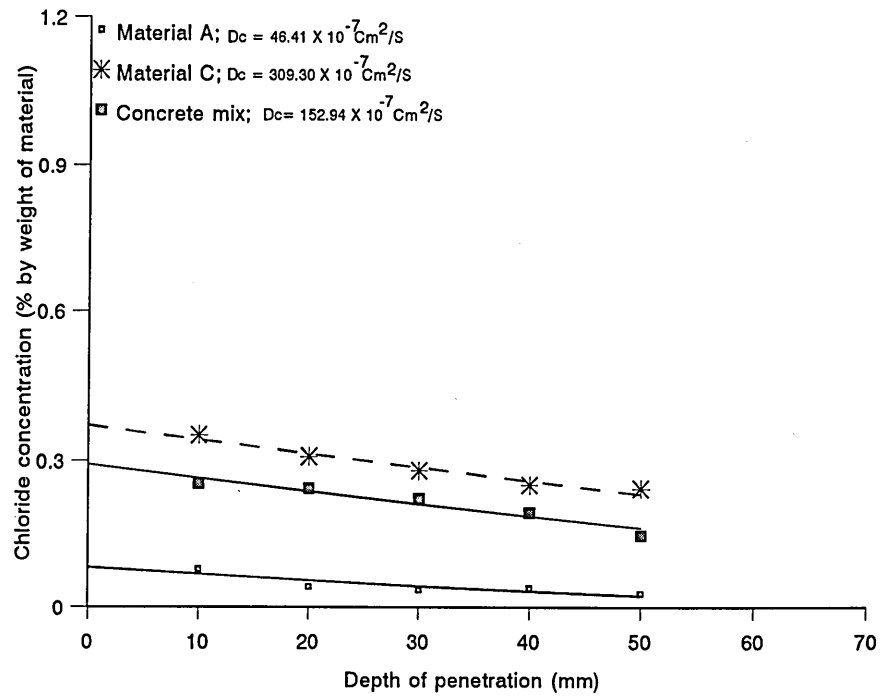


Figure 5.10
Chloride diffusion for repair materials at 28 days, water cured at 20 °C

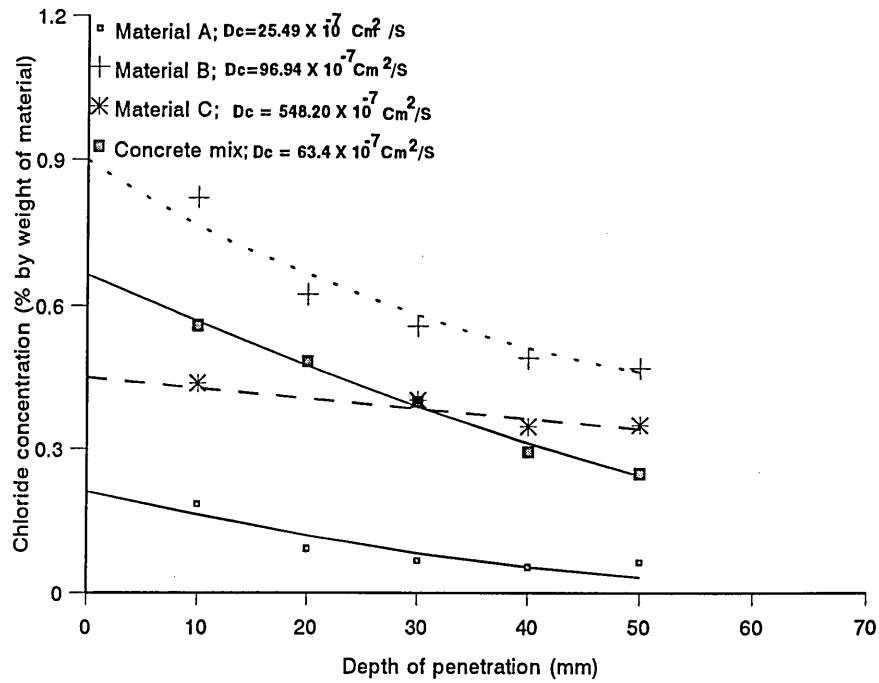


Figure 5.11
Chloride diffusion for repair materials at 28 days, air cured at 20 °C & 55% r.h.

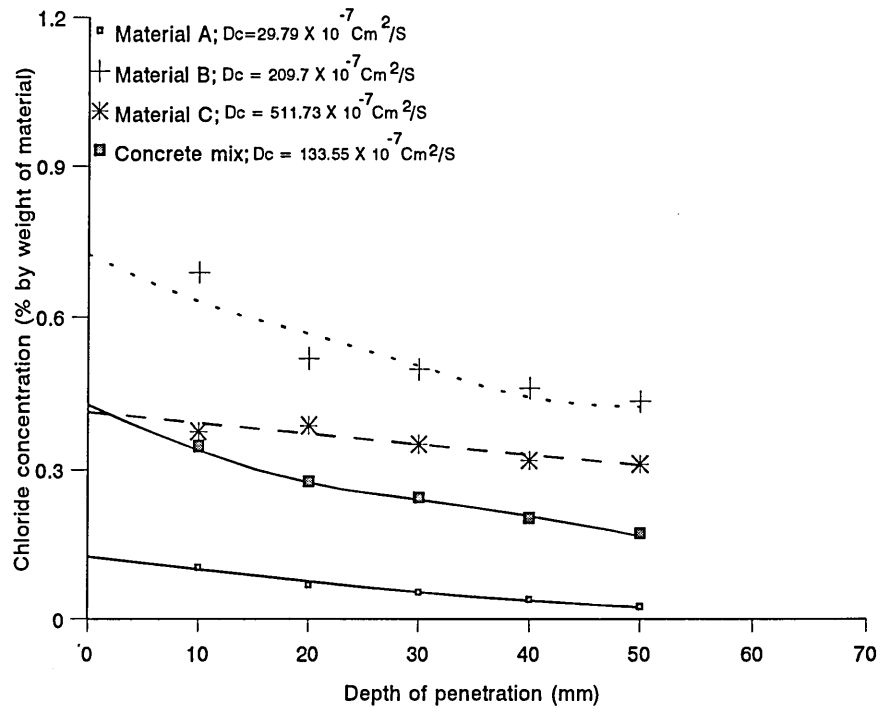


Figure 5.12
Chloride diffusion for repair materials at 28 days, wet/air cured at 20°C

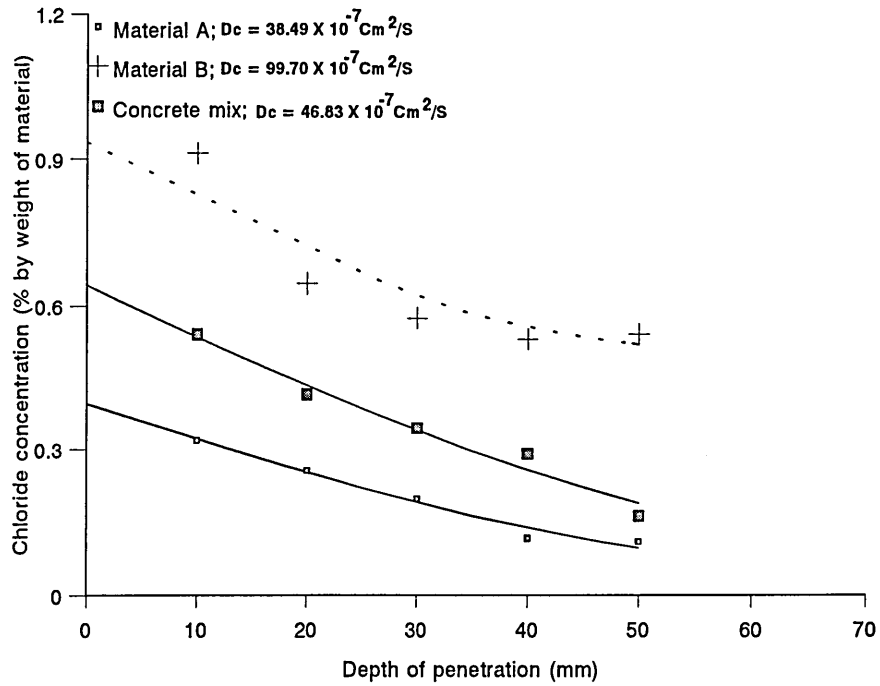


Figure 5.13
Chloride diffusion for repair materials at 28 days, cured under ambient conditions.

It is also clear from the figures 5.10 to 5.13, that chloride concentration profiles for high strength repair material were lower compared to other three materials. For example from figure 5.12, the value of equilibrium chloride concentration on the surface of materials B, C and concrete mix were 0.69, 0.41 and 0.29% by weight of material respectively compared to 0.12% for high strength material A. The relatively flatter chloride diffusion profiles of repair material C is also noticeable from this figures.

5.4.1.2 Chloride ingress after 90 days

Chloride diffusion profiles after 90 days of immersion in the chloride solution are presented in figures 5.14 to 5.17 for materials A, B, C and concrete mix respectively under initially air curing at 20°C, 55%RH and water curing at 20°C. It appears that the initially air cured specimens at 20°C, 55% RH still possess higher chloride uptake than water cured specimens at 20°C, for all repair materials. For example, figure 5.15 shows chloride diffusion profiles for the repair material B for the two curing conditions. Specimens initially air cured at 20°C, 55% R.H. showed higher chloride uptake than the specimen water cured at 20°C. The effect of initial curing conditions on chloride levels for the first 20 mm depth were quite high and beyond that for the curing methods employed show a constant difference in chloride concentration.

The effect of initial curing conditions on material C is shown in figure 5.16, while figure 5.17 represents chloride concentration profiles for plain concrete mix, under two initial curing conditions. Similar to the results of material A, B and C, initially air cured (at 20°C, 55% R.H.) specimens of concrete showed the highest values of chloride concentrations at all

the depths. It is also clear from figures 5.14 to 5.17 that the mineral based material B and plain concrete mixes are more sensitive to the initial curing conditions compared to materials A and C. A high uptake of chloride is found in chloride diffusion profiles for a repair mortar which is based on a mineral cement binder, material B, as represented in figure 5.15. High chloride concentration can be explained by the higher permeability property of material B compared to other materials as discussed in chapter 3.

In figure 5.14 the equilibrium chloride concentrations on the surface are 0.35 and 0.39% by weight of material for water cured specimens at 20°C and air cured specimens at 20°C, 55% RH respectively. The same trend of lower chloride concentration in initially water cured specimens is seen at other depths.

The diffusion coefficients after 90 days of immersion in the chloride solution are considerably smaller than those obtained after 28 days of immersion, especially for materials B and C. For example, the diffusion coefficients of initially water cured specimens of material C at 20°C after 90 days is $107 \times 10^{-7} \text{ Cm}^2/\text{sec}$ in comparison to $309 \times 10^{-7} \text{ Cm}^2/\text{sec}$ after 28 days. Also the diffusion coefficients of the initially water cured specimens at 20°C is lower than that of the air cured specimens at 20°C, 55% RH, as shown in figures 5.16 and 5.17.

Results of all water cured specimens at 20°C and all air cured specimens at 20°C, 55% RH after 90 days of immersion in the chloride solution are presented in figures 5.18 and 5.19 respectively. The trend is similar to that of 28 days results as shown in figures 5.11 and 5.12.

5.4.1.3 Chloride ingress after 180 days

Chloride diffusion profiles after 180 days of immersion in the chloride solution are presented in figures 5.20 to 5.23 for repair materials A, B, C and plain concrete respectively. From the figures 5.20 to 5.22, it is clear that the initial curing method has very little or no influence on the chloride uptake in repair materials. While from the figure 5.23, it is clear that concrete mix is more sensitive to the initial curing condition.

The results in figures 5.24 and 5.25 represent chloride diffusion profiles for all the materials for each of the initial curing conditions, after 180 days of immersion in the chloride solution. The trend is similar to that in figures 5.18 and 5.19 after 90 days immersion. It is clear from these figures that the repair mortar which is based on a mineral cement binder (material B) possesses higher chloride concentration than the other materials under both initial curing conditions. From the results of materials C it is also clear that its surface chloride levels are similar to those of good quality concrete (figures 5.24 and 5.25) but the chloride diffusion rate is extremely high. This would lead to unacceptable high chloride penetration for long-term chloride exposure, with the consequent danger of reinforcement corrosion and spalling of concrete in repaired zone.

Consider figure 5.24, which shows chloride diffusion profiles for the four different mixes considered in this investigation after 180 days of immersion in chloride solution for initially water cured specimens at 20°C. The equilibrium chloride concentration on the material surfaces were 0.59, 0.97, 0.41 and 0.61% by weight of material for the repair materials A, B, C and concrete mix respectively. At a depth of 30 mm and greater the chloride concentration profiles for all the materials, except material B, were found closer. It is also clear from figure 5.24, that chloride concentration profiles for material with polymer additives (material C) has lower concentration compared to other materials.

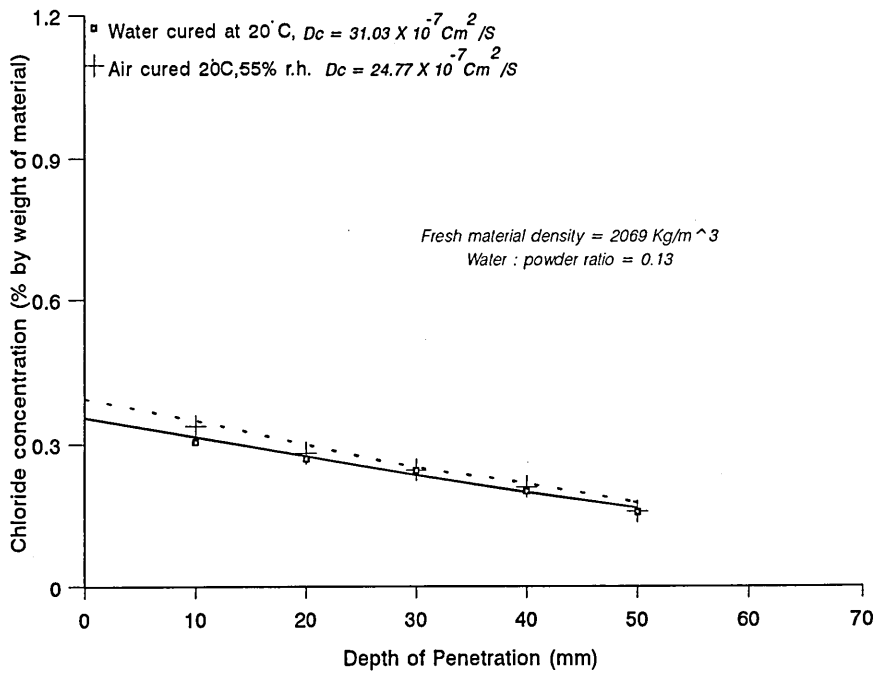


Figure 5.14
Influence of initial curing conditions on chloride diffusion for Material A (at 90 days)

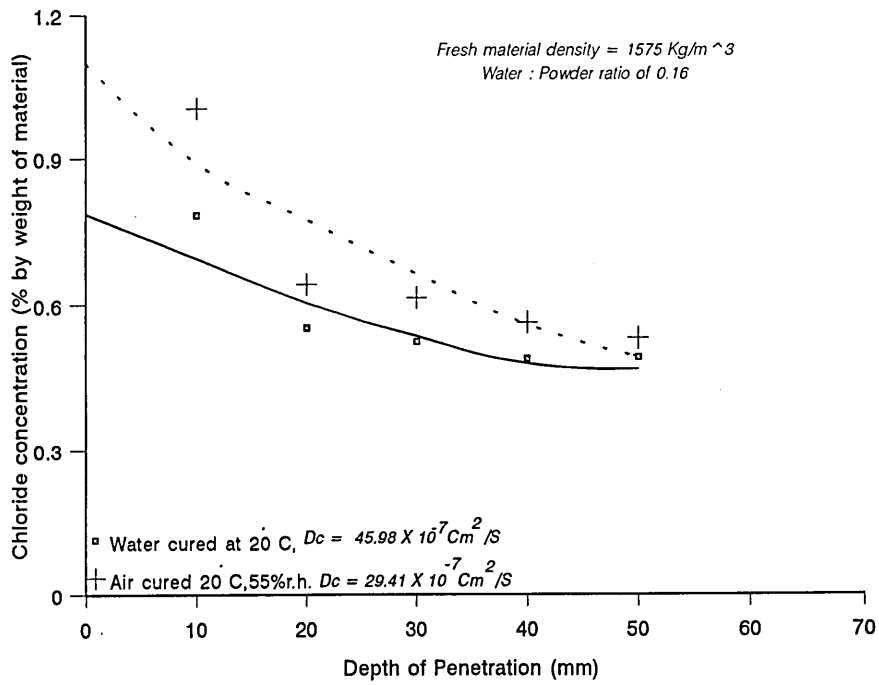


Figure 5.15
Influence of initial curing conditions on chloride diffusion for Material B (at 90 days)

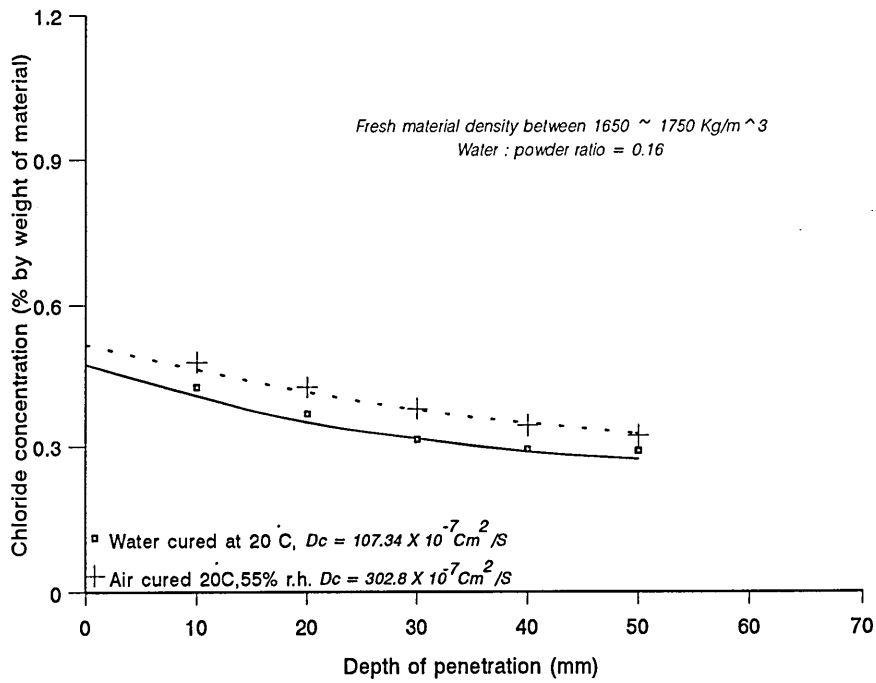


Figure 5.16
 Influence of initial curing conditions on chloride diffusion for
 Material C (at 90 days)

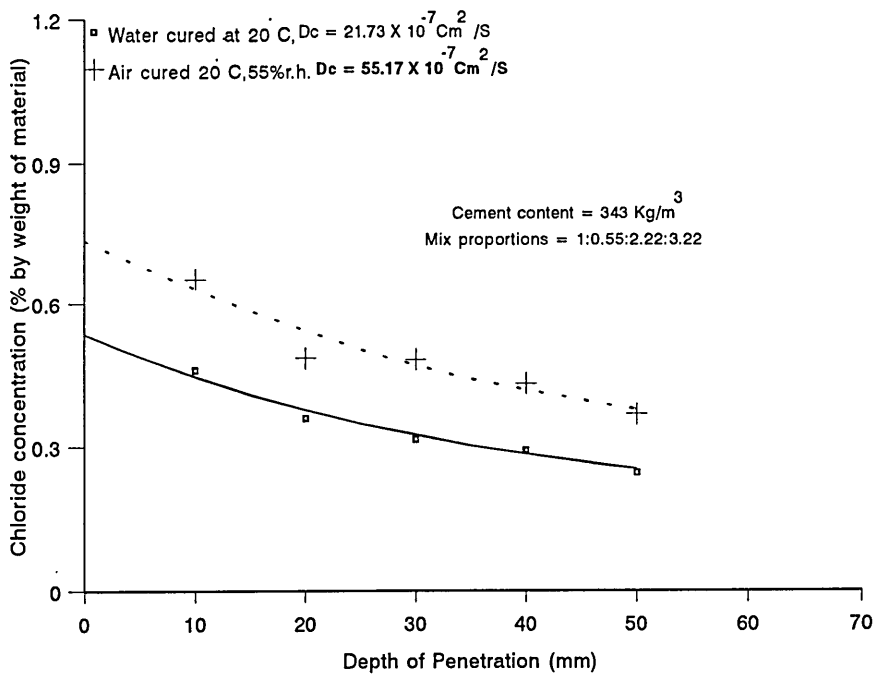


Figure 5.17
 Influence of initial curing conditions on chloride diffusion for
 control concrete (at 90 days)

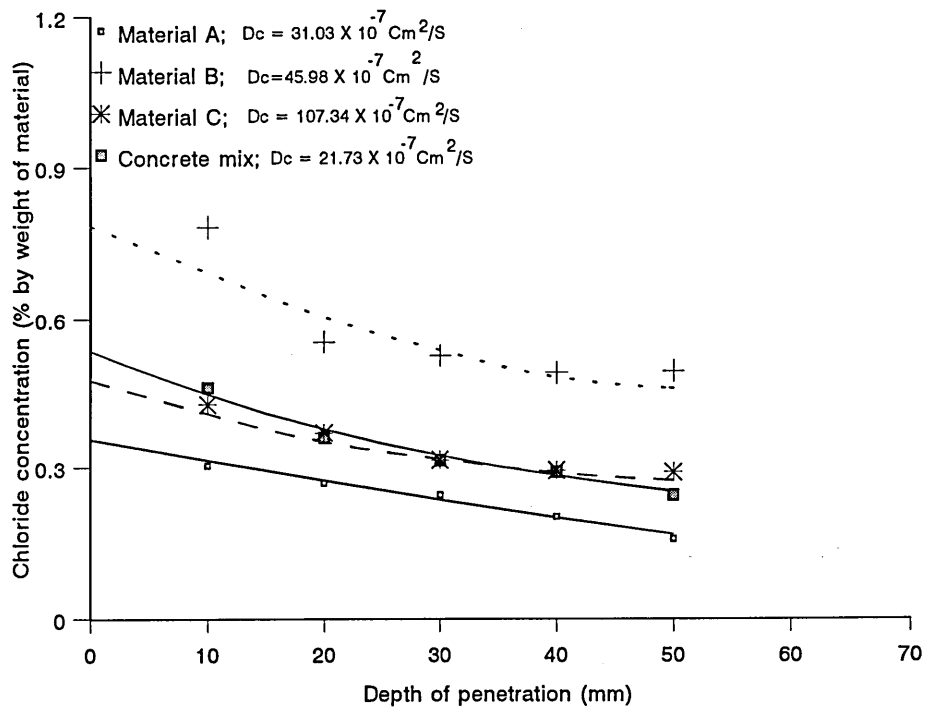


Figure 5.18
Chloride diffusion for repair materials at 90 days, water cured at 20 °C

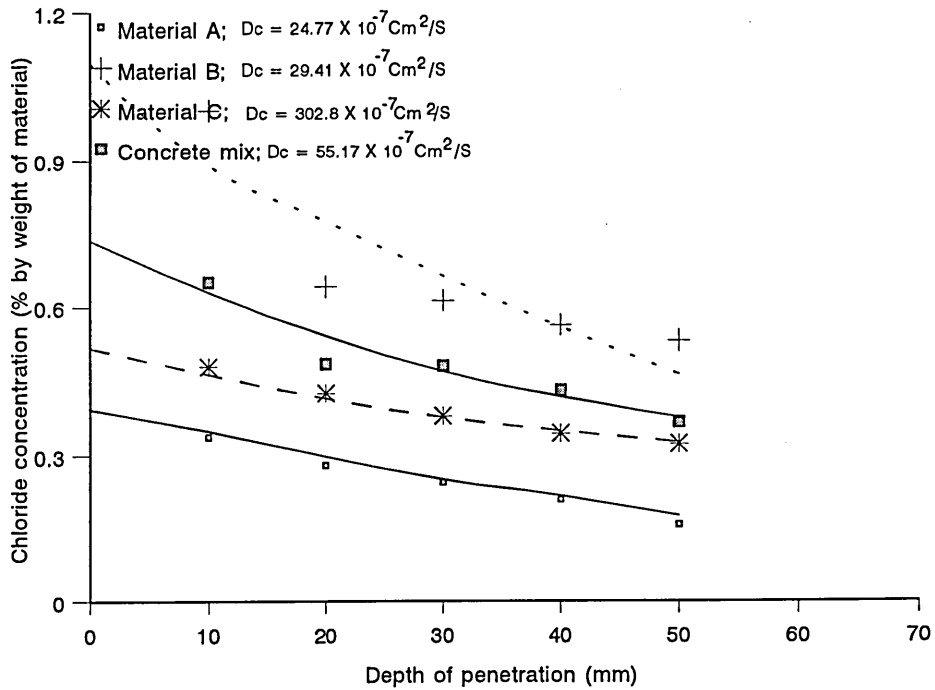


Figure 5.19
Chloride diffusion for repair materials at 90 days, air cured at 20 °C and 55% r.h.

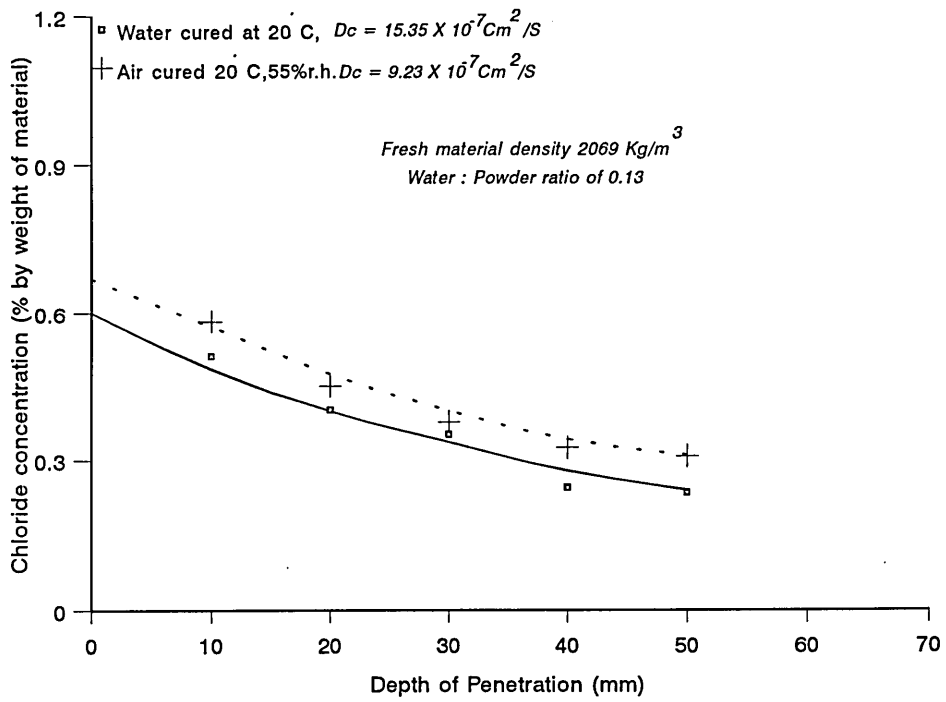


Figure 5.20
Influence of initial curing conditions on chloride diffusion for Material A (at 180 days)

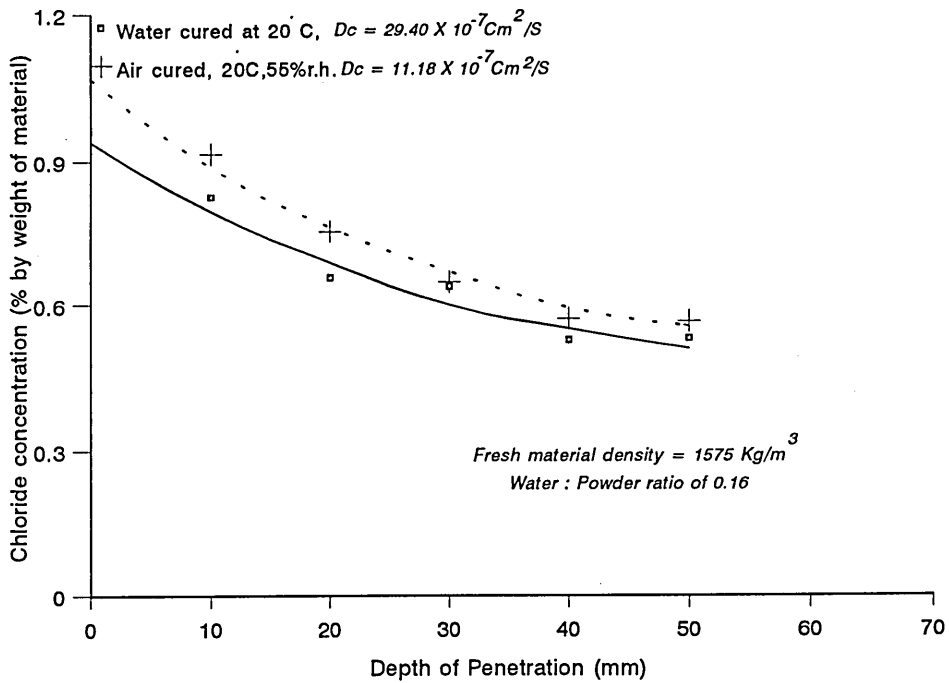


Figure 5.21
Influence of initial curing conditions on chloride diffusion for Material B (at 180 days)

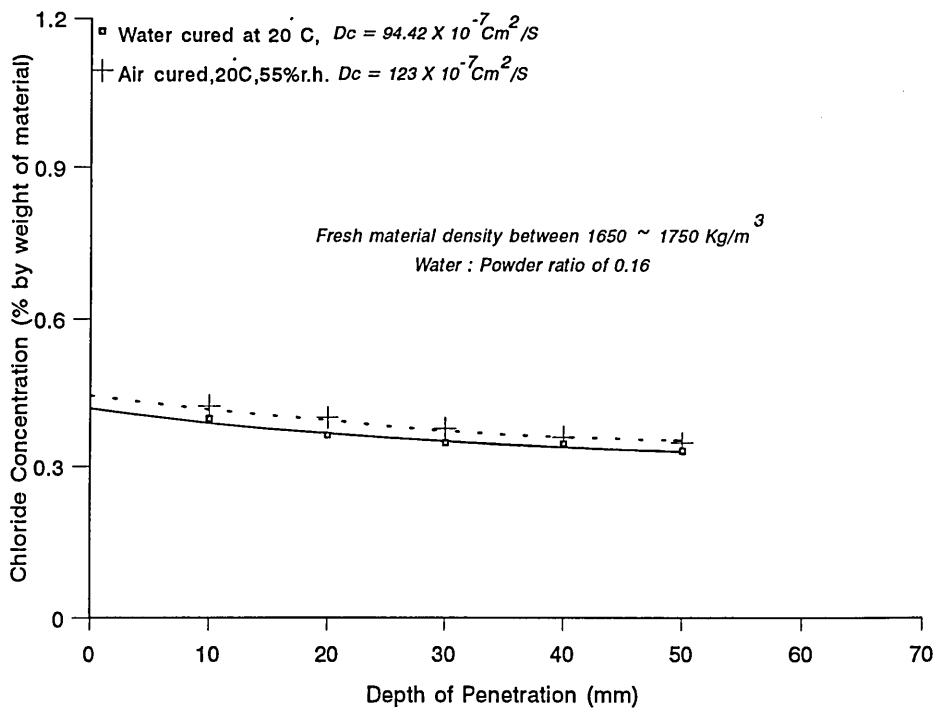


Figure 5.22
Influence of initial curing conditions on chloride diffusion of Material C (at 180 days)

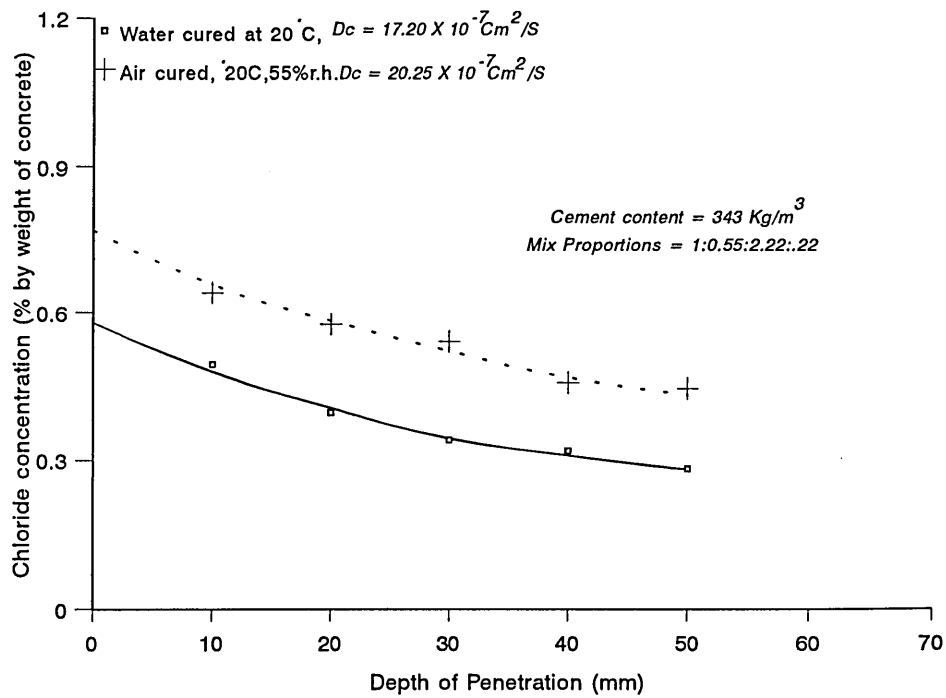


Figure 5.23
Influence of initial curing conditions on chloride diffusion for control concrete (at 180 days)

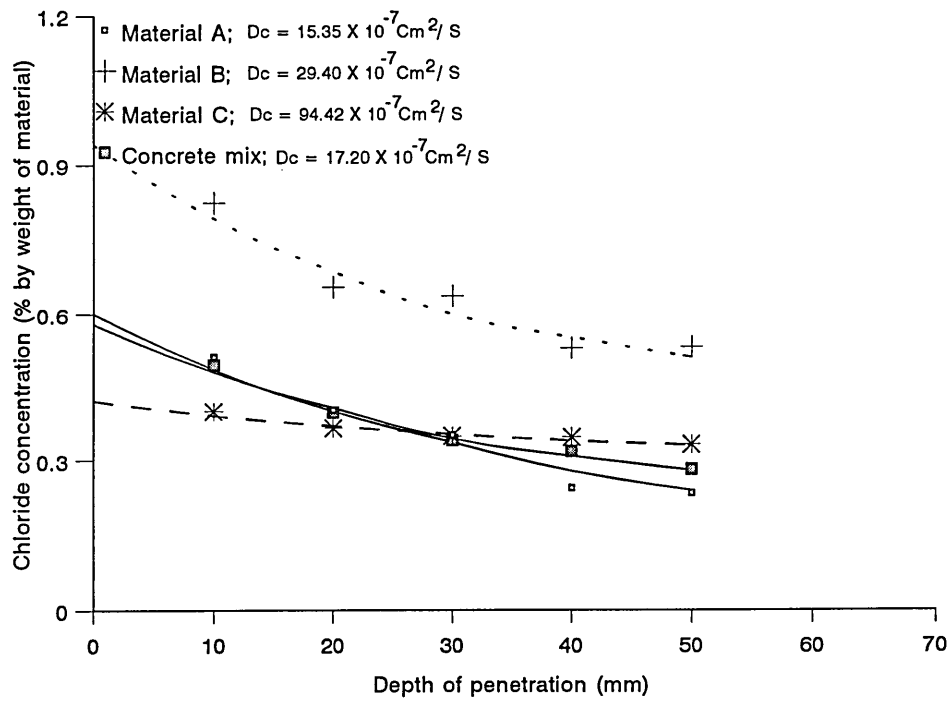


Figure 5.24
Chloride diffusion for repair materials at 180 days, water cured at 20 °C

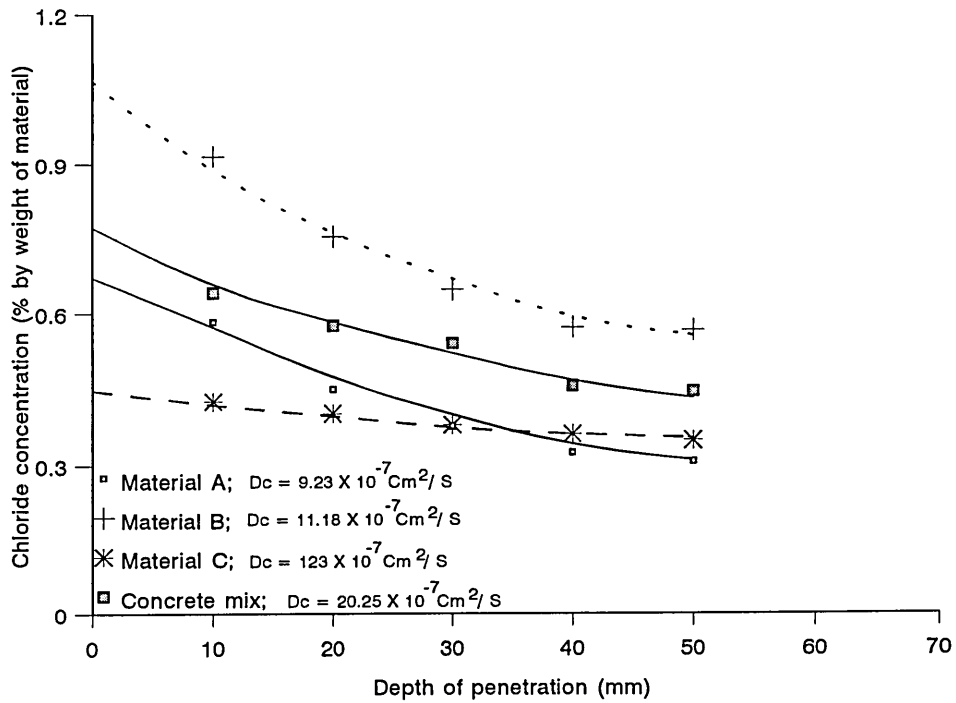


Figure 5.25
Chloride diffusion for repair materials at 180 days, air cured at 20 °C and 55% r.h.

Diffusion coefficient values of specimens after 180 days of exposure to chloride solution are generally smaller than those obtained after 28 and 90 days of exposure for the various curing regimes adopted in this investigation. Values of diffusion coefficient ranged from $15.35 \times 10^{-7} \text{ Cm}^2/\text{Sec}$ to $94.42 \times 10^{-7} \text{ Cm}^2/\text{Sec}$ for the initial water cured specimens, and from $9.23 \times 10^{-7} \text{ Cm}^2/\text{Sec}$ to $123 \times 10^{-7} \text{ Cm}^2/\text{Sec}$ for the initial air cured specimens.

5.4.2 Influence of early exposure to chloride solution

Chloride diffusion profiles for Materials exposed to chloride solution after 24 hours of casting are presented in figures 5.26 to 5.28 for 28, 90 and 180 days of immersion in the chloride solution. These results are obtained from the specimens of Batch II (section 5.3.3). Each figure displays chloride diffusion profiles for the repair materials and the concrete mix considered in this investigation. As for the previous results (of Batch I), a high uptake of chloride is found in the repair mortar B which is based on a mineral cement binder. This seems to be true in most of the results obtained. For example, from figure 5.26 the values of chloride concentrations at a depth of 10 mm from the unsealed surface for material B is 0.66% compared to 0.24, 0.49 and 0.26% for materials A, C and concrete mix respectively. However, early exposure to chloride (24 hours after casting) has very little effect on chloride penetration compared to the specimen cured for 28 days prior to exposure to chloride solution. So it is clear that exposing these materials to chloride environment at early age has no serious consequences.

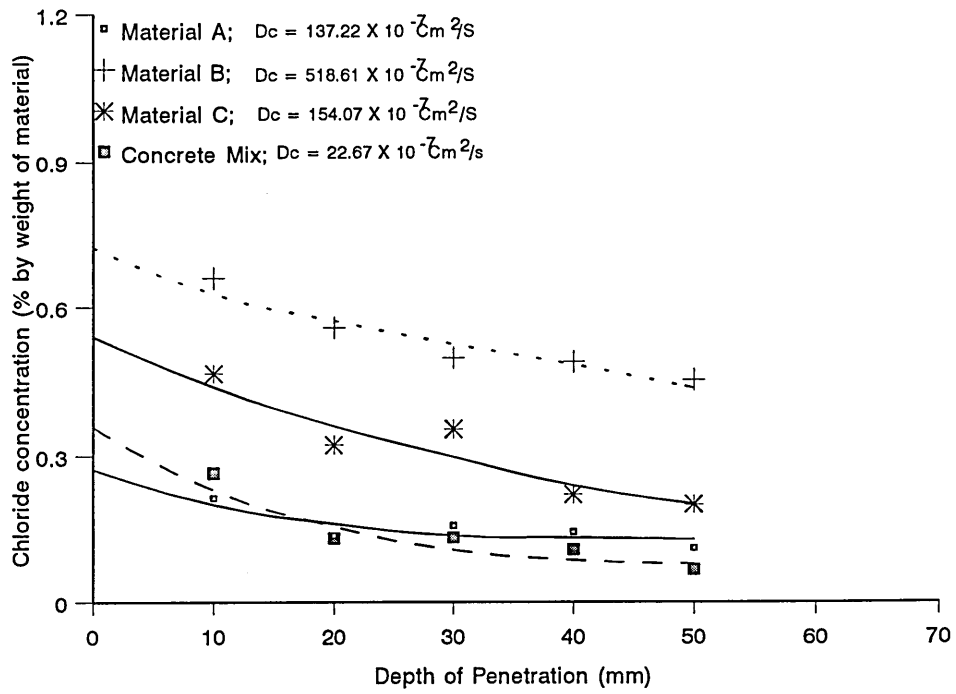


Figure 5.26
 Influence of early exposure (24 hours after casting) on chloride diffusion after 28 days

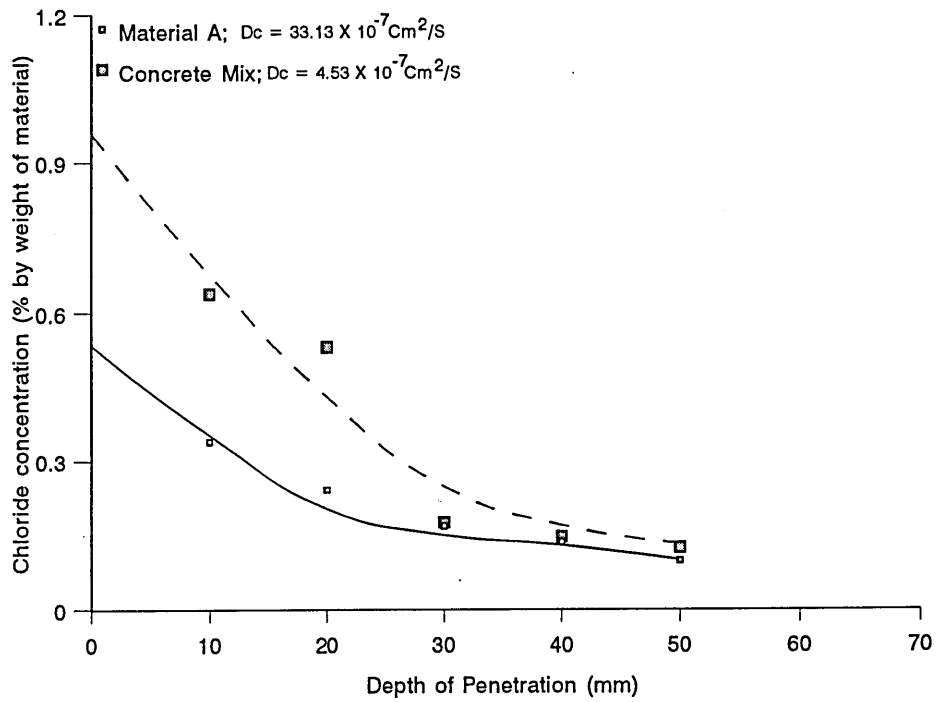


Figure 5.27
 Influence of early exposure (24 hours after casting) on chloride diffusion after 90 days

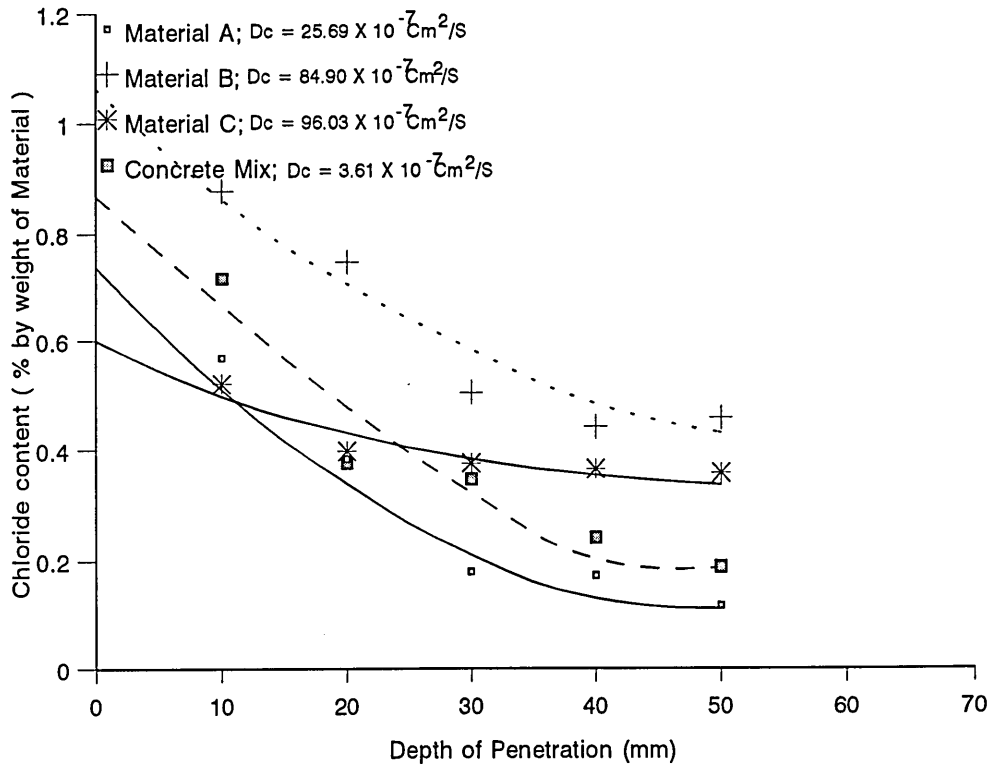


Figure 5.28
 Influence of early exposure on chloride diffusion after 180 days

5.4.3 Influence of duration of exposure to chloride environment

5.4.3.1 Chloride diffusion profiles at different ages of exposure

Influence of duration of exposure to chloride environment on chloride uptake is shown for the specimens initially cured for 28 days (batch I) and initially cured for 24 hours (batch II) of this investigation in figures 5.29 to 5.40 for the various materials used in this study. It appears from the results of figures 5.31 to 5.35, where specimens were either water cured at 20°C or air cured at 20°C, 55% RH for first 28 days prior to immersion in a chloride solution, that material C did not show an increase in chloride uptake even after 180 days of immersion in the chloride solution. The other three materials (materials A, B and concrete mix) showed increased chloride uptake with increase in duration of exposure to chloride environment (figures 5.29, 5.30 and 5.32). This is probably due to the very low permeability of material C, as discussed in chapter 3.

Considering figure 5.29, which presents the chloride diffusion profiles for the repair Material A at various periods of exposure to chloride solution, it shows that there is a considerable increase in the chloride uptake beyond the 28 days of immersion. Figures 5.30 and 5.31, on the other hand, show that there is a relatively small increase in chloride uptake at periods beyond 28 days of immersion for the materials B and C.

In figure 5.33, results of high strength repair material A are presented for three different periods of immersion to a chloride environment. Initial curing for 28 days was at 20°C and 55% RH. It shows a consistent increase in chloride uptake at all ages of immersion. Chloride diffusion profiles for the concrete mix at different ages of immersion are presented in figures 5.32 and 5.36 for initial water cured at 20°C and air cured at 20°C, 55% RH respectively. It is also clear from these figures that the chloride uptake increases as the age of immersion increases. It also shows effect of initial curing condition on the

chloride uptake in concrete.

Gjorv and Vennestand [123] also showed progressively increasing depths of chloride penetration with time for a mortar mix with ordinary portland cement at water to cement ratio of 0.4. Specimens were cured in water for at least 2 to 3 months. Midgley and Illston [124] also found a consistent increase in the chloride uptake after one year of immersion in chloride solution compared with the chloride uptake after 6 months of immersion in chloride solution. The work was conducted on cement pastes with water/cement ratios of 0.23, 0.47 and 0.71. Paste cylinders of 23 mm diameter X 70 mm length were initially stored for one month in a saturated solution of calcium hydroxide at a temperature of $21 \pm 1^{\circ}\text{C}$, then specimens were forced into undersized rubber tubes of 20 mm diameter and only one end of each sample was left exposed. Some cylinders were then placed in a solution of sodium chloride containing 30 grams per litre NaCl and some others were left in sodium chloride solution containing 150 grams per litre. At a water/cement ratio of 0.47, the chloride concentrations at a depth of 7 mm were about 0.62% at the age of 6 months of immersion and 1.1% at the age of 12 months in chloride solution (150 grams NaCl per litre). A similar trend was obtained at other water/cement ratios regardless of the concentration of the chloride solution.

Influence of early exposure to chloride environment on the chloride profiles of the repair materials and the concrete is shown in figures 5.37 to 5.40. For the repair materials A, B and the concrete mix, an increase in chloride uptake occurred with increase in age of exposure to chloride solution, while in case of material C (figure 5.39) duration of exposure has relatively small influence on the chloride diffusion profile.

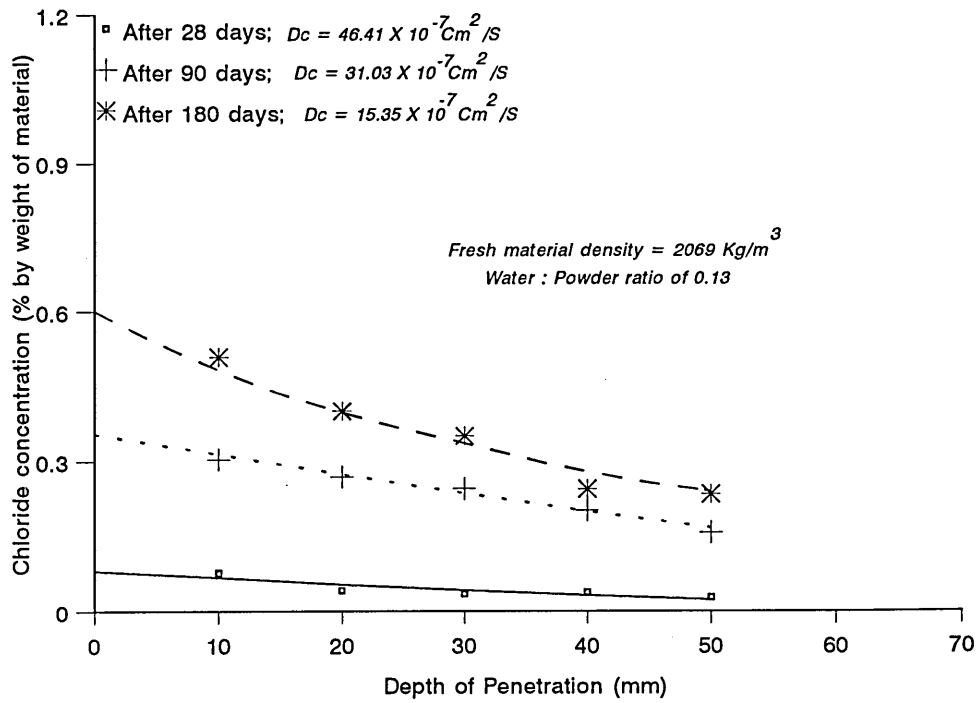


Figure 5.29
 Chloride diffusion profiles for repair material A at various periods of exposure to chloride
 (initial water cured at 20 C for the first 28 days)

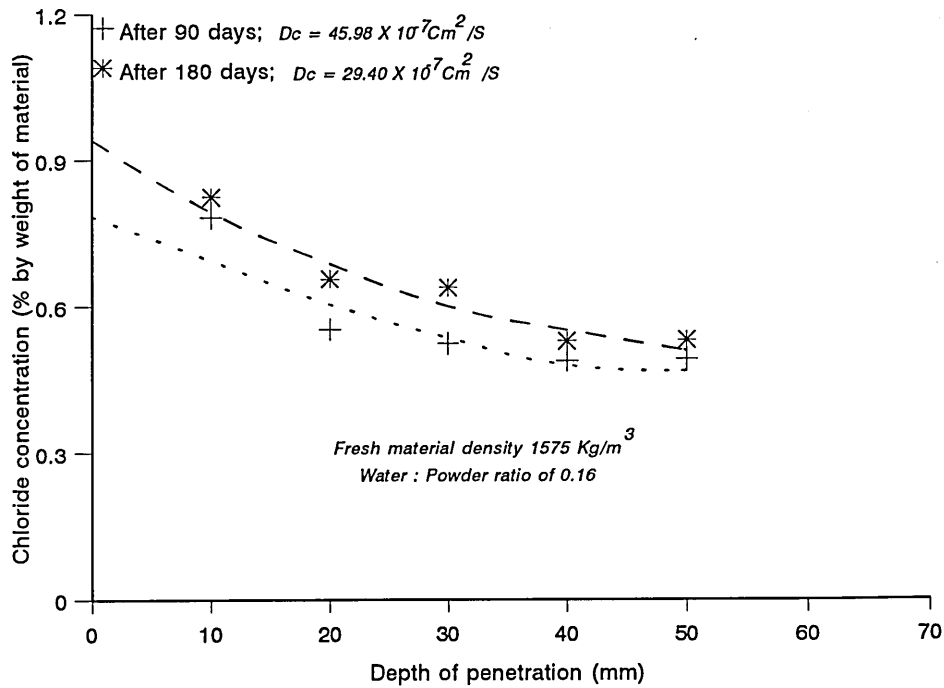


Figure 5.30
 Chloride diffusion profiles for repair material B at various periods of exposure to chloride
 (initial water cured at 20 C for the first 28 days)

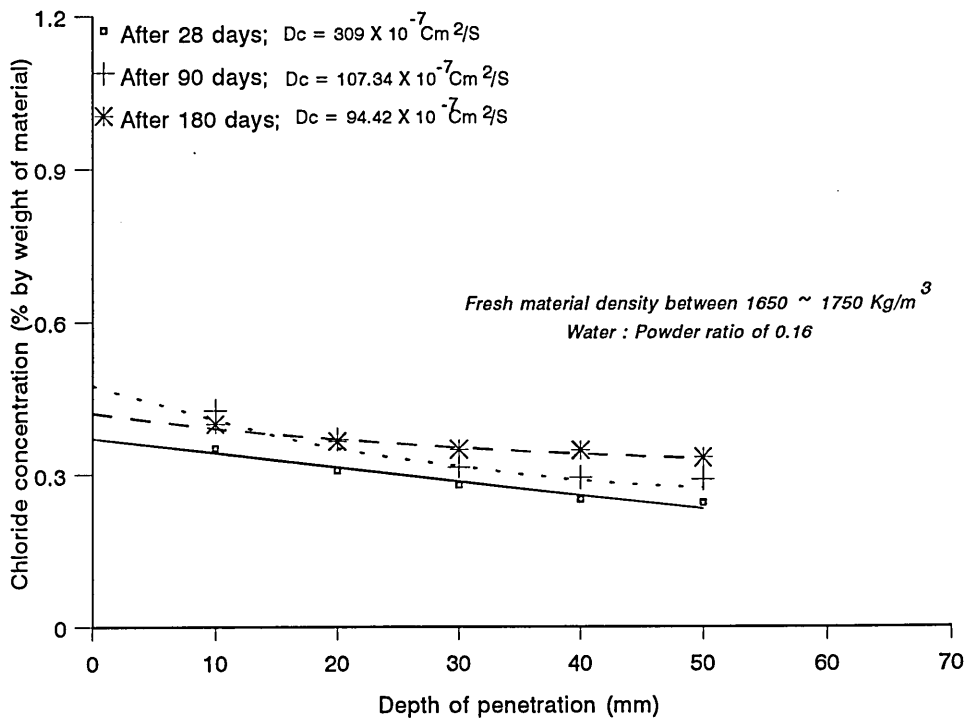


Figure 5.31
 Chloride diffusion profiles for repair material C at various periods of exposure to chloride
 (initial water cured at 20 °C for the first 28 days)

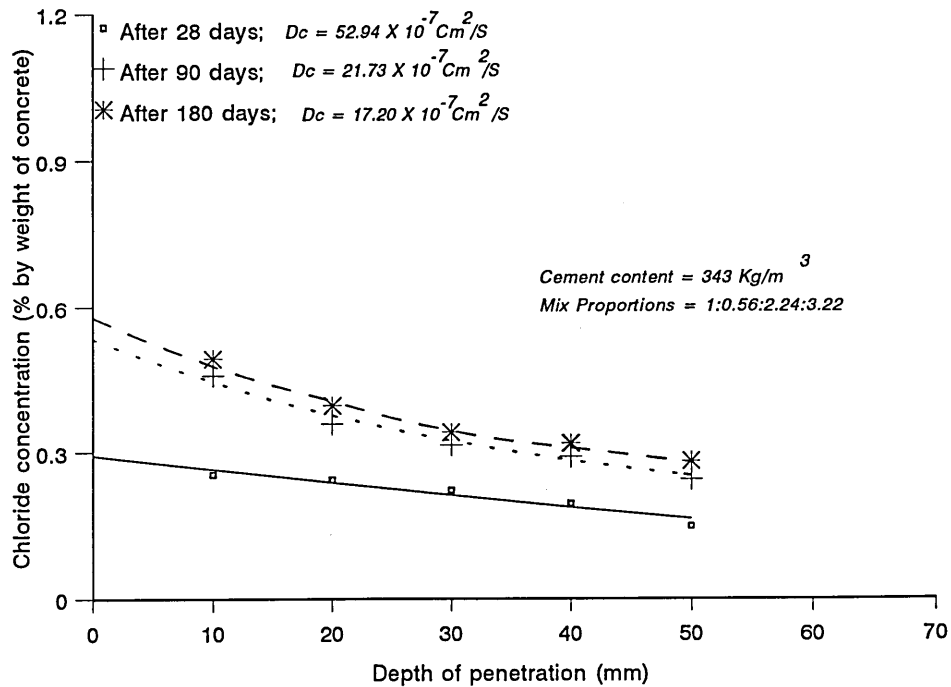


Figure 5.32
 Chloride diffusion profiles for concrete mix at various periods of exposure to chloride
 (initial water cured at 20 °C for the first 28 days)

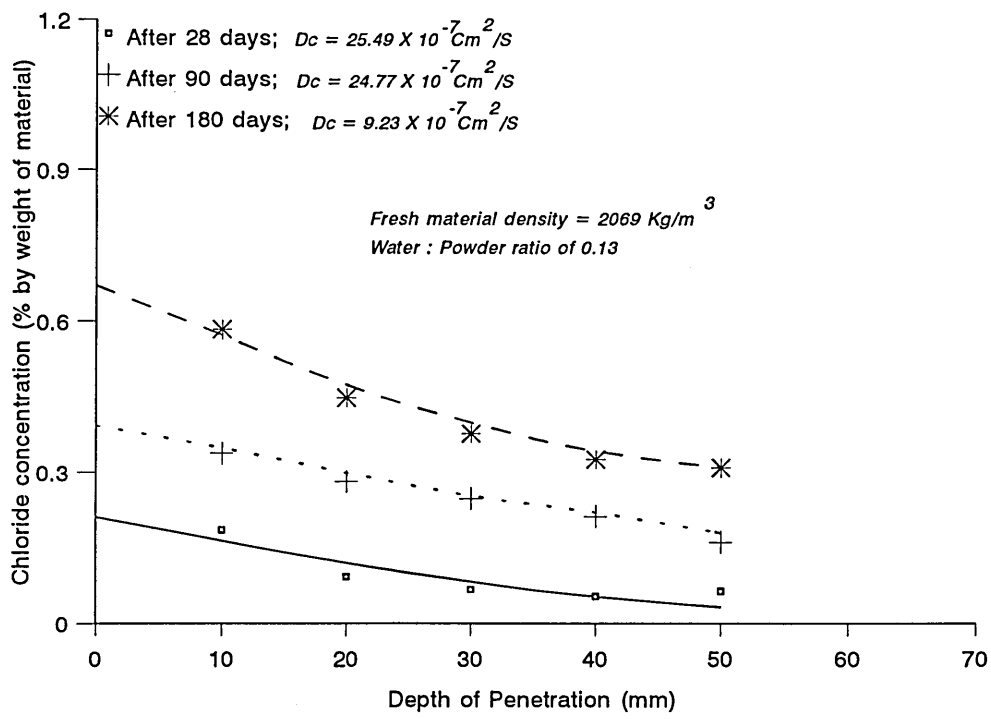


Figure 5.33
Chloride diffusion profiles for repair material A at various periods of exposure to chloride (initial air cured at 20 C, 55% r.h. for the first 28 days)

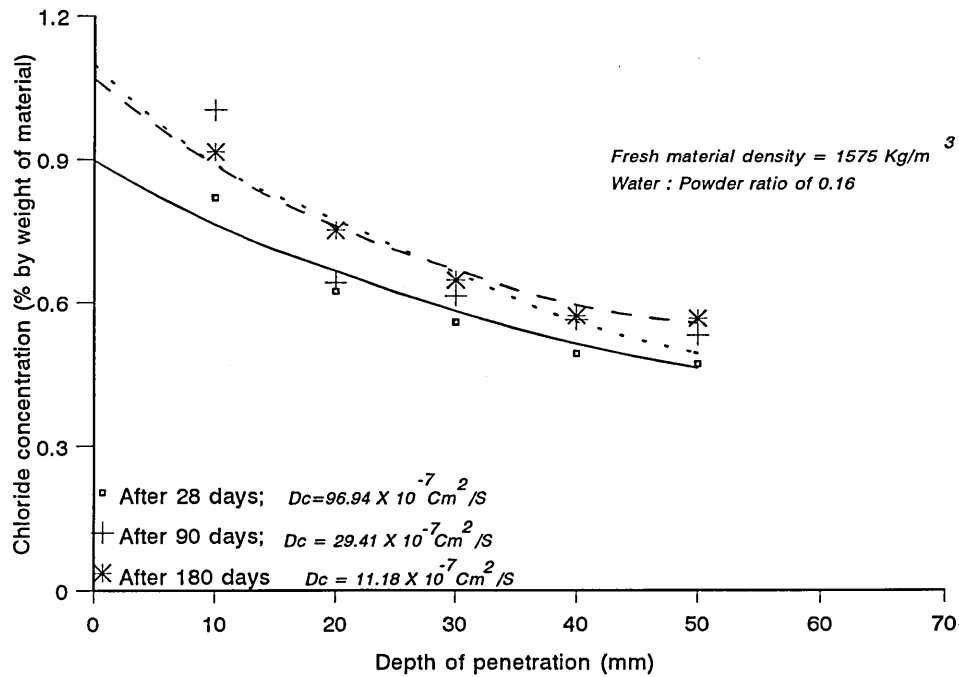


Figure 5.34
Chloride diffusion for repair material B at various periods of exposure to chloride (initial air cured at 20 C, 55% r.h. for the first 28 days)

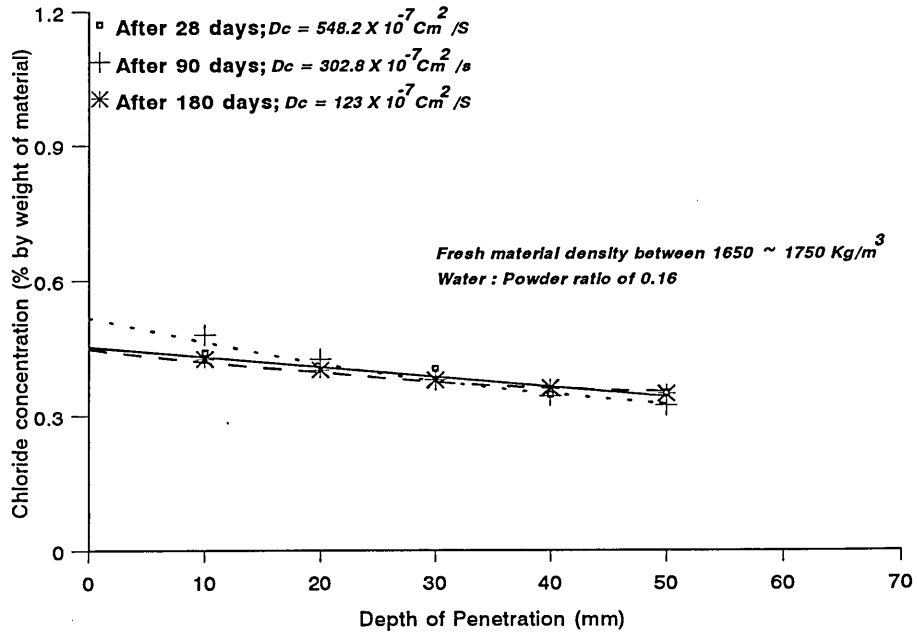


Figure 5.35
 Chloride diffusion profiles for repair material C at various periods of exposure to chloride
 (initial air cured at 20 C, 55% r.h. for the first 28 days)

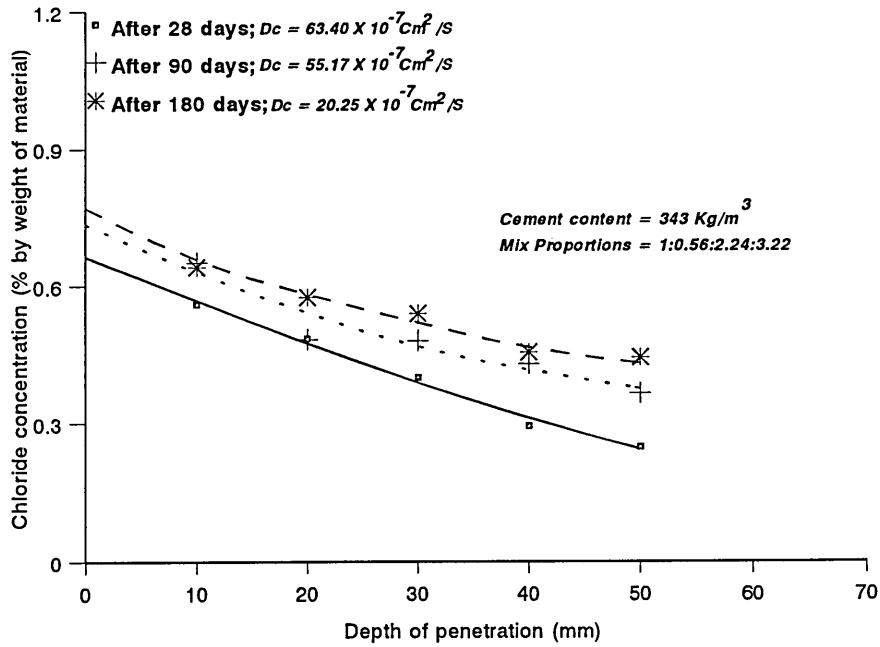


Figure 5.36
 Chloride diffusion profiles for concrete mix at various periods of exposure to chloride
 (initial air cured at 20 C, 55% r.h. for the first 28 days)

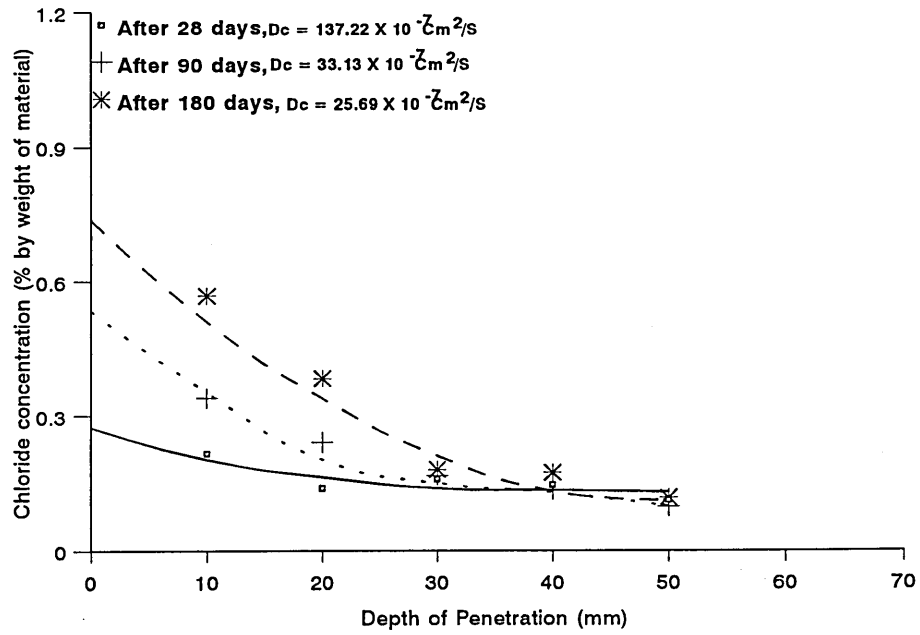


Figure 5.37
Chloride diffusion profiles for material A at various periods of exposure to chloride (early exposure - 24 hours after casting)

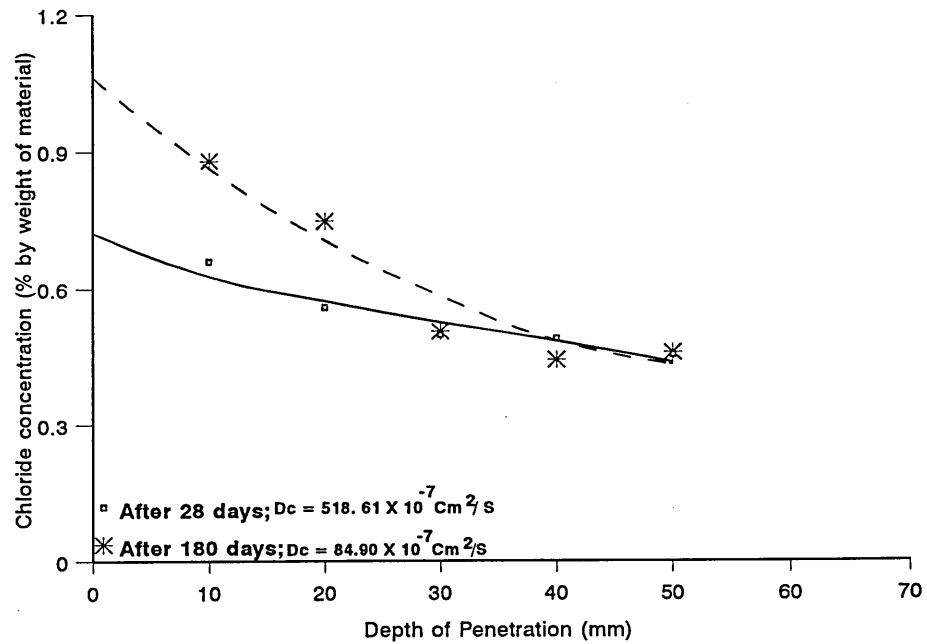


Figure 5.38
Chloride diffusion profiles for material B at various periods of exposure to chloride (early exposure - 24 hours after casting)

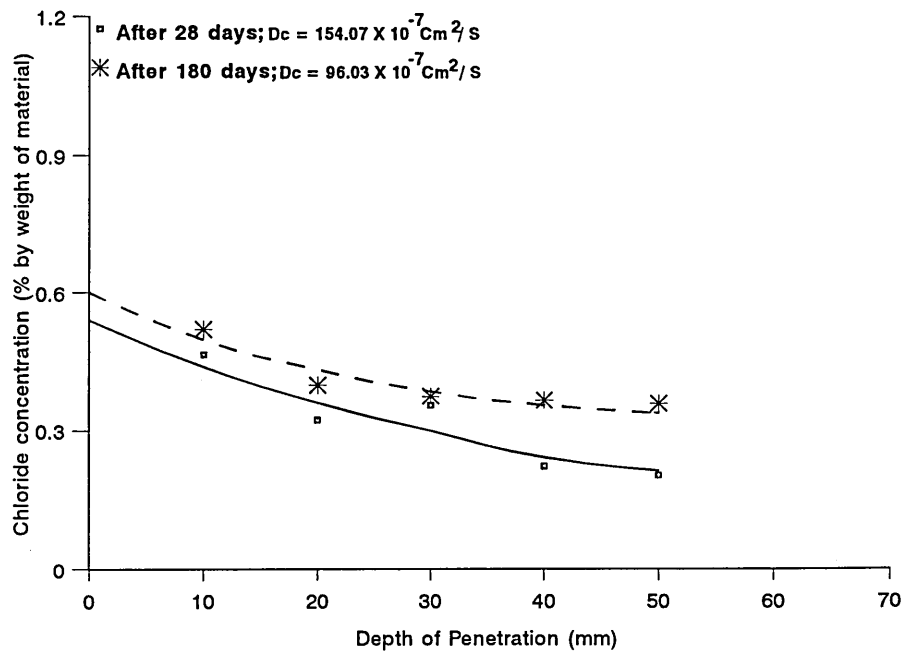


Figure 5.39
Chloride diffusion profiles for material C at various periods of exposure to chloride
(early exposure - 24 hours of casting)

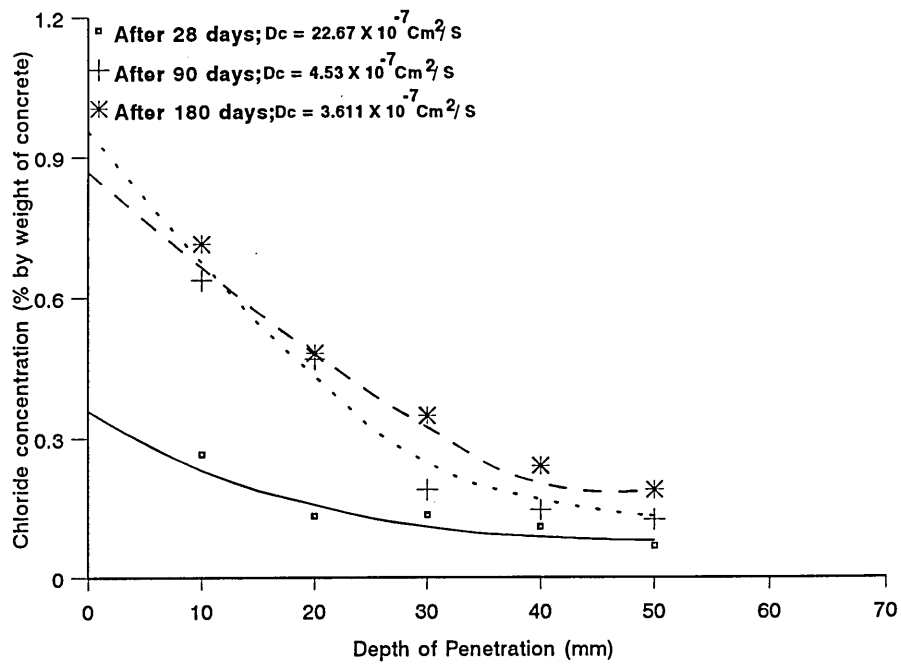


Figure 5.40
Chloride diffusion profiles for concrete at various periods of exposure to chloride
(early exposure - 24 hours after casting)

By comparing the results of mixes exposed after 24 hour and after 28 days of initial curing, it is shown that specimens exposed to chloride environment after 24 hours of casting has no serious consequences on long-term chloride concentration.

5.4.3.2 Relationship between Diffusion coefficient and duration of exposure

Results obtained on the variation of diffusion coefficient with duration of exposure, together with the results of other workers are reported. The variation in the diffusion coefficient with the duration of exposure to chloride solution for the results of this investigation are shown in figures 5.41 to 5.43 for initially air cured specimens at 20°C, 55% RH, water cured specimens at 20°C and early exposed specimens respectively. The diffusion coefficient values ranged from $63.4 \times 10^{-7} \text{ cm}^2/\text{Sec}$ after 28 days of exposure to $20.25 \times 10^{-7} \text{ cm}^2/\text{Sec}$ after 180 days of exposure, for initially air cured concrete specimens.

El-Khatib [125] reported values of diffusion coefficients for different mixes of concrete with various durations of exposure to chloride solution. Four different concrete mixes were used. Mixes A1, B1, C1 and D1 of proportions by weight of Cement : Binder (which comprises cement and cement replacement material) : Water : Fine aggregate : Coarse aggregate of 1 : 0.45 : 2.0 : 3.44. The mixes were identified as follows:-

- a) Mix A1 is the control mix made with OPC, without the addition of cement replacement materials;
- b) Mix B1 was made with 22% replacement of cement with PFA;

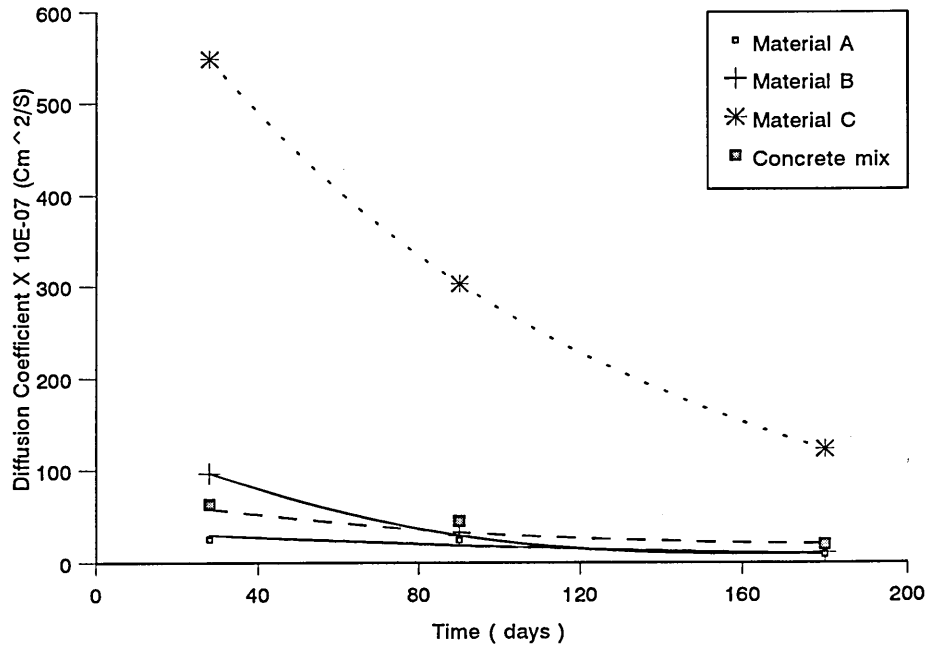


Figure 5.41
Diffusion coefficient versus exposure time for repair materials A,B,C and concrete mix
(initial curing for 28 days 20°C, 55% RH)

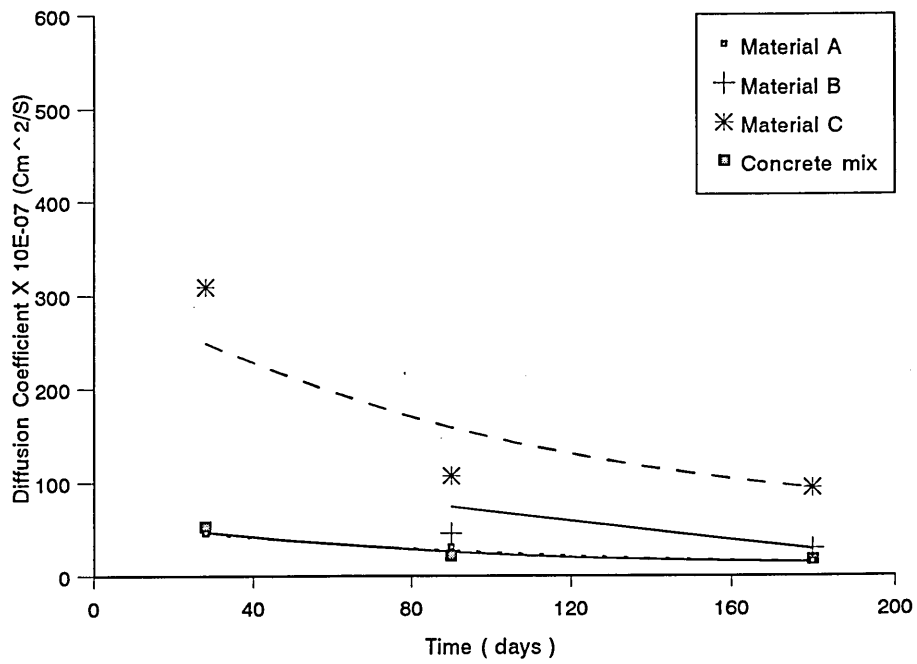


Figure 5.42
Diffusion coefficient versus exposure time for repair materials A, B, C and concrete mix
(initial water curing for 28 days at 20°C)

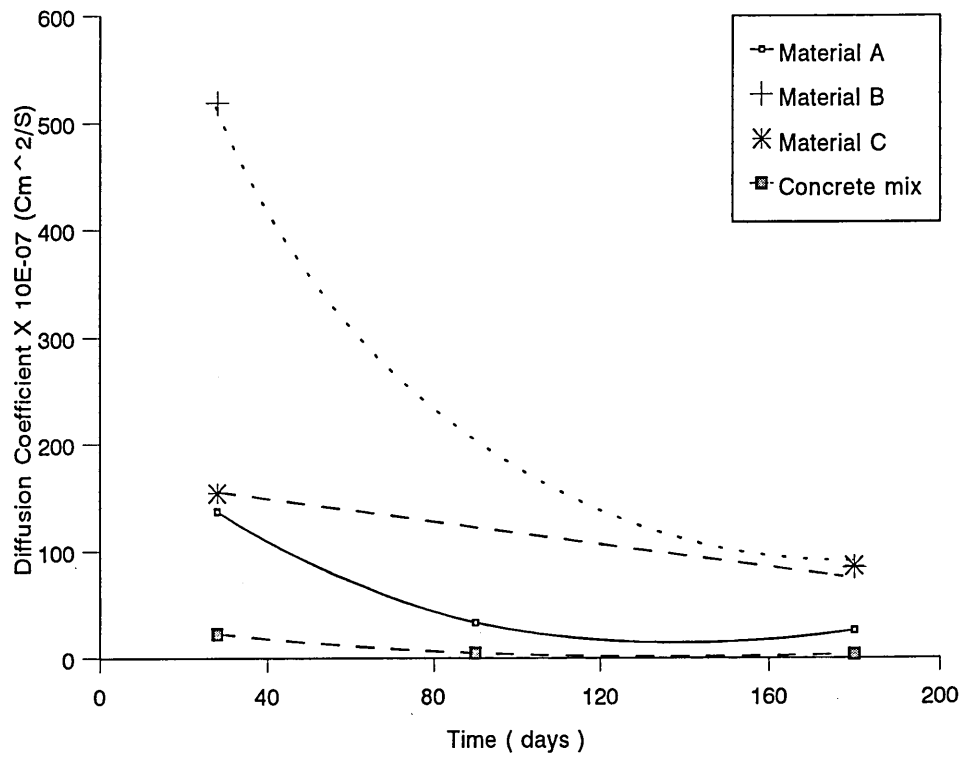


Figure 5.43
 Diffusion coefficient versus exposure time for repair materials A, B, C and concrete mix
 (early exposure 24 hours after casting)

c) Mix C1 is the mix where 9% of cement was replaced by silica fume, and

d) Mix D1 was made with replacing 40 of cement GGBF slag.

Further details of the mixes are given in Table 5.3.

Table 5.3 Details of mixes used by El-Khatib [125]

| Mix proportions (Kg/m ³) | | | | | | | |
|--------------------------------------|--------|-----|-------------|-----------|-------|----------------|------------------|
| Mix | Cement | PFA | Silica Fume | GGBF Slag | Water | Fine Aggregate | Coarse Aggregate |
| A1 | 350 | - | - | - | 157.7 | 708.6 | 1201.4 |
| B1 | 273 | 77 | - | - | 157.7 | 687.1 | 1201.4 |
| C1 | 318.5 | - | 31.5 | - | 157.5 | 698.1 | 1201.4 |
| D1 | 210 | - | - | 140 | 157.5 | 698.6 | 1202.4 |

1.2% by weight of cement or cementitious materials (binder) of Superplasticiser SP2000 was added in mixes A1, B1 and D1, and 1.5% was added in mix C1 to provide satisfactory workability. 95ml of air entraining agent (AEI) per 50 kg of cement or cementitious material (binder) were added in mixes A1, C1, and D1, While 118 ml per 50 kg of cementitious material were added in mix B1 which contained 22% of PFA. Owing to

the presence of carbon in PFA, the air content of the concrete mix was reduced, so that it maintain the same level of air content in mix 1 compared with other three mixes, the dosage of air entraining agent had to be increased as recommended by the manufacturer. After casting, specimens (100X100X500 mm) were initially cured in air at 37°C, 25% RH, wet/air cured at 37°C, 25% RH and air cured at ambient conditions. The chloride diffusion values ranged from 7×10^{-7} Cm²/Sec after 28 days of exposure to 0.1×10^{-7} Cm²/Sec after 12 months of exposure for initial wet/air curing (at 37°C, 25% R.H.) condition, as shown in figure 5.44.

Molloy [126] reported values of diffusion coefficients for different concrete mixes with various durations of exposure to sea water. Six different mixes were used. Control mix A3, mix D3 with 25% replacement of cement with PFA, mix E3 with 60% replacement of cement with GGBF slag, and F3 with 15% replacement of cement with silica fume. The binder content of mixes A3, D3, E3 and F3 was 430 kg/m³ and water/binder ratio of 0.58. Mixes B3 and C3 were mixes with cement only. Mix B3 had a cement content of 430 kg/m³ and water/cement ratio of 0.58. Details of the mixes are given in Table 5.4. After casting, specimens (100 X 100 X 500 mm) were initially cured in air under laboratory ambient conditions for one month before exposure to sea water. Chloride diffusion values ranged from about 2.0×10^{-7} Cm²/Sec to 12.6×10^{-7} Cm²/Sec, but after 9 months of exposure, the values ranged from 0.42×10^{-7} to 1.51×10^{-7} Cm²/Sec. Results on variation of chloride diffusion coefficient for mixes A3, B3, C3, D3, E3 and F3 are presented in figure 5.45.

Thomas' et al results [127] show that the values of diffusion coefficients were always found to be lower after two years of exposure compared to those after one year of exposure. This further indicates that the diffusion coefficient decreases as the period of exposure to the chloride environment increases.

Table 5.4 Details of Mixes used by Molloy [126].

| Mix | Mix Proportions by weight | | | | | | | Water/ Binder Ratio | Binder Content |
|-----|---------------------------|----------------|--------------------------|--------|-------------------|---------------------|--|---------------------------|-------------------|
| | pfa | Silica Fume | Blast Furnace Slag | Cement | Fine Aggregate | Coarse Aggregate | | | |
| A3 | 0.0 | 0.0 | 0.0 | 1.0 | 2.5 | 1.2 | | 0.58 | 430 |
| B3 | 0.0 | 0.0 | 0.0 | 1.0 | 2.73 | 1.31 | | 0.45 | 430 |
| C3 | 0.0 | 0.0 | 0.0 | 1.0 | 2.67 | 0.8 | | 0.58 | 530 |
| D3 | 0.25 | 0.0 | 0.0 | 0.75 | 2.43 | 1.20 | | 0.58 | 430 |
| E3 | 0.0 | 0.0 | 0.6 | 0.4 | 2.46 | 2.20 | | 0.58 | 430 |
| F3 | 0.0 | 0.15 | 0.0 | 0.85 | 2.49 | 1.20 | | 0.58 | 430 |

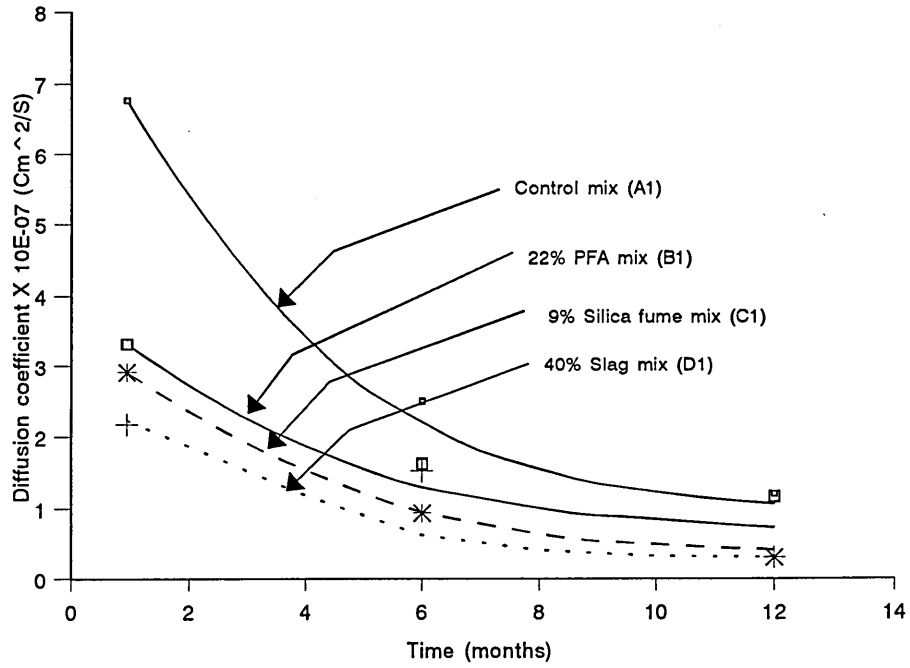


Figure 5.44
Diffusion coefficient versus time for mixes A1, B1, C1 and D1,
after El-Khatib [125]

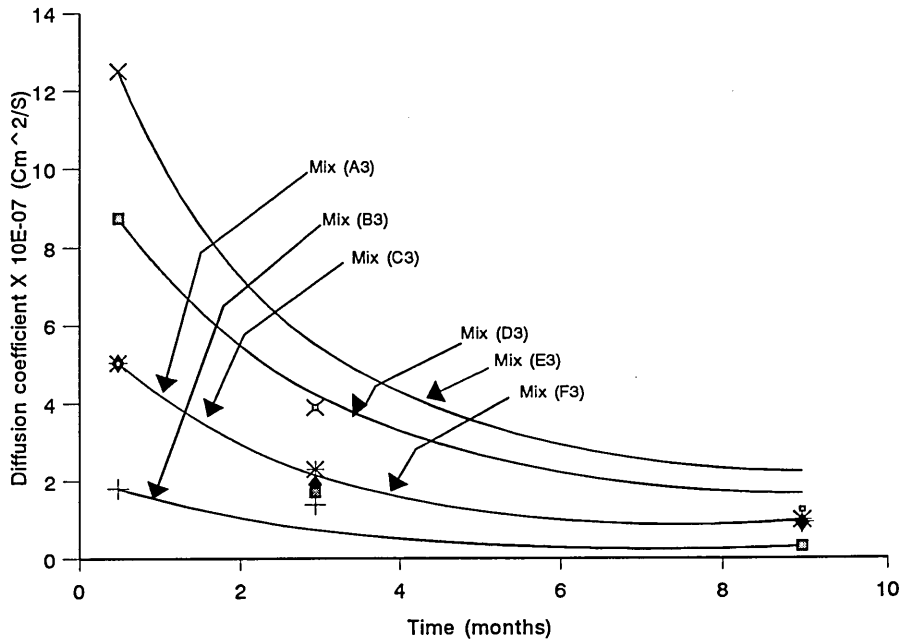


Figure 5.45
Diffusion coefficient versus time for mixes A3, B3, C3, D3, E3 and F3,
after Molloy [126]

It is observed from experimental results of this investigation and others [102,103, 125-127] that the rate of chloride diffusion into repair materials and concrete diminishes with time. The values of D_c for materials A, B, C and concrete are shown in figures 5.41 and 5.42 for exposure periods up to 180 days for specimens water cured at 20°C and air cured at 20°C, 55% RH for first 28 days prior to exposure to chloride solution. It is evident from these figures that the rate of decrease in D_c values is sharp at early age. The implication of decreasing D_c values with time is that prediction of long-term chloride concentrations in repaired concrete structures by simply using D_c values measured at earlier ages will result in an overestimation of these concentrations. The diffusion coefficient values ranged from $29 \times 10^{-7} \text{ cm}^2/\text{Sec}$ after 28 days of exposure to $9.23 \times 10^{-7} \text{ cm}^2/\text{Sec}$ after 180 days of exposure for initial air cured specimens of material A. In the case of material B, the diffusion coefficient value after 28 days of immersion was $209.7 \times 10^{-7} \text{ cm}^2/\text{sec}$ for initial water cured specimens at 20°C as shown in figure 5.30. The overwhelming evidence indicates that the diffusion coefficient decreases as the duration of exposure to chloride environment increases.

5.5 PREDICTION OF LONG-TERM CHLORIDE PENETRATION

The basic Fick's 2nd law equation and its solution as applied to chloride diffusion in concrete were presented in section 5.2.2 [Equations (5.1) and (5.2)]. The effective diffusion coefficient is assumed to be constant with respect to time in these equations. Figures 5.41 to 5.43 show, however, that D_c is time dependent. So incorporating the time-dependency of D_c into the chloride diffusion model used for calculating long-term chloride concentrations will lead to greater accuracy. Hence, the relationship between D_c and time may be approximated by an empirical relationship of the form,

$$D_c = D_1 t_m^{-m} \quad (5.3)$$

Where,

- D_c = effective diffusion coefficient (Cm²/Sec)
 t_m = time (months)
 D_1 = effective diffusion coefficient at time t equal to one month
 m = empirical coefficient, which depends on the diffusion characteristic of the material.

Equation (5.3) can be written in a linear form as;

$$\log D_c = \log D_1 - m \log t_m \quad (5.4)$$

In order to determine the values of D_1 (from the intercept) and the constant m (slope) for the various materials, the data for the mixes reported in this chapter are plotted in the form of equation (5.4) in figures 5.46 to 5.48. Since repair materials are generically different and sensitive to the initial curing condition, separate values of constants for initial water cured and air cured specimens are listed in Table 5.5. Table 5.6 gives values of constants (m and D_1) for early exposed specimens.

The profiles of the diffusion coefficient as a function of time have been calculated using equation 5.4 using the values of m and D_1 tabulated in Tables 5.5 and 5.6. These have been plotted together with the experimental data in figures 5.49 to 5.51 for different curing conditions. The experimental results of diffusion coefficients obtained in this investigation are generally in good agreement with the profiles obtained from different m and D_1 values, which are shown by the solid line. It appears that equation 5.3 is suitable for the prediction of long-term chloride diffusion coefficient with reasonable accuracy.

TABLE 5.5 D_1 and m values for the various materials for initially either air cured or water cured for 28 days

| Materials | initially water cured | | initially air cured | |
|-----------|-----------------------|--|---------------------|--|
| | m | D_1 ($\times 10^{-6}$) Cm ² /Sec | m | D_1 ($\times 10^{-6}$) Cm ² /Sec |
| A | 0.50 | 4.70 | 0.57 | 3.91 |
| B | 1.10 | 19.06 | 1.41 | 13.85 |
| C | 0.69 | 25.88 | 0.65 | 56.88 |
| Concrete | 0.58 | 4.70 | 0.52 | 7.06 |

TABLE 5.6 D_1 and m values for the various materials for early exposed (24 hours after casting) specimens

| Materials | m | D_1 ($\times 10^{-6}$) Cm ² /Sec |
|-----------|------|--|
| A | 0.91 | 11.88 |
| B | 0.98 | 48.31 |
| C | 0.58 | 14.96 |
| Concrete | 0.92 | 1.88 |

5.5.1 Surface Chloride Concentration, C_0 , and Diffusion Coefficient, D_c

The values of surface chloride concentration, C_0 , were obtained from experimental data available at different periods of exposure to a chloride environment by applying Fick's second law (equation 5.2), to obtain a best-fit curve. These values of surface concentration obtained from the experimental data are plotted against exposure period in figures 5.52 to 5.54. The results in these figures indicate that generally there is an increase in C_0 values as the period of immersion increases. It is important to state that a high concentration of the

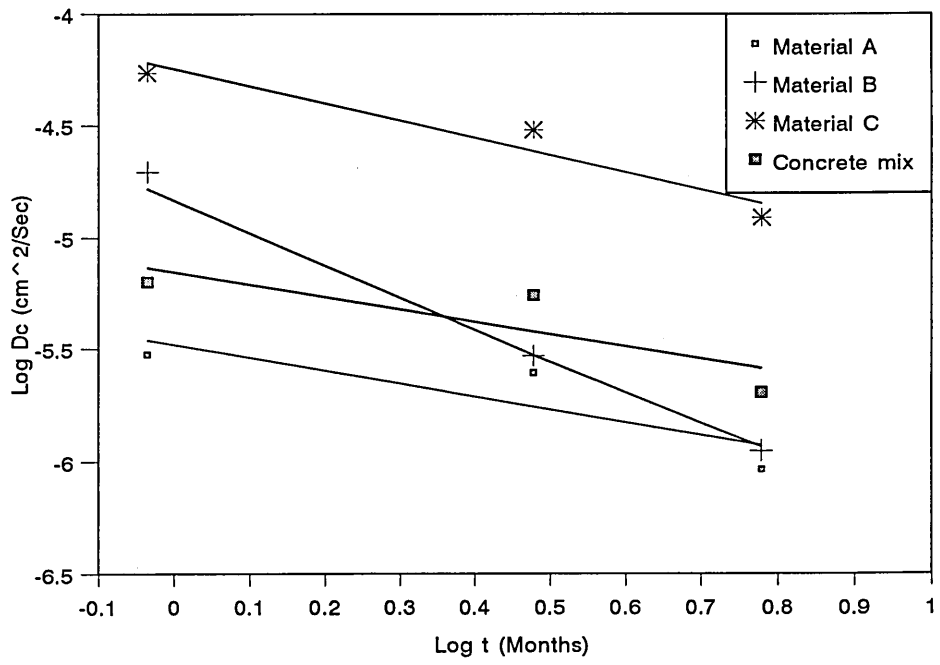


Figure 5.46
 Relation between effective diffusion coefficient (D_c) and time for repair materials A, B, C and concrete mix exposed to chloride solution (initially air cured for 28 days at 20 C, 55% r.h.)

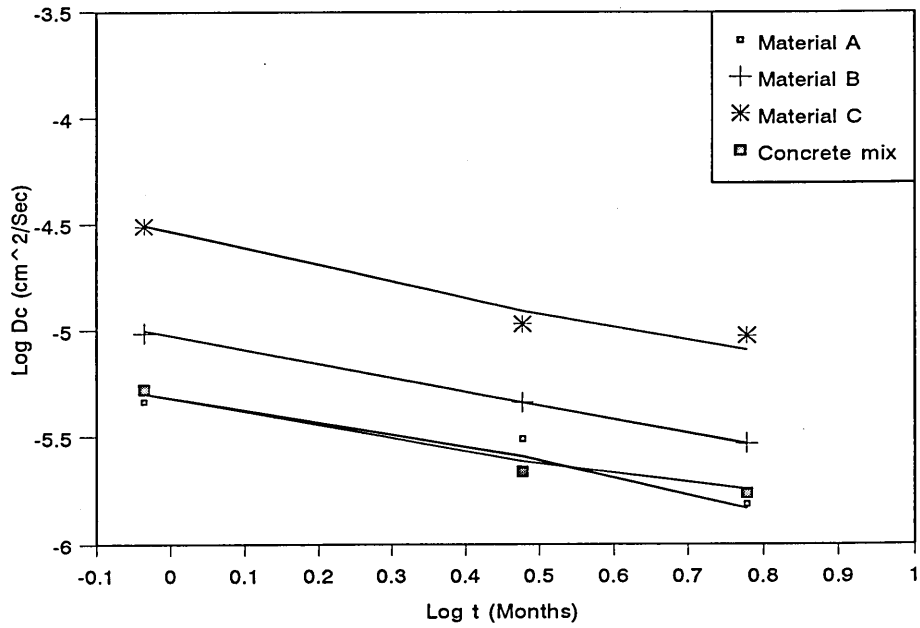


Figure 5.47
 Relation between effective diffusion coefficient (D_c) and time for repair materials A, B, C and concrete mix exposed to chloride solution (initially water cured for 28 days at 20 C)

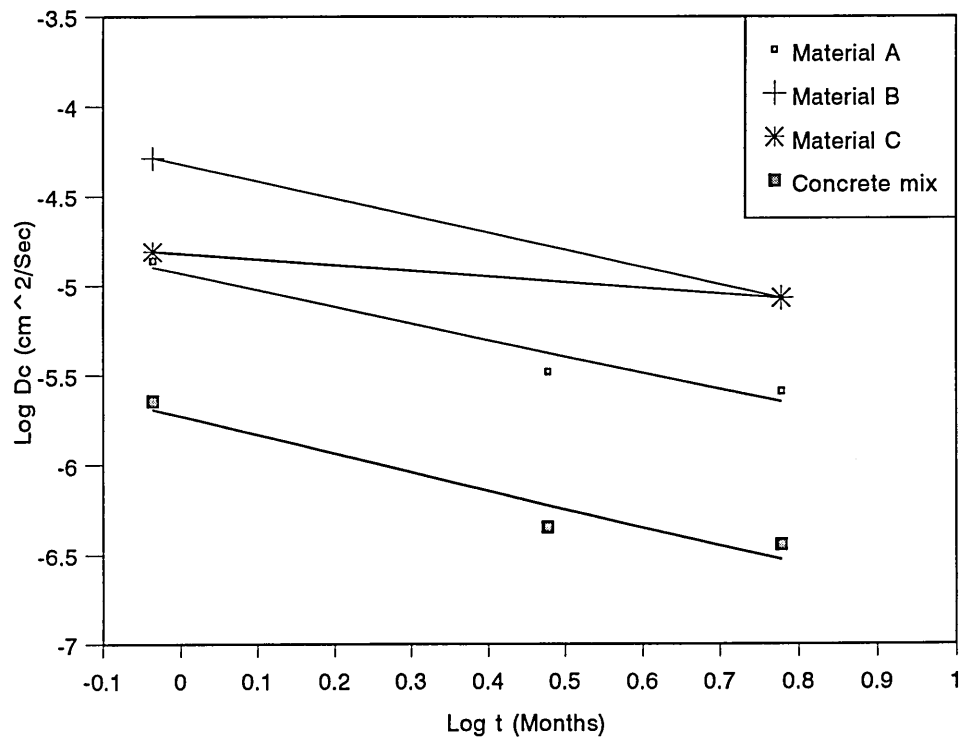


Figure 5.48
 Relation between effective diffusion coefficient (Dc) and time for repair materials A, B, C and concrete mix exposed to chloride solution (24 hours after casting)

chloride solution was used for the exposure test; 175 gm NaCl per litre was used. The vast majority of C_0 values obtained from the experimental data ranged between 0.3 to 0.8 % by weight of material. By comparing equilibrium chloride concentration of figure 5.54 (early exposed) with those obtained from specimens which were exposed to chloride solution after 28 days initial curing (figures 5.52 and 5.53) show no significant difference in the C_0 values of different materials in the long-term.

Also, an attempt is made to see whether there is any relationship between C_0 and D_c . In figure 5.55, each value of equilibrium chloride concentration on the surface (C_0) associated with a value of diffusion coefficient (D_c) is plotted for the mixes considered in this investigation (materials A, B, C and concrete) after 28 days, 90 days and 180 days of immersion in the chloride solution. There seems to be no specific trend between C_0 and D_c . This is further repeated in figure 5.56 for the data of El-Khatib [125] on mixes A1, B1, C1 and D1.

In figure 5.57, the relationship between C_0 and D_c obtained from other research data [102,103,123] is presented. The figure shows that there is no relationship between C_0 and D_c . In mix B1 the value of D_c decreases as the value of C_0 increases. whereas in mix A1, the D_c values seems to have increased as the values of C_0 increased. Also, Gjorv and Vennesland's results show no particular trend.

From the above results in figures 5.55 to 5.57, it can be concluded that surface chloride concentration (C_0) and diffusion coefficient (D_c) are not related. This can be due to the fact that D_c is primarily related to the properties of material and C_0 is a function of the chloride concentration of the solution to which a concrete specimen is exposed.

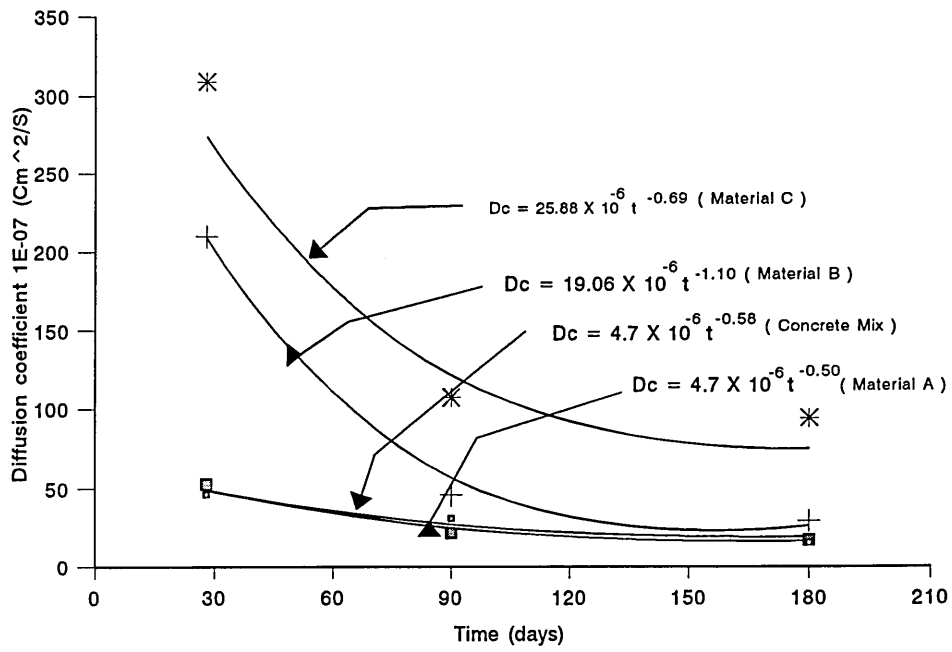


Figure 5.49
Relationship between diffusion coefficient and time for initial water cured specimens, using m and D1 values from Table 5.5

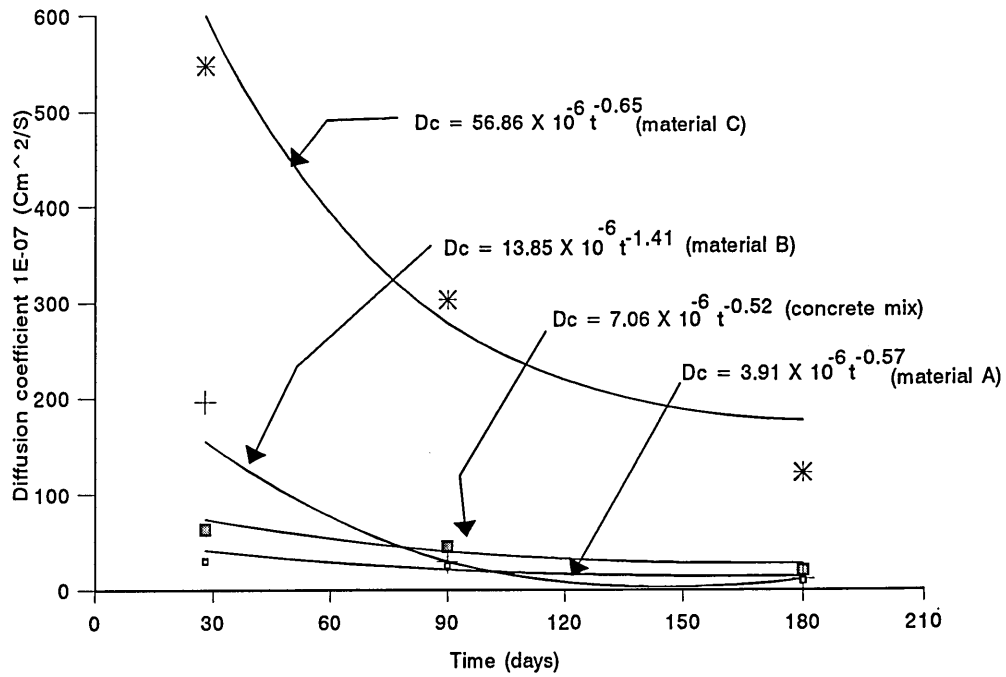


Figure 5.50
Relationship between diffusion coefficient and time for initial air cured specimens, using m and D1 values from Table 5.5

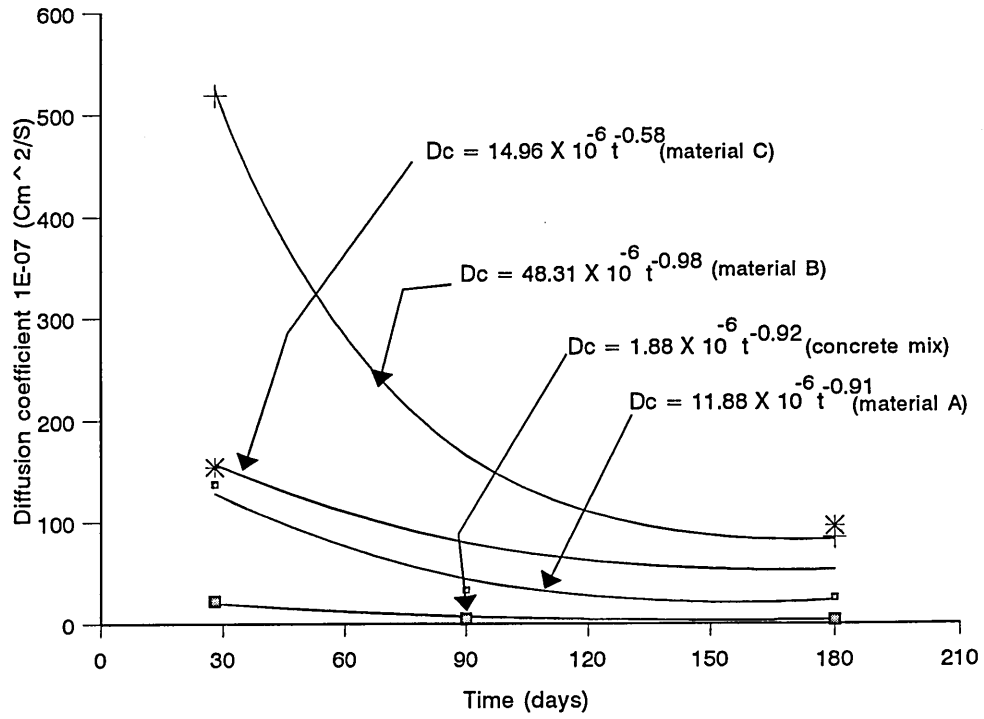


Figure 5.51
 Relationship between diffusion coefficient and time for early exposed (24 hours after casting)
 specimens using m and D_1 values from Table 5.6

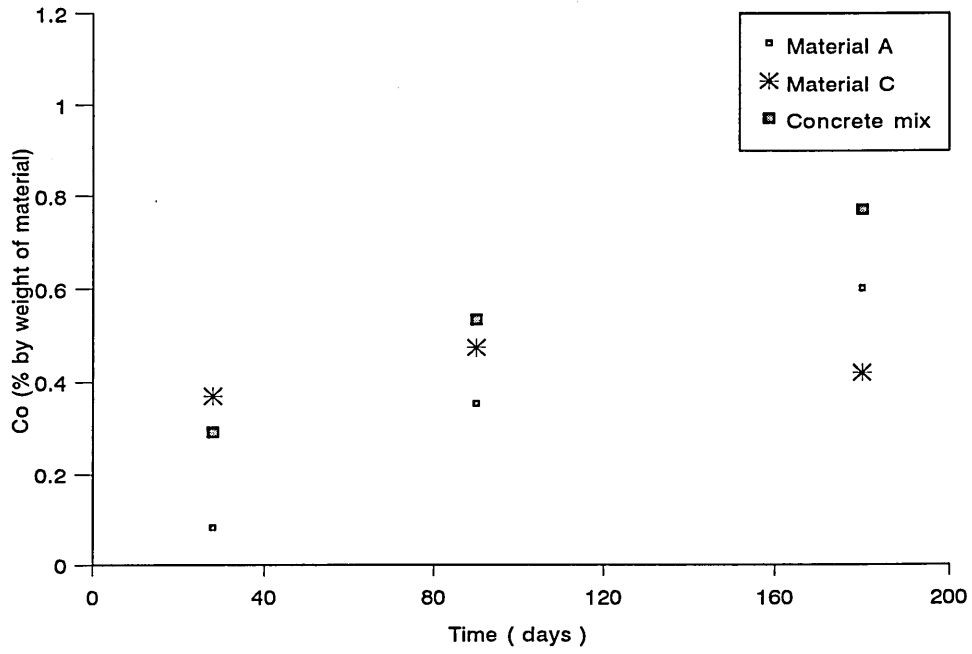


Figure 5.52
Equilibrium chloride concentration with time for repair materials A, B, C and concrete mix
(for initial water curing at 20°C)

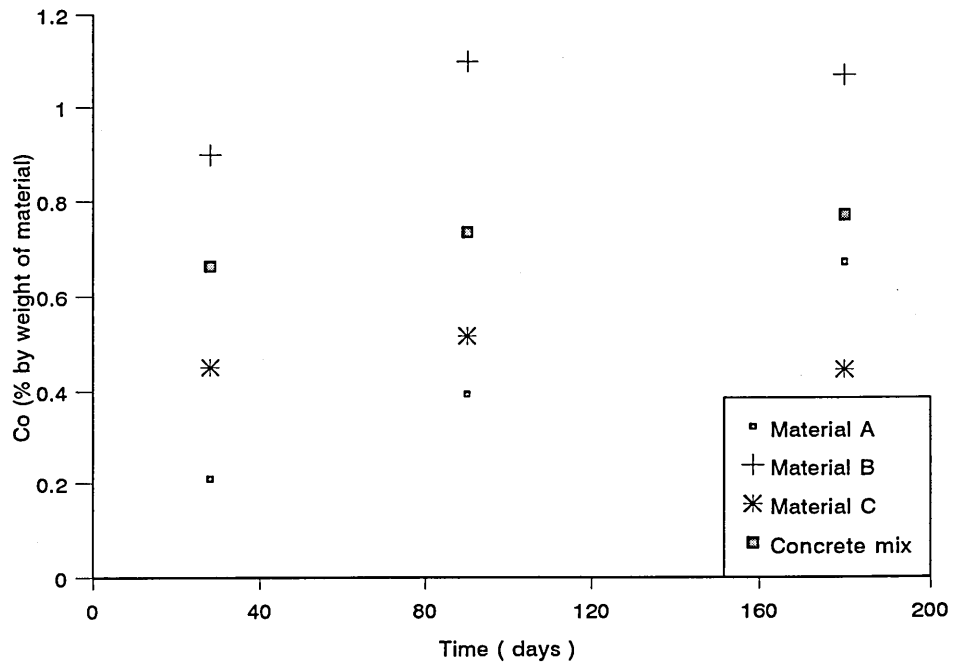


Figure 5.53
Equilibrium chloride concentration with time for repair materials A, B, C and concrete mix
(for initial air curing at 20°C, 55% RH)

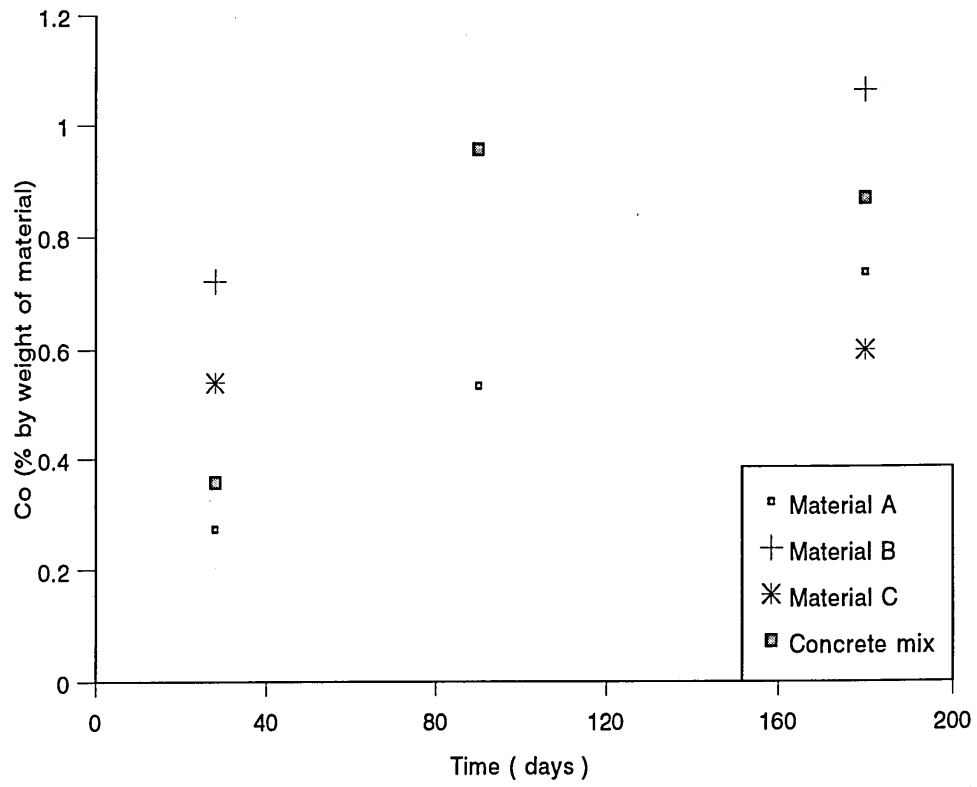


Figure 5.54
 Equilibrium chloride concentration with time for repair materials A, B, C and concrete mix
 (for specimens immersed in the chloride solution at 24 hours after casting)

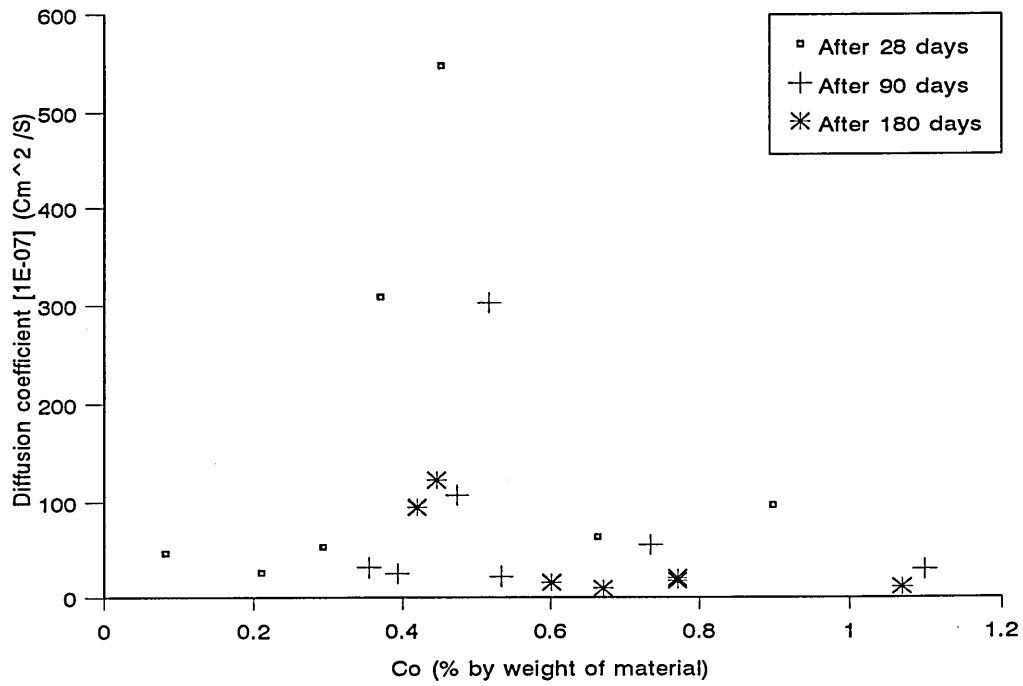


Figure 5.55 Relationship between Co and Dc for repair materials A, B, C and concrete mix

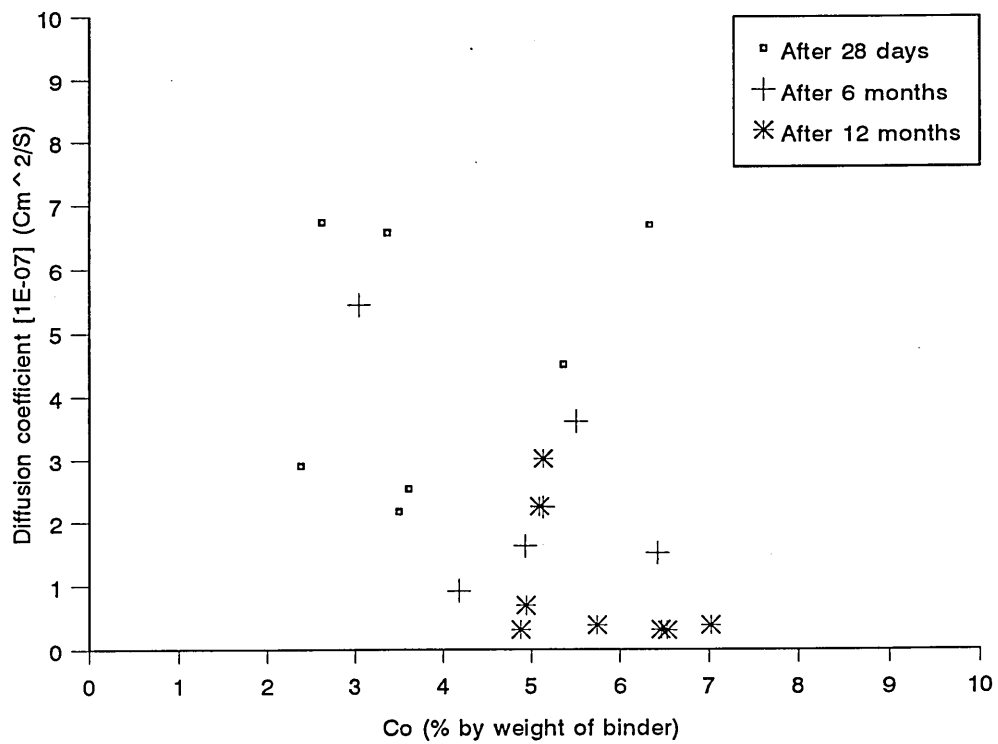


Figure 5.56 Relationship between Co and Dc for mixes used by El-Khatib [125]

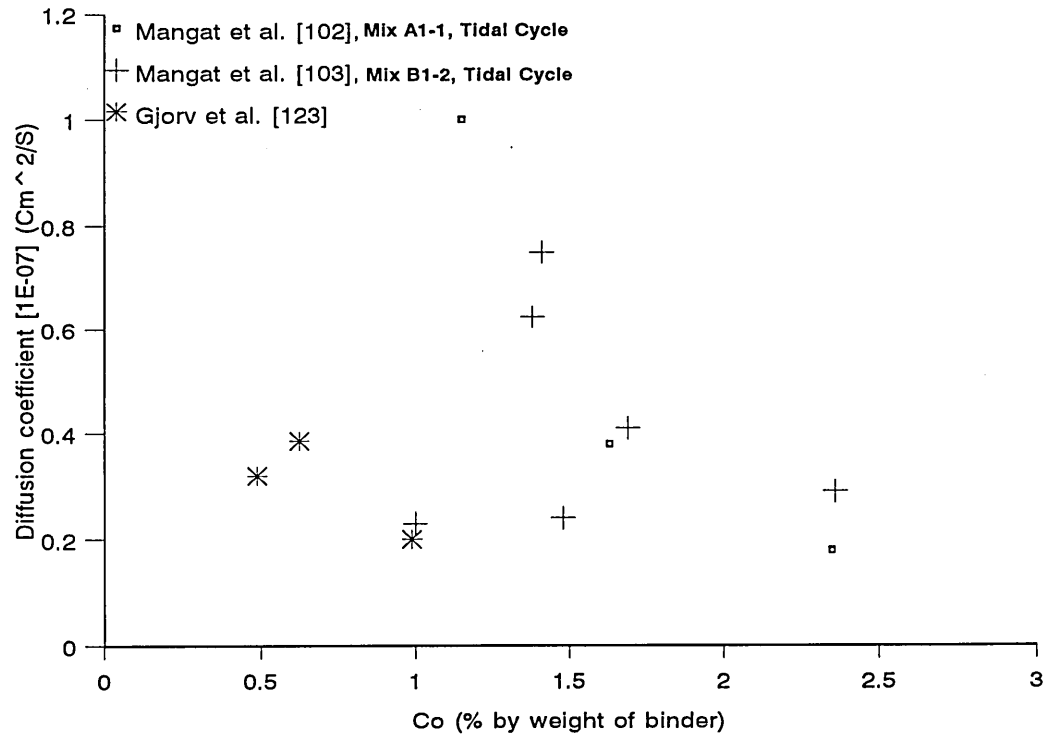


Figure 5.57 Relationship between Co and Dc for mixes used by different researchers

5.5.2 Theory for predicting long-term chloride diffusion

As discussed in section 5.5.1, the diffusion coefficient decreases as the period of exposure to chloride environment increases. The following empirical equation was derived to describe that change, which was as follows :-

$$D_{ct} = D_1 t_m^{-m} \quad (5.3)$$

The value of constants, D_1 and m , for the various materials are given in the Tables 5.5 and 5.6.

In order to derive an equation for the determination of long-term chloride concentration in repair materials, the time-dependence of the diffusion coefficient, D_{ct} , which is represented by equation 5.3, needs to be incorporated in the theory based on Fick's second law of diffusion which governs chloride penetration into material.

By converting the time in months into seconds, equation 5.3 becomes,

$$D_{ct} = K_s t^{-m} \quad (5.5)$$

Where,

t = time of exposure to chloride solution in seconds,

Table 5.6(a) The values of constant K_s

| Materials | K_s | |
|-----------|-------------------------|-------------------------|
| | initially water cured | initially air cured |
| A | $0.153 \times 10^4 D_1$ | $0.430 \times 10^4 D_1$ |
| B | $0.108 \times 10^8 D_1$ | $10.49 \times 10^8 D_1$ |
| C | $2.53 \times 10^4 D_1$ | $1.4 \times 10^4 D_1$ |
| Concrete | $0.498 \times 10^4 D_1$ | $0.205 \times 10^4 D_1$ |

For example, diffusion coefficient, D_{ct} , for initially water cured material A is as follows:

$$D_{ct} = (0.153 \times 10^4) D_1 t^{-m} \quad (5.6)$$

For initially air cured repair material A, substituting the time-variable expression for D_{ct} from equation 5.5 into equation 5.1 (Fick's second law of diffusion equation) gives:

$$\frac{\partial C}{\partial t} = (K_s t^{-0.57}) \frac{\partial^2 C}{\partial x^2} \quad (5.7)$$

Where,

$$m = 0.57, \text{ from Table 5.5.}$$

$$\therefore \frac{1}{(K_s t^{-0.57})} \frac{\partial C}{\partial t} = \frac{\partial^2 C}{\partial x^2} \quad (5.8)$$

$$\text{Assuming } \partial T = (K_s t^{-0.57}) \partial t \quad (5.9)$$

and substituting into equation (5.8) gives:

$$\frac{\partial C}{\partial T} = \frac{\partial^2 C}{\partial x^2} \quad (5.10)$$

Integrating equation (5.9) gives :

$$T = \int_0^t (K_s t^{-0.57}) \partial t$$

Solving the integral gives :

$$T = 2.326 K_s t^{0.43} \quad (5.11)$$

The standard solution of equation (5.10) is

$$C = C_0 \left[1 - \operatorname{erf} \left(\frac{x}{2\sqrt{T}} \right) \right] \quad (5.12)$$

Substituting for T from equation (5.11) and for K_s from equation (5.5) as listed in Table 5.7 gives :

$$C(x, t) = C_0 \left[1 - \operatorname{erf} \left(\frac{x}{196\sqrt{D_1 t^{0.43}}} \right) \right] \quad (5.13)$$

Hence, if the diffusion coefficient after one month (30 days) of exposure to a chloride environment, D_1 , is known together with the equilibrium chloride concentration on the material surface, C_0 , then the chloride concentration at a depth x from the surface after time t, $C(x,t)$, may be calculated from equation (5.13).

Similarly, using different values of K_s and m of the various materials for initial curing conditions of this investigation, the chloride concentration at a depth x from the surface after time t, $C(x,t)$, can be calculated as follows:-

For initial water cured Material A

$$C(x, t) = C_0 \left[1 - \operatorname{erf} \left(\frac{x}{109 \sqrt{D_1 t^{0.5}}} \right) \right] \quad (5.14)$$

For initial water cured Material C

$$C(x, t) = C_0 \left[1 - \operatorname{erf} \left(\frac{x}{555 \sqrt{D_1 t^{0.31}}} \right) \right] \quad (5.15)$$

For initial air cured Material C

$$C(x, t) = C_0 \left[1 - \operatorname{erf} \left(\frac{x}{391 \sqrt{D_1 t^{0.35}}} \right) \right] \quad (5.16)$$

For initial water cured Concrete Mix

$$C(x, t) = C_0 \left[1 - \operatorname{erf} \left(\frac{x}{213 \sqrt{D_1 t^{0.42}}} \right) \right] \quad (5.17)$$

For initial air cured Concrete Mix

$$C(x, t) = C_0 \left[1 - \operatorname{erf} \left(\frac{x}{129 \sqrt{D_1 t^{0.48}}} \right) \right] \quad (5.18)$$

In order to see the validity of equations (5.14) to (5.18), chloride diffusion profiles obtained from experimental data should be compared with those obtained from above equations. All equations are based on the assumption that the equilibrium chloride concentration on the surface, C_0 , is constant during the period of exposure to chloride

environment. By considering figures 5.52 to 5.54 (section 5.5.2) for the results of this investigation, C_0 seems to increase slightly as the period of exposure to chloride increases. However, a constant value has been assumed. The values of C_0 shown in figures 5.52 to 5.54 suggest that a value of 0.4% (by weight of material) for Material C and 0.6% (by weight of material) for other materials.

Consider the high-performance repair Material A under air curing at 20°C, 55%RH. The chloride diffusion profiles obtained from the experimental data after 180 days of exposure to chloride solution and those obtained from the equation (5.13) after the same period are shown in figure 5.58.

The values obtained from equation (5.13) are calculated as follows:

$$\begin{aligned} C_0 &= 0.6\% \text{ by weight of material (assumed)} \\ t &= (180 \times 24 \times 60 \times 60) = 15552000 \text{ Seconds} \\ D_1 &= 3.91 \times 10^{-6} \text{ Cm}^2/\text{Sec as given in Table 5.5.} \end{aligned}$$

It can be seen from figure 5.58 that predicted values obtained from equation (5.13) are slightly higher than those obtained from the experimental data. The difference becomes larger as the depth of penetration increases.

Similar differences are obtained in figure 5.59, for material C (initially water cured at 20°C) for 180 days of exposure. The same trend is seen in figures 5.60 and 5.61 for the concrete mix under initial air curing at 20°C, 55%RH and initial water curing at 20°C respectively, after 180 days of exposure.

Generally, the predicted chloride profiles are in acceptable agreement with the experimental data obtained in this investigation. Therefore the method outlined in this chapter

represents a convenient means of predicting chloride concentration in concrete and the three generic repair materials.

5.5.3 Application of prediction model to field data

The procedure for predicting long-term (after 20 years) chloride concentration profiles is applied to the field data of two Arabian Gulf reinforced concrete dock structures exposed to a marine environment, at Port Rashid and Jebel Ali Port. The calculations were performed for control concrete and concrete cast using zemdrain formwork. Splash zone, tidal zone and top of dock zones of marine exposure were considered. The structures were constructed using two types of formwork, standard formwork followed by normal curing and zemdrain formwork manufactured by DuPont de Nemours (Luxembourg) which allows absorption of moisture from top layers of concrete so that the surface layers of concrete are expected to be less permeable and consequently allow less chloride diffusion.

Using the chloride concentration data at various depths, as shown in Tables 5.7 and 5.8, values of diffusion coefficients (D_c) and equilibrium chloride concentration on the surface (C_0) were calculated by employing the BMDP computer programme to determine the chloride penetration profile. The computed values of diffusion coefficients and the C_0 are presented in Tables 5.9 and 5.10. Together with the corresponding values for constants D_1 and m calculated from equation 5.4, and 24 months surface chloride concentration (assumed to be constant for each exposure conditions).

The predicted chloride concentration profiles after 20 years of exposures were, hence, determined and are plotted in figures 5.62 to 5.73 together with the chloride diffusion profiles assuming constant D_c (of 24 months age).

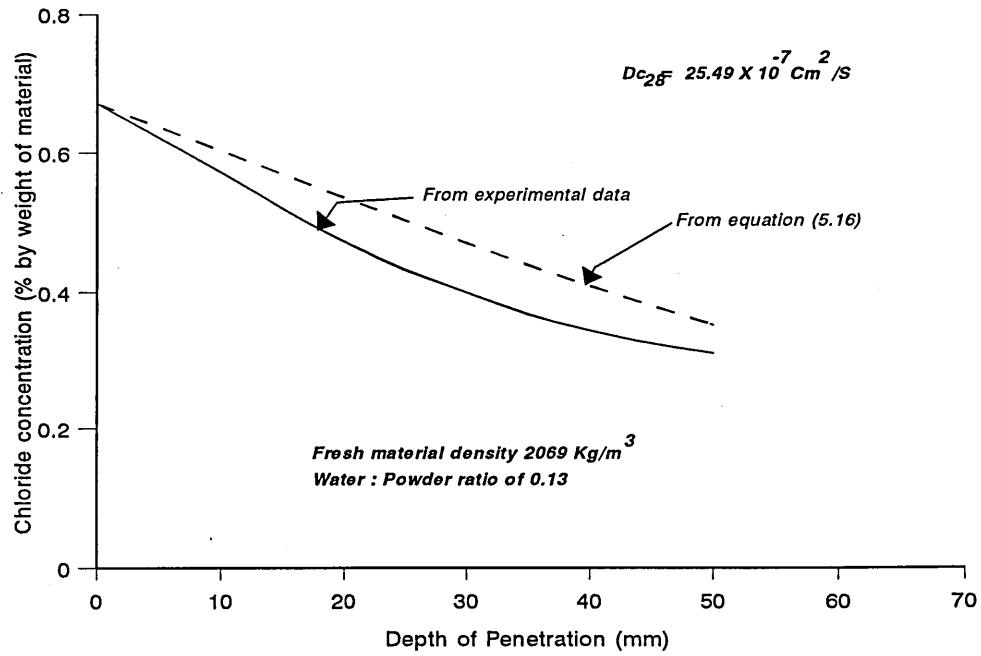


Figure 5.58
 Predicted chloride diffusion profile for material A (initially air cured at 20°C, 55% r.h. - after 180 days)

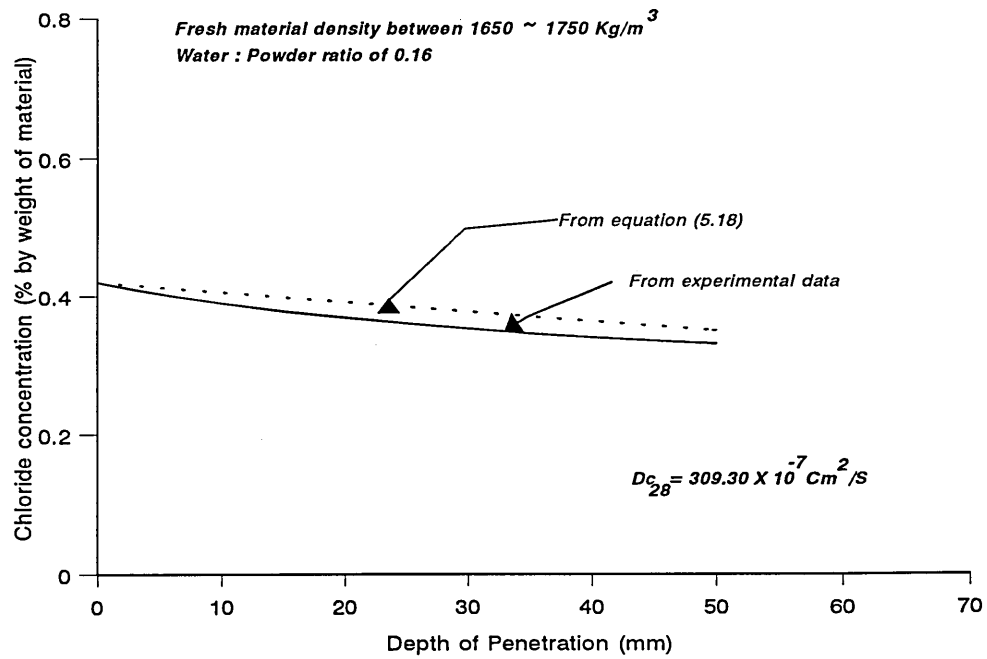


Figure 5.59
 Predicted chloride diffusion profile for material C (initially water cured at 20°C - after 180 days)

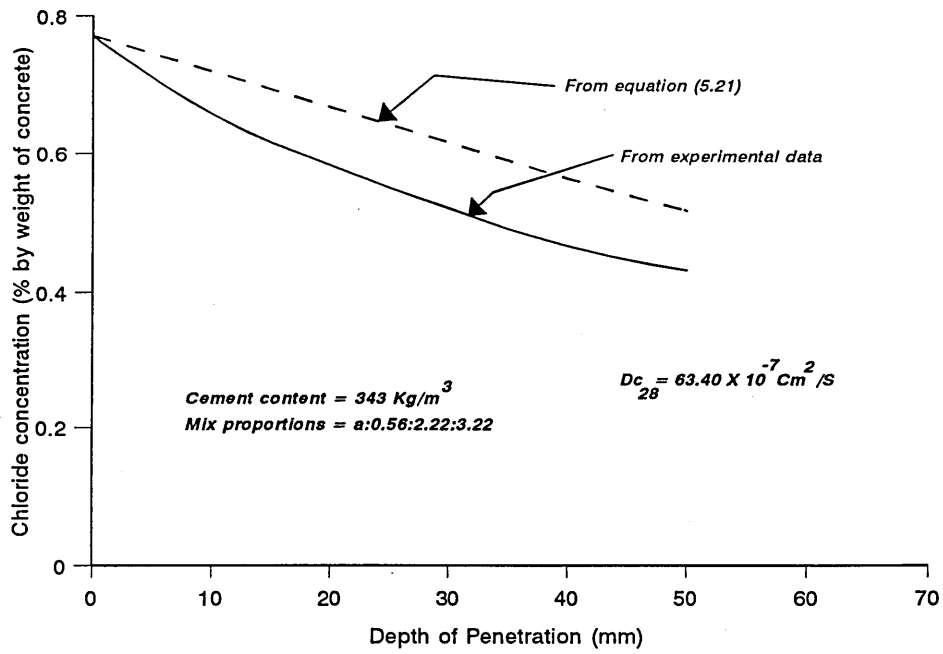


Figure 5.60
 Predicted chloride profile for concrete mix (initially air cured at
 20° C, 55% r.h. - after 180 days)

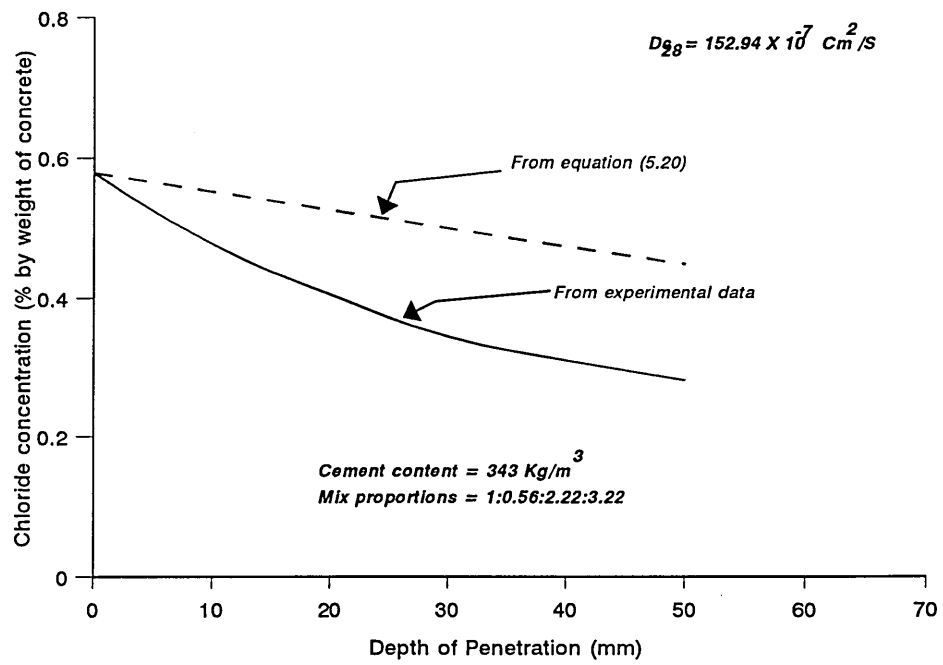


Figure 5.61
 Predicted chloride profile for concrete mix (initially water cured at
 20° C - after 180 days)

Table 5.7 Percentage of chloride (by weight of cement) at given depth and location of PORT RASHID

| Age | Depth (mm) | TIDAL ZONE | | SPLASH ZONE | | TOP OF DOCK | |
|--------------|---------------|------------|----------|-------------|----------|-------------|----------|
| | | Control | Zamdrain | Control | Zamdrain | Control | Zamdrain |
| 12 months | 0 - 10 | 2.39 | 1.05 | 1.26 | 0.77 | 1.12 | 0.39 |
| | 10 - 25 | 0.22 | 0.21 | 0.22 | 0.07 | 0.19 | 0.06 |
| | 25 - 50 | 0.11 | 0.09 | 0.07 | 0.06 | 0.09 | 0.05 |
| | 50 - 75 | 0.08 | 0.06 | 0.06 | 0.05 | 0.08 | 0.05 |
| | 75 - 100 | 0.07 | 0.06 | 0.05 | 0.05 | 0.05 | 0.05 |
| 18 months | 0 - 10 | 3.76 | 2.63 | 2.90 | 1.91 | 2.43 | 1.21 |
| | 10 - 25 | 2.28 | 0.83 | 1.12 | 0.27 | 0.66 | 0.08 |
| | 25 - 50 | 1.06 | 0.29 | 0.16 | 0.06 | 0.11 | 0.06 |
| | 50 - 75 | 0.52 | 0.08 | 0.06 | 0.05 | 0.05 | 0.05 |
| | 75 - 100 | 0.23 | 0.05 | 0.05 | 0.05 | 0.05 | 0.05 |
| 24 months | 0 - 10 | 3.94 | 2.72 | 2.30 | 1.50 | 2.45 | 1.12 |
| | 10 - 25 | 2.49 | 1.14 | 0.91 | 0.33 | 0.62 | 0.19 |
| | 25 - 50 | 1.49 | 0.68 | 0.31 | 0.16 | 0.19 | 0.08 |
| | 50 - 75 | 1.04 | 0.23 | 0.16 | 0.06 | 0.06 | 0.06 |
| | 75 - 100 | 0.81 | 0.06 | 0.06 | 0.06 | 0.06 | 0.06 |

Table 5.8 Percentage of chloride (by weight of cement) at given depth and location of JEBEL ALI PORT

| Age | Depth (mm) | TIDAL ZONE | | SPLASH ZONE | | TOP OF DOCK | |
|--------------|---------------|------------|----------|-------------|----------|-------------|----------|
| | | Control | Zamdrain | Control | Zamdrain | Control | Zamdrain |
| 12 months | 0 - 10 | --- | --- | 2.00 | 0.68 | 0.80 | 0.12 |
| | 10 - 25 | --- | --- | 0.16 | 0.09 | 0.14 | 0.09 |
| | 25 - 50 | --- | --- | 0.13 | 0.08 | 0.12 | 0.07 |
| | 50 - 75 | --- | --- | 0.10 | 0.06 | 0.09 | 0.05 |
| | 75 - 100 | --- | --- | 0.10 | 0.06 | 0.07 | 0.05 |
| 18 months | 0 - 10 | 2.47 | 1.95 | 2.38 | 1.91 | 2.14 | 0.54 |
| | 10 - 25 | 0.29 | 0.25 | 0.25 | 0.23 | 0.43 | 0.20 |
| | 25 - 50 | 0.25 | 0.16 | 0.20 | 0.08 | 0.16 | 0.07 |
| | 50 - 75 | 0.11 | 0.11 | 0.13 | 0.06 | 0.11 | 0.05 |
| | 75 - 100 | 0.11 | 0.08 | 0.11 | 0.06 | 0.07 | 0.05 |
| 24 months | 0 - 10 | 3.45 | 2.12 | 2.80 | 2.28 | 1.14 | 0.20 |
| | 10 - 25 | 0.58 | 0.11 | 0.48 | 0.11 | 0.19 | 0.08 |
| | 25 - 50 | 0.37 | 0.08 | 0.42 | 0.08 | 0.16 | 0.06 |
| | 50 - 75 | 0.15 | 0.06 | 0.19 | 0.08 | 0.12 | 0.06 |
| | 75 - 100 | 0.08 | 0.08 | 0.11 | 0.06 | 0.08 | 0.06 |

Table 5.9 D_c and C_0 values used in the analysis of **PORT RASHID**

| Exposure durations | | Control mix | | | Zamdrain | | |
|--------------------|---------|---|--------|-------------|---|--------|-------------|
| | | $D_c (X 10^{-7}) \text{ Cm}^2/\text{Sec}$ | | | $D_c (X 10^{-7}) \text{ Cm}^2/\text{Sec}$ | | |
| | | Tidal | Splash | Top of Dock | Tidal | Splash | Top of Dock |
| 12 months | | 0.13 | 0.19 | 0.19 | 0.21 | 0.13 | 0.18 |
| 18 months | | 1.22 | 0.31 | 0.19 | 0.25 | 0.11 | .074 |
| 24 months | | 2.18 | 0.28 | 0.13 | 0.49 | 0.12 | .096 |
| C_0 | 12 mths | 4.10 | 1.93 | 1.72 | 1.56 | 1.33 | 0.61 |
| | 18 mths | 4.10 | 3.76 | 3.41 | 3.52 | 3.05 | 2.2 |
| | 24 mths | 3.98 | 2.87 | 3.48 | 3.06 | 2.19 | 1.72 |

Table 5.10 D_c and average C_0 values used in the analysis of **JEBEL ALI PORT**

| Exposure durations | | Control mix | | | Zamdrain | | |
|--------------------|---------|---|--------|-------------|---|--------|-------------|
| | | $D_c (X 10^{-7}) \text{ Cm}^2/\text{Sec}$ | | | $D_c (X 10^{-7}) \text{ Cm}^2/\text{Sec}$ | | |
| | | Tidal | Splash | Top of Dock | Tidal | Splash | Top of Dock |
| 12 months | | -- | 0.12 | 0.20 | -- | 0.16 | 13.1 |
| 18 months | | 0.099 | 0.093 | 0.13 | 0.1 | 0.11 | 0.33 |
| 24 months | | 0.09 | 0.097 | 0.09 | 0.05 | 0.05 | 2.99 |
| C_0 | 12 mths | --- | 3.52 | 1.22 | --- | 1.1 | 0.11 |
| | 18 mths | 4.07 | 4.0 | 3.67 | 3.16 | 3.16 | 0.69 |
| | 24 mths | 5.32 | 4.29 | 1.76 | 4.01 | 4.36 | 0.16 |

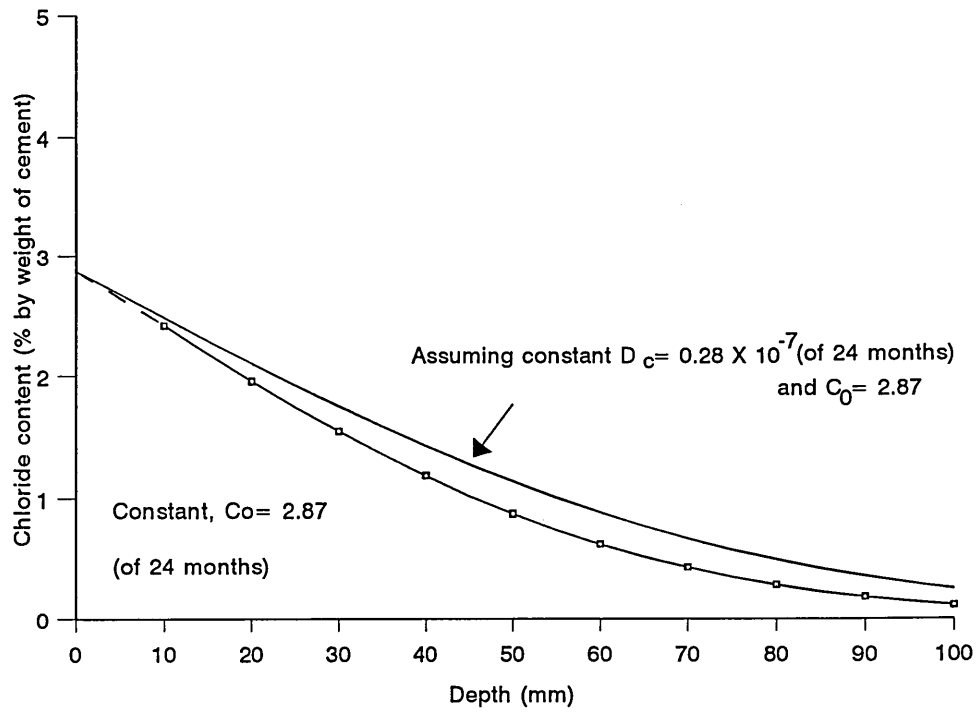


Figure 5.62
 Prediction of chloride concentration after 20 years exposure, Port Rashid (Control - Splash Zone)
 $m = 0.53$ (from experimental data).

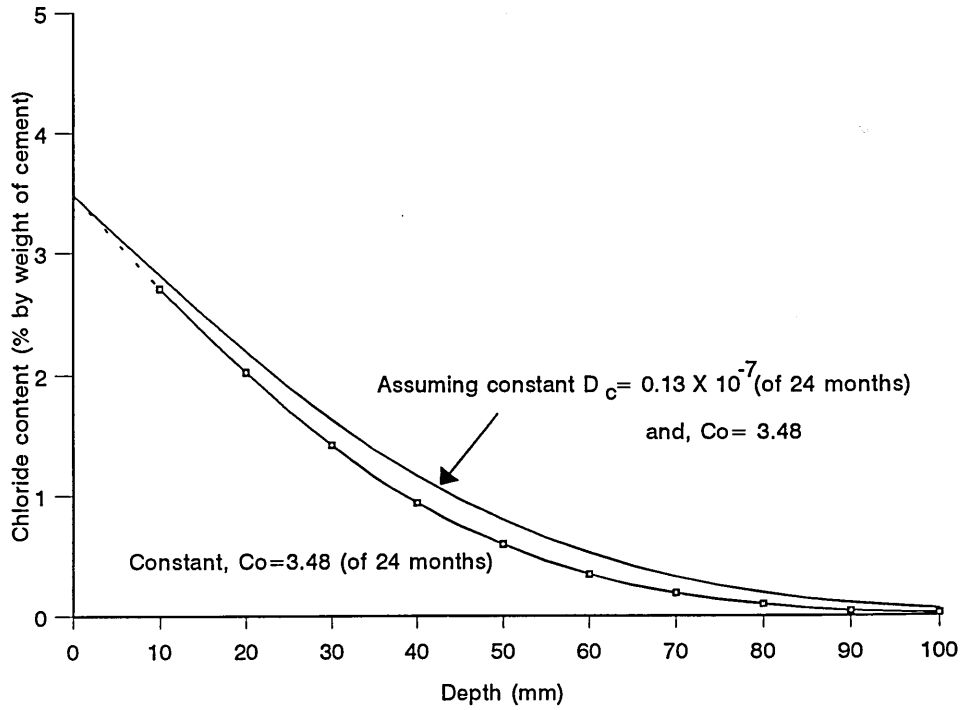


Figure 5.63
 Prediction of chloride concentration after 20 years exposure, Port Rashid (Control - Top of Dock)
 $m = -0.51$ (from experimental data).

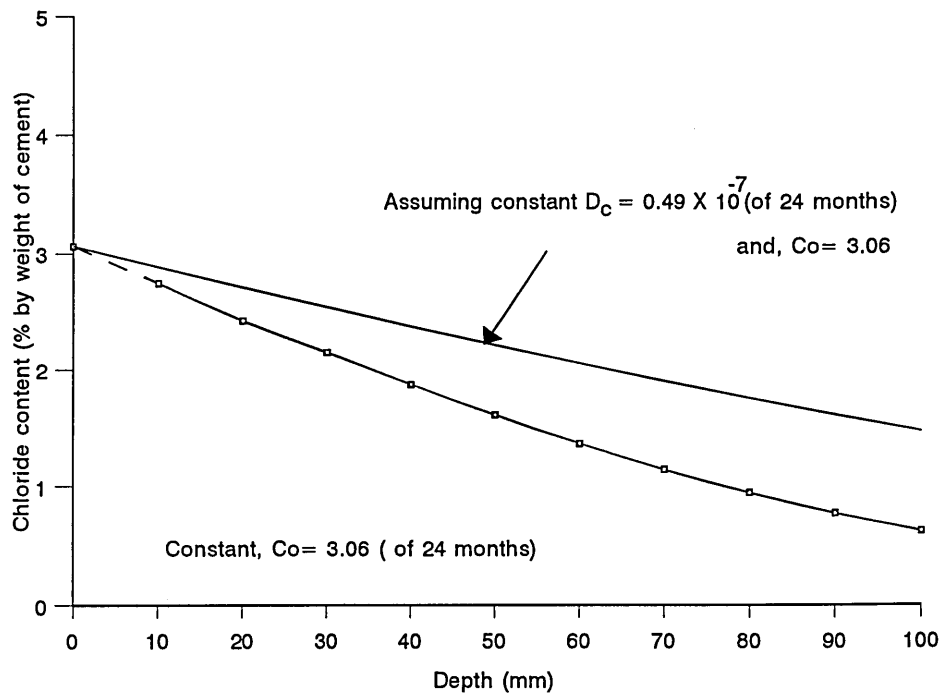


Figure 5.64
Prediction of chloride concentration after 20 years exposure, Port Rashid (Zamdrain - Tidal Zone)
 $m = +1.10$ (from experimental data)

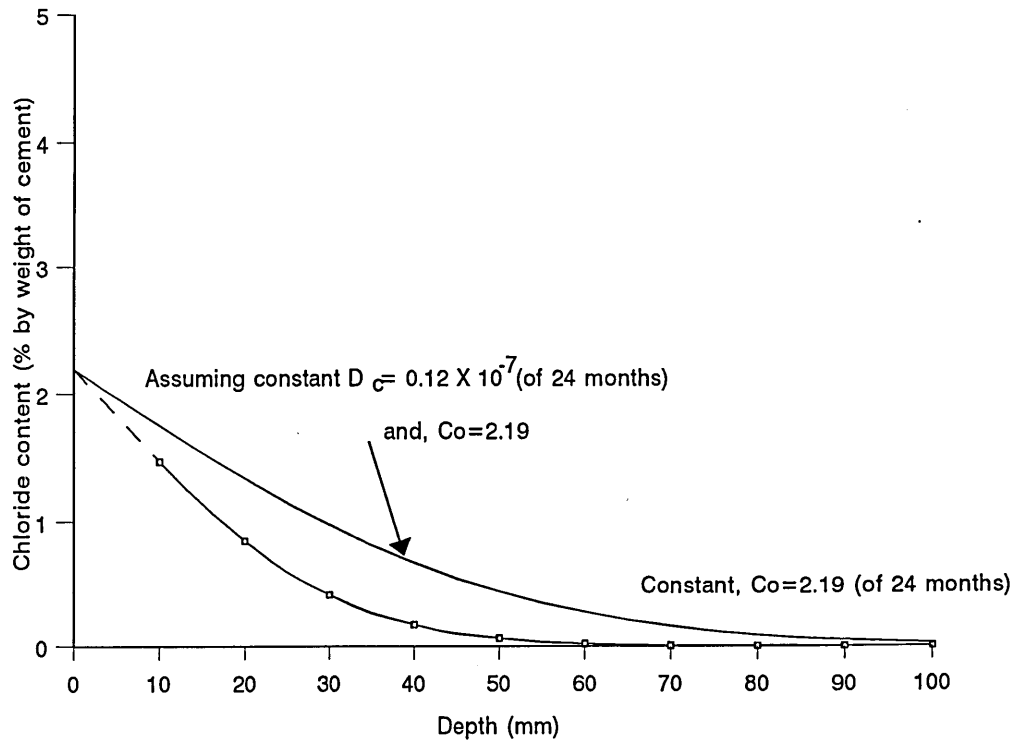


Figure 5.65
Prediction of chloride concentration after 20 years exposure, Port Rashid (Zamdrain - Splash Zone)
 $m = -0.18$ (from experimental data).

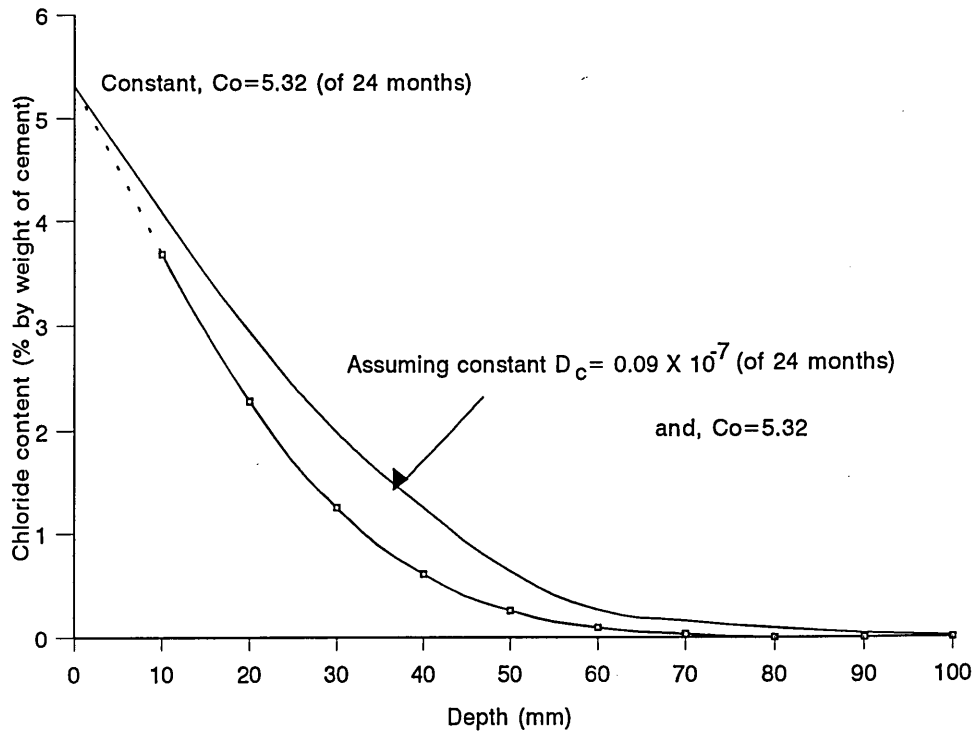


Figure 5.66
 Prediction of chloride concentration after 20 years exposure, Jebel Ali Port (Control - Tidal Zone)
 $m = -0.04$ (from experimental data).

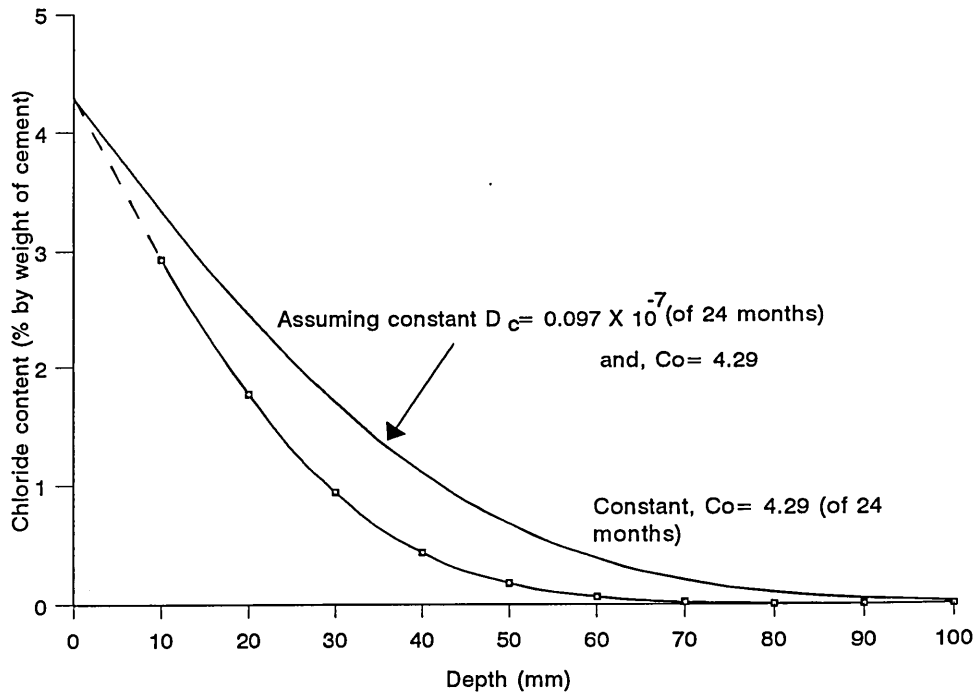


Figure 5.67
 Prediction of chloride concentration after 20 years exposure, Jebel Ali Port (Control - Splash Zone)
 $m = -0.35$ (from experimental data).

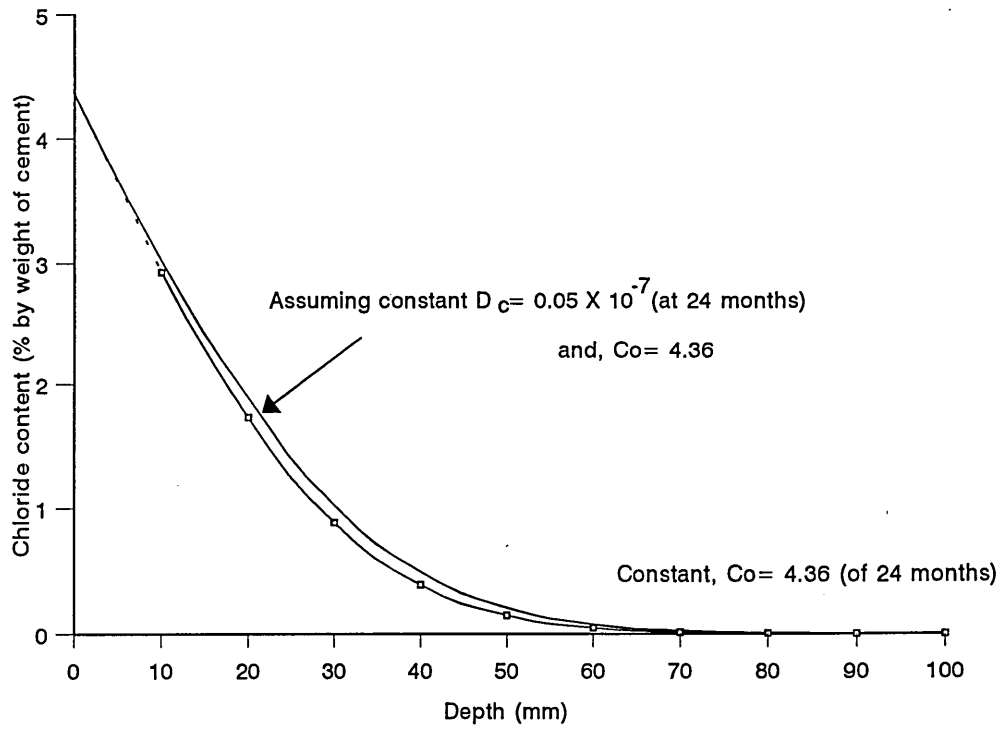


Figure 5.68
 Prediction of chloride concentration after 20 years of exposure, Jebel Ali Port (Zamdrain - Splash Zone) $m = -0.99$ (from experimental data).

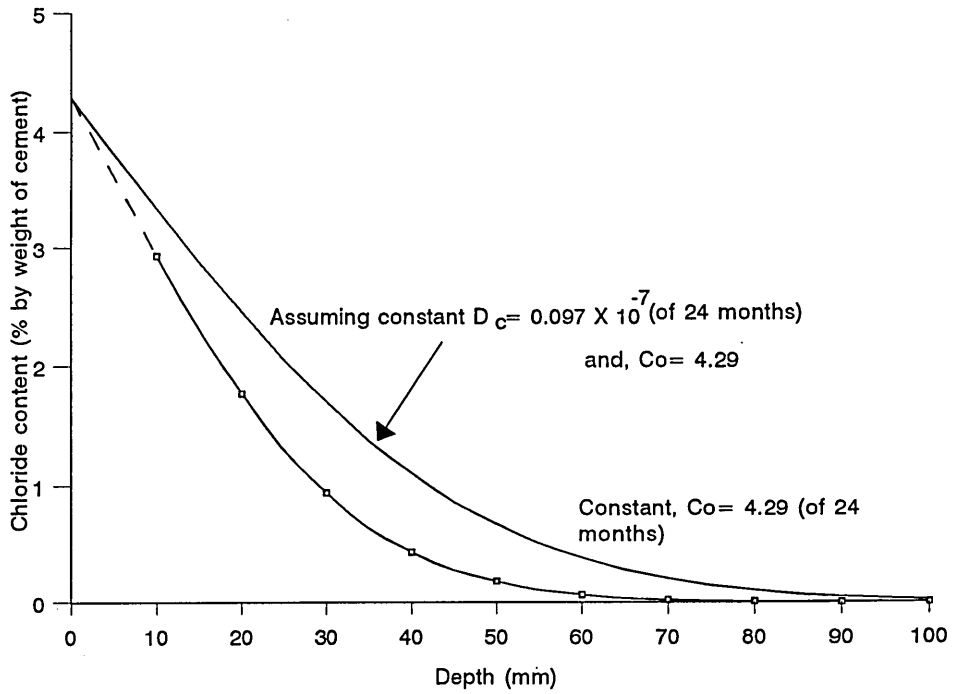


Figure 5.69
 Prediction of chloride concentration after 20 years exposure, Jebel Ali Port (Control - Splash Zone) $m = -0.35$ (from experimental data).

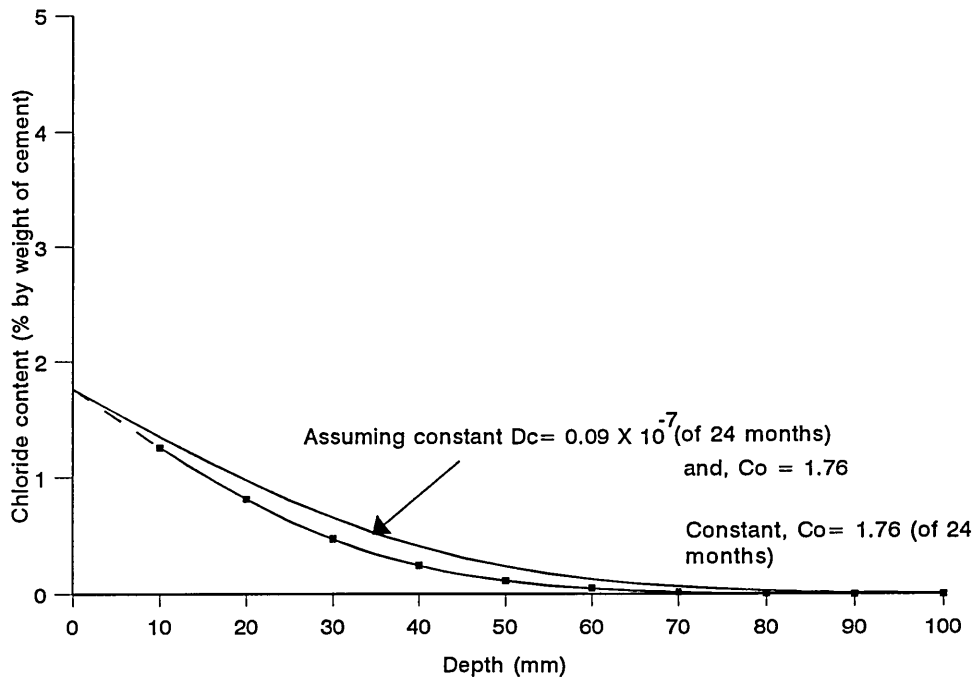


Figure 5.70
 Prediction of chloride concentration after 20 years exposure, Jebel Ali Port (Control - Top of Dock)
 $m = -0.98$ (from experimental data)

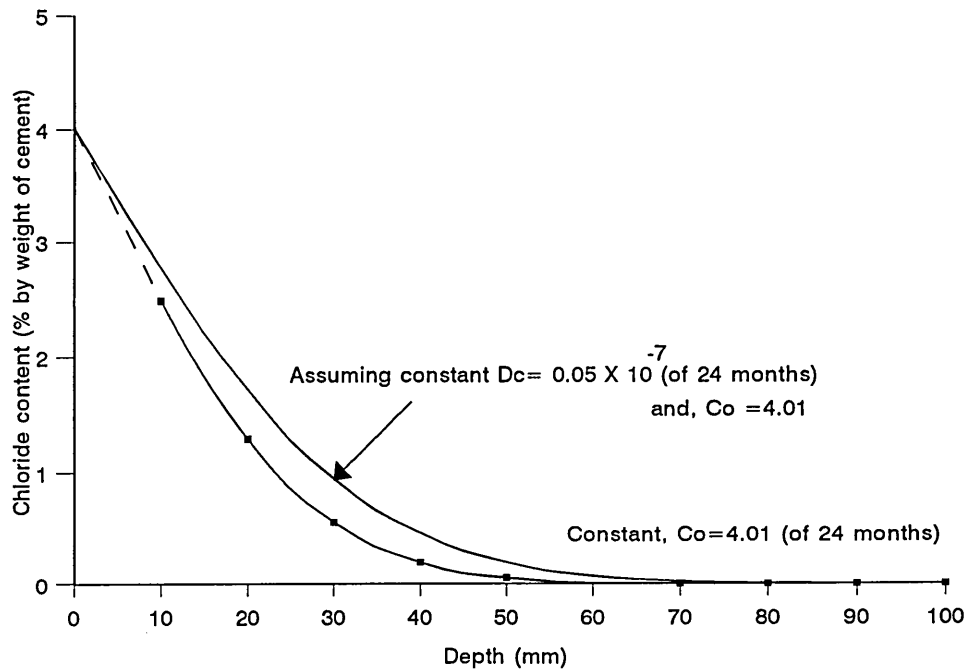


Figure 5.71
 Prediction of chloride concentration after 20 years exposure, Jebel Ali Port (Zamedrain -Tidal Zone)
 $m = -0.99$ (from experimental data)

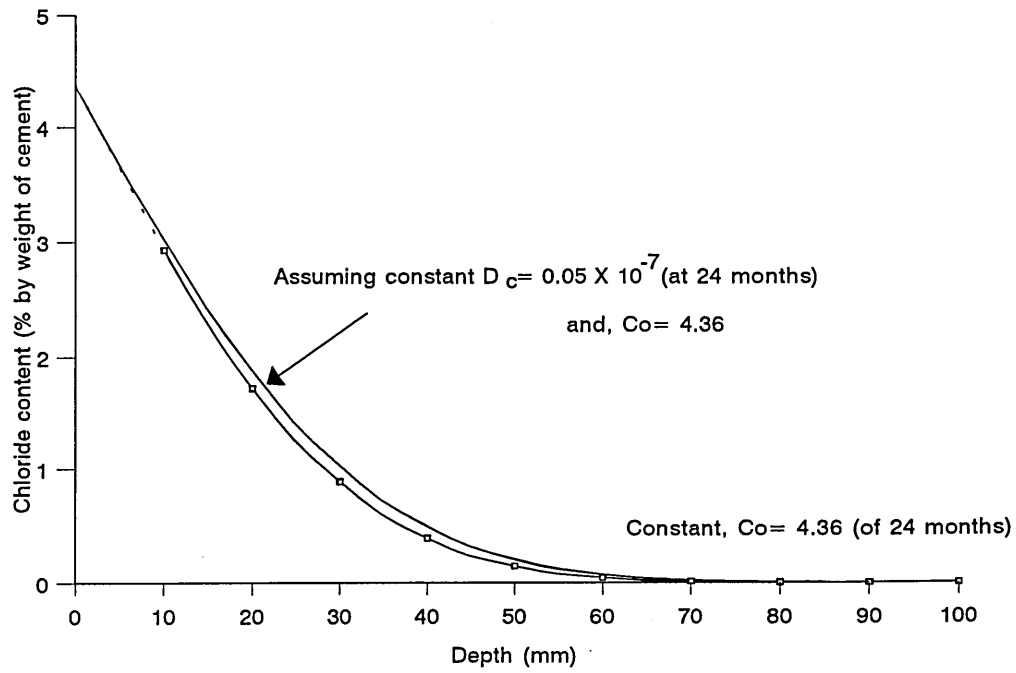


Figure 5.72
Prediction of chloride concentration after 20 years of exposure, Jebel Ali Port (Zamdrain - Splash Zone) $m = -0.99$ (from experimental data).

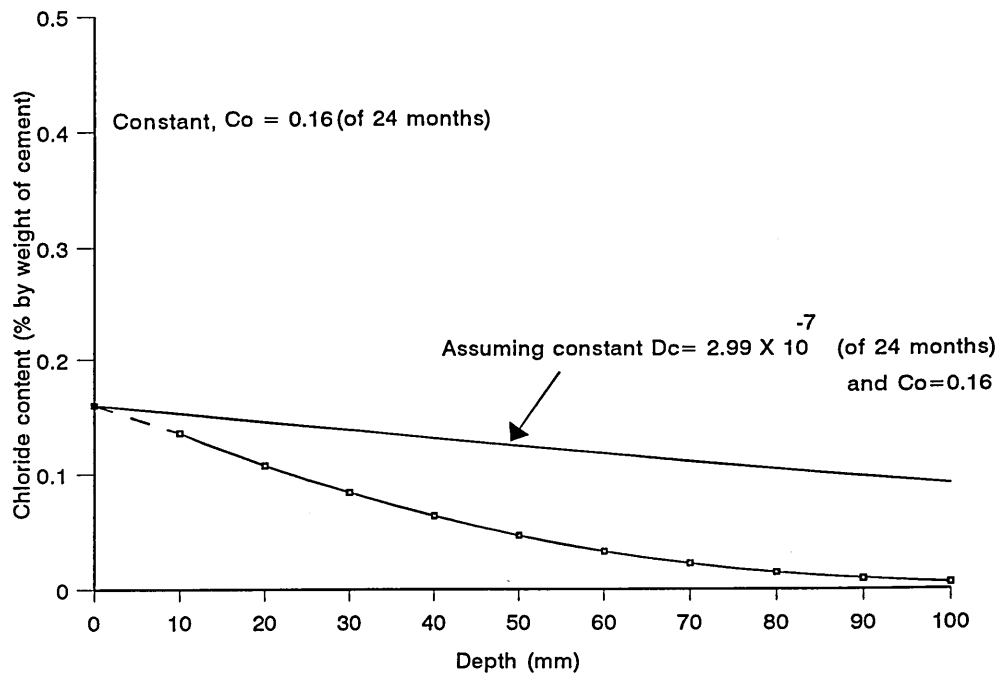


Figure 5.73
Prediction of chloride concentration after 20 years of exposure, Jebel Ali Port (Zamedrain - Top of Dock), using experimental data

5.6 CONCLUSIONS

The following conclusions are based on results obtained for specimens of generic repair materials (namely A, B, C) and concrete mix exposed to a chloride environment.

1. The chloride concentration profiles show a strong dependency on the initial curing conditions, especially during the early periods of exposure to chloride environment. But after a long period of exposure the effect of initial curing on chloride penetration is reduced.
2. High performance non-shrink repair material A showed the lowest chloride penetration under all the initial curing conditions considered in this investigation, while cementitious repair material B showed the highest chloride uptake among all materials.
3. The diffusion coefficient of a material at a given time, D_c , showed a strong dependency on time of exposure to a chloride environment. The different chloride concentration profiles for different materials are related to the diffusion coefficient at one month (30 days) of exposure. The relationship can be expressed in the form

$$D_{ct} = D_1 t_m^{-m}$$

Where,

D_{ct} = diffusion coefficient (Cm^2/Sec) after time t ,

D_1 = effective diffusion coefficient at time t equal to one month (30 days),

t_m = the time of exposure in months(30 days),

m = an empirical coefficient which can be assumed constant for particular mix.

4. The equilibrium chloride concentration on the material surface, C_0 , and diffusion coefficient, D_c , are not related.
5. Incorporation of the time-dependency of the diffusion coefficient into Fick's Second Law of Diffusion gives the following equation;

$$C(x, t) = C_0 \left[1 - \operatorname{erf} \left(\frac{x}{K \sqrt{D_1 t^m}} \right) \right]$$

Which can be used to predict long-term chloride concentration in the different materials.

Where,

$C(x,t)$ = chloride concentration at distance, x , and at time, t ,

C_0 = Chloride concentration at the surface

K & m = Constants which depends on the material property and initial curing conditions.

6. Based on the above expressions, prediction of long-term chloride concentrations in repair can be made using routine inspection data such as chloride concentration values at a known depth in materials at a given period of exposure.
7. The early exposure to chloride environment (after 24 hours of casting) has no serious consequences on long-term chloride concentration.

CHAPTER 6

INFLUENCE OF REPAIR MATERIALS ON THE STRUCTURAL PERFORMANCE OF REINFORCED CONCRETE COMPRESSION MEMBERS

6.1 INTRODUCTION

A patch repair is an effective restoration technique when an element of a structure shows signs of distress, especially spalling and delamination [5]. Repair should be carried out with sound material of similar properties to the original substrate. Repair materials which can be packed into the repair zone with little or no support [128] are required in most situations. These restrictions explain the fairly natural choice of sand-cement mortars for the repair of damaged concrete, but the durability of such repair is not always satisfactory. Dissatisfaction with this state of affairs has led to the search for better repair materials. In the mid-1960's polymer and epoxy resin-based mortars became available [128,129]. Their adhesive bonding capacity, rapid development of high strength and their outstanding chemical resistance offered clear advantages over simple cementitious mortars - sufficient to justify their considerably higher cost [128-130].

However, while these materials continue to give excellent service when used in appropriate situations, their indiscriminate substitution soon led to other problems. For example, the rapid curing reactions of these chemicals were often accompanied by a considerable rise in temperature, and in some cases substantial shrinkage of the resin binder, which could induce severe stresses in the parent concrete adjacent to the bond line [131,84]. Ignorance of these aspects led to unfortunate experiences in the repair industry, which spurred interest in the reappraisal of cementitious mortars to overcome their shortcomings. The outcome has been a swing back to cementitious repair materials, modified in more

sophisticated forms [128,84], such as the incorporation of fibres to improve crack resistance, abrasion and impact resistance and durability of the repair [132].

In chapters three and four conclusions were drawn about the significance of property mismatch on the structural behaviour of patch repaired concrete members. These were based on material properties determined for three generic repair materials and a plain concrete mix of similar strength. In this investigation, the influence of generic repair materials on the structural performance of defective reinforced concrete columns is studied. This includes the load-strain characteristics and the failure mode of defective and repaired reinforced concrete members. Short compression members simulating deterioration due to reinforcement corrosion on one face and on two faces were considered in this investigation.

Prior to presenting the results of this investigation, however, a brief literature review is made of the current information available on the load-deformation behaviour of reinforced concrete compression members under axial loading. This also includes the effect of creep and shrinkage deformations on the structural behaviour of repaired members, which forms relevant literature review for the topics covered in the next chapter.

6.2 LITERATURE REVIEW

The information available on the effect of generic repair materials on the load-deformation characteristics of reinforced concrete compression members is very limited. Such available information [10,13] shows that repair materials have a significant effect on the load-deformation properties of reinforced concrete columns. In order to understand the principal features of the behaviour of repaired members, a general knowledge of the load-deformation properties of reinforced concrete compression members under axial loading is essential. In the following sections the salient points on the load deformation behaviour of conventionally

reinforced compression members under short-term and long-term loading will be discussed.

6.2.1 Reinforced concrete compression members

A reinforced concrete compression member basically consists of concrete, longitudinal steel reinforcement and lateral steel reinforcement (stirrups). The stirrups are provided primarily to prevent the longitudinal steel from buckling. If the stirrups are closely spaced, the ductility of the member is improved. The diameter and spacing of the stirrups are related to the diameter of the longitudinal steel bars for design purposes. The behaviour of a reinforced concrete compression member under axial loading is mainly governed by the load-deformation properties and cross-sectional areas of the longitudinal steel and concrete. At small stresses, concrete and steel can be considered to behave elastically. Under these conditions the load carried by each phase of the composite material can be determined from elastic theory which will be discussed in section 6.2.1.1. However, actual observations show that the steel stress is much larger than elasticity calculation would indicate, because of both shrinkage and creep of concrete which increase with age under load.

The results of several tests on reinforced concrete compression members [10,13,134] indicate that there is no fixed ratio of steel stress to concrete stress in column specimens. The ratio of these stresses depends on the amount of shrinkage, which in turn depends on the age of the concrete and the method of curing. It also depends on the amount of creep in the concrete phase of the column specimens. Creep is greater when the load is applied at an early stage of the hardening process [135-137]. The amount of creep is influenced by any of the factors which determine the quality of concrete, such as cement content, water to cement ratio, additives, curing and even type of aggregate used.

If a load is applied for only a short time, such as an ordinary live load, it causes little

creep especially after the concrete is well cured. The live load thus produces an increment of stress in steel and concrete which can be calculated reasonably accurately by elastic theory. However, stress produced by dead load or any permanent or semi permanent load depends on the entire load history of the columns.

Although tests show that the actual working stresses cannot be estimated with any reasonable accuracy, they also show that the ultimate strengths of column specimens do not vary appreciably with the history of loading [138]. This is due to the fact that, if under load, the longitudinal steel reaches its yield stress first, the resulting increased deformation builds up the stress in the concrete until its ultimate strength is reached. If, however, the concrete approaches its ultimate strength before the steel reaches its yield, the increased deformation of the concrete near its maximum stress, forces the steel stress to build up more rapidly. Thus regardless of loading history, a reinforced concrete compression member reaches its ultimate strength only when the load causes a stress approximately equal to 67 percent of the ultimate strength of the concrete plus the yield stress of the longitudinal steel reinforcement [138]. The 67 percent factor for the concrete is due to a number of possible factors:-

- columns have a much larger height/width ratio than standard cubes and hence the effect of end restraints is almost insignificant compared with that in a cube test;
- the apparent concrete strength increases with the rate of loading [139,140], and since the rate of loading in a column test is much slower than that in a cube test, the apparent strength is reduced;
- the compaction of the concrete in a reinforced concrete column is likely to be less complete than in a cube.

The following equation can therefore be used for the ultimate strength of reinforced compression members;

$$P_U = 0.67f_{cu}A_c + f_yA_s \quad (6.1)$$

Where,

- P_U = Ultimate strength of column specimens
- f_{cu} = Compressive cube strength
- f_y = Yield stress of the longitudinal steel bars
- A_c = Cross-sectional area of concrete
- A_s = Cross-sectional area of steel.

6.2.1.1 Elastic theory

When a load, P , is applied to a reinforced concrete compression member, it is shared between the concrete and steel phase of the composite material. The proportion of load carried by each phase depends on the cross-sectional area and stiffness of each phase. The conditions of equilibrium of forces, leads to the following equation,

$$P = \sigma_c A_c + \sigma_s A_s \quad (6.2)$$

Where,

- P = Applied axial load
- σ_s = Stress in the reinforcement
- σ_c = Stress in the concrete.

When the stresses in concrete and the reinforcement are within the elastic limit and the interfacial bond is intact then the strains in the two phases are equal. Therefore, from the condition of strain compatibility, it follows that;

$$\frac{\sigma_c}{E_c} = \frac{\sigma_s}{E_s} \quad (6.3)$$

Where,

E_c = Modulus of elasticity of concrete, and

E_s = Modulus of elasticity of steel.

Substituting for σ_c or σ_s from equation (6.3) into equation (6.2), leads to the following equation;

$$\sigma_c = \frac{P}{A_c + \beta A_s} \quad (6.4)$$

$$\sigma_s = \frac{\beta P}{A_c + \beta A_s} \quad (6.5)$$

Where,

β = modular ratio (E_s / E_c)

In equations (6.4) and (6.5), the term ($A_c + \beta A_s$) represents the area of the transformed section.

6.2.1.2 Effects of creep and shrinkage

Equations (6.4) and (6.5) may give the false impression that the stresses σ_c and σ_s in a given column are uniquely defined once the load P is specified. In fact, as mentioned earlier, it is almost impossible to determine these stresses accurately because of the effects of creep and shrinkage of concrete. In practice, σ_s is usually much larger than predicted by the elastic theory (equation 6.5). This is due to the fact that under a sustained load, the

effective stiffness of concrete decreases with time due to creep. Hence, the modular ratio, β , in equations (6.4) and (6.5) increases, leading to an increase in the steel stress. If the effective values of β for various durations of loading are inserted in equations (6.4) and (6.5), it will be found that for a reinforced compression member under a constant load, there is a gradual but significant redistribution of stress with time, the concrete gradually sheds off part of the load it carries and this is picked up by the steel. This redistribution may continue for years until the effective modular ratio settles down to an approximately constant value [139], which cannot be determined with precision [141]. For practical concrete mixes, the effective modular ratio for long-term loading may be two to three times that for short-term modular ratio; BS 8110: Clause 2.5.2 [92] recommends that the effective modular ratio should be taken as 15.

If the sustained load on a compression member is removed, there is an immediate elastic recovery and residual stresses are set up. The steel reinforcement ends up in compression and the concrete in tension [141]. The residual tensile stress in the concrete may sometimes be high enough to cause cracking.

The effect of shrinkage of concrete causes further redistribution of stresses. A plain concrete specimen undergoing uniform shrinkage will experience no stresses, but in a reinforced concrete member, the reinforcement bars resist the shrinkage and set up tensile stresses in concrete and compressive stresses in the steel.

It is clear from the above discussion that the actual stresses in a reinforced compression member may be quite different from the values predicted from equations (6.4) and (6.5). The difficulty of determining the creep and shrinkage with precision means that the actual stresses cannot be determined accurately. If the member is subjected to a history of load applications and removals, the residual stresses constitute further complications.

The requirements of a repair system will vary within a broad classification of structural and cosmetic application. Within each of these classes, the mechanical properties must be defined which will identify the ability of a material to fulfil the required application. The structural application of a repair patch (i.e its stress carrying ability) is made more complicated by the load relief during the repair operation. Thus, analysis of the transmission and distribution of load through patch repairs in real structural members presents a complex problem. Emberson et al [13] found complex patterns of stress gradient for the relatively simple symmetrically reinforced repaired compression members.

6.3 EXPERIMENTAL WORK

An experimental investigation was carried out in two batches to understand the behaviour of defective and repaired column specimens. Batch (I) deals with a single void repair, while batch (II) deals with voids on two opposite faces of reinforced concrete columns. Three commercially available generic repair materials, labelled as A, B, and C, were used for repair work and the repaired specimens were axially loaded to failure. Results of these tests are provided in this chapter.

6.3.1 Details of column specimens

A total of twenty six 150 X 150 X 750mm column specimens and nine cube specimens were cast in three different series. All the column specimens were reinforced longitudinally with four 12mm diameter high yield steel bars. The centroid of each longitudinal bar was located at 26mm from the face of a specimen, as shown in figure 6.1. Mild steel bars of 6mm diameter were used for stirrup reinforcement.

To simulate deterioration due to reinforcement corrosion, the defective columns were

cast with centrally located voids of depth 55mm and length of 220mm, as shown in figure 6.2. The longitudinal steel bars were cast in the voids with 10% loss of cross-section due to corrosion. Twelve columns were cast for each batch (I and II) with the centrally located voids as shown in figure 6.2, and a further two columns were cast for each batch as control column specimens which did not contain any void representing defective concrete.

6.3.2 Details of mix and materials

Details of repair materials and concrete mix are given in Table 6.1. Concrete mix proportions (by weight) of 1 : 2.24 : 3.22, with a water to cement ratio of 0.56, were used throughout. The cement content was 343 kg/m³. The chosen concrete mix proportions are designed to give a 28 days cube strength of 40 N/mm² (± 1 N/mm²), and a slump of 10-20 mm. Further details of these materials are given in section 3.3.1 of chapter 3.

As stated earlier, the longitudinal reinforcement consisted of four 12mm diameter high yield steel (HYS) bars. The links provided to prevent outward buckling of the longitudinal bars were 6mm diameter mild steel. The concrete at each end of a column specimen was confined by closely placed links to a depth of 90 mm, as shown in figure 6.1, in order to prevent premature localised failure during destructive testing. In order to facilitate strain measurements in the longitudinal steel, studs of 10mm diameter were welded on to the longitudinal bars in the reinforcing cage over a gauge length of 200mm.

Three commercially available generic repair materials which are labelled A,B and C were used for repair of the defective reinforced concrete columns, as shown in Table 6.1. Material A is a high performance non-shrinkable mix, Material B is a mineral based cementitious mortar with no aggregate size particles or additives and Material C is a single component cementitious mortar with polymer additives.

TABLE - 6.1 Details of Mixes and Materials.

| MIX | MATERIALS AND DESCRIPTION | QUANTITY (kg/m ³) | W/C RATIO |
|-----------------|---------------------------|-----------------------------------|--------------|
| CONCRETE | Ordinary Portland Cement | 342.54 | 0.56 |
| | Fine aggregate | 767.04 | |
| | 10mm Coarse aggregate | 1102.04 | |

REPAIR MATERIALS

| | | Mixed Density | Water Addition |
|----------|---|------------------|------------------------------|
| A | High performance, non-shrink concrete | 2069 | 4 litres per 30 kg pack |
| B | Mineral based cementitious mortar with no additives | 1575 | 3 litres per 20 kg pack |
| C | Single component cementitious material with polymer additives | 1725 | 2.5 litres per 20 kg pack |

Further information and detailed mechanical characteristics of these materials are given in section 3.3.1 of chapter 3.

6.3.3 Casting and curing

Prior to casting, polystyrene pieces was carefully cut to prepare voids around corroded reinforcement when concrete was cast. These were then cut into smaller sections and assembled around the reinforcing bars to completely occupy the area in the mould where the void was required in the cast concrete. Any cracks and joints between the pieces were covered with insulating tape and in some areas plasticine was used to ensure that accurately dimensioned voids remained after casting. The welded studs, as described in section 6.3.2.1, were fitted with thin cylindrical polystyrene blocks during casting. The polystyrene blocks were removed before the column specimens were tested to ensure unrestrained movement of the studs during the deformation of the reinforcing bars.

Prior to casting, the column moulds were cleaned and lightly oiled to ensure easy removal of the concrete. The reinforcement cage was positioned within the column mould and the polystyrene pieces for the voided section were positioned carefully. All concrete mixing was carried out using a rotary pan mixer. Mixing was continued until a uniform consistency confirmed that concrete was thoroughly mixed. All the specimens were cast horizontally in three layers, each layer being adequately compacted. The fresh concrete was covered with a polythene sheet. After 24 hours the specimens were removed from their moulds and allowed to cure in water for 28 days. Three reinforced columns of each series were repaired with each repair material A, B and C respectively after 14 days of curing. They were subsequently cured in water for a further 14 days prior to test. A fourth voided specimen was taken as defective column specimen to study effect of void on the performance of such columns. In this column, the void was not filled with patch repair. The full details of the column specimens is given in Table 6.2.

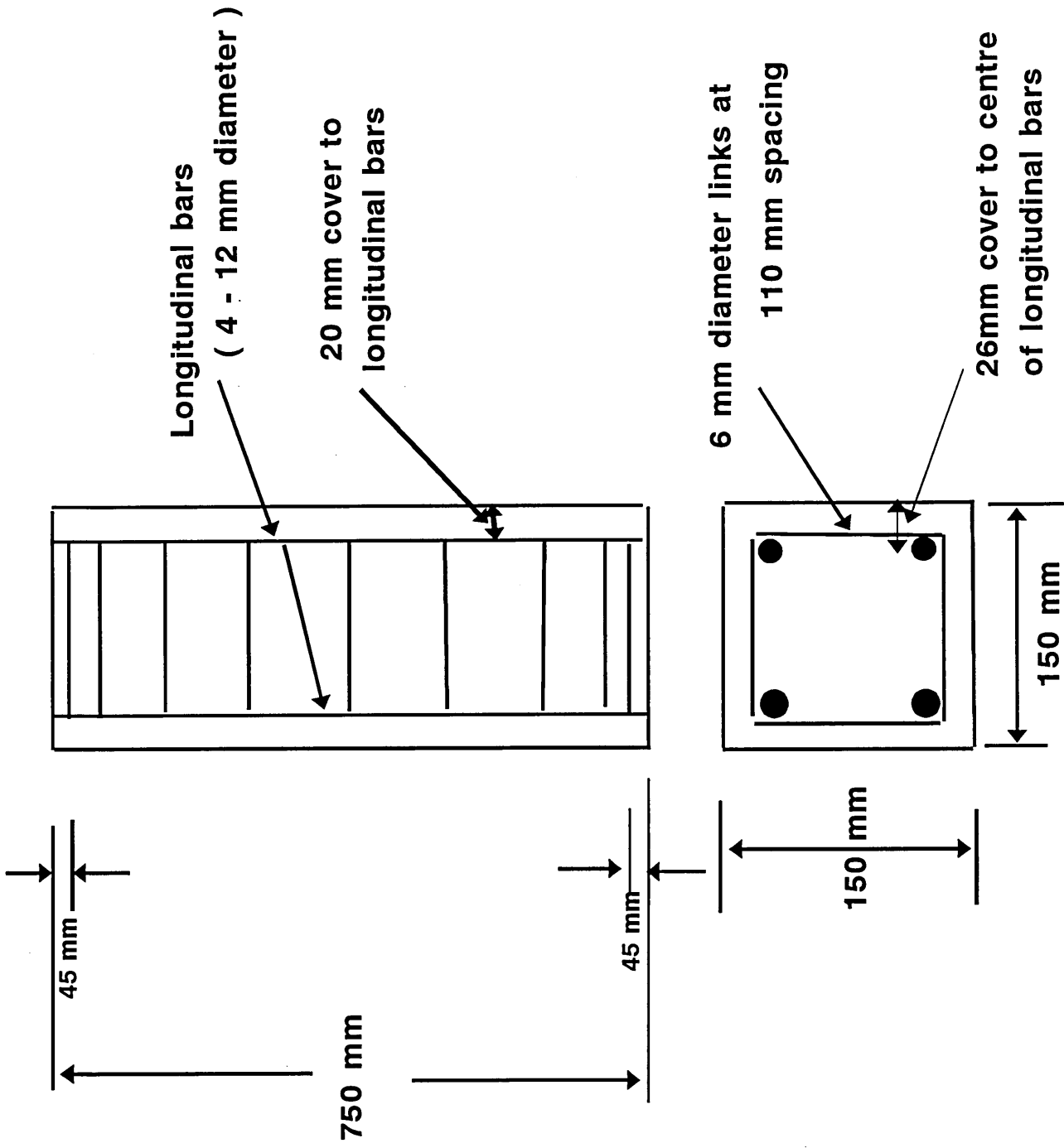


Figure 6.1 Reinforcement Details

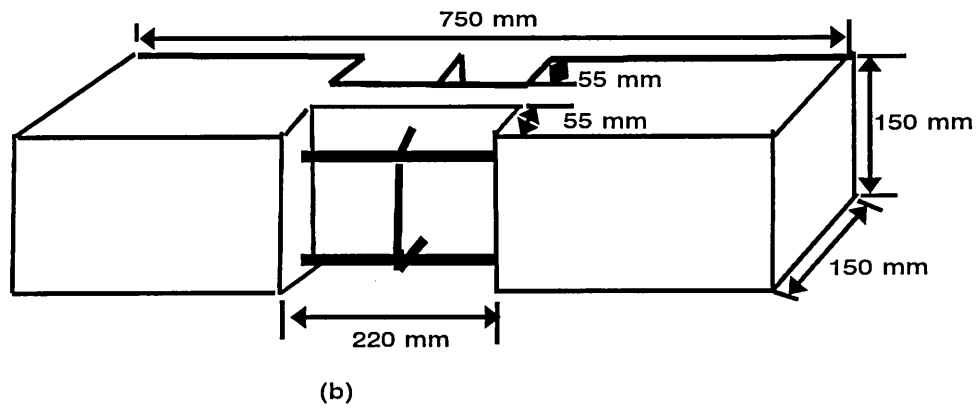
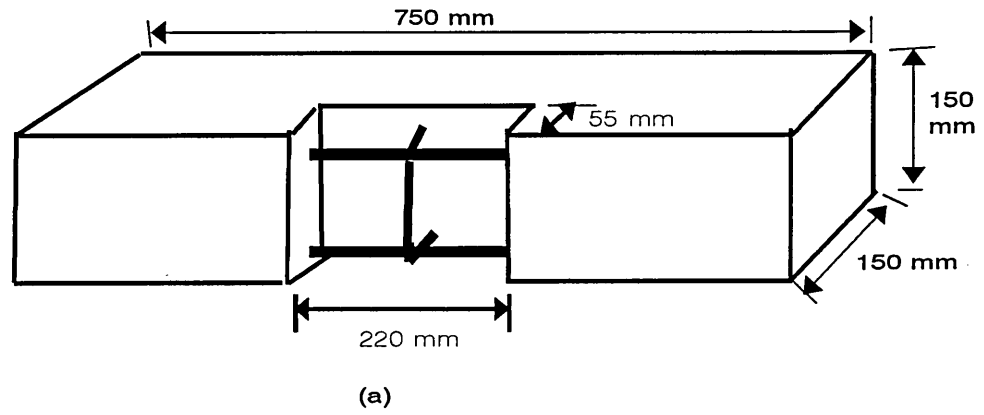


Figure 6.2
Details of void for (a) batch I, and (b) batch II specimens

Table 6.2 Details of column specimens.

| Batch I and II Specimens | Description |
|---------------------------------|---|
| Control Columns | Reinforced concrete columns with no voids |
| Columns A | Repaired using Repair Material A |
| Columns B | Repaired using Repair Material B |
| Columns C | Repaired using Repair Material C |
| Voided Columns | Void was not filled with patch repair |

(Batch I- void on one face; Batch II- void on opposite faces and three specimens were tested for each batch I and II)

6.3.4 Repair of columns

Timber formwork was cut to cover two sides of each void and it was clamped in place by using G clamps. This formed a tightly sealed joint on two sides of the void leaving the third side open to allow the placing of the repair material.

At the age of 14 days, the columns to be repaired were taken out of water, and the void surface was roughened by hand using a hammer and chisel to ensure good bonding. At the same time, by using a wire brush, it was ensured that impurities were cleaned from the corroded exposed reinforcement.

The repair mix was prepared according to the manufacturer's literature. The material was manually poured and compacted into the voids until full, when the exposed surface was levelled off. Upon completion of the repair, the specimens were kept covered with a polythene sheet for 24 hours, after which they were cured in water until the test date.

Strains at different positions were measured by using a demec extensometer of 200mm

gauge length. Demec discs were attached for this purpose and their locations on the specimens are as shown in figures 6.3 to 6.5.

6.3.5 Test procedure

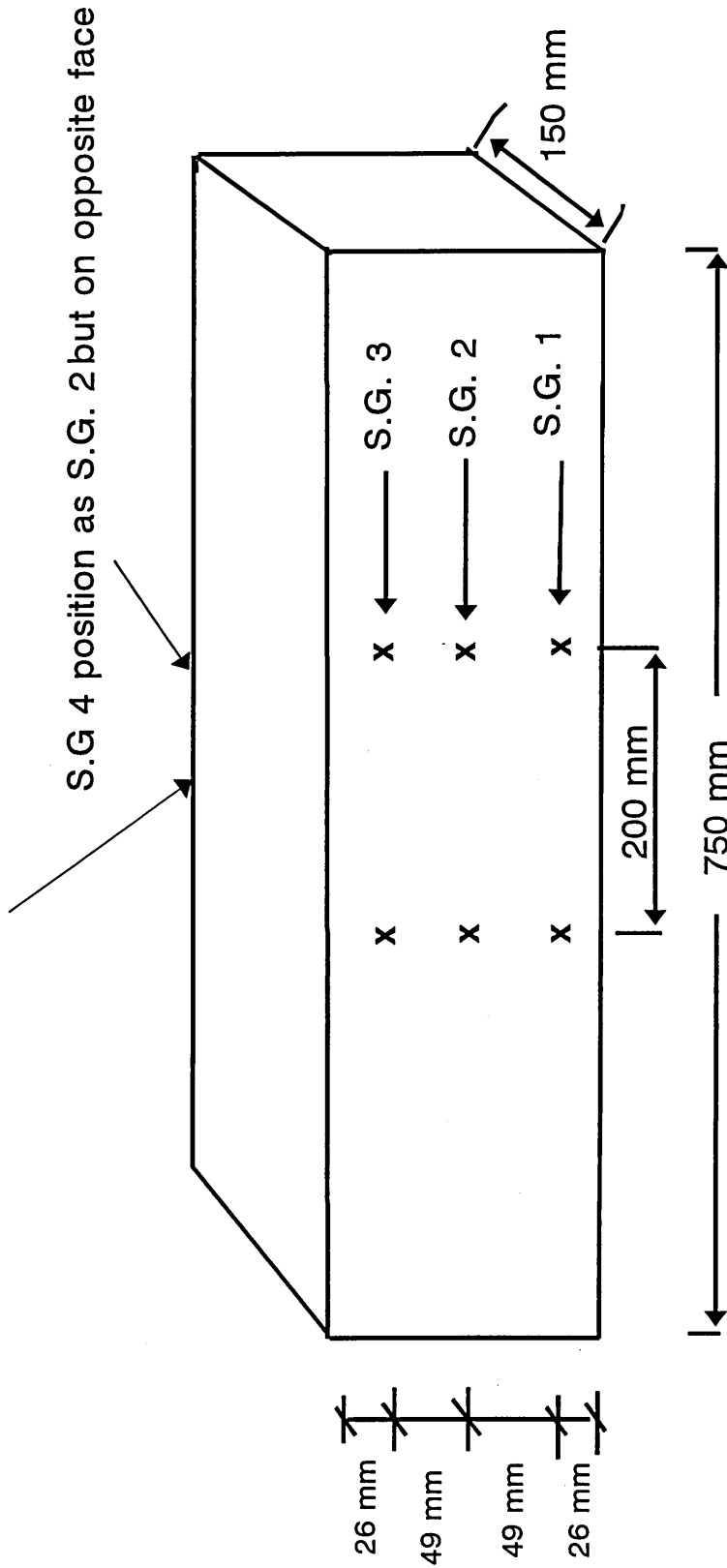
Uniaxial compression tests were performed on the column specimens in an ELE (International) 3000 kN compression machine under a constant stress rate of loading. Initial strain readings at the locations described in the previous section were taken using a Demec extensometer and the column was loaded in 25 kN increments. At each load increment longitudinal strain were measured and the column was examined to check for any cracking. Loading was continued at a steady rate to failure and the failure load was noted. The specimen was then taken out of the testing machine and any crushed material was removed to expose the reinforcement. Demec gauge calibration factors were used to determine the strains in each column at the various load intervals.

6.4 ANALYSIS OF VOIDED SECTIONS OF COMPRESSION MEMBERS

6.4.1 Elastic Analysis

Consider the axially loaded short reinforced concrete column with a void as shown in figure 6.6. An equivalent section for a voided section (A-A) is drawn in figure 6.7, because the voided section A-A is the determinant feature for failure. The applied force P is assumed to act through the centroid of the original section and so acts at a depth of $D/2$ as shown in figure 6.7. It is obvious that due to presence of void this force is not centroidal about the equivalent section, so it will cause bending as well as compression. It means that in this case the column specimen is subjected to an axial load P and bending moment M , or the column is eccentrically loaded with a load P at an eccentricity $e = M/P$. This combined action gives a strain distribution on the voided portion as shown in figure 6.8.

S.G. 5 and S.G. 6 position as S.G. 1 and S.G. 3 but on opposite face



* Strain Gauges 1,3,5,6 are on steel studs and measure strain on outside face of steel reinforcement which is at 20 mm from the surface

* S.G. 2 and S.G. 4 are on concrete surface

Figure 6.3 Location of Demec points on reinforced concrete column (control)

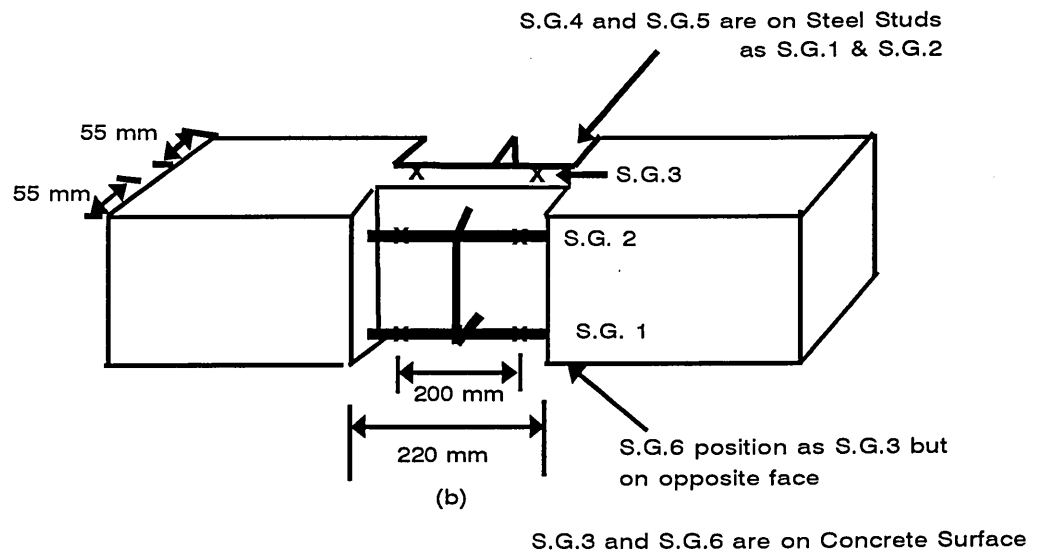
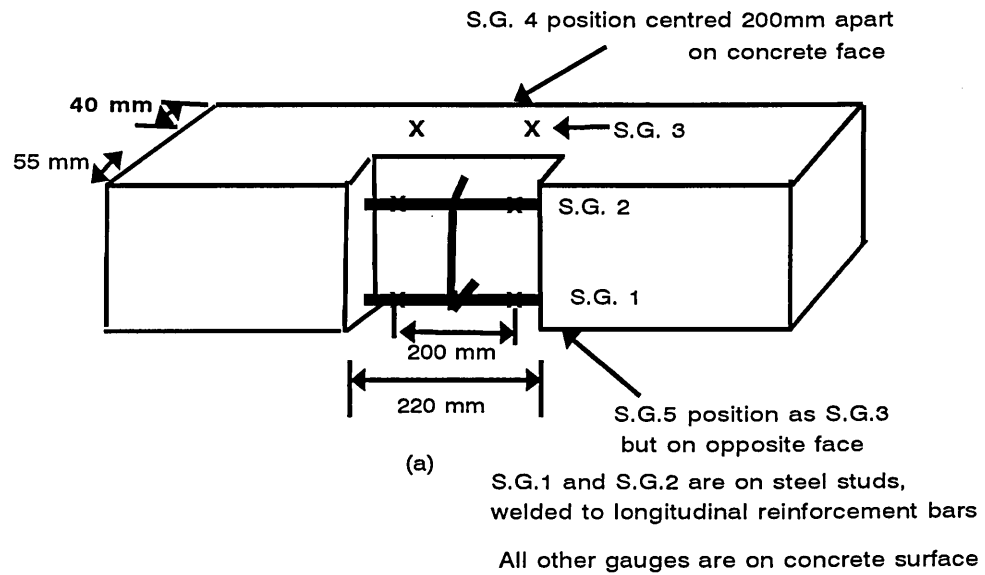
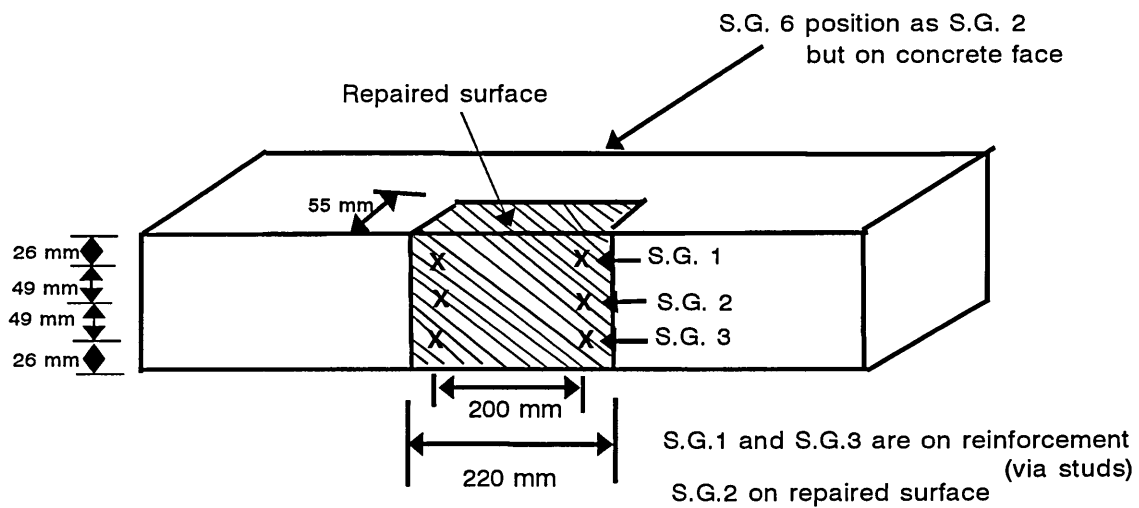
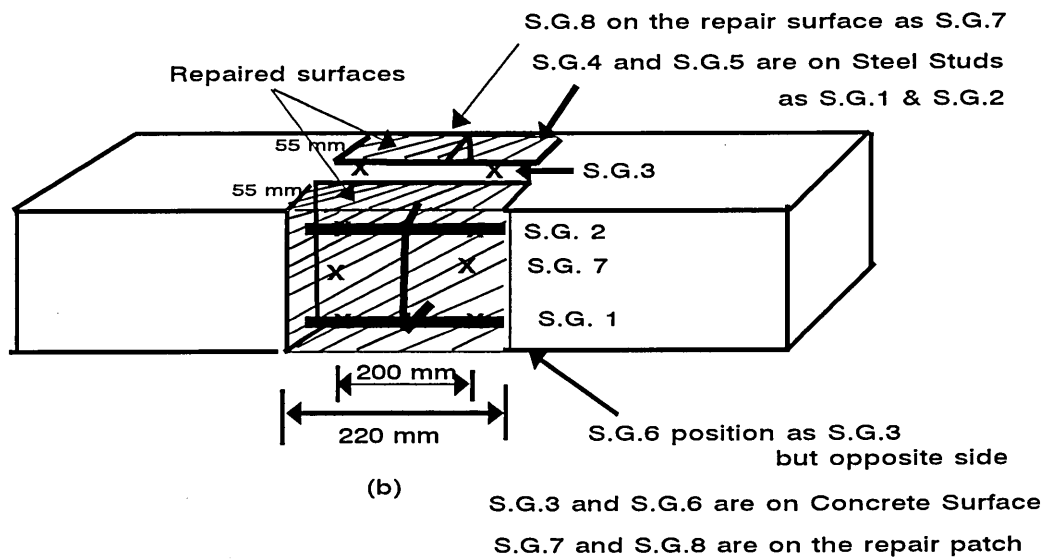


Figure 6.4

Location of demec points on voided column specimens; (a) void on one face (batch I), and (b) void on two opposite faces (batch II)



(a)



(b)

Figure 6.5
Location of demec points on repaired column specimens; (a) void on one face (batch I), and (b) void on two opposite faces (batch II)

For small applied loads, both materials will be in their elastic ranges and so stress is directly proportional to strain. In this case, stress variation across the equivalent section will be identical to the strain variation. The stress due to the axial load P , σ_{cp} , from equation (6.4) is given by;

$$\sigma_{cp} = \frac{P}{A_c + \beta A_{s1} + \beta A_{s2}} \quad (6.6)$$

The stress due to the moment M , σ_{cM} , at any depth x from the un-voided face is given by,

$$\sigma_{cM} = \frac{M(\bar{x}-x)}{I_c} \quad (6.7)$$

Where,

I_c = the second moment of area of the equivalent section about its centroidal axis and

\bar{x} = depth of centroid axis (voided section).

Combining equations (6.6) and (6.7), the stress variation due to both the axial load and bending, σ_{cpM} , across the equivalent section in the elastic range is given by,

$$\sigma_{cpM} = \frac{P}{A_c + \beta A_{s1} + \beta A_{s2}} + \frac{M(\bar{x}-x)}{I_c} \quad (6.8)$$

By equating to zero and substituting $e = M / P$, the position of the neutral axis is given by,

$$\bar{x} = x - \frac{I_c}{(A_c + \beta A_{s1} + \beta A_{s2}) e} \quad (6.9)$$

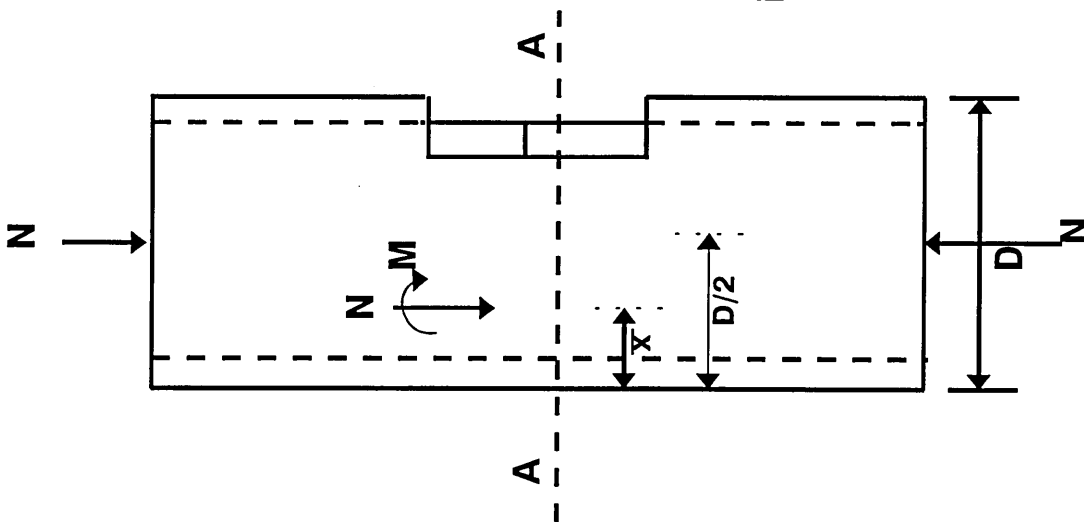


Figure 6.6
Axially loaded voided column

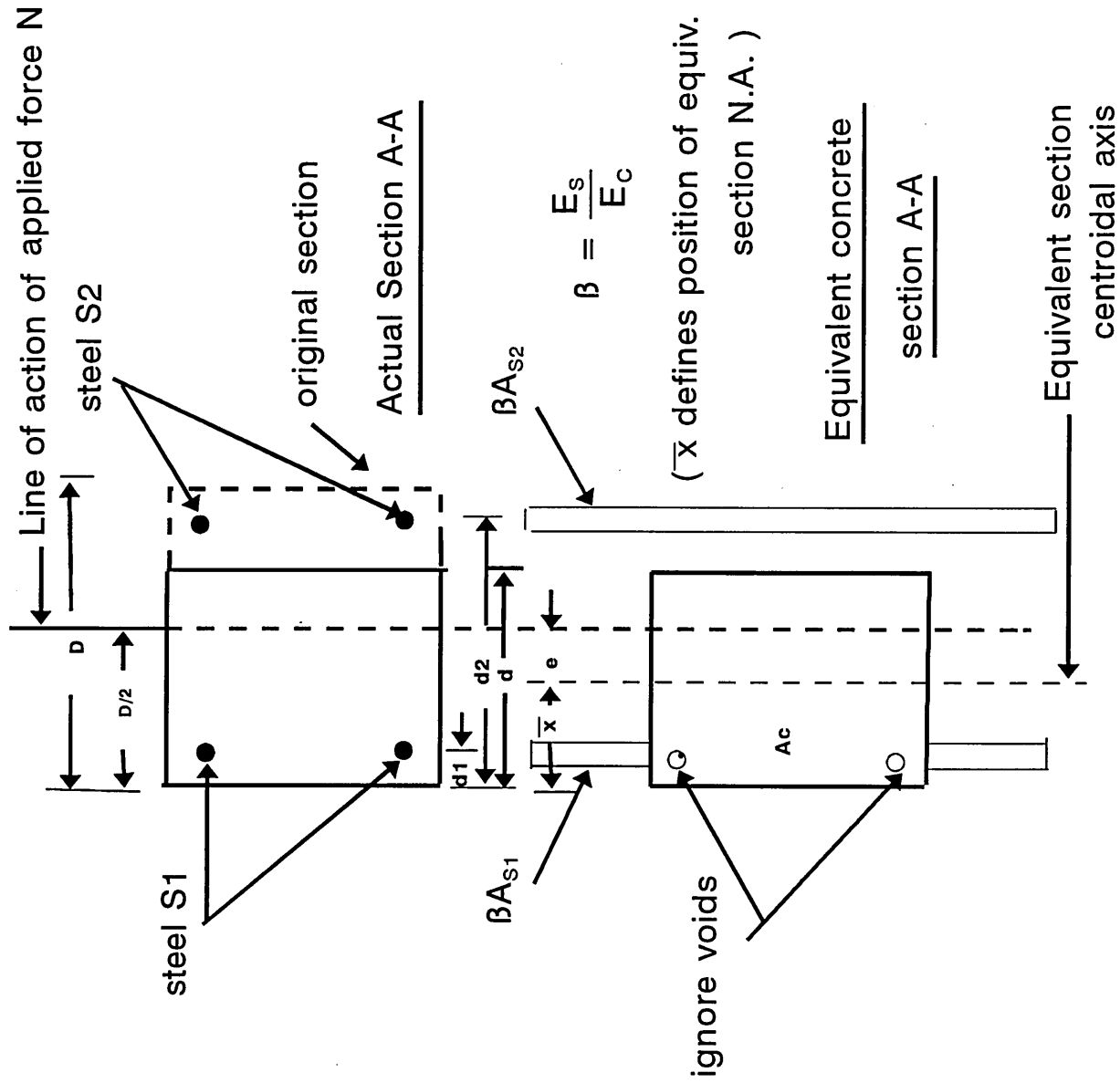


Figure 6.7
Voided Cross-Section

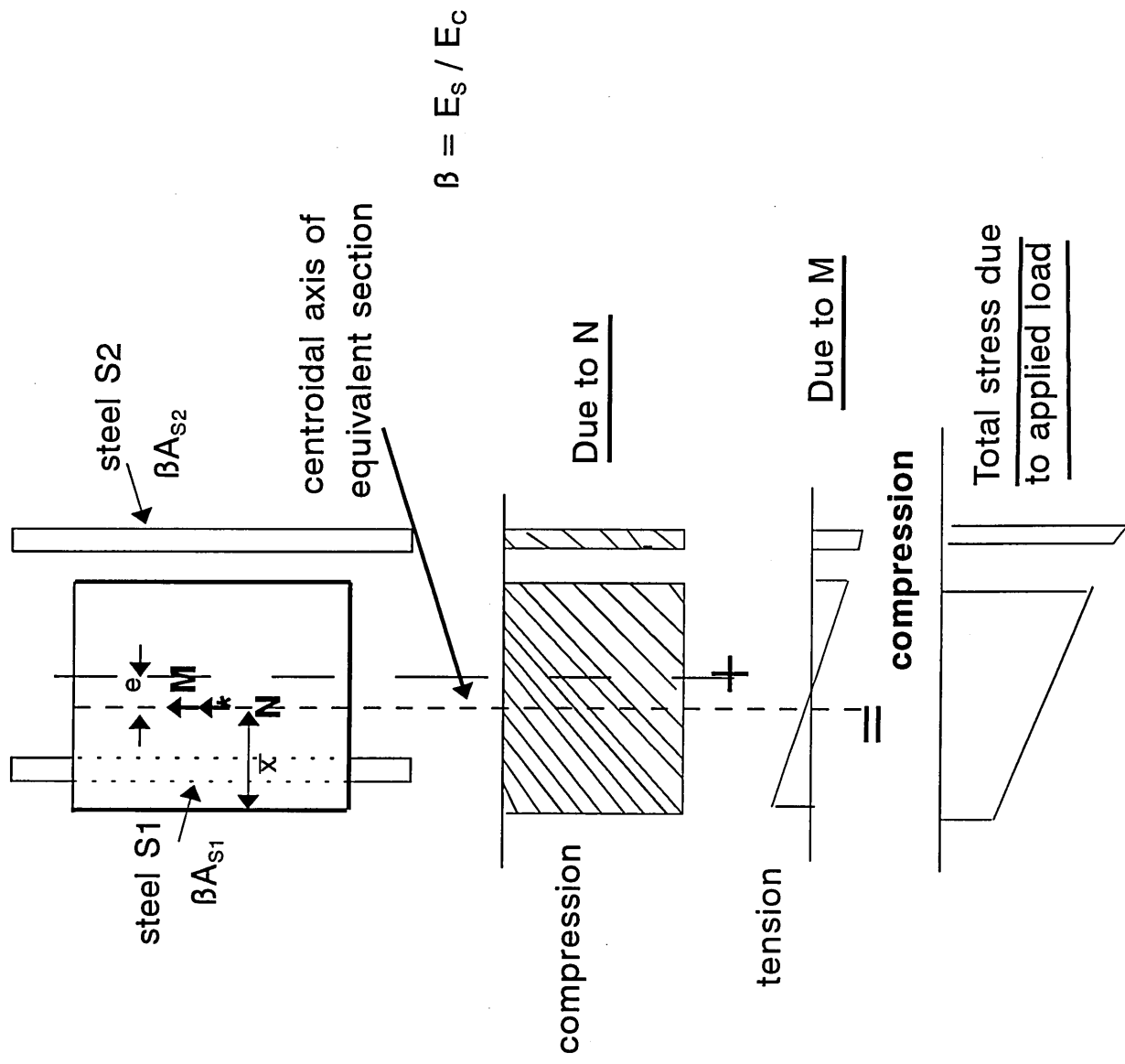


Figure 6.8

Stress distribution on voided cross-section of column

6.4.2 Ultimate Analysis

For the rectangular void used in this investigation, the concrete reaches its maximum compressive strain first on the voided face. Also, at maximum load, the concrete begins to crush and this propagates across the column causing it to fail. Figure 6.9 shows possible mode of failure for eccentrically loaded voided columns. As there is compatibility of strains between the reinforcement and the adjacent concrete, the steel strains (ϵ_{s1} and ϵ_{s2}) and concrete strain on unaffected face (ϵ_c) can be determined from the strain diagram (figure 6.9). The relationship between the depth of neutral axis (\bar{x}) and the ultimate concrete strain ($\epsilon_{cc} = 0.0035$) and steel strains are given by,

$$\epsilon_{s2} = \left(\frac{d_2 - \bar{x}}{d - \bar{x}} \right) \times 0.0035 \quad (6.10)$$

$$\epsilon_{s1} = \left(\frac{d_1 - \bar{x}}{d - \bar{x}} \right) \times 0.0035 \quad (6.11)$$

$$\epsilon_c = \left(\frac{\bar{x}}{d - \bar{x}} \right) \times 0.0035 \quad (6.12)$$

Figure 6.8 represents the total strain diagram for the voided columns considered in this investigation and corresponding stress distribution across the voided section is as shown in figure 6.10. As shown in the figure, the concrete stress variation is part parabola and part rectangular and the stress on voided face is $0.67 f_{cu}$. A detailed stress analysis would be required for the calculation of the area of the part parabola and part rectangular concrete stress block as shown in figure 6.10. The simplification for the rectangular parabolic concrete

stress distribution is the rectangular block as suggested in BS 8110 [92]. This gives a stress distribution as shown in figure 6.11.

Assuming idealised stress strain curves of steel reinforcement, BS 8110 [92] as shown in figure 6.12, the steel stresses can be easily calculated as follows:-

$$f_{s1} = E_s \epsilon_{s1} \text{ or } f_y \quad 6.13 \text{ (a)}$$

$$f_{s2} = E_s \epsilon_{s2} \text{ or } f_y \quad 6.13 \text{ (b)}$$

Where the lesser of the two values is used.

Using simplified stress distribution as shown in figure 6.11, for the known stress distribution (figure 6.9), the ultimate load, P_u , can be calculated as follow;

$$P_u = [0.9 d B (0.67 f_{cu})] + [f_{s1} A_{s1}] + [f_{s2} A_{s2}] \quad (6.14)$$

The axial loading on the column may cause buckling of the longitudinal reinforcement and subsequent cracking and spalling of the adjacent concrete cover. So, checking for steel buckling:-

The maximum load, P , that can be carried by any reinforcing bar is given by,

$$P = f_y A_s \quad (6.15)$$

Where,

A_s = the cross sectional area of the bar.

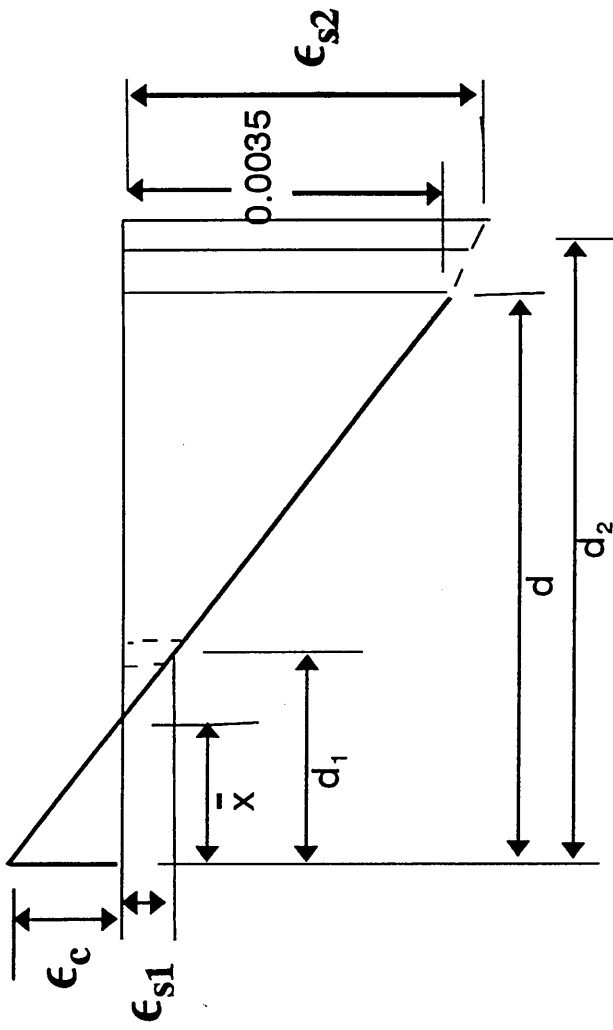
Buckling will be the controlling factor when the applied load exceeds the buckling load. An approximation of the buckling load, P_{CR} , can be gained using Euler's formula for the two fixed ends,

$$P_{CR} = 4 \pi^2 EI / L^2 \quad (6.16)$$

Where,

I = the second moment of area about the buckling axis,

L = the length over which the steel can buckle.



Where,

- ϵ_c = strain on concrete at the unvoided face
- ϵ_{s1} = strain in steel S_1 , and
- ϵ_{s2} = strain in steel S_2 , at the point of failure

Figure 6.9
Strain distribution on voided cross-section at
point of failure

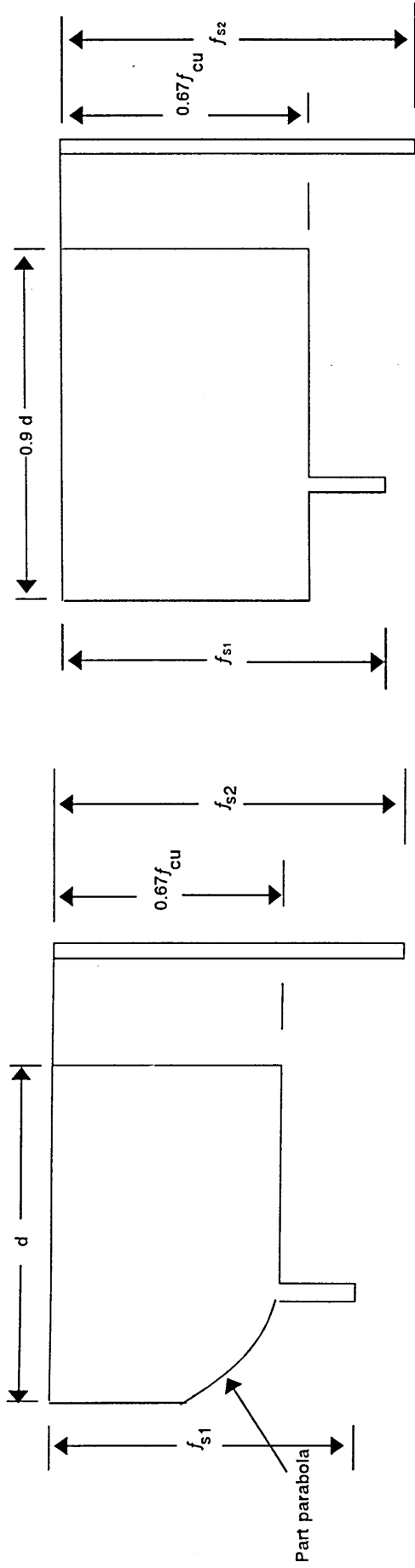


Figure 6.10
Stress distribution for the single void specimen

Figure 6.11
Simplified stress distribution as suggested in BS 8110 [92]

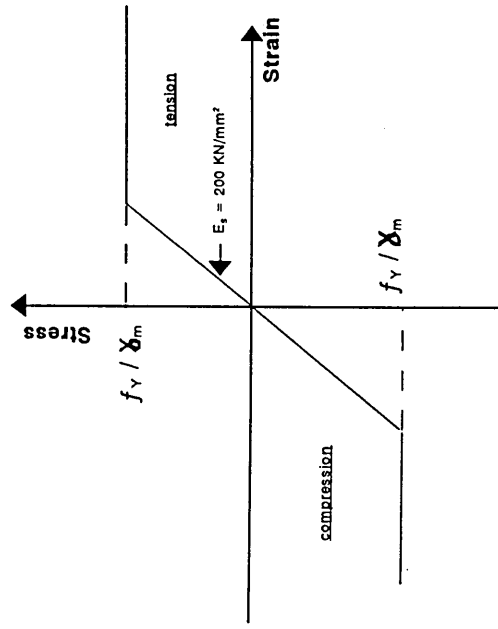


Figure 6.12
Design stress-strain curve for reinforcement [92]

From equating the loads from equations (6.15) and (6.16), a critical length, L_{CR} , of exposed reinforcing bar is,

$$L_{CR} = 2\pi\sqrt{\frac{EI}{f_y}A_s} \quad (6.17)$$

Substituting values for I and A_s , for a circular bar, gives

$$L_{CR} = \frac{\pi D}{2}\sqrt{\frac{E}{f_y}} \quad (6.18)$$

The critical length, L_{CR} , gives a guideline as to possibility of buckling failure. For example, if the exposed length of reinforcement is greater than L_{CR} then the mode of reinforcing bar failure will be controlled by buckling.

6.5 RESULTS AND DISCUSSION

A wide range of experimental data are presented to describe the load-strain characteristics of the control, voided and repaired reinforced concrete short compression members.

The effect of different generic repair materials on the ultimate strength and fracture process of concrete under short term uniaxial compression were established. Each result for the compression members presented in this investigation is an average of three column specimens.

6.5.1 Mode of failure

Plates 6.1 and 6.2 shows the failure mode for the repaired specimens of Batch I and II, respectively. A careful observation of these photographs shows that the basic mechanical properties of repair materials govern the failure mode of the repaired columns when loaded under compression. For example, the failure of columns repaired with high strength material A (both Batches I and II) is due to simultaneous crushing of the concrete and buckling of steel reinforcement in substrate concrete adjacent to the repair patch while the repair patch itself (repair material and reinforcement within it) does not fail. Similarly it is evident from a plates 6.1 and 6.2 that failure of the column specimens repaired with cementitious mortar B is due to crushing of repair material and buckling of steel bars within repair zone. Extensive spalling of the repair patch leading to a pronounced failure zone was found for the columns repaired with materials B and C, the spalling in the repair patch being even more extensive for the weaker repair material C.

Repair materials having higher values of strength and consequently higher elastic modulus than the substrate concrete can cause significant changes in the stress fields developed during transmission of load through repair patch. The value of poisson's ratio contributes to these changes but in patch repairs the mismatch of the modulus values is primarily responsible for their magnitude [11,13].

6.5.2 Load distribution in Steel, Concrete and Repair phases

When repaired reinforced concrete column specimens are subjected to uniaxial compression, the applied load is shared between the materials. The magnitude of load carried by the repair material, steel and concrete phases depends on their cross-sectional area and stiffness.

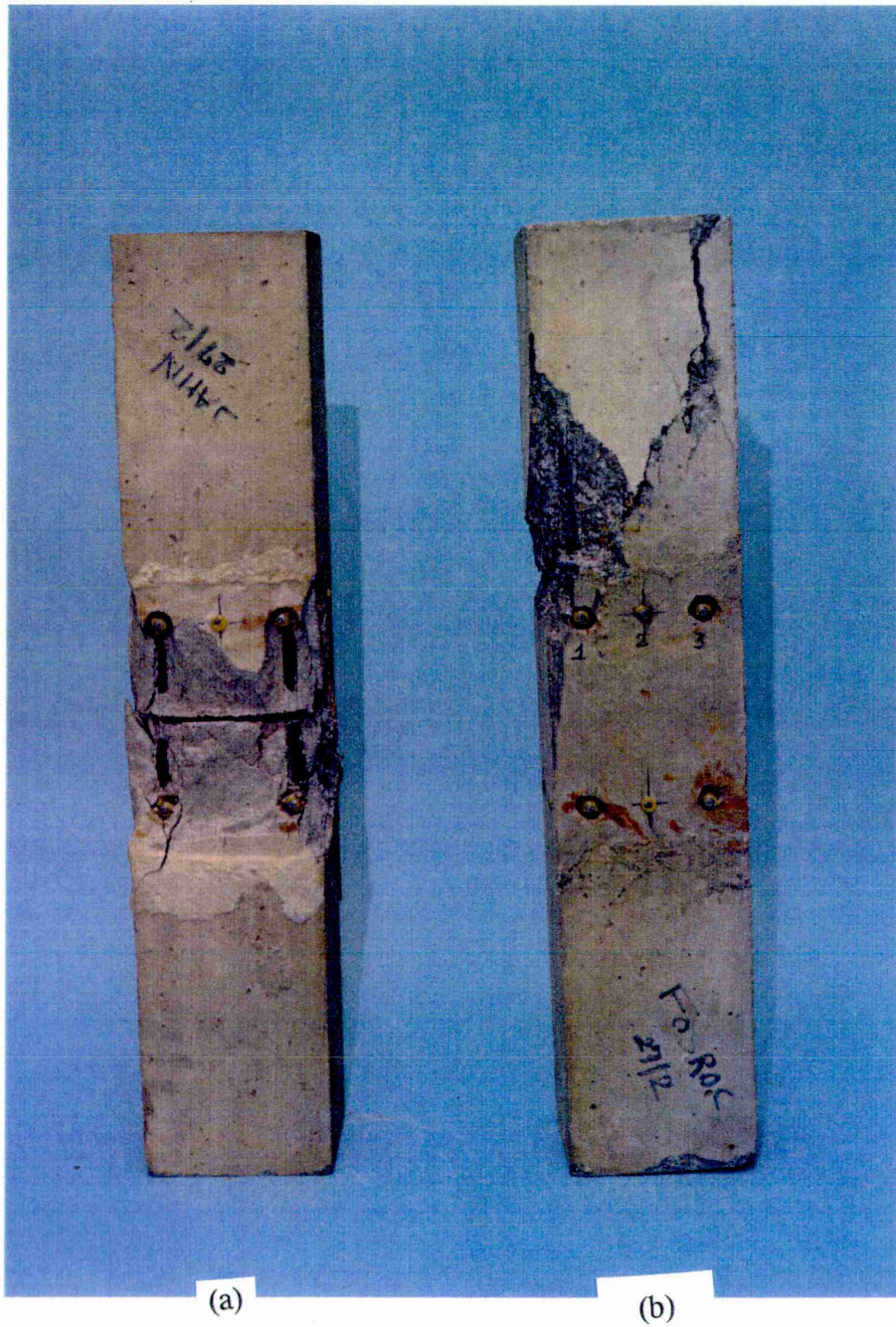


Plate 6.1 Failure mode for the specimens, (a) repaired with Material B and (b) repaired with Material A, of Batch I.

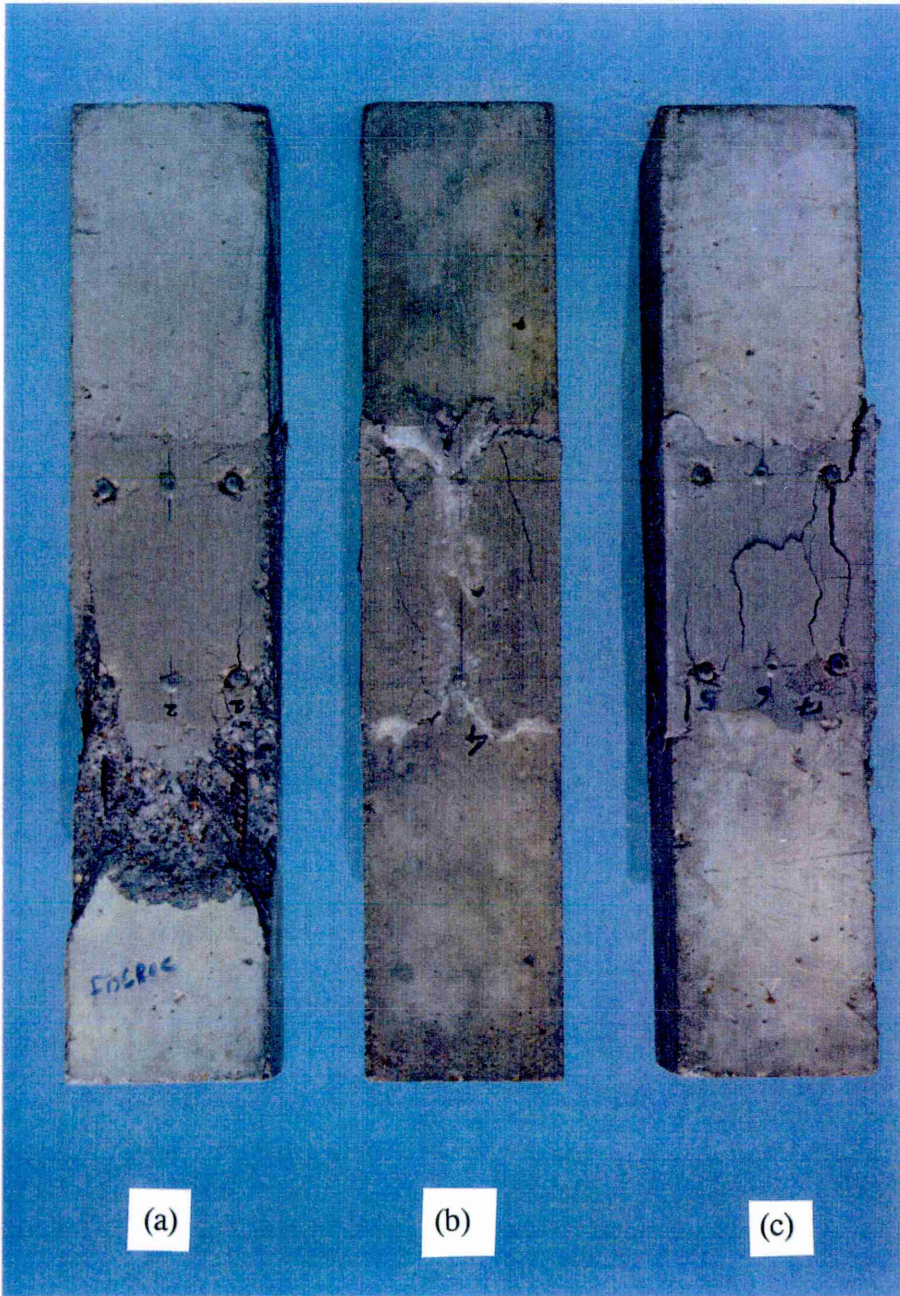


Plate 6.2 Failure mode for the specimens, (a) repaired with Material A, (b) repaired with Material B and (c) repaired with Material C, of Batch II.

The load-strain curves of column specimens (batch I) under uniaxial compression are shown in figures 6.13 to 6.16. Each curve represents the average of three column specimens. As the applied load increases, stresses and strains in the column specimens increase. In this investigation, the loads carried by the steel, concrete and repair phases are determined from a knowledge of the strains in the longitudinal steel and repair materials at each increment of applied load. The stress and hence the load, P_s and P_R , carried by the steel and repair patch are obtained from figures 6.17 and 6.18 which represents the complete stress-strain relationship of the longitudinal steel and repair materials. The load in the concrete phase of the specimen, P_C , is then determined from the following expression for composite materials:-

$$P_C = P - P_s - P_R$$

Where,

P_s = load carried by Longitudinal steel,

P_C = load carried by substrate concrete,

P_R = load carried by repair patch, and

P = total applied load on column specimen at each increment of loading.

The ultimate load carried by the column specimen is taken as the load causing the concrete or repair materials to reach its ultimate strain, and buckling of the steel reinforcement. Due to safety reasons it was decided to take strain readings up to about 40% of the failure load.

The load distribution in the steel, repair and concrete phases of the compression members as obtained using the above procedure is presented in figures 6.19 to 6.20, where

the abscissa represents the incremental applied load in form P/P_U and the ordinate represents the proportion of applied load shared by the concrete, repair and steel phases which are represented by P_C/P , P_R/P and P_S/P respectively.

The results in figure 6.19 show that the high strength and high stiffness of material A has a significant effect on the load distribution in the repaired reinforced concrete column specimens. It also shows that, with increment in load, stress concentration on substrate concrete becomes high, as a result concrete begins to crush and this propagates across the column causing it to fail.

From the load distribution curve for column specimens repaired with material B, repaired surface carries slightly lower stress compared to substrate concrete as shown in figure 6.20. In this case, the repaired column failed by crushing of the repair material. This was followed by crushing of the concrete, then buckling of reinforcing bars. The buckling occurred between the links, and was within the repair zone. In column specimens repaired with material B, some crushing started to appear on repaired surface at about 95% of failure load and propagated to concrete and across the column causing it to fail. Also, from figure 6.21, with increase in load, stress concentration on substrate concrete becomes high for reinforced concrete specimens repaired with material C.

In case of voided column specimens, the concrete crushed on the voided face then crushing propagated across the column. The exposed corroded steel buckled between the links and consequently the steel on unaffected side buckled as the column collapsed.

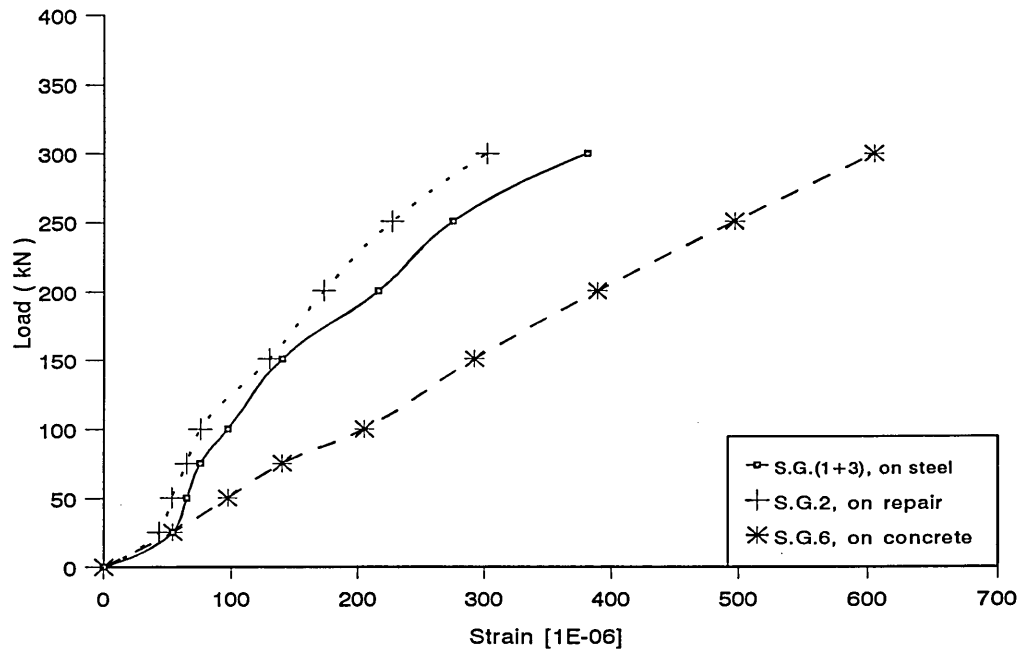


Figure 6.13
 Load-strain relationship for columns A (batch I), repaired with Material A
 Failure Load = 1014 kN

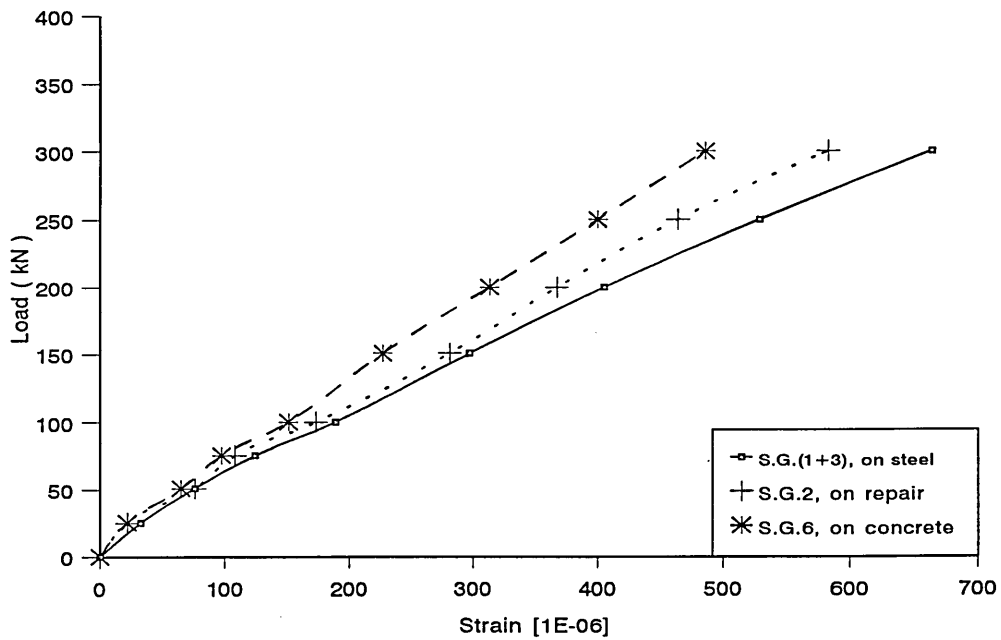


Figure 6.14
 Load-strain relationship for column 2 (Batch I), repaired with Material B
 Failure Load = 857.10 kN

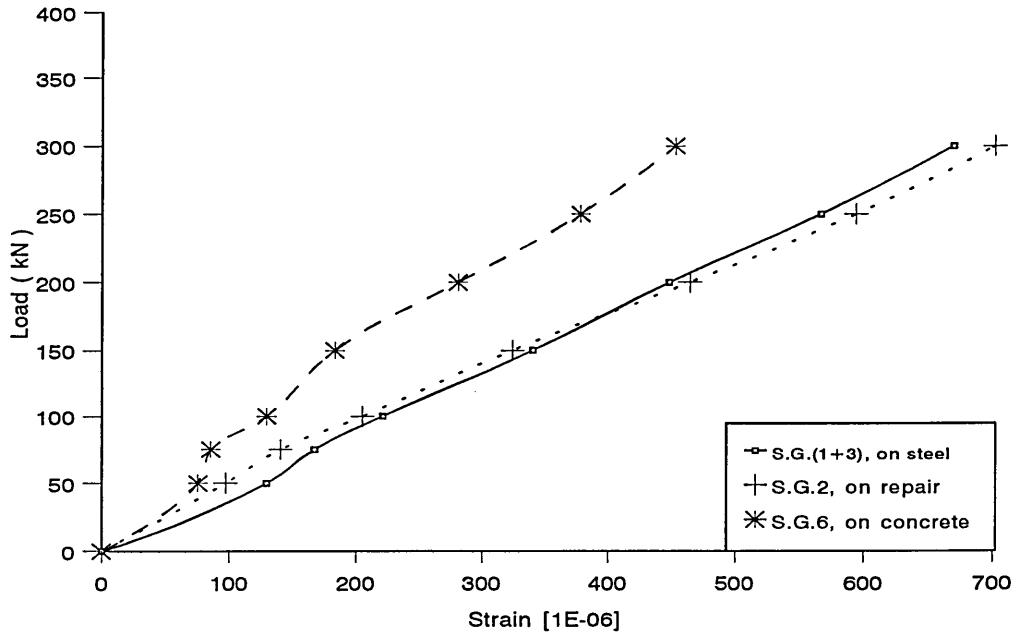


Figure 6.15
 Load-strain relationship for columns C (batch I), repaired with Material C
 Failure Load = 910.80 kN

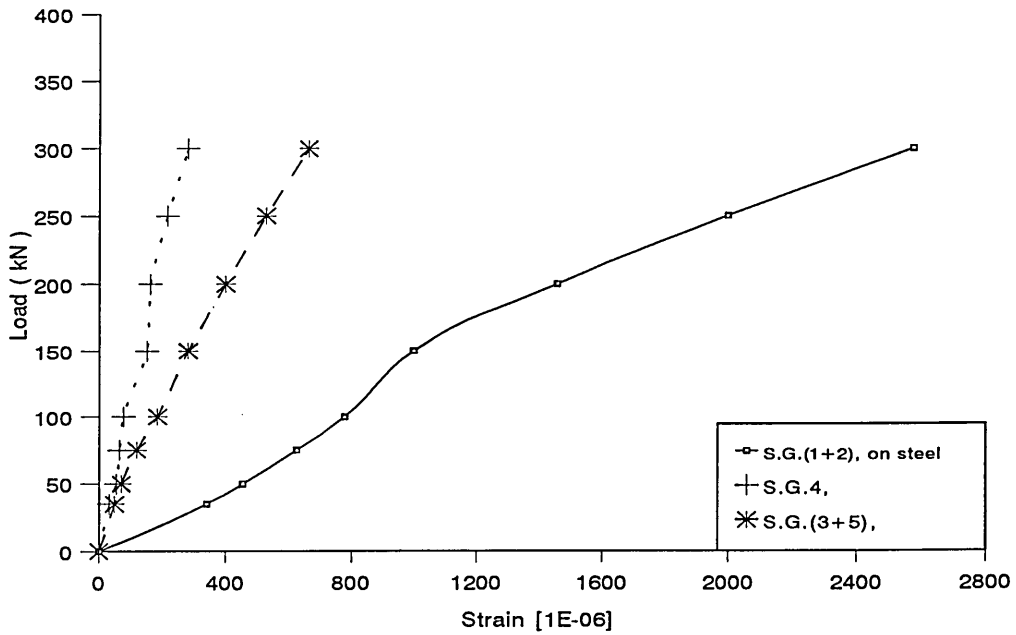


Figure 6.16
 Load-strain relationship for voided columns (batch I),
 Failure Load = 592.60 kN

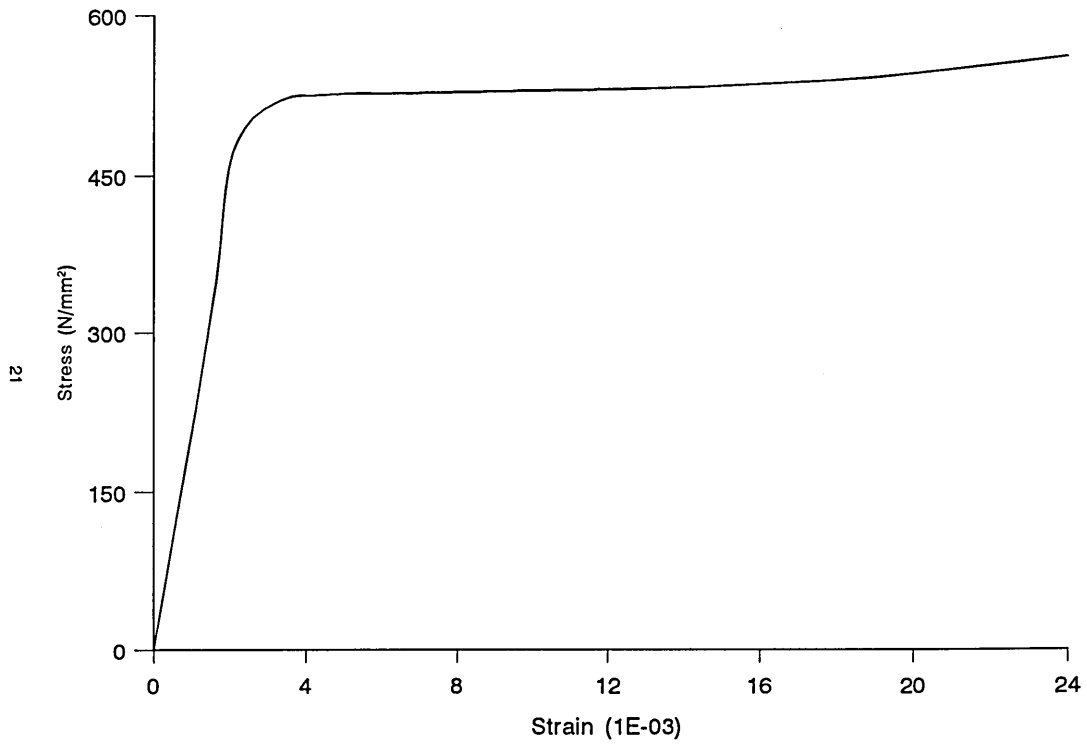


Figure 2.5
Stress-Strain curve for the longitudinal steel reinforcement

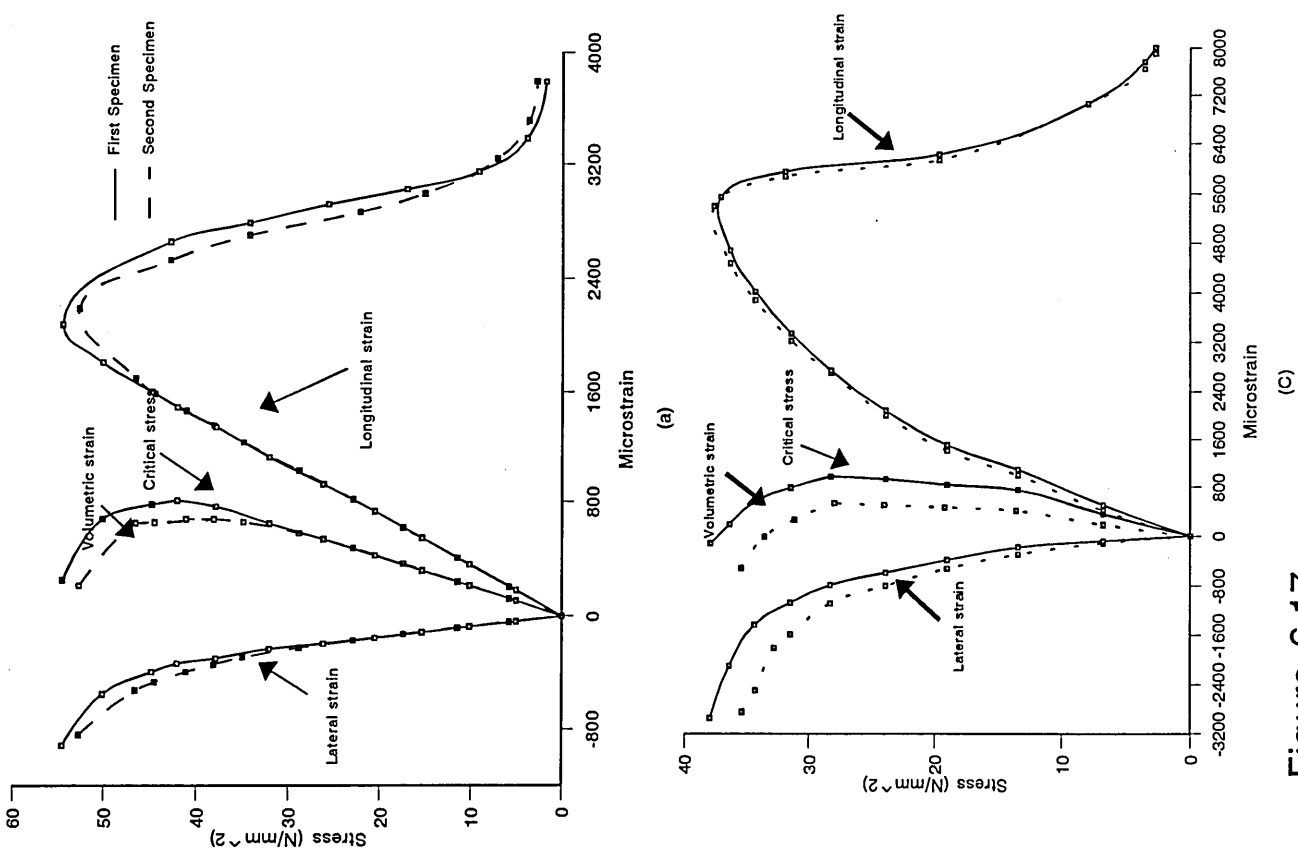
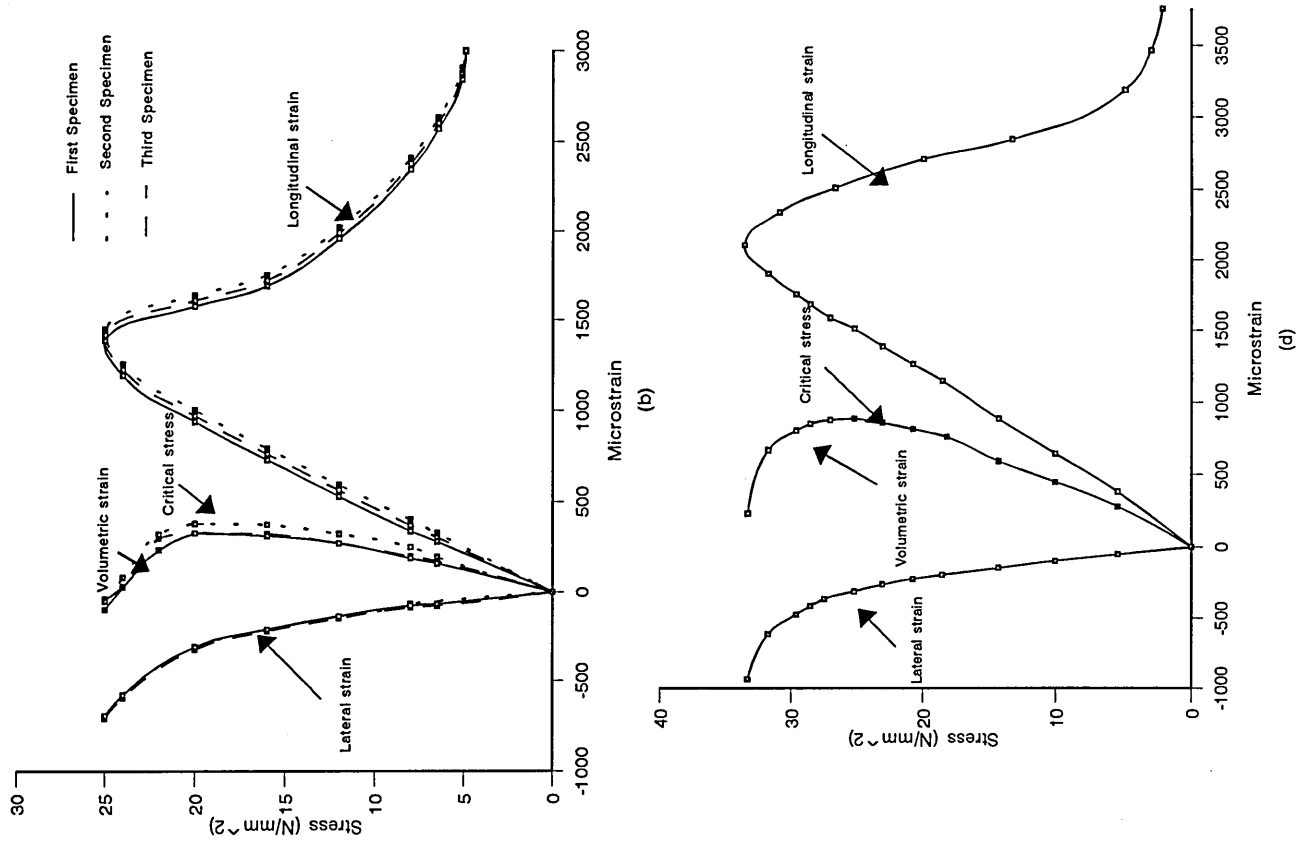


Figure 6.17 Stress-strain relationship for (a) Material A, (b) Material B, (c) Material C and (d) Concrete

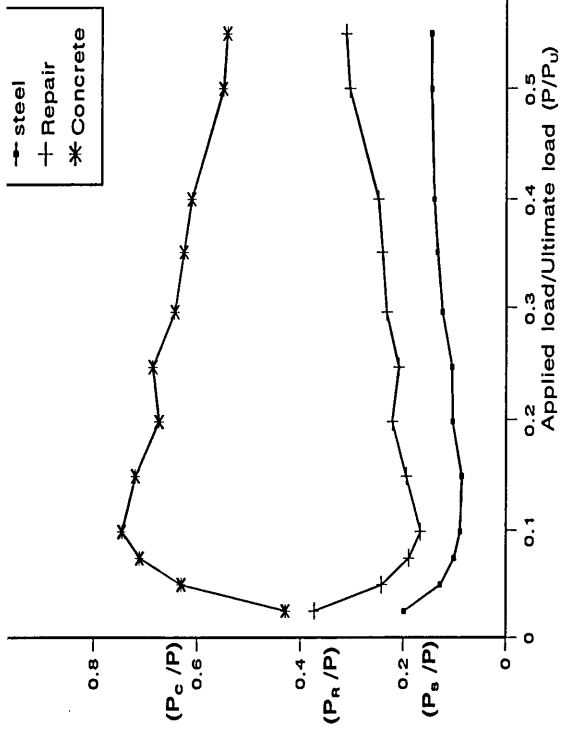


Figure 6.19
Load distribution in the concrete, repair and steel phases of column specimens (Repaired with Material A). Batch I
Failure Load = 1014 kN

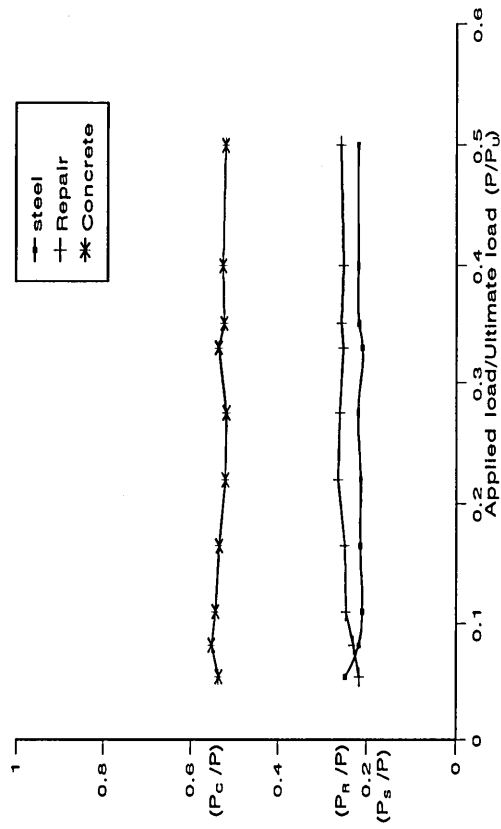


Figure 6.21
Load distribution in the concrete, repair and steel phases of column specimens (Repaired with Material C). Batch I
Failure Load = 910.8 kN

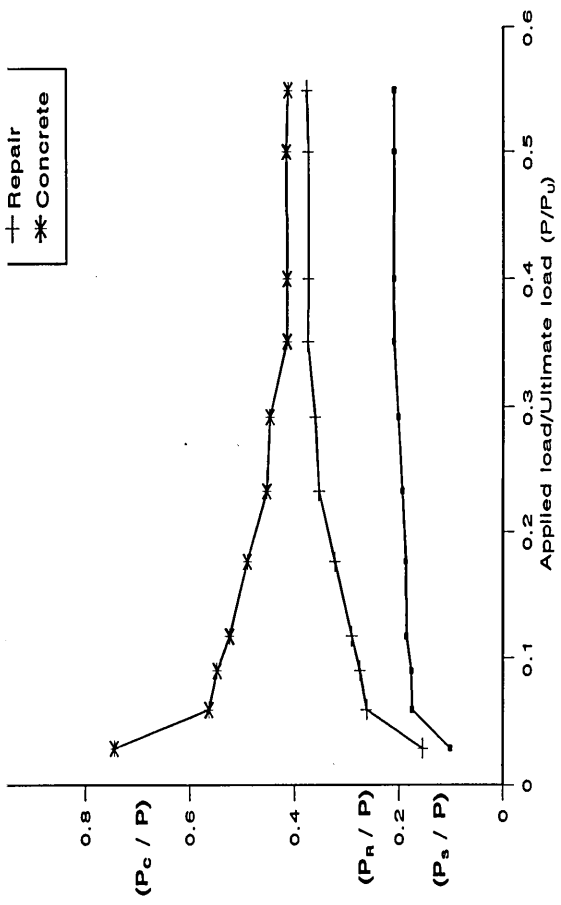


Figure 6.20
Load distribution in the concrete, repair and steel phases of column specimens (Repaired with Material B). Batch I
Failure Load = 857.1 kN

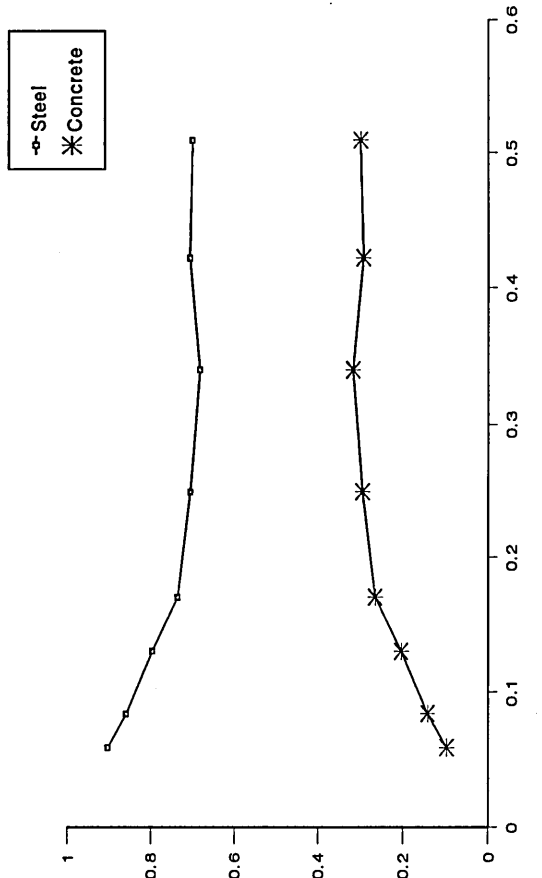


Figure 6.22
Load distribution in the concrete and steel phases of voided column specimens (Batch I)
Failure Load = 592.60 kN

Figures 6.24 to 6.27 represent experimental results of batch II tests (double sided void), of this investigation. The load distribution in the concrete, repair and steel phases of repaired column specimens are given in figures 6.28 to 6.31- these are determined from the strain data plotted in figures 6.24 to 6.27 and the stress-strain curves of materials given in figures 6.17 and 6.18. Repair materials strength and stiffness have similar effect as in batch I on the load sharing by the concrete, repair and steel phases of the repaired column specimens. The results in figures 6.28 to 6.31 shows that, with increase in load, stress concentration on substrate concrete becomes lower. This is due to large cross-sectional area of the repair patch. Column specimens repaired with Material A exhibited more convergent performance compared to other column specimens. Also, the magnitude of load carried by the repair material and substrate concrete phases depends on their cross-sectional area and stiffness. While figure 6.32 represents load distribution in the concrete and steel phases of control column specimens.

The results in figures 6.33 and 6.34 show the comparison between the experimental and theoretical load distribution (batch I) using serviceability analysis. These curves are determined from the equation of total stress (equation 6.8) and the stress strain curve of concrete given in figure 6.18. Generally all the predicted load distribution are in agreement with the experimental data obtained in this investigation.

6.5.3 Ultimate strength

Figures 6.35 and 6.36, represent the effect of the repair material on the ultimate failure load (as percentage of the ultimate strength of the control column) of repaired column specimens of batches I and II, respectively.

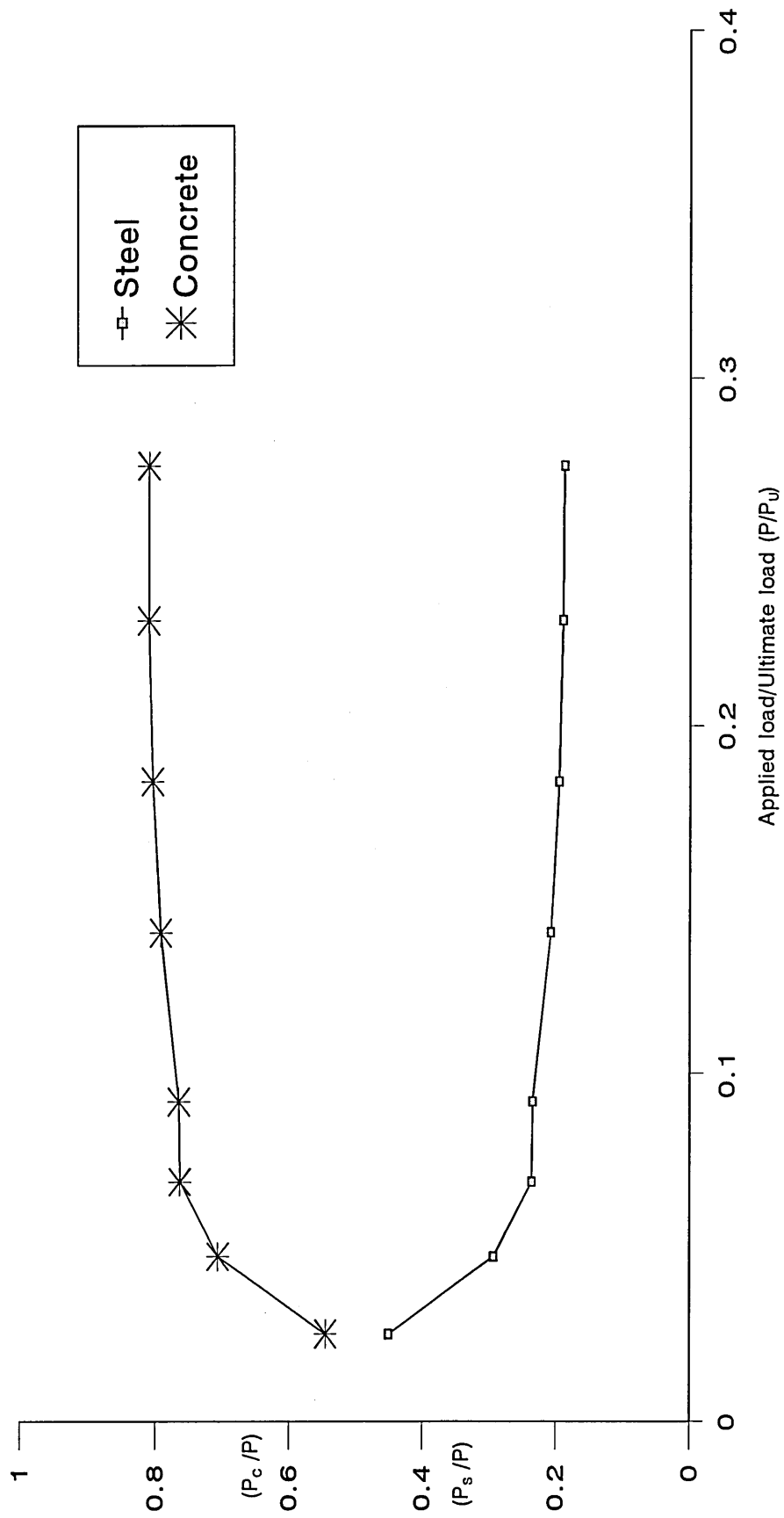


Figure 6.23
Load distribution in the concrete and steel phases of control column specimens. Batch I

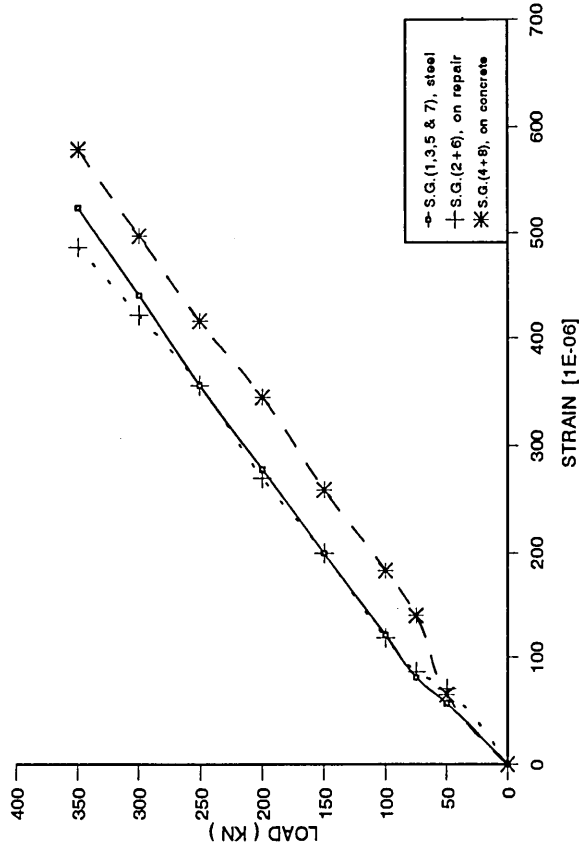


Figure 6.24
Strain distribution for columns A (batch II), repaired with Material A
Failure Load = 1072 KN

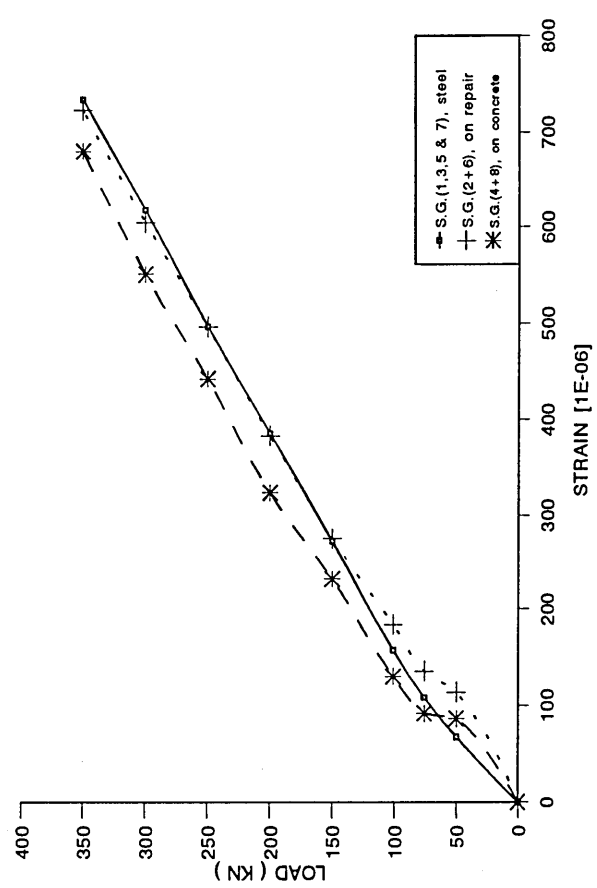


Figure 6.25
Strain distribution for Columns B (batch II), repaired with Material B
Failure Load = 825.40 KN

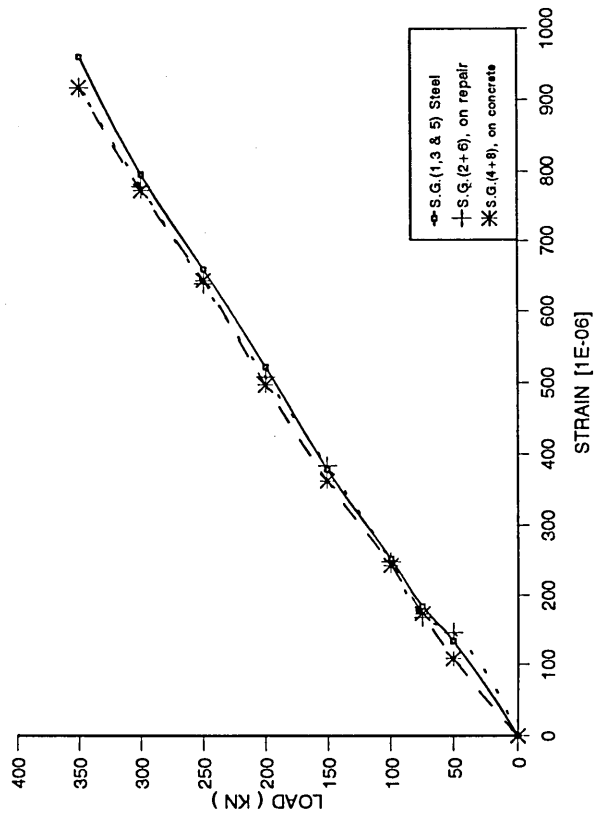


Figure 6.26
Strain distribution for Columns C (batch II), repaired with Material C
Failure Load = 815.80 KN

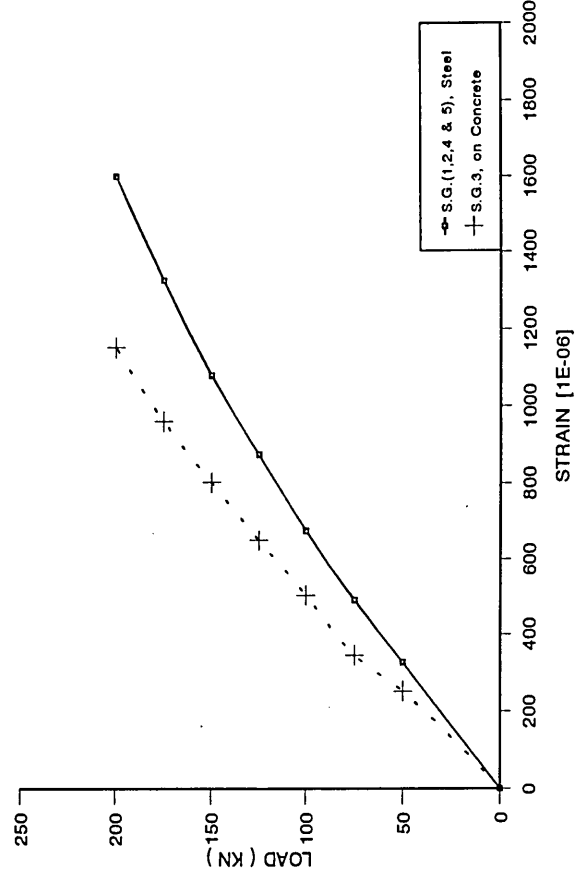


Figure 6.27
Strain distribution for voided columns (batch II)
Failure Load = 249.90 KN

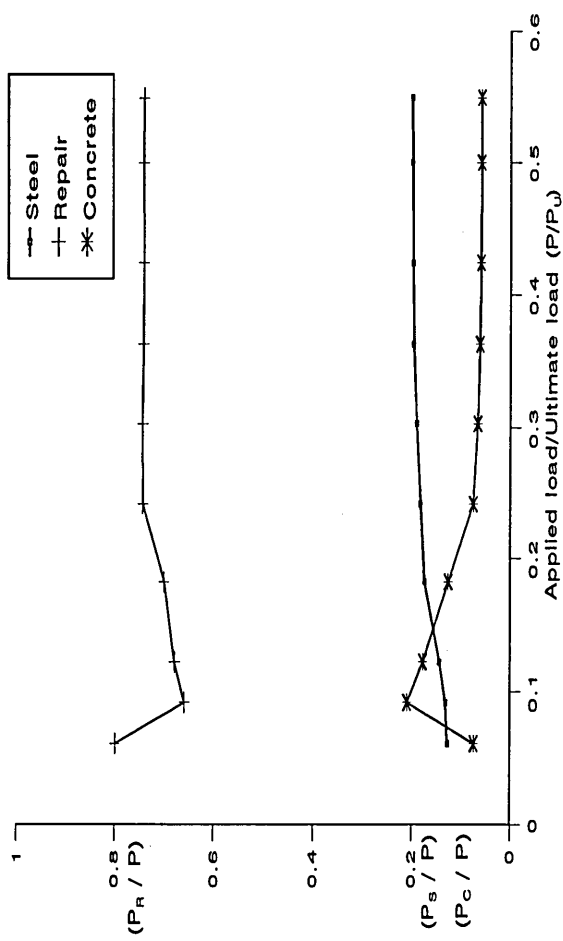


Figure 6.29
Load distribution in the concrete, repair and steel phases of
column specimens (Repaired with Material B). Batch II
Failure Load = 825.40 kN

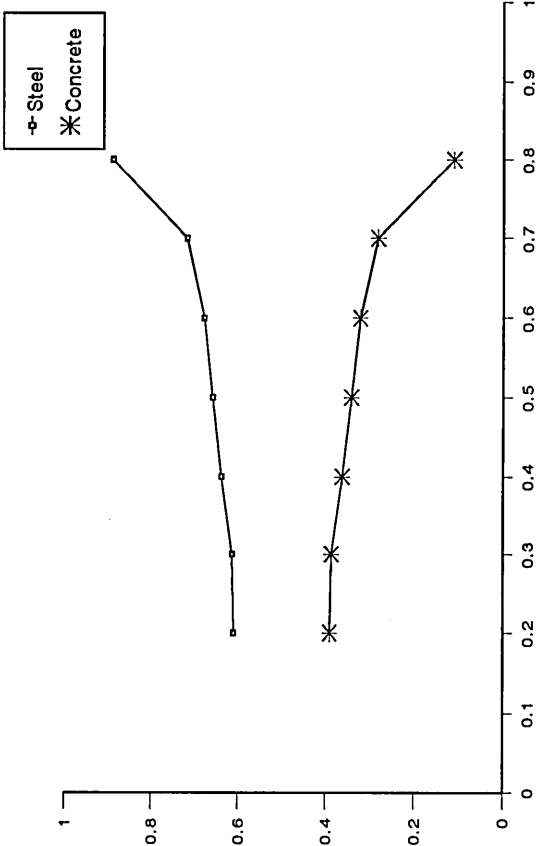


Figure 6.31
Load distribution in the concrete and steel phases of voided column specimens (Batch II)
Failure Load = 249.90 kN

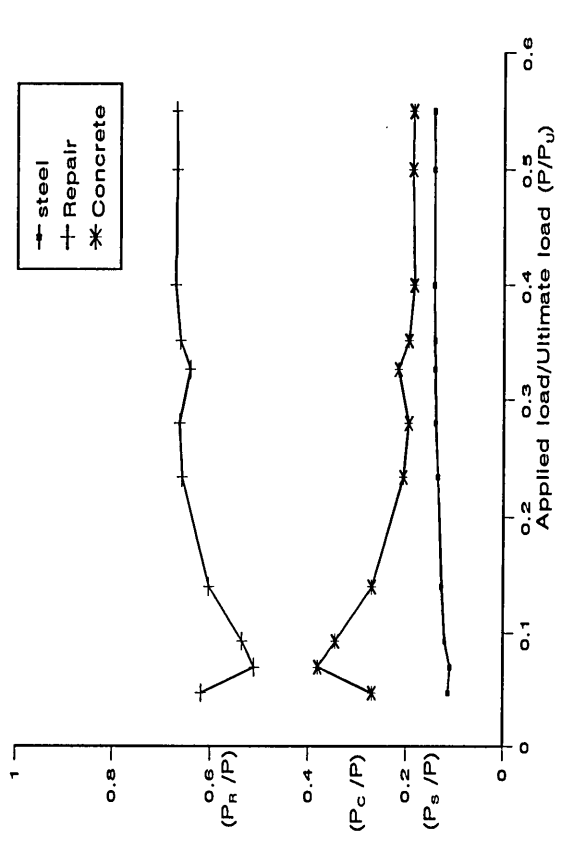


Figure 6.28
Load distribution in the concrete, repair and steel phases of
column specimens (Repaired with Material A). Batch II
Failure Load = 1072 kN

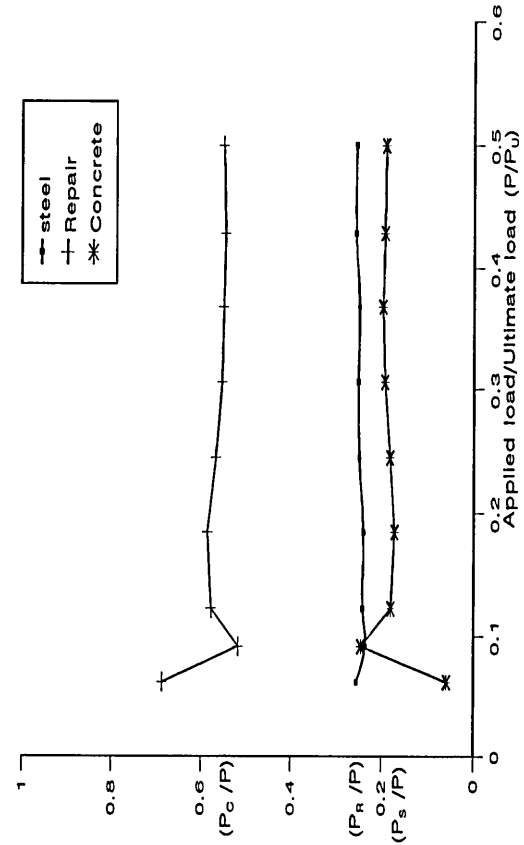


Figure 6.30
Load distribution in the concrete, repair and steel phases of
column specimens (Repaired with Material C). Batch II
Failure Load = 815.8 kN

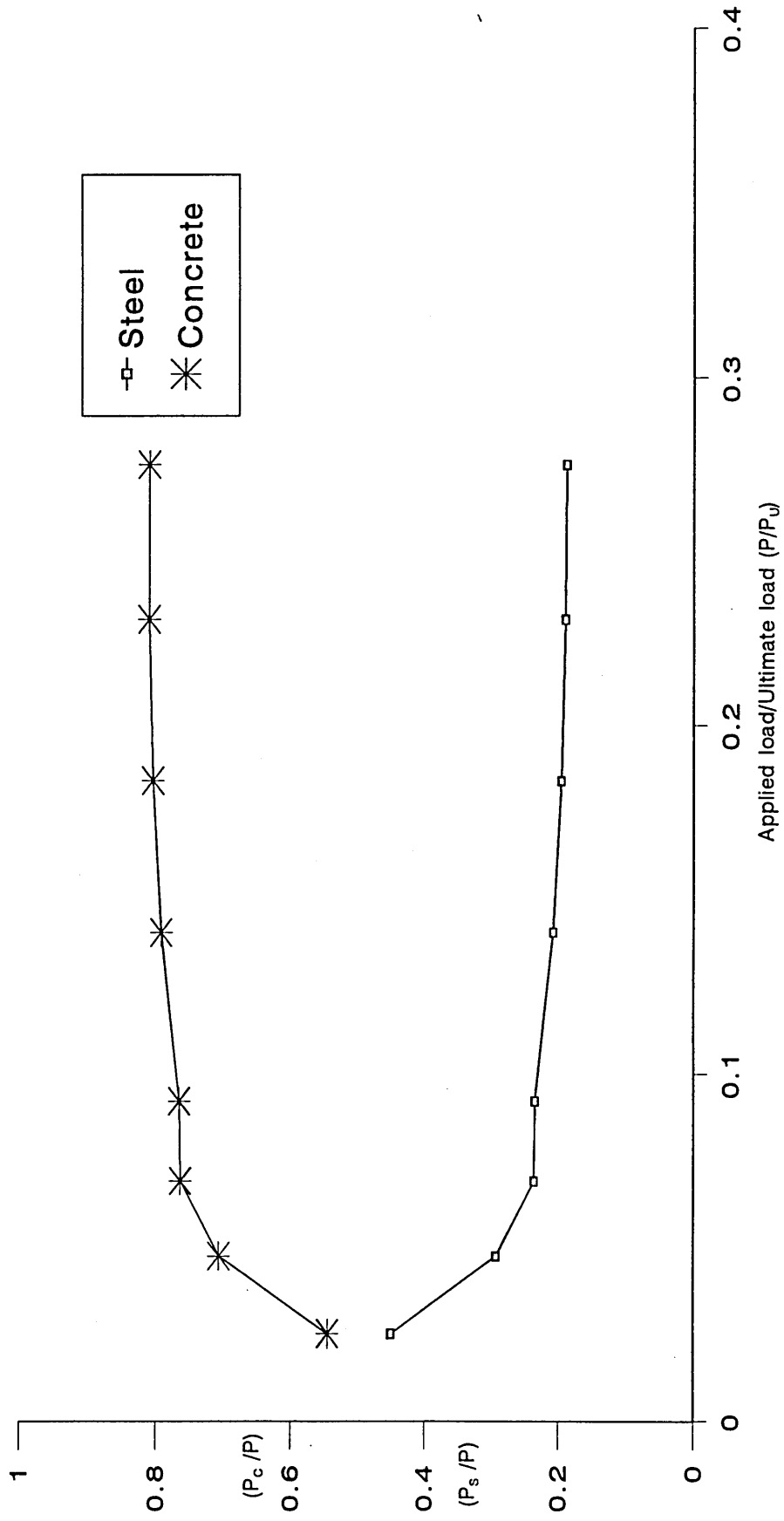


Figure 6.32
 Load distribution in the concrete and steel phases of control column specimens
 (average of three)

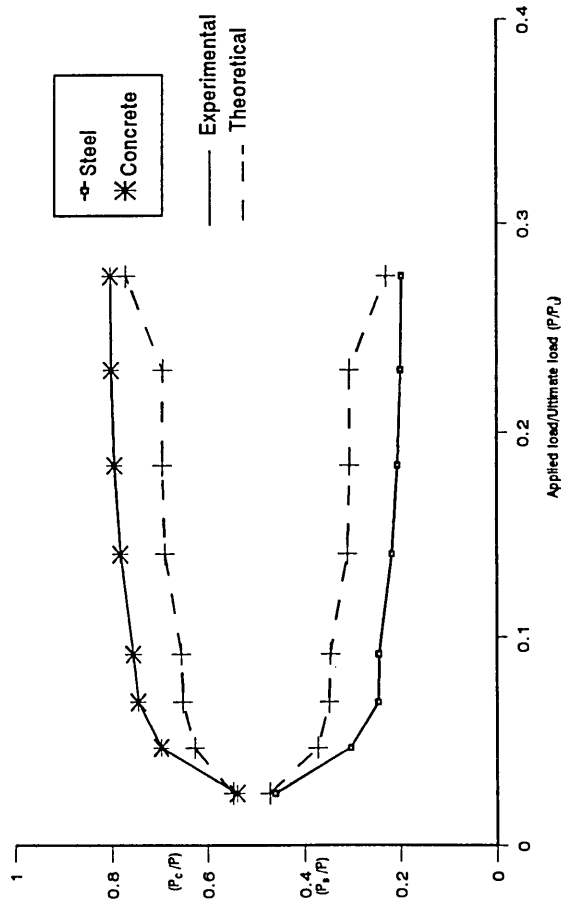


Figure 6.33
Comparison of theoretical and experimental load distribution for control reinforced concrete columns

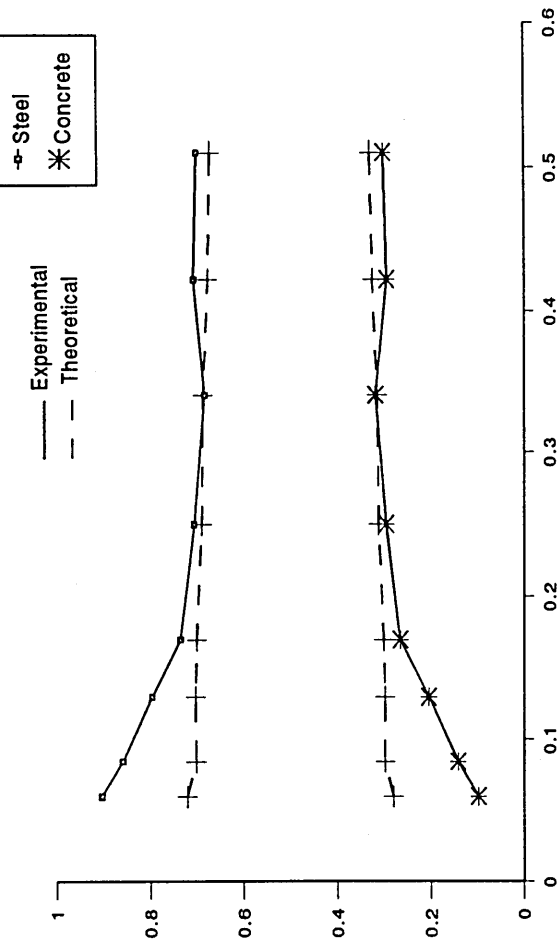


Figure 6.34
Comparison of theoretical and experimental load distribution for voided (batch I) reinforced concrete columns

According to these figures, the properties of repair material have a significant effect on the load carrying capacity of the repaired column specimens. The average residual strength of column specimens repaired with material A was found in the range of 93 to 94% of the compressive strength of control column.

While values of 76 and 80% were found for the column specimens repaired with materials B and C, respectively. So, the ultimate failure load of the repaired reinforced concrete depends on the cross-sectional area, strength and stiffness of repair materials.

The effect of different generic materials on the failure load and the ultimate strength of the defective and repaired short compression members are highlighted in Table 6.3. The presence of a single and double voids on two opposite faces in the reinforced concrete column due to corrosion of reinforcement and subsequent spalling reduces its strength by approximately 46 and 79%, respectively.

Repair of defective reinforced concrete columns using three generic repair materials A, B and C restore the strength of the column by 94, 72 and 71 percent for a voids on two opposite faces (Batch II) respectively.

Table 6.3 Results of a failure load and residual strength of Batch I and Batch II tests.

| Specimens | Repair Materials | Failure Load (KN) | | Failure load compare to control column (%) | |
|-----------|------------------|-------------------|----------|--|----------|
| | | Batch I | Batch II | Batch I | Batch II |
| Control | ---- | 1093 | 1143 | 100 | 100 |
| Columns A | A | 1014 | 1072 | 92.77 | 93.79 |
| Columns B | B | 857.1 | 825.4 | 78.42 | 72,21 |
| Columns C | C | 910.8 | 815.8 | 83.33 | 71.37 |
| Voided | nil | 592.6 | 249.9 | 54.22 | 21.86 |

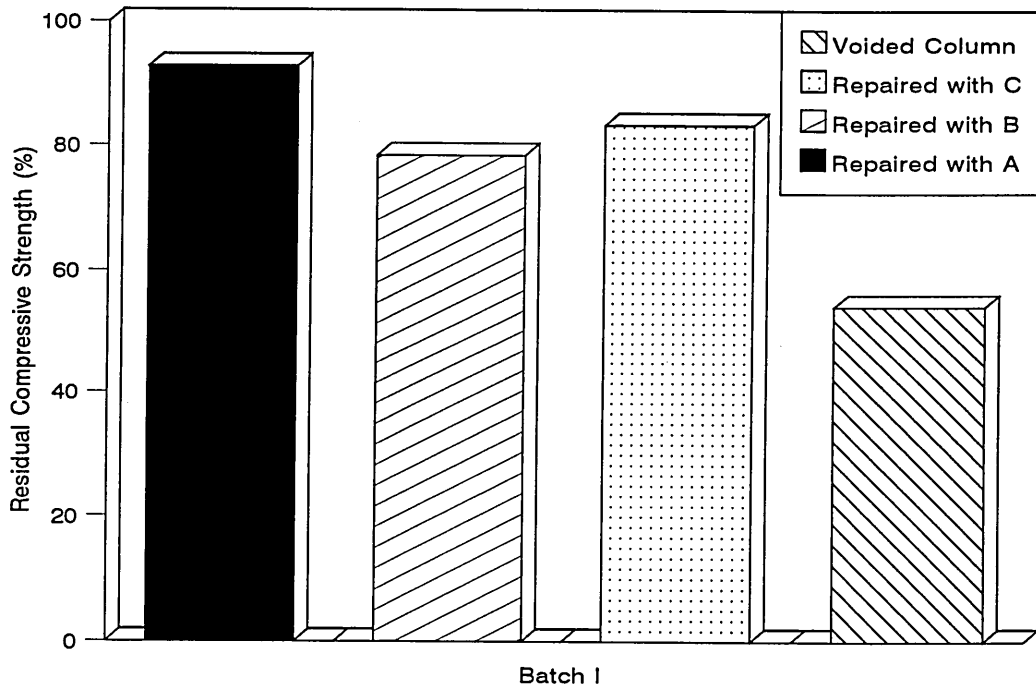


Figure 6.35
The residual compressive strength of repaired columns (relative to control columns)

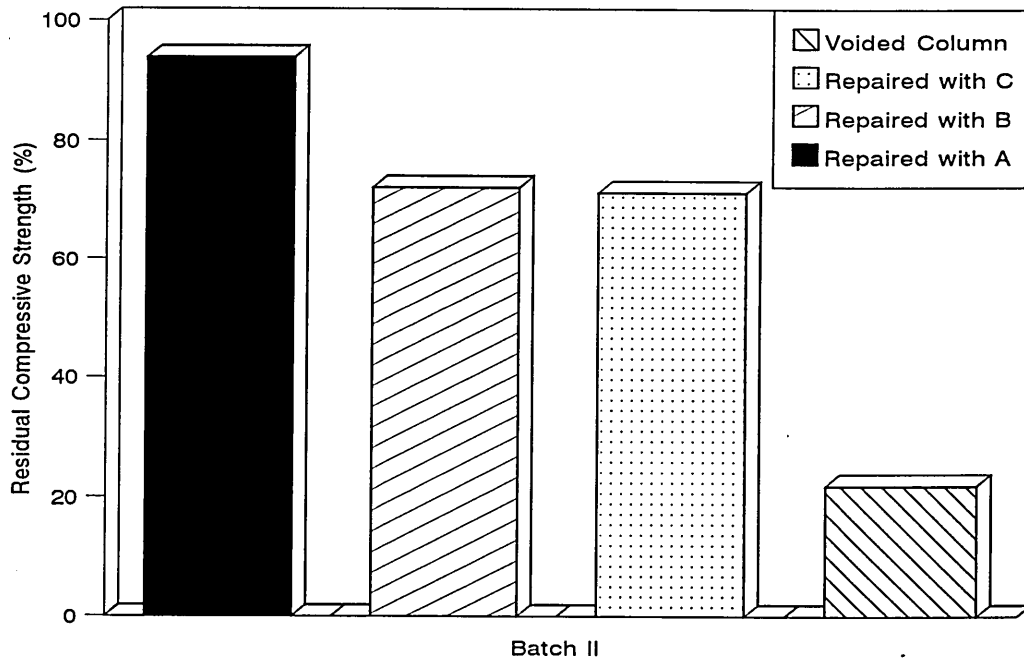


Figure 6.36
The residual compressive strength of repaired columns (relative to control columns)

6.5.4 Theoretical analysis

Theoretical analysis of voided column specimens of batch I test using the method described in section 6.4 is as follows:-

The voided cross-section dimensions are:-

$$B = D = 150 \text{ mm}, d = 95 \text{ mm}, d_1 = 26 \text{ mm}, d_2 = 124 \text{ mm}$$

$$A_c = (150 \times 95) = 14250 \text{ mm}^2, A_{s1} = 226 \text{ mm}^2, A_{s2} = 203 \text{ mm}^2$$

The material properties are:-

$$f_{cu} = 42 \text{ N/mm}^2, f_y = 470 \text{ N/mm}^2, E_s = 210 \text{ kN/mm}^2,$$

$$E_c = 21 \text{ kN/mm}^2$$

This gives an equivalent section area A_T of:

$$\begin{aligned} A_T &= A_c + \alpha A_{s1} + \alpha A_{s2} \quad \text{where, } \alpha = E_s / E_c \\ &= 14250 + 10 (226 + 203) \\ &= 18540 \text{ mm}^2 \end{aligned}$$

From the design stress-strain curve of concrete [92], the maximum concrete strain (ϵ_o) is given by:-

$$\begin{aligned} \epsilon_o &= (f_{cu}/\gamma_m)^{0.5} / 4100 \\ &= 1.581 \times 10^{-3} \end{aligned}$$

Now the length of exposed reinforcing bar (L) is = 220 mm.

Using equation (6.18), the critical length (L_{CR}) of the exposed reinforcing bar is,

$$L_{CR} = 398.4 \text{ mm.}$$

$$\text{Hence, } L < L_{CR}.$$

Therefore, mode of reinforcement failure is not controlled by buckling.

The neutral axis position of the equivalent section is given by:-

$$x = (14250 \times 47.5) + (10 \times 226 \times 26) + (10 \times 203 \times 124)/18540 = 53.26 \text{ mm.}$$

Therefore, the eccentricity e of the applied load is,

$$e = 150/2 - 53.26 = 21.74 \text{ mm.}$$

The second moment of area, I , of the equivalent section at the voided section is,

$$\begin{aligned} I &= \{150 \times 95^3/3\} + \{10 \times 226 \times (95-26)^2\} \\ &\quad + \{10 \times 203 \times (124-95)^2\} \\ &= 4.473 \times 10^7 \text{ mm}^4 \end{aligned}$$

Therefore,

$$\begin{aligned} I_c &= (4.473 \times 10^7) - (18540 \times 21.74^2) \\ &= 3.597 \times 10^7 \text{ mm}^4 \end{aligned}$$

Using equation (6.9) the neutral axis position \bar{x} due to the applied load is:-

$$\bar{x} = -35.98 \text{ mm}$$

and, from equations (6.10) to (6.12) the critical strains at point of failure are:-

$$\begin{aligned} \epsilon_{s1} &= 1.646 \times 10^{-3} \\ \epsilon_{s2} &= 4.275 \times 10^{-3}, \text{ and} \\ \epsilon_c &= -0.961 \times 10^{-3}. (\because \epsilon_c < \epsilon_o) \end{aligned}$$

Also from equations 6.13(a) and 6.13(b) the steel stresses f_{s1} and f_{s2} at point of failure is,

$$\begin{aligned} f_{s1} &= 417.00 \text{ N/mm}^2 && \text{i.e.} < f_y \\ f_{s2} &= 897.75 \text{ N/mm}^2 && \text{i.e.} > f_y, \text{ So } f_y = 470 \text{ N/mm}^2 \end{aligned}$$

Applying equation (6.14), failure load, P_u , can be calculated as follows:-

$$P_u = [0.9 \times 95 \times 150 \times 0.67 \times 42] + [417 \times 226] + [470 \times 203]$$
$$= 546.20 \text{ kN}$$

The failure load value determined from the above procedure for the single voided column specimen shows acceptable agreement with experimental result as shown in Table 6.4.

Table 6.4 Comparison between the experimental and theoretical failure load of defective reinforced concrete column of Batch I.

| Failure Load (kN) | | % Error |
|-------------------|-------------|---------|
| Experimental | Theoretical | 8 |
| 592.60 | 546.20 | |

6.6 CONCLUSIONS

From the experimental results described in this chapter, the following conclusions can be made :-

- Column specimens repaired with material A, failed without giving any warning, while columns repaired with materials B and C developed cracks on the repair surface at about 90% of failure load and propagated to concrete and across the column causing it to failure.
- The elastic modulus of the repair material is of importance in reinforced concrete patch repairs. To avoid stress concentrations and brittle failure, the modulus of the

repair material should not differ significantly from that of the substrate concrete. For example, repair material A - a high strength and high elastic modulus material causes relatively high stress concentration and fails in a brittle manner. Conversely, those with low elastic modulus values transfer load into the substrate concrete.

- The magnitude of load carried by the repair material and substrate concrete phases depends on their cross-sectional area and stiffness.

CHAPTER 7

LONG TERM STRUCTURAL INTERACTION IN REPAIRED COMPRESSION ELEMENTS

7.1 INTRODUCTION

The importance of long-term deformation, such as creep and shrinkage, in concrete structures is already well established. Creep can affect internal stresses in two ways: it can reduce existing internal stress concentrations so that they are of a continuous nature, and it can create its own new internal stresses when materials with different creep characteristics interact in a given cross section. One example would be a reinforced concrete column under permanent load. Creep causes contraction of concrete but not of steel. Since plane sections remain plane, the stresses decrease in the concrete over time as the stresses increase in the steel. The same redistribution is produced by shrinkage ; these internal stresses are, in turn, reduced by creep. As a result of this redistribution caused by creep and shrinkage, compression reinforcement in under-reinforced columns may reach the yield point even under working loads. Similar redistribution of stresses can be expected in repaired reinforced concrete elements due to grossly different creep and shrinkage characteristics of a repair patch relative to the substrate material. However, there is little information available on the long-term stress distribution in repaired elements.

In this chapter, the long term structural interaction between a repair patch and substrate reinforced concrete were investigated. Three commercially available generic repair materials, namely A, B and C, are used for repair work. Results of an experimental investigation on the long term structural interaction between a repair patch and the substrate in short compression members of reinforced concrete are given in this chapter. A theoretical

procedure is derived to relate the interaction with basic properties of these repair materials and substrate concrete, e.g. creep, shrinkage and modulus of elasticity. The validity of the theory is established on the basis of the experimental data obtained in this study. Also, an attempt is made to predict the long-term creep deformation of repaired reinforced concrete by using the creep model proposed by Samra [144]. Before presenting the results of this study, however, a brief literature review is made on the practical methods of predicting time-dependent deformations of reinforced concrete.

7.2 LITERATURE REVIEW

Although it is known that the presence of reinforcement in concrete reduces elastic strain, shrinkage and creep, there are surprisingly few published papers reporting experimental data. Troxell et. al [145] and Lambotte et. al [146] demonstrated the reduction in shrinkage and, to a lesser degree, in creep for symmetrically distributed reinforcement.

For designers, there are various practical methods available for estimating time-dependent deformations of reinforced concrete: Okada[147], Abeles[148], CEB[149], Dilger[150] and Branson[151]. These five methods apply reduction factors to the creep and shrinkage of plain concrete to allow for the presence of reinforcement, these factors are based mainly on elastic analysis either on a constant modulus of elasticity for concrete or on an age-adjusted effective modulus to allow for creep. Except for the Okada method [147], the general form of the reduction factor (**F**) is :

$$F = \frac{1}{1 + \rho n}$$

$$F = \frac{1}{1 + \rho n_0 (1 + \chi \phi)} \quad (7.1)$$

Where,

n is the modular ratio

n_0 is the initial modular ratio

ρ is the reinforcement ratio

χ is the ageing coefficient

ϕ is the creep coefficient of plain concrete

(the ratio of creep to the elastic strain is termed the creep coefficient)

Okada's reduction factors are:

$$\text{Creep } F = \left[\frac{1 + 0.5 \rho n_0}{1 + \rho n_0} \right] \frac{E_{co}}{E_{ro}} \quad (7.2 \text{ (a)})$$

Where,

E_{co} is the modulus of elasticity of plain concrete at loading,

E_{ro} is the reinforced concrete modulus of elasticity at loading.

$$\text{Shrinkage } F = \frac{1 - 0.5 \rho n_0 \phi}{1 + \rho n_0} \quad (7.2 \text{ (b)})$$

Details of the parameters of equations (7.1) and (7.2) for each method are listed in Table 7.1. It is clear that all the above predicting methods rely on a knowledge of creep and shrinkage of plain concrete specimens of the same size and shape. Therefore, it is necessary to have experimental data on plain concrete to compare the results.

Table 7.1 Parameters of deformation reduction factors (eqns. (7.1) and (7.2)) for the various methods of predicting deformation of reinforced concrete.

| Method | Deformation | Initial modular ratio n_0 | Rein. ratio | Aging coeff (χ) | Creep coeff (ϕ) | Remark |
|------------------|--------------------|------------------------------|------------------------|------------------------|------------------------|--------------------------------------|
| CEB70 [149] | Creep Shrinkage | - 20 | - a_s/a_g | - - | - 0 | No influence Time-independent |
| Abeles [148] | Creep Shrinkage | E_s/E_{c0} | a_s/a_c | - - | 0 0 | Time-independent Time-independent |
| Branson [151] | Creep Shrinkage | E_s/E_{c0} | a_s/a_g | 0.82 | Variable | Time-dependent Time-dependent |
| Dilger [150] | Creep Shrinkage | E_s/E_{c0} | a_s/a_c | 0.82 | Variable | Time-dependent Time-dependent |
| Okada [147] | Creep Shrinkage | E_s/E_{c0} E_s/E_{c0} | a_s/a_c a_s/a_c | - - | Variable | Time-independent Time-dependent |

E_s is the modulus of elasticity of steel

E_{c0} is the modulus of elasticity of plain concrete at loading

a_s is the area of steel

a_c is the area of concrete

a_g is the area of section ($= a_s + a_c$)

Assessment of the above five methods of predicting time-dependent deformations of reinforced concrete has been carried out by Brooks et. al [152]. The objectives were to compare experimental and predicted axial deformations of reinforced concrete with symmetrical and unsymmetrical distribution of reinforcement, as used for non-tensioned steel in the partially prestressed beam tests [153]. The specimens were twelve rectangular prisms,

100 X 180mm in cross-section and 435mm in length, the percentage of reinforcement being 0, 0.63, 1.62, 1.74, 3.66 and 4.47, as shown in figure 7.1. Axial creep was determined under a stress of 5MPa on two sets of three prisms loaded in series by two dead-weight lever arm test rigs, the remaining six prisms were used for the determination of shrinkage. Concrete surface strain measurement was by a 200mm Demec gauge, the gauge positions being at the top and bottom reinforcement levels and at midheight of the 180mm sides of the prism. Figures 7.2 and 7.3 show the average time-dependent total deformation of the prisms under load and the average shrinkage of the load-free prisms for the various amounts of reinforcement. In the case of symmetrical reinforcement, the strain is the average of six gauge positions, i.e. at two reinforcement levels and midsection depth on two sides. For the unsymmetrically reinforced prisms, the strain is the average of two gauge positions, i.e. at the reinforcement level on two sides. Comparison of measured creep strains of reinforced concrete specimens after the test duration of 8 months [152] with the theoretically predicted strains, by the methods of Okada [147] and Abeles [148] are in close agreement, whereas the Dilger [7] and Branson [8] methods underestimate creep. In a majority of cases, shrinkage is overestimated by the prediction methods.

On the other hand, a rational approach for calculating the serviceability effects of creep on reinforced concrete columns is proposed by Samra [144]. In this approach, a simple procedure for predicting the effects of creep in reinforced concrete is devised. The approach is based on a study of the behaviour of reinforced concrete members under sustained load, with the resulting increase in deformations and stress redistribution between concrete and steel. The solution incorporates an effective modulus of elasticity for a member with reinforcement.

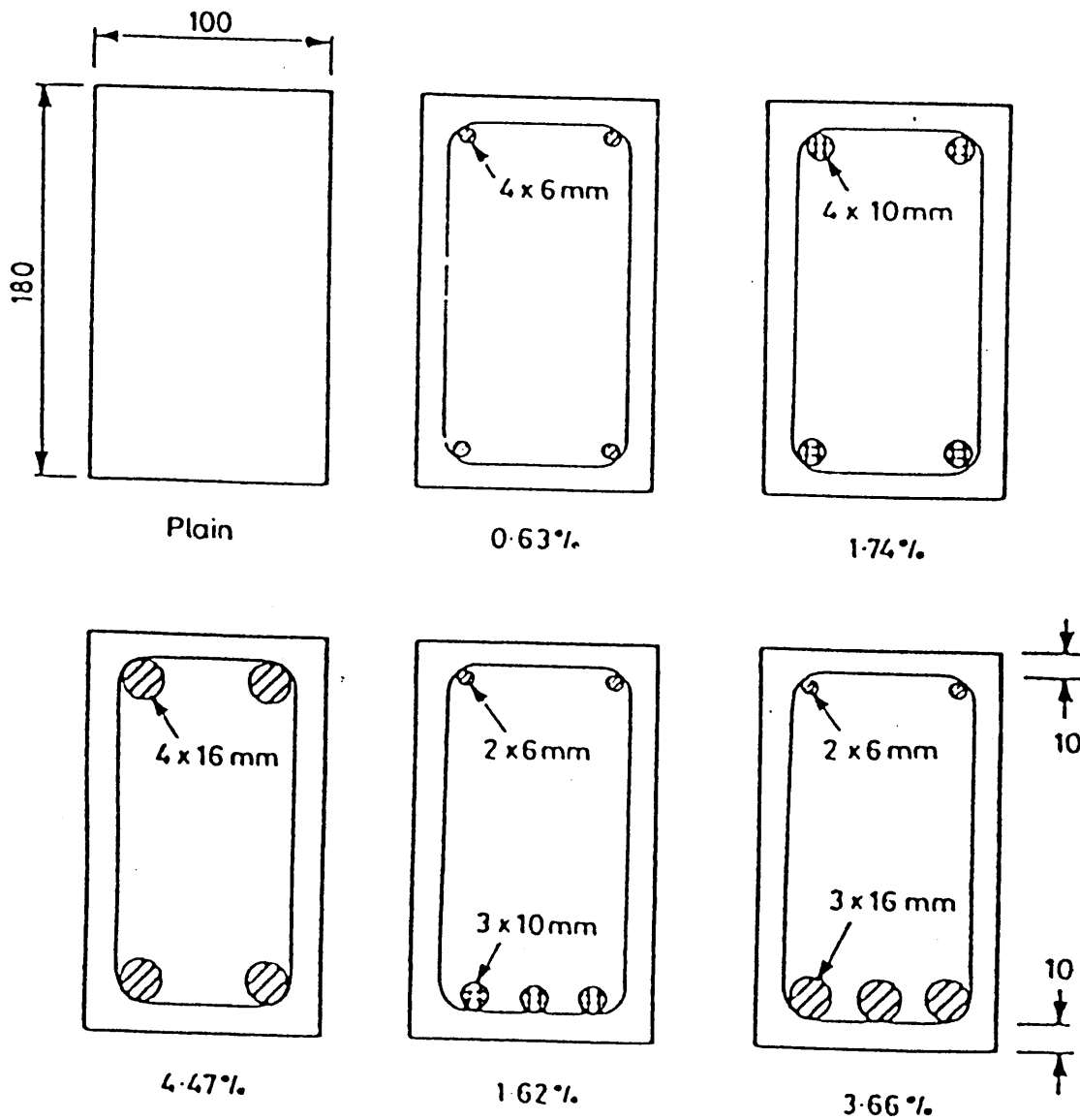
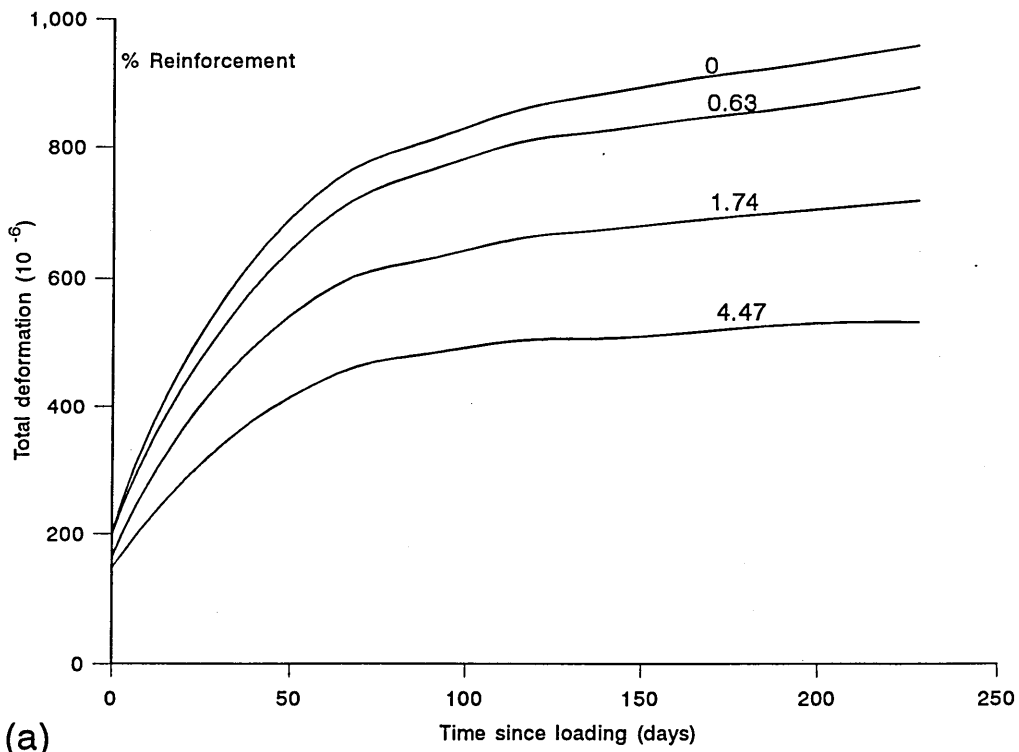
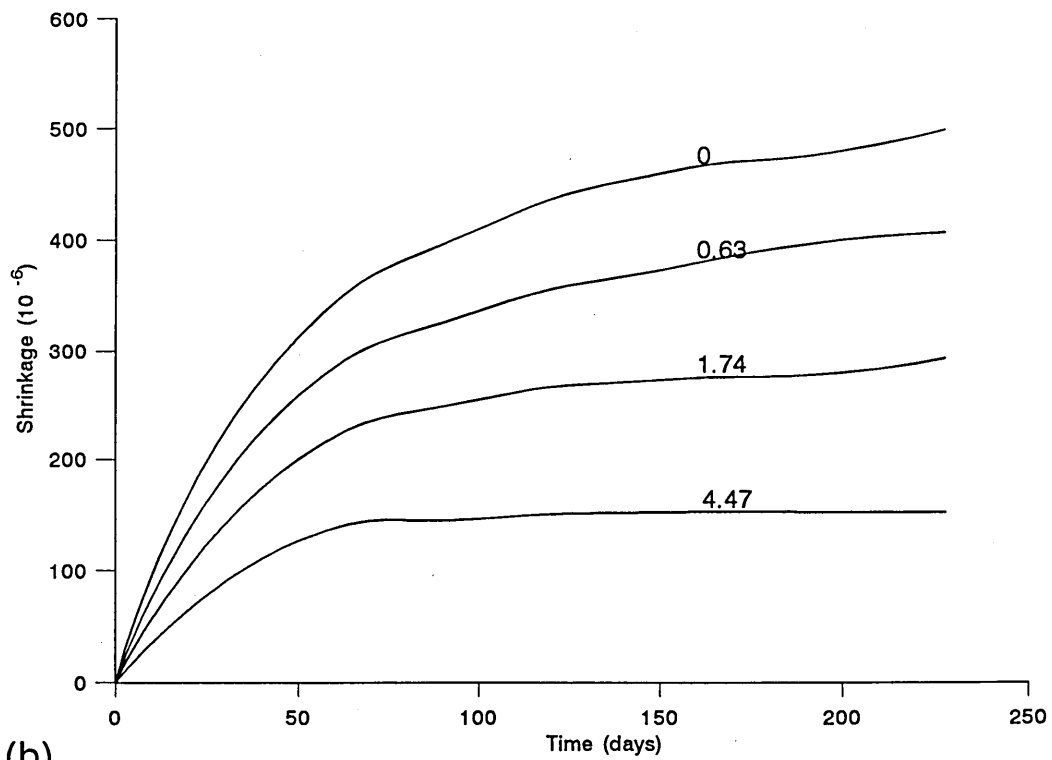


Figure 7.1 Details of creep and shrinkage test specimens. Rectangular plain, symmetrically reinforced and unsymmetrically reinforced concrete prisms, after Brooks et al [152]



(a)



(b)

Figure 7.2

(a) Total deformation under a stress of 5Mpa and (b) shrinkage, of symmetrically reinforced concrete prisms, after Brooks et al [152].

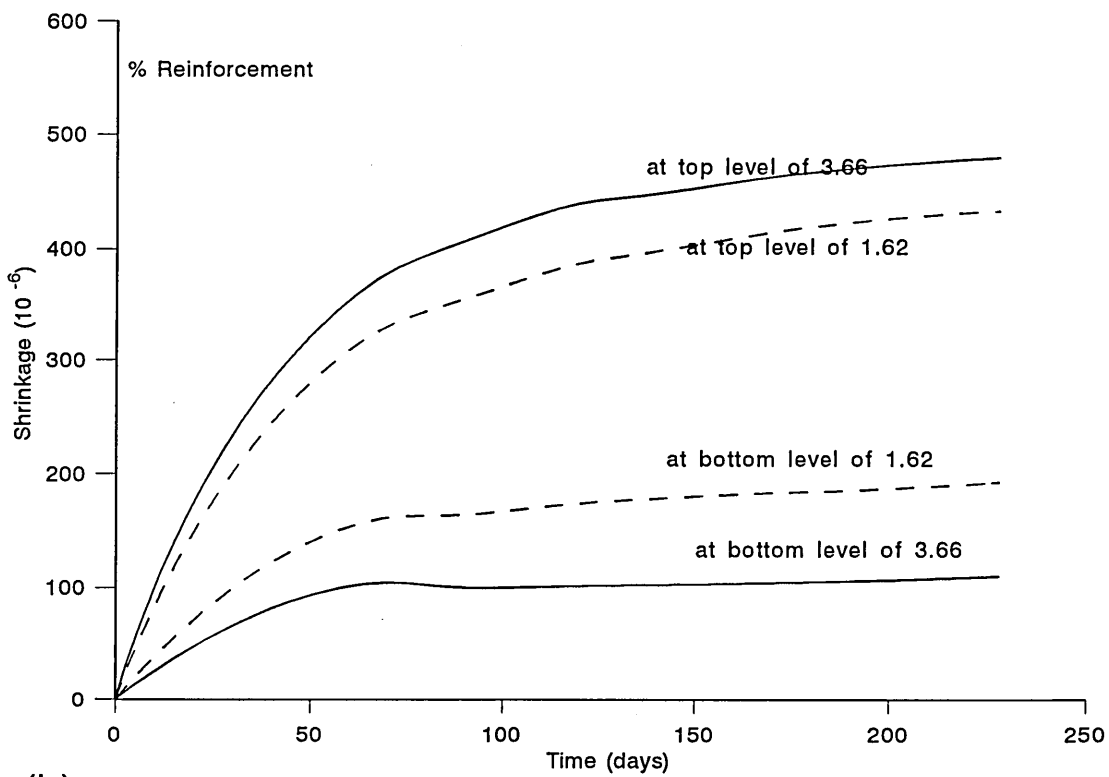
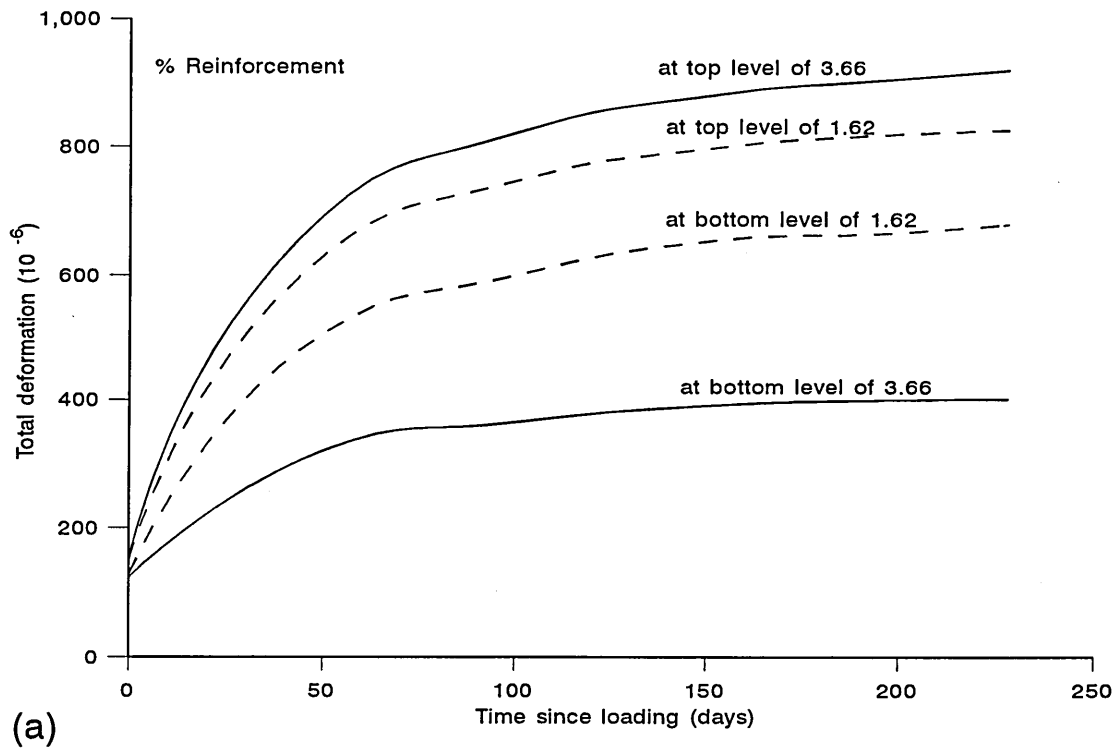


Figure 7.3

(a) Total deformation under a stress of 5 Mpa and (b) shrinkage, of unsymmetrically reinforced concrete prisms, after Brooks et al [152]

According to the creep model suggested by Samra [144] for a reinforced concrete member the final strain in concrete, after a period t of sustained load, may be expressed by the following equation,

$$\epsilon_{ct} = \epsilon_{ci}(1 + \phi_t) - \int_0^{\phi_t} \frac{\Delta f_i}{E_c} d\phi_t - \frac{\Delta f_t}{E_c} \quad (7.3)$$

i.e.

$$\epsilon_{ct} = \begin{array}{l} \text{initial strain} \\ \text{plus creep strain} \end{array} - \begin{array}{l} \text{Creep recovery} \\ \text{strain} \end{array} - \begin{array}{l} \text{Short-term} \\ \text{recovery} \end{array}$$

in which,

- ϵ_{ct} = strain in concrete after time t , under sustained load
- ϵ_{ci} = elastic strain in concrete upon application of load
- Δf_t = stress decrement in concrete due to transfer of force from concrete to steel, during time t and
- Δf_i = stress decrement in concrete during an infinitesimal time interval i .

Equation (7.3) describes the well-known phenomenon that columns under sustained load exhibit a continuous, but decreasing, transfer of force from concrete to steel.

The concrete stress f_{ct} , after a time t , is given by

$$f_{ct} = f_{ci} - \Delta f_t \quad (7.4)$$

The term under the integral sign in equation (7.3) may be approximated as $\Delta f_t \phi_t / 2E_c$ and substituting in equation 7.3 gives:-

$$\epsilon_{ct} = \frac{f_{ci}}{E_c} (1 + \phi_t) - \frac{\Delta f_t}{E_c} \left(1 + \frac{1}{2} \phi_t\right) \quad (7.5)$$

or,

$$\epsilon_{ct} = \frac{f_{ci}}{E_c} \left[(1 + \phi_t) - \frac{\Delta f_t}{f_{ci}} \left(1 + \frac{1}{2} \phi_t\right) \right]$$

Hence, the final strain in concrete ϵ_{ct} may now be written simply as :-

$$\epsilon_{ct} = \frac{f_{ci}}{E_{ca}} \quad (7.6)$$

and

$$E_{ca} = \frac{E_c}{(1 + \phi_t) - \left(1 + \frac{1}{2} \phi_t\right) \frac{\Delta f_t}{f_{ci}}} \quad (7.7)$$

Where,

E_{ca} = an apparent effective modulus of elasticity for the composite reinforced section

ϕ_t = creep coefficient

$\Delta f_t / f_{ci}$ = ratio of the stress transfer.

The analysis of an axially loaded column under sustained service loads using the above creep model proceeds as follows:-

1. The stress and strain distributions in concrete and steel are determined under

short-term loading by using transformed section analysis.

2. After a time (t) of sustained load, and due to creep effects, concrete stresses are reduced while the steel stress is increased. The stress reduction Δf_t is assumed. Then, knowing the creep coefficient after time (t) for the given concrete mix and substituting into equation (7.7), the apparent modulus of elasticity is determined.
3. From equation (7.6), the final strain in the concrete is calculated. Because of strain compatibility, this strain is equal to the steel strain, i.e., $\epsilon_{st} = \epsilon_{ct}$. The final stresses in concrete and steel are computed from equation (7.4) for the concrete, and by multiplying the steel strain determined in step (3) by its modulus of elasticity. Thus for concrete: $f_{ct} = f_{ci} - \Delta f_t$, and for steel: $f_{st} = \epsilon_{st} E_s$.

Equilibrium is then checked by verifying $P_s + P_c = P$, where P_s and P_c represent the forces in the steel and the concrete respectively, and P is the applied axial compressive force on the column. If this condition is not satisfied, a new stress decrement is assumed, and steps (2) and (3) are repeated until equilibrium is satisfied. The solution involves an iterative procedure and may require several trials.

7.3 EXPERIMENTAL PROGRAMME

Experimental work was carried out to establish long-term deformations of reinforced concrete short column specimens which incorporated repair patches in them.

7.3.1 Materials and Mix proportions

Concrete mix proportions of 1: 2.24 : 3.21 (by weight), with a water-cement ratio of 0.56, were used throughout. The concrete constituents were ordinary portland cement, fine aggregate conforming to Zone 'M' of BS 882, and the coarse aggregates of a maximum size of 10mm. The concrete mix was designed to give a 28-days cube strength of 45 N/mm² (\pm 1 N/mm²), and a slump of 10 - 30mm. Details of the materials are given in section 3.3.1 of chapter 3.

Three commercially available generic repair materials which are labelled A, B and C were used in this study. Details of these repair materials are given in chapter 3.

The longitudinal reinforcement consisted of four 12mm diameter HYS bars. The links provided to prevent outward buckling of the longitudinal bars were 6mm diameter mild steel. Four studs were welded onto the longitudinal bars to ensure correct cover to the reinforcement. In order to prevent premature localised failure of specimens during testing, extra links at both ends were provided, as shown in figure 7.4. In order to facilitate strain measurements in the longitudinal steel, studs of 10mm diameter were welded on the longitudinal bars in the reinforcing cage and demec points were attached to these providing a gauge length of 200mm for strain monitoring.

7.3.2 Details of Specimens, Casting, Curing and Testing

All the column specimens were reinforced longitudinally with four 12mm diameter high yield steel bars, the centroid of each bar was located at 26mm from the adjacent faces of the specimen as shown in figure 7.4. Mild steel bars of 6mm diameter were used for stirrup reinforcement in each column specimen.

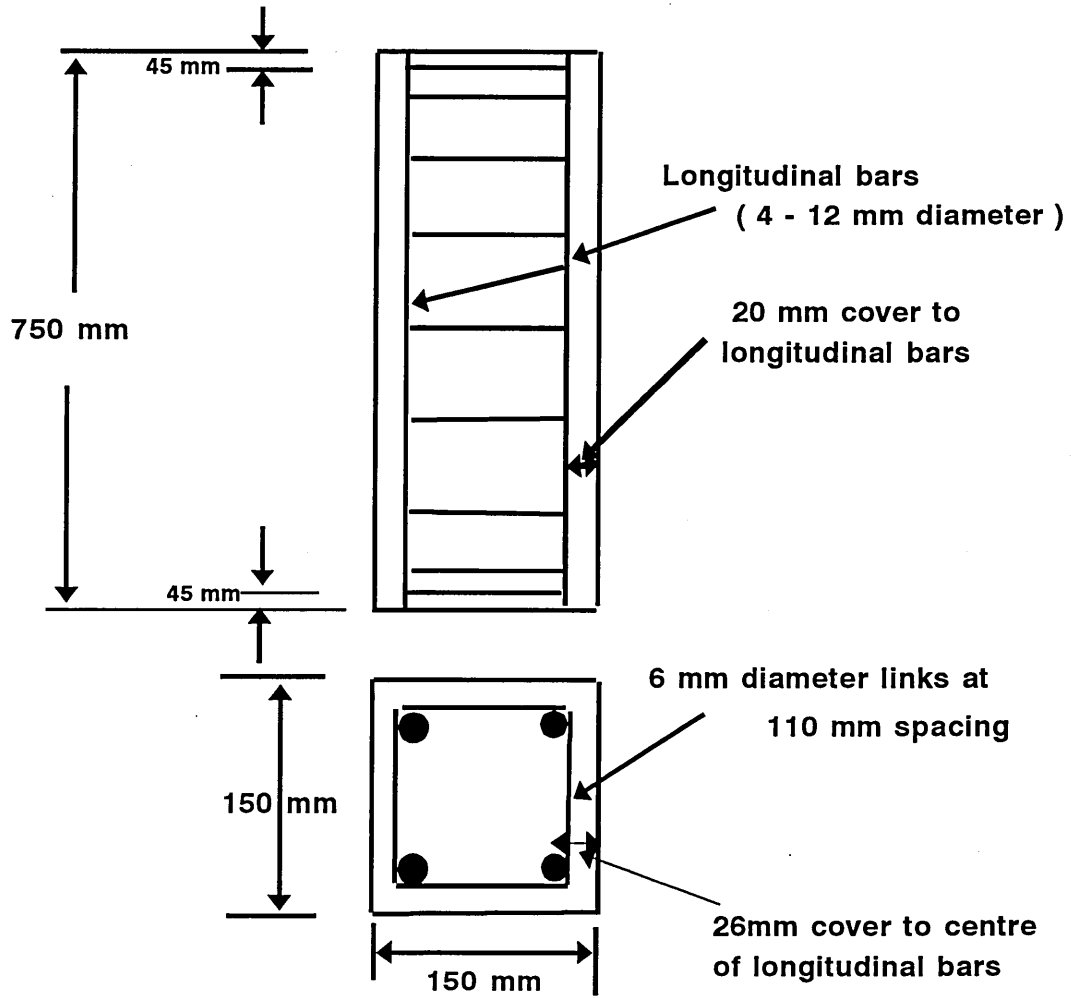


Figure 7.4 Reinforcement Details

A total of twenty four 150 x 150 x 750mm column specimens and eighteen cube specimens of dimensions 100 x 100 x 100mm were cast in four batches (columns I, II, III and IV) as shown in Table 7.2. From the six column specimens of each batch, three were used for the uniaxial creep test and three for measuring shrinkage strains.

All the column specimens were cast in a horizontal position in three layers, each layer was compacted on a vibrating table for a few seconds. The fresh concrete was covered with a polythene sheet for the first 24 hours and then, specimens were demoulded. Subsequently, all the specimens were cured at 20°C and 55% R.H. in a temperature and humidity controlled room for 28 days prior to testing.

Tests for uniaxial creep and shrinkage commenced at 28 days after casting and regular strain measurements were taken thereafter for 120 days. To simulate deterioration due to reinforcement corrosion, after 120 days, centrally located voids on two opposite faces of the columns were cut to a depth of 55mm and length 220mm using a hammer and chisel, as shown in figure 7.5. Subsequently, patch repair work was carried out using the three generic repair materials. Prior to patch repairing a void in a column, timber formwork was cut to cover two sides of each void and it was clamped in place by using G clamps. This formed tightly sealed joints on two faces of the void leaving the third face open to allow the placing of the repair material. The repair mix was prepared according to the manufacturer's instructions. The material was manually poured and compacted into the voids until full, when the open surface was levelled off. Upon completion of the repair, the specimens were kept covered with a polythene sheet for 24 hours, after which they were cured at 20°C and 55% RH for a further 7 days, prior to testing.

Table 7.2 Experimental programme

| Column Specimens* | Remark |
|-------------------|---|
| Columns I | Repaired with Material A after 120 days |
| Columns II | Repaired with Material B after 120 days |
| Columns III | Repaired with Material C after 120 days |
| Columns IV | Control column specimens of reinforced concrete |

(* 6 columns, each repaired with materials A, B and C respectively and 6 control columns)

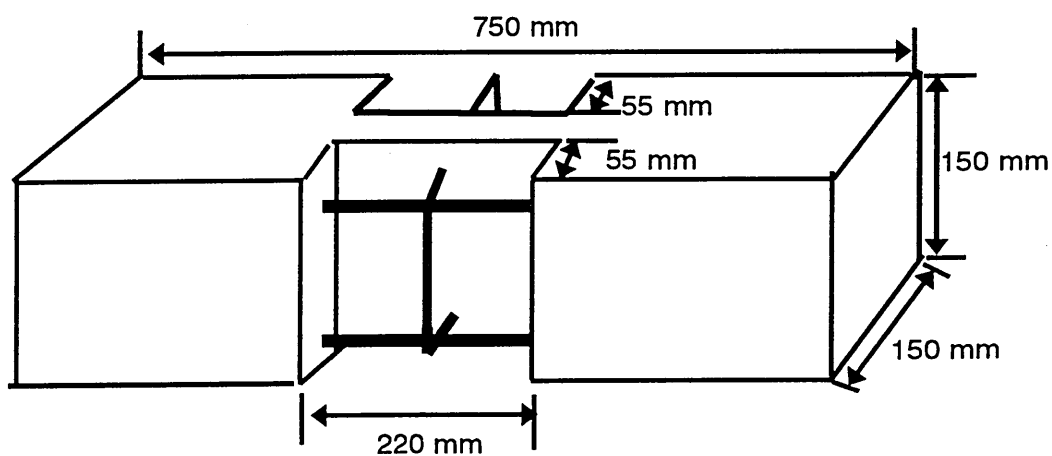


Figure 7.5 Column specimens showing the voids before patch repair

A total of twelve specimens were tested for compression creep characteristics, by maintaining a sustained axial load for a period of 210 days after patch repairing the voids in a column and curing for 7 days. The creep tests were carried out in accordance with standard practice [26]. Each specimen was loaded independently in a standard creep rig which comprised of steel end plates bolted on to four 36mm diameter high yield steel tie rods. The axial sustained load was applied to the specimen by means of a hydraulic jack and was maintained at a constant level by regular application of load and tightening of the nuts on the supporting steel rods. The nut loss was assumed to be 10 percent of the applied load in all cases. The concentricity of the applied load was ensured by achieving reasonably similar strains on the four steel tie rods of the creep rigs. In order to calculate the net creep strain, shrinkage was measured on separate reinforced concrete column specimens and deducted from the total strain measured on specimens in the creep rig. The loaded creep specimens along with their corresponding shrinkage specimens were stored in the temperature and humidity controlled room, at 20°C and 55% R.H.

At regular intervals, the creep and shrinkage strains of concrete were measured on the four faces of each column specimen. The strains were measured by using a demec extensometer of 200mm gauge length. Locations of demec points on specimens are given in figures 7.6 and 7.7. Strain measurements in the steel reinforcement were made across two demec points attached to the protruding ends of steel studs which were welded to the reinforcement as described in section 6.3.2. Each shrinkage value presented in this chapter is an average of strains measured across four faces of three identical reinforced concrete specimens.

7.3.2.1 Determination of sustained stress-strength ratio for Uniaxial creep test

At the serviceability limit state, the condition of equilibrium of forces in a column results in the following expression:

$$N = f_c A_c + f_s A_s \quad (7.8)$$

Where,

- N = applied axial load
- f_c = compressive stress in the concrete
- f_s = compressive stress in the longitudinal reinforcement
- A_c = cross-sectional area of the concrete, and
- A_s = cross-sectional area of the longitudinal reinforcement.

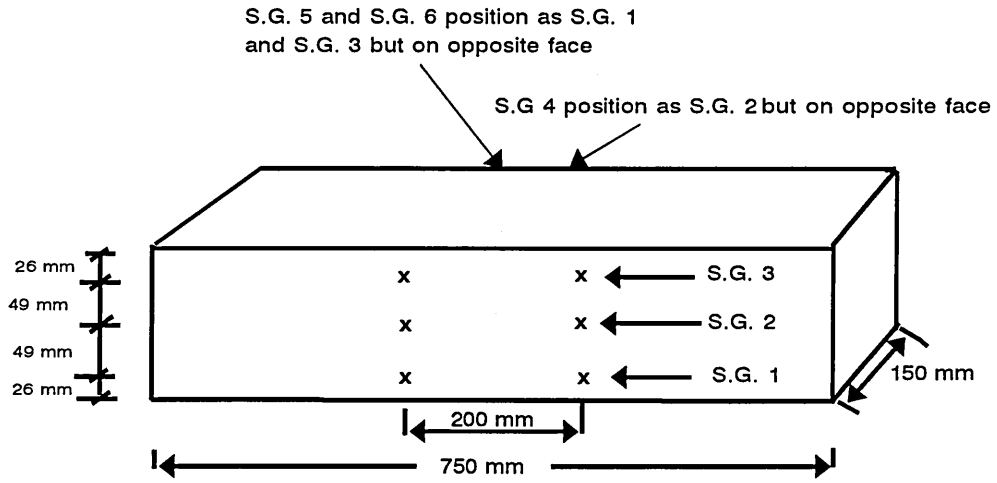
For the ultimate limit state [136],

$$N = 0.4 f_{cu} A_c + 0.75 f_y A_s \quad (7.9)$$

Where,

- f_{cu} = the characteristic strength of concrete
- f_y = the characteristic strength of the reinforcement

In limit state design a structural member is usually designed for the ultimate limit state and then checked for the serviceability limit states of cracking and deflection.



* Strain Gauges 1,3,5,6 are on steel studs and measure strain on outside face of steel reinforcement which is at 20 mm from the surface

* S.G. 2 and S.G. 4 are on concrete surface

Figure 7.6 Location of Demec points on reinforced concrete column (control)

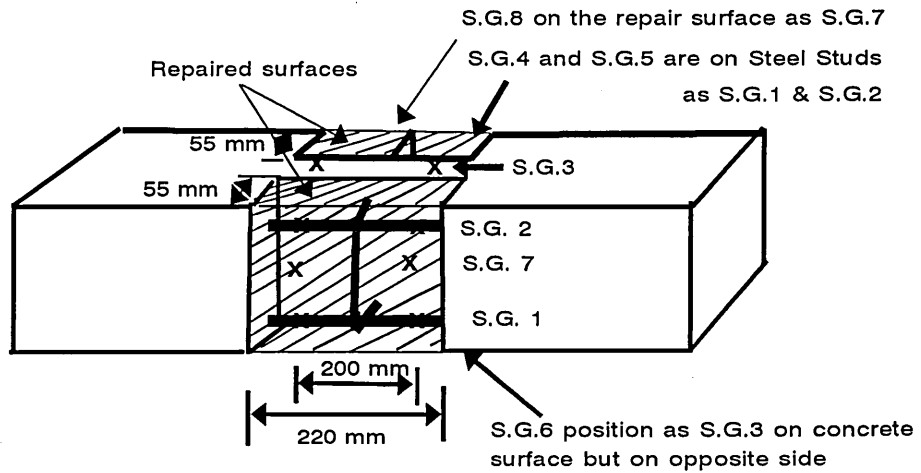


Figure 7.7 Location of demec points on repaired column specimens

The loading on a column at the serviceability condition under limit state design procedure is taken as:-

$$N_s = 1.0G_k + 0.9Q_k \quad (7.10)$$

Where,

G_k = characteristic dead load,

Q_k = Characteristic live load.

1.0 and 0.9 are partial factors of safety.

The ultimate design load is taken as:-

$$N_u = 1.4G_k + 1.6Q_k \quad (7.11)$$

where,

1.4 & 1.6 are the appropriate partial safety factors for load.

Assuming $G_k = Q_k = Q$ gives:

$$N_s = 1.9Q, \text{ and}$$

$$N_u = 3Q$$

Therefore, the ratio of serviceability load to ultimate load is,

$$\frac{N_s}{N_u} = \frac{1.9}{3} = 0.63 \quad (7.12)$$

Hence, in order to determine the serviceability sustained load to be applied to a creep specimen, the ratio of applied load to ultimate column load of 0.63 is taken as a suitable value.

7.4 RESULTS AND DISCUSSION

Experimental results are presented on the long-term deformations of short reinforced concrete column specimens together with the structural interaction between a repair patch and the substrate concrete.

7.4.1 Influence of Longitudinal Steel reinforcement on the Shrinkage of Concrete

The shrinkage of plain concrete and repair materials has been established in chapter 4. The restraining effect of longitudinal steel reinforcement on shrinkage is assessed in this chapter by comparing the shrinkage curves for reinforced concrete column specimens with corresponding unreinforced prisms of similar mix proportions (from chapter 4), as shown in figure 7.8. The top curve in figure 7.8 shows shrinkage of plain concrete prisms of dimension 100 X 100 X 500mm which were considered in chapter 4. In order to make these data suitable for comparison with reinforced concrete columns of dimension 150 X 150 X 750mm, a volume/surface correction has been made [141]. The corrected shrinkage curve for plain concrete is shown in figure 7.8. The shrinkage curves of the three reinforced concrete specimens (control columns) are also plotted in figure 7.8. It can be seen that the longitudinal reinforcing steel leads to significant reduction in the shrinkage measured on the surface of plain concrete. For example, for control column specimens of reinforced concrete, the surface shrinkage at 120 days decreases by about 43 percent relative to the surface shrinkage of the plain concrete specimens of similar volume/surface.

7.4.2 Influence of Patch Repair on the Shrinkage of Concrete

Figures 7.9 to 7.11 show the shrinkage strains with age of reinforced concrete columns which have been repaired with repair materials A, B and C. The graphs in figures

7.9 to 7.11 show the shrinkage strains of the concrete surface of the unreinforced columns upto 120 days of age (strain measured on gauges 3 and 6, figure 7.7). After the application of repair patch at 120 days age, the effect on the shrinkage of the concrete surface (gauges 3 and 6, figure 7.7), repair patches (gauges 7 and 8, figure 7.7) and the strain in steel reinforcement (gauges 1,2 and 4,5, figure 7.7) is also shown in these figure. For comparison purpose, the free shrinkage curve of each repair material is also plotted. It is clear in figures 7.9 and 7.10 that after application of the repair patch, the shrinkage on the concrete surface (gauge 3 and 6) and the shrinkage of the repair patch are similar. Also the strain of the steel reinforcement is similar. In the case of material C, however (figure 7.11), the shrinkage strains in the repair patch (gauges 7 and 8) are considerably greater than the strains on the concrete surface after repair (gauges 3 and 6). The strains in the steel reinforcement have an intermediate value, greater than the substrate concrete surface but less than the repair material surface. In each of figures 7.9 to 7.11, the free shrinkage of the repair materials is much greater than the shrinkage strains measured on the repair patch. This is due to the restraining effect provided by both the substrate concrete and the steel reinforcement on the repair patch.

The volume/surface ratio of the repair patch is higher than that of the 100X100X500mm prism specimens and hence the free shrinkage of the repair patch will be even higher than free shrinkage curves plotted in figures 7.9 to 7.11.

It has been established in chapter 4 that the creep characteristics of repair materials A and B are quite similar at a constant stress/strength ratio. However, the creep strains of material C are relatively quite high. So high shrinkage strains on the repair patch repaired with material C can be due to the significantly high creep at a given stress/strength ratio.

The total volume of repair patch and the surfaces which are exposed to drying can be used to obtain volume/surface ratio, but drying will also take place from the restrained faces due to absorption by the substrate concrete and this cannot be quantified accurately. Therefore, volume/surface ratio of repair cannot be determined accurately in this case, so a volume/surface ratio correction to the free shrinkage of prism 100 X 100 X 500mm dimensions have not made in this investigation.

Glanville and Thomas [154] found that the total creep in compression and in tension is equal under the same applied stress/strength ratio. On the other hand, Davis et al [155] found that the rate of creep in tension is initially higher than in compression under the same stress/strength ratio . After about one month under load, the creep rate under tension decreases considerably than in compression. This behaviour was found to apply both to mass-cured concrete and to concrete drying at a relative humidity of 50 per cent. Mamillan's tests [156] indicate the total specific creep of neat cement paste at a relative humidity of 50 percent to be about five times higher in tension than in compression. However, on a stress/strength basis, the creep in tension is the lower of the two. Brooks et. al [157] reveal that, for concrete loaded at a latter age after shrinkage has taken place, total creep in tension is less than total creep in compression. Also, whereas age reduces basic creep in compression, basic creep in tension is not appreciably reduced, because the increase of tensile strength with age is small. In this investigation, the substrate concrete shrinkage strains start increasing after the application of the repair patch whereas the repair patch itself shrinks less than its free shrinkage. This results in a varying tensile stress on the repair patch.

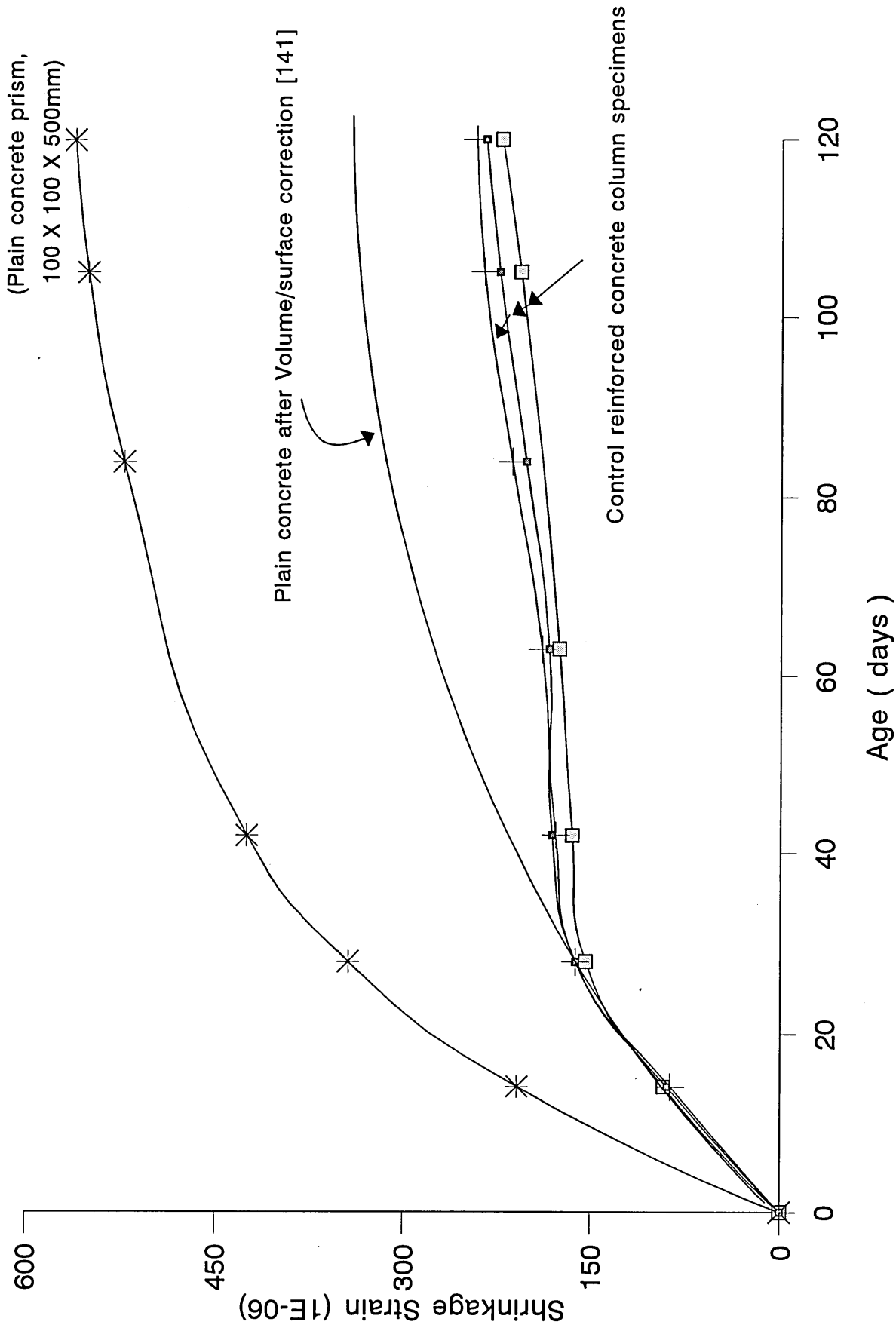


Figure 7.8
Influence of reinforcing steel on the shrinkage of concrete [column dimensions 150 X 150 X 750mm]

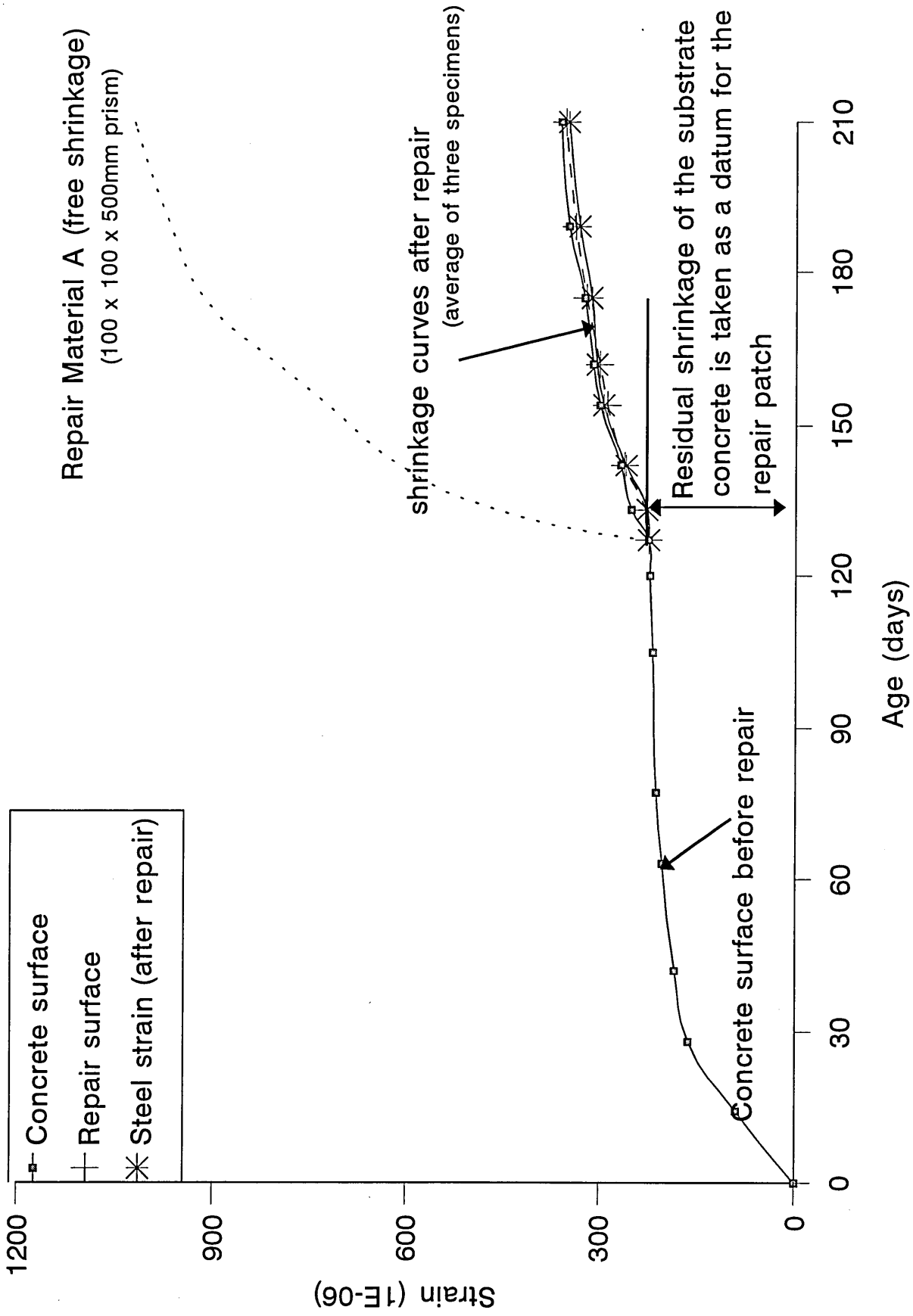


Figure 7.9
Influence of repair material A on the shrinkage of reinforced concrete column

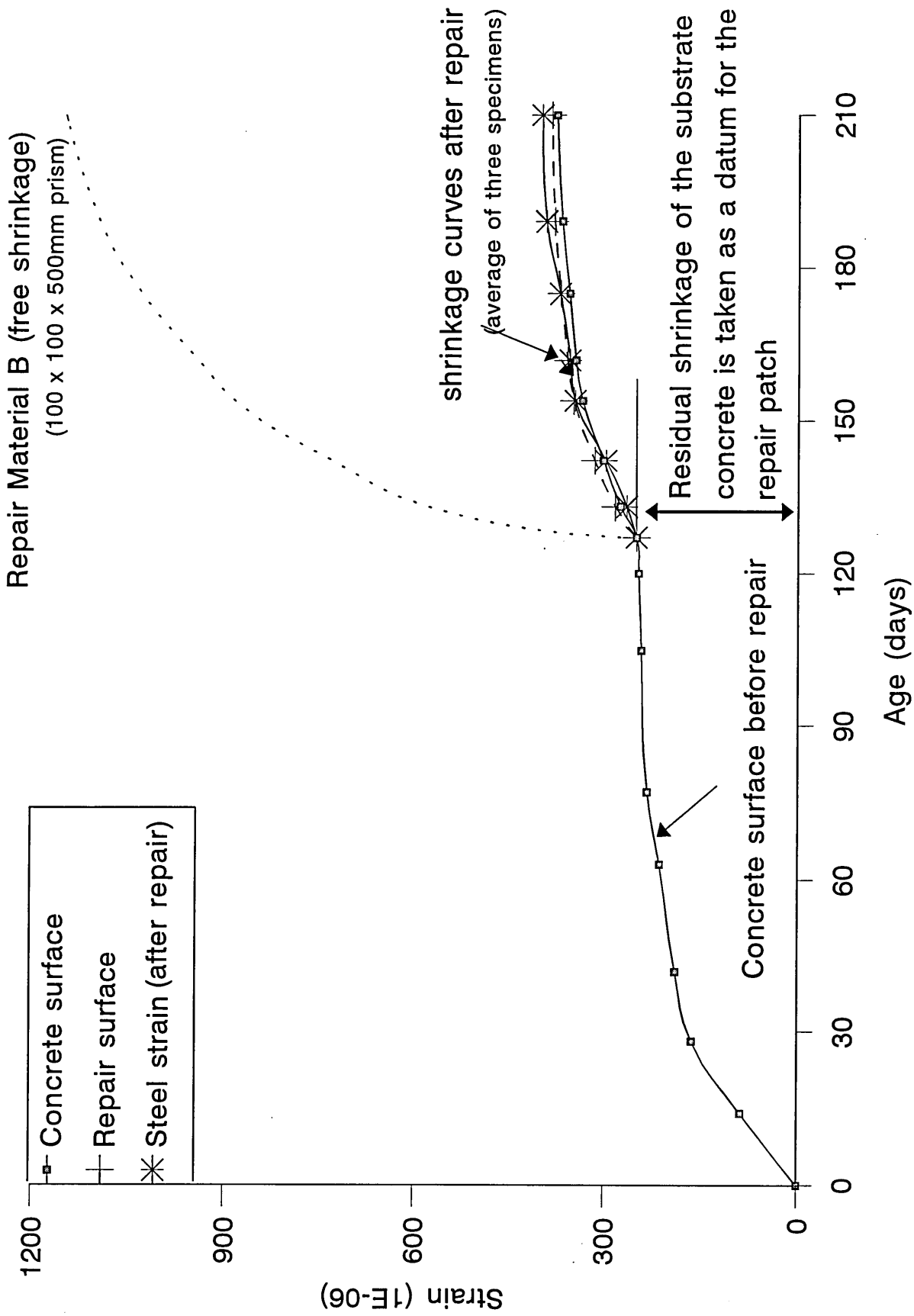


Figure 7.10
Influence of repair material B on the shrinkage of reinforced concrete column

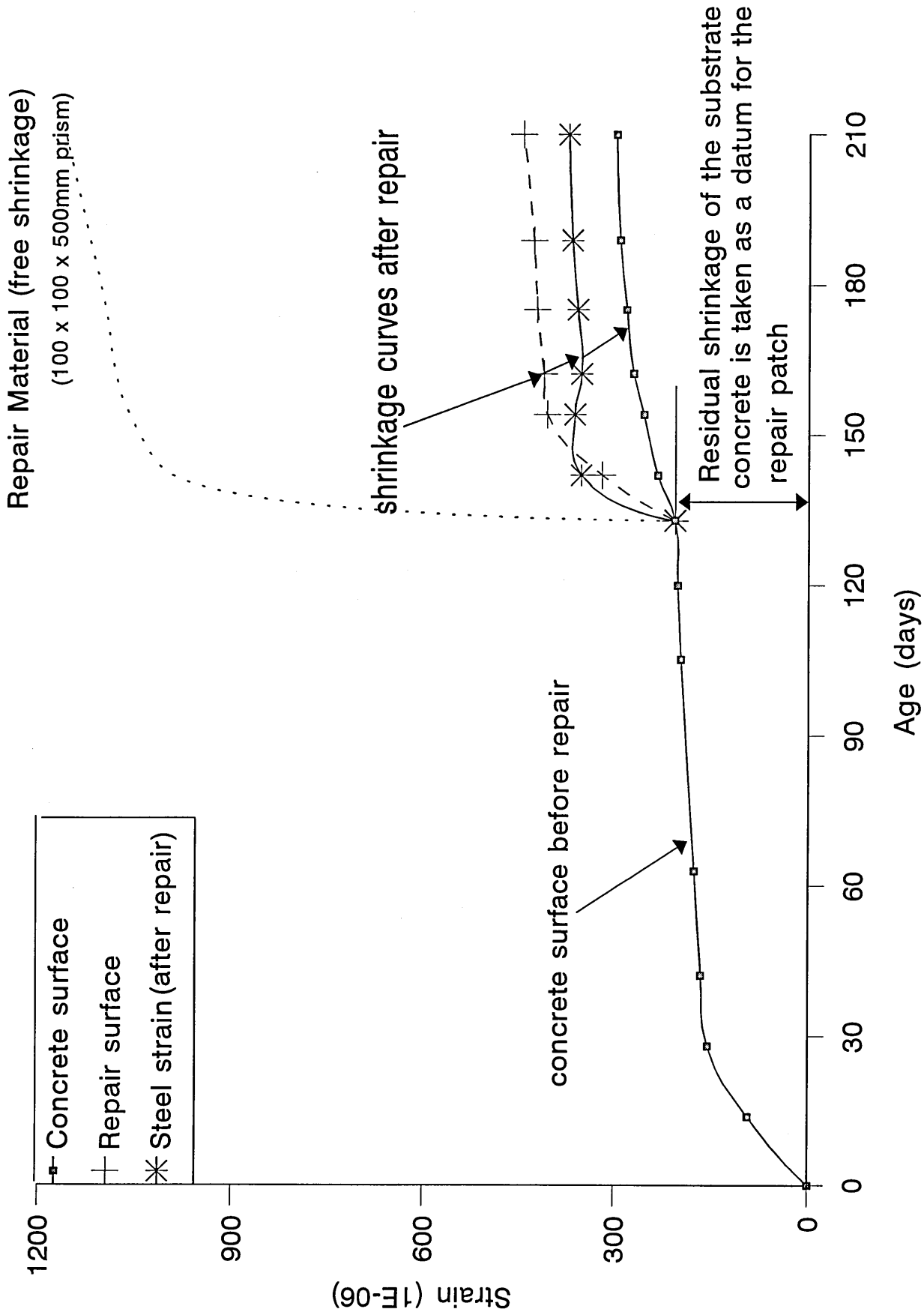


Figure 7.11 Influence of repair material C on the shrinkage of reinforced concrete column

7.4.3 Load distribution in reinforced concrete column specimens under sustained axial loading

When reinforced concrete columns are kept under a constant sustained load, redistribution of stress from concrete to steel takes place continuously until the reinforcing steel reaches its yield stress. Once the steel has attained its yield stress, it can no longer carry any additional load, thus preventing the concrete from transferring its load to steel. This stage represents the end of stress redistribution from concrete to steel and is referred to as the "Steady state".

7.4.3.1 Schematic Representation

In order to identify clearly the factors which influence the load distribution in the concrete and reinforcing steel phases of columns under sustained loading, a schematic representation is made in this section. The load distribution in concrete and steel can be represented by the idealised curves in figure 7.12, where the load in concrete, P_c , and in steel, P_s , are related to the total applied load, P , as follows :-

$$P = P_s + P_c \quad (7.17)$$

The concrete matrix, in figure 7.12, carries a proportion of the applied sustained load immediately after the application of load. However, as the age under load increases concrete undergoes creep and hence it transfers some of the load to the longitudinal steel reinforcement, thus leading to an increase in the share of load carried by the steel until it reaches a steady state. This process of load redistribution leads to a continuous reduction in the sustained stress of concrete until the steady state of stress is reached beyond which it remains unchanged.

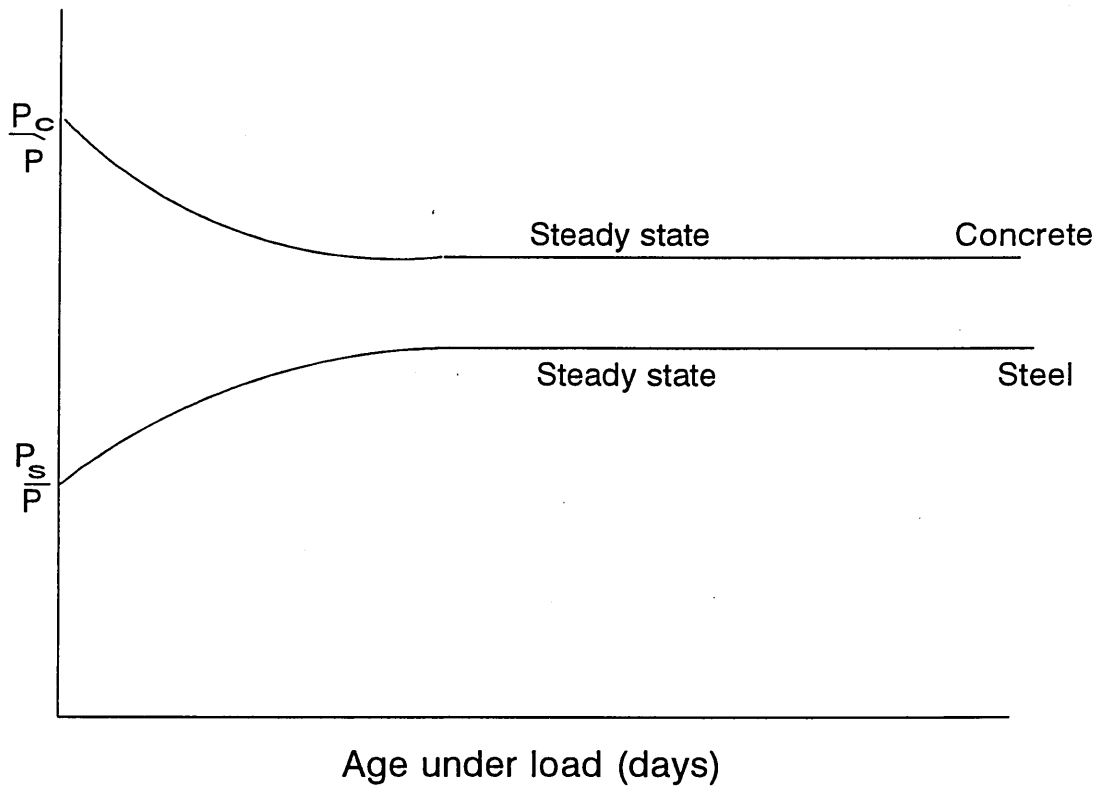


Figure 7.12

Schematic load distribution in reinforced concrete compression members under sustained load.

The load carried at different ages by the concrete and reinforcing steel phases in the column specimens tested in this investigation was determined from the strain measurements on the longitudinal steel reinforcement, which were made at regular intervals as shown by a typical example in figure 7.13. The stress corresponding to these strains was determined from the stress-strain curves of the steel reinforcement bars which is given in figure 7.14. Hence, a knowledge of the total applied load, P , and the force in the longitudinal steel, P_s , lead to the determination of load P_c in the concrete phase using equation 7.17. In order to confirm the accuracy of this procedure for determining P_s and P_c , an alternative approach was made to determine the instantaneous values only of these loads, as described below.

Assuming a condition of strain compatibility between the concrete and longitudinal steel phases of the column specimens, equation 7.17 can be re-written in the form of:

$$P = P_c + P_c \left(\frac{E_s}{E_c} \right) \left(\frac{A_s}{A_c} \right) \quad (7.18)$$

Where,

P = total applied load

P_c = load carried by the concrete phase

E_s = Young's modulus of steel (= 210 KN/mm²)

E_c = Secant modulus of elasticity of concrete (= 22 KN/mm²)

A_s = cross-sectional area of steel reinforcement

A_c = cross-sectional area of concrete.

A knowledge of the total applied load, P , the cross-section dimensions and elastic properties of concrete and steel reinforcement allows the determination of the instantaneous value of P_c from equation 7.18 and consequently of P_s from equation 7.17. These instantaneous values of P_c and P_s , as determined from the above two procedures, are given in Table 7.3 and show acceptable agreement with experimental results.

The loads carried by the concrete and reinforcing steel phases of the column specimens, as a proportion of the total applied load, against the age under loading are shown in figure 7.15 as obtained from figures 7.13 and 7.14, for two control column specimens. It is evident from figure 7.15 that the steel reinforcement took a gradually increasing share of the compressive load, with a corresponding decrease in compressive load taken by the concrete. Also, the sustained load causes redistribution of stresses, so that the stress decreases in the concrete over time as the stress increases in the steel. From the results in figure 7.15, it is not possible to detect the steady state of stress as mentioned in section 7.4.2.1. This is so because when the applied sustained load on the column specimens is small it requires longer period before the longitudinal steel reinforcement attains its yield stress.

Table 7.3 Comparison between the instantaneous loads in concrete and steel as determined by the two procedures

| Column | P (kN) | Procedure 1* (kN) | | Procedure 2** (kN) | | Maximum % error | |
|-------------------------|-----------|----------------------|-------|-----------------------|-------|--------------------|-------|
| | | P_s | P_c | P_s | P_c | P_s | P_c |
| control (specimen 2) | 320 | 64 | 256 | 54 | 266 | 14 | 4 |
| control (specimen 3) | 320 | 65 | 254 | 54 | 266 | 15 | 5 |

* Procedure 1 is based on steel stress-strain in figure 7.12, and

** Procedure 2 uses equation 7.18.

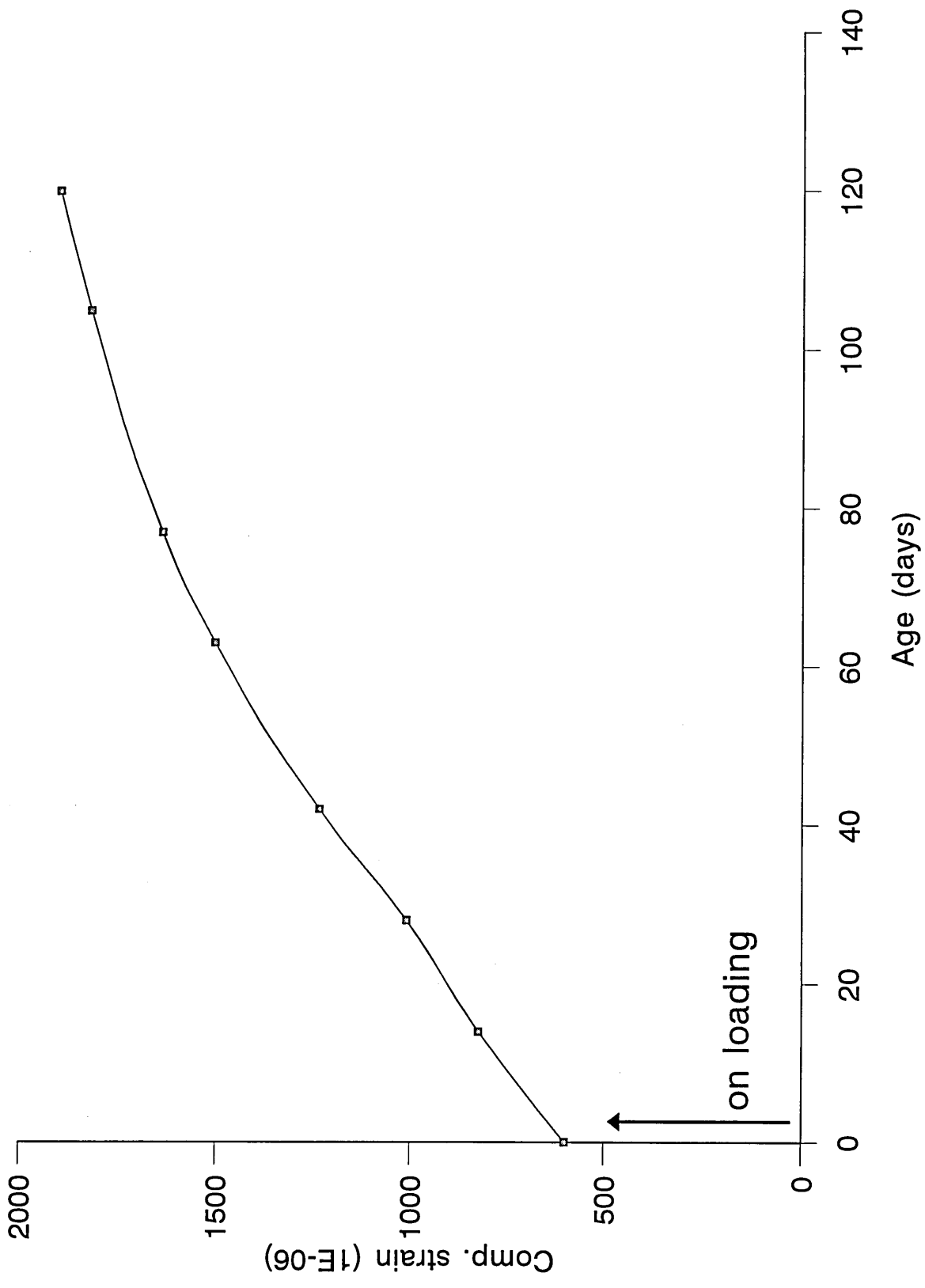


Figure 7.13
 Strain in steel reinforcement of control reinforced concrete column specimens
 under sustained loading

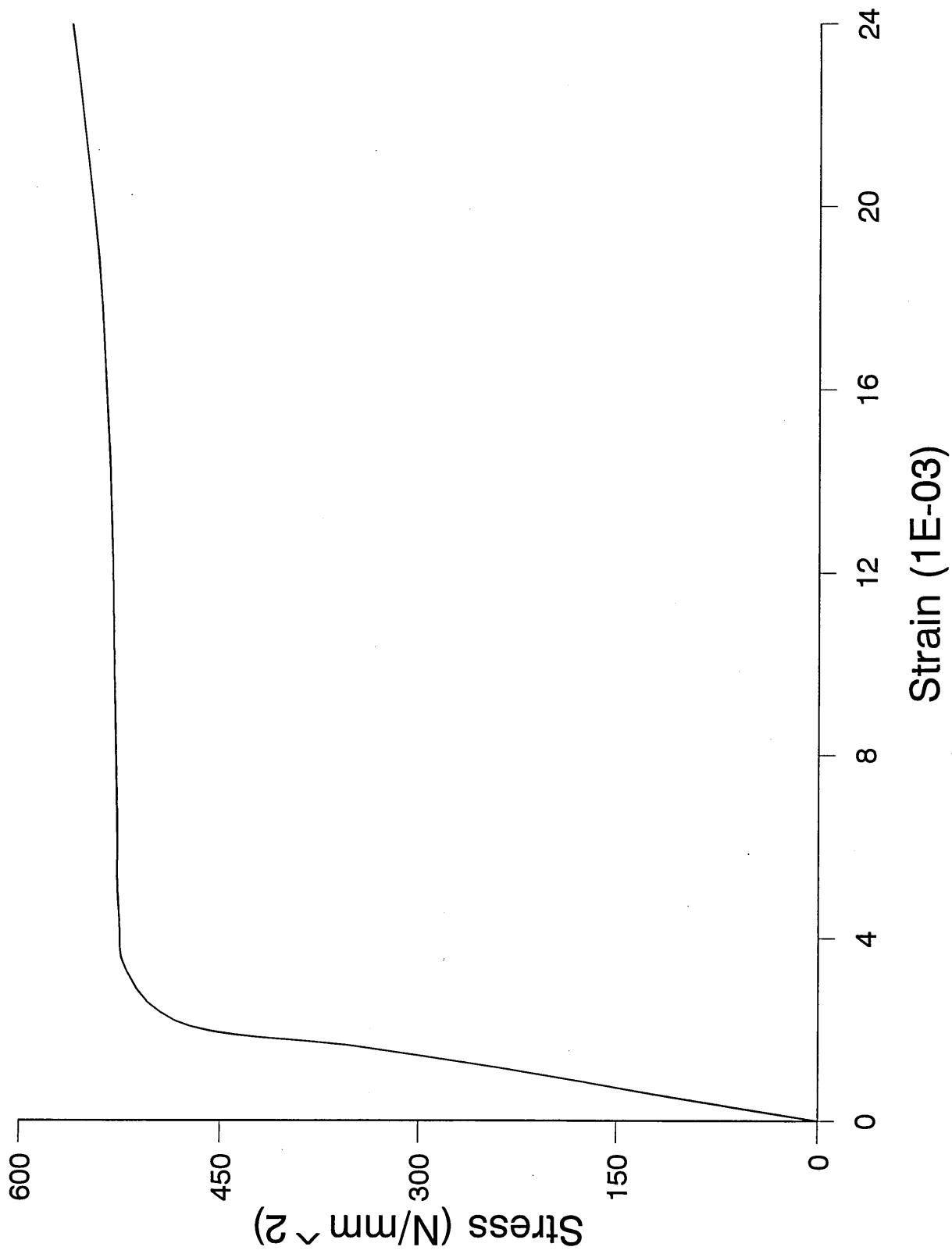


Figure 7.14 Stress-strain curve for the longitudinal steel reinforcement (12mm diameter HYS)

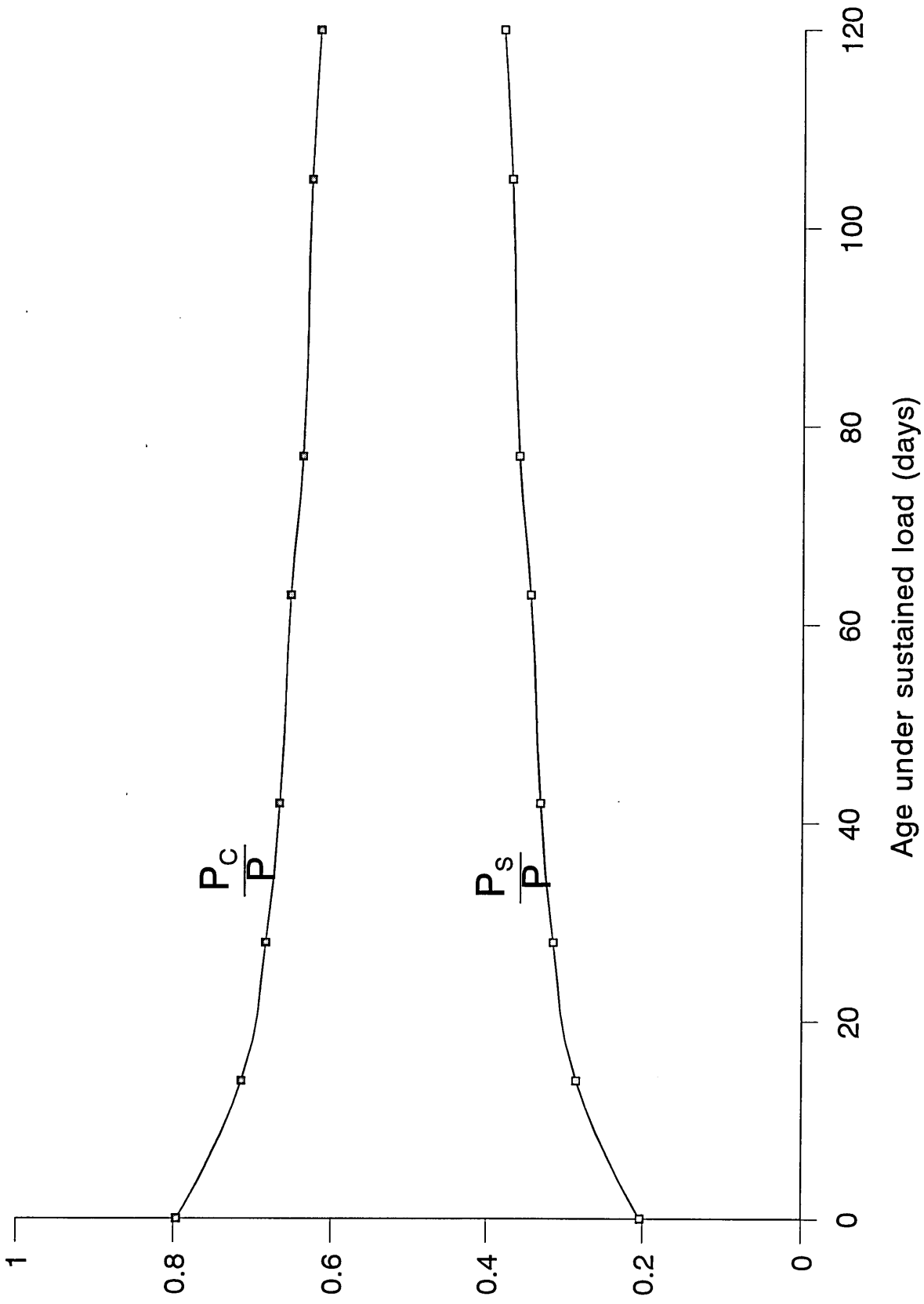


Figure 7.15
Experimental load distribution under sustained load of control column (average of three) specimens

7.4.4 Creep Deformation

The creep characteristics of repair materials and plain concrete under different stress/strength ratios have already been investigated in chapter 4. In this section the creep curves of the concrete phase and patch repair phase in reinforced concrete columns will be discussed. The effect of longitudinal reinforcing steel on the creep of concrete and repair materials will be investigated by comparing the creep curves of reinforced concrete column specimens with those for unreinforced prisms under similar sustained stresses.

7.4.4.1 Creep curves for short reinforced concrete columns

The results in figure 7.16 show the creep curves of the control short reinforced concrete column specimens and of prism specimens of the plain concrete mix which was used in the reinforced concrete columns. In order to make creep data of plain concrete prism of 100 X 100 X 500mm suitable for comparison with reinforced concrete columns of dimension 150 X 150 X 750mm, volume/surface and stress/strength ratio corrections have been made to achieve common values for the prism and column specimens [141]. The specimens were loaded at 28 days age after casting. The load was maintained for up to 120 days in the case of the reinforced concrete column specimens and for 90 days in the case of plain concrete prism specimens. The sustained stress level on the unreinforced prism specimens was 0.35 percent of the 28 day cube strength. The axial sustained load on the reinforced concrete columns was 0.63 percent of the ultimate column load.

Comparing the creep curves for the reinforced concrete columns (average of three specimens) and prism specimens (average of three specimens), as shown in figure 7.16, it can be concluded that reinforcement leads to a reduction in creep, but not as significant as

in shrinkage deformation curves, as shown in figure 7.8. For example, for a specimen of control column, the creep strain at 90 days after loading decreases only by 3 percent relative to the creep of the unreinforced prism specimen compared to 36 percent decreases in the case of the surface shrinkage at 90 days. Results of other investigators also show that the effect of reinforcement is to reduce shrinkage to a much greater extent than creep [147-149, 157]. In fact, it is assumed in the CEB 70 design recommendations that there is little influence on creep for amounts of reinforcement up to 2% [149].

In this investigation, the following creep model [144] as described in section 7.2 is used to investigate its correlation with the experimental data on reinforced concrete columns.

The final strain in concrete ϵ_{ct} [144] is :-

$$\epsilon_{ct} = \frac{f_{ci}}{E_{ca}} \quad (7.6)$$

and

$$E_{ca} = \frac{E_c}{(1+\phi_t) - (1+\frac{1}{2}\phi_t) \frac{\Delta f_t}{f_{ci}}} \quad (7.7)$$

Where,

E_{ca} = an apparent effective modulus of elasticity for the composite reinforced section

ϕ_t = creep coefficient

$\Delta f_t/f_{ci}$ = ratio of the stress transfer.

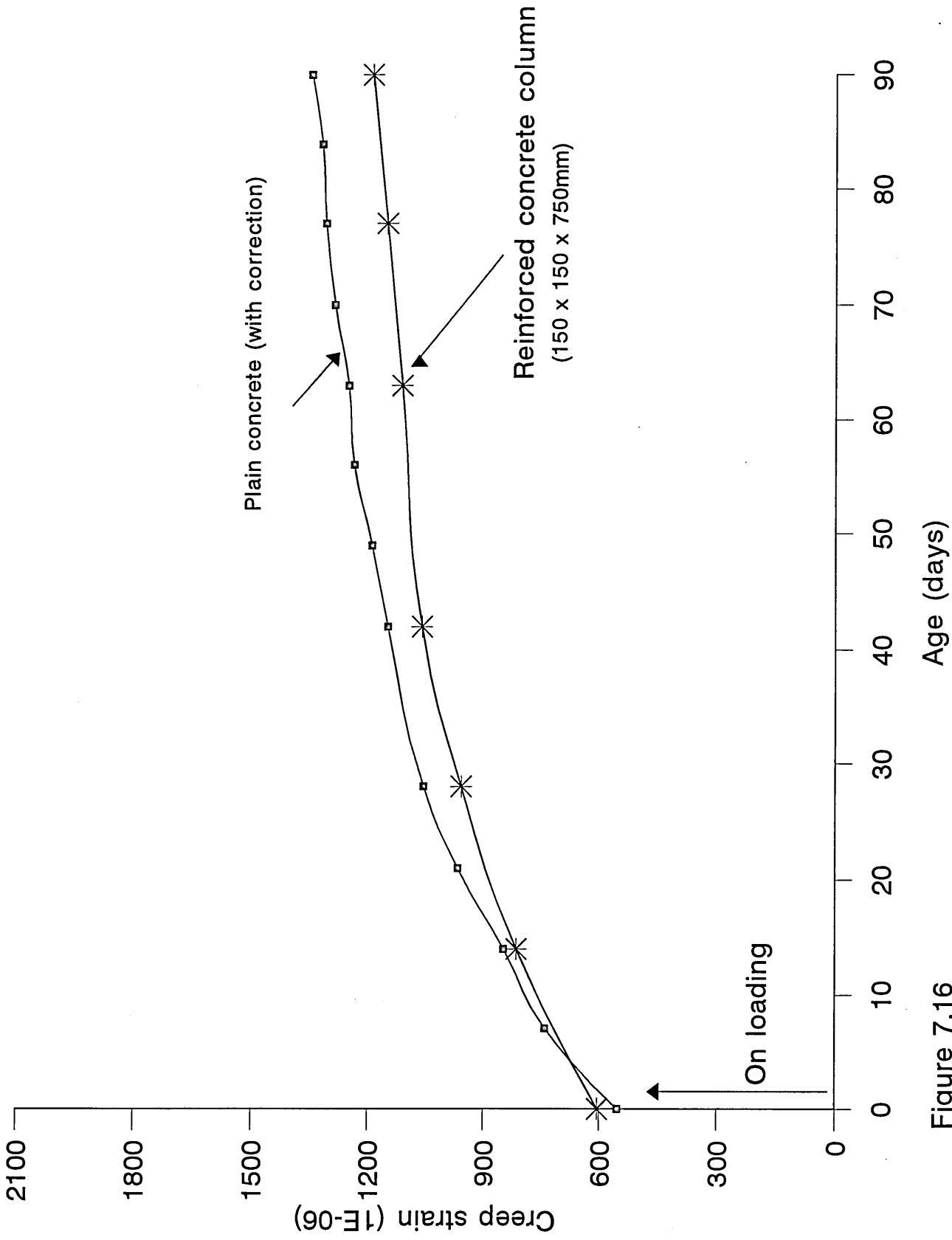


Figure 7.16
 Creep curves of short reinforced concrete column specimens
 (average of three) and unreinforced prisms
 [stress/strength = 0.6]

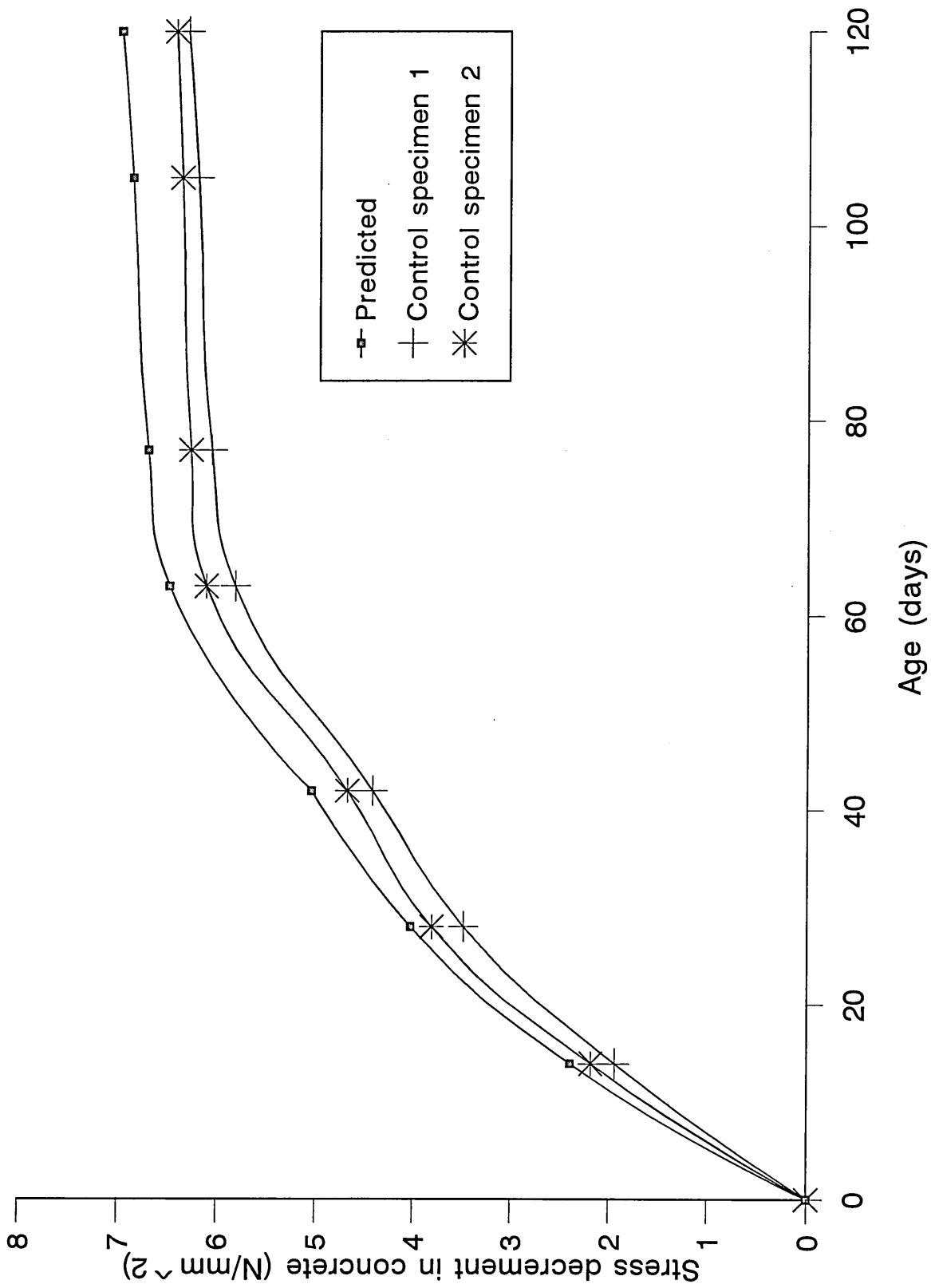


Figure 7.17 Comparison of measured stress decrement in concrete with predicted using creep model suggested by Samra [144]

Predictions made on the basis of an apparent effective modulus of elasticity used in the creep model suggested by Samara [144], are compared with the experimental data of this study, and very good agreement is found as shown in figure 7.17. It is clear from this figure that creep is overestimated by the creep model [144], and it gives overestimates within 12%.

7.4.4.2 Creep of substrate concrete and repair phase in reinforced columns

Creep deformation of the three repair materials A, B and C and plain concrete has already been investigated in chapter 4. In this section creep curves of the substrate concrete and repair phases in repaired reinforced concrete columns are presented. The total strains on concrete and repair materials were measured on two opposite faces on each column specimens, as described in section 7.3.2 (figure 7.7, gauges 3,6,7 and 8). The net creep strains were then obtained by deducting the shrinkage strains of corresponding unstressed column specimens.

Typical creep curves of repaired and control reinforced concrete columns (average of three specimens) are given in figures 7.18 to 7.20, showing the instantaneous elastic strain upon loading and the rate at which creep strains increase with time for both the concrete surface and the patch repair surface.

From the results of figure 7.18 to 7.20, it is not possible to detect the influence of repair material on the proportion of load distribution in the concrete, repair and reinforcing steel phases of the repaired column specimens owing to different cross-section and properties of materials. The loads carried by the concrete, repair and steel phases of the repaired

reinforced concrete columns (average of three specimens) are determined as a proportion of the total applied load and plotted against the age under load in figures 7.21 to 7.23. While figure 7.24 represents load distribution in the concrete and steel phases of the control column specimens under sustained load.

Both the concrete and repair material, in figures 7.21 to 7.23, carry a different proportion of the applied sustained load immediately after the application of load since the cross-sectional area, strength and stiffness of the materials comprising the column specimens are not the same. However, as the age under load increases both concrete and repair patch undergo creep and hence transfer of their share of load takes place.

It is clearly evident from figures 7.21 to 7.23 that, with time, load distribution from the repair to substrate concrete is much more marked in the reinforced concrete columns repaired with material B and C as compared to columns repaired with material A. This is primarily due to relatively low modulus and high creep characteristics of repair materials B and C compared to substrate concrete. This trend is clearly in agreement with the repair material properties which influence long-term performance of concrete structures as discussed in chapters 3 and 4. An additional factor is the fact that the creep of repair materials is more sensitive to stress/strength ratio than plain concrete (chapter 4).

So, the long-term load sharing by the repair patch is primarily controlled by the creep characteristics of the repair materials. The elastic modulus is also an important property - a high strength and consequently high elastic modulus of the repair material A increases the load sharing capacity of the repair patch, but it also increases the possibility of cracking and failure in long-term.

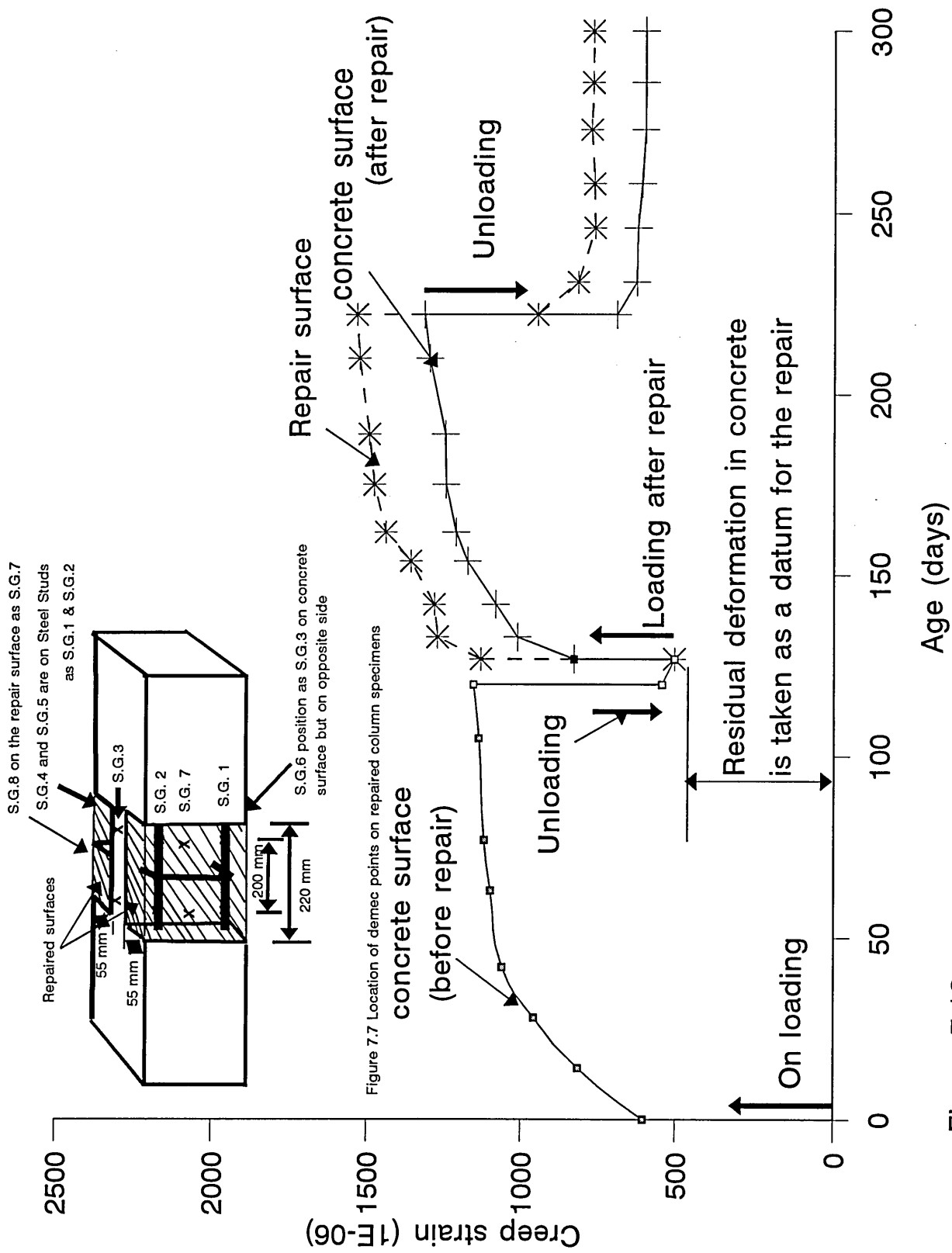


Figure 7.7 Location of demec points on repaired column specimens

Figure 7.18 Influence of patch repair (material A) on the creep of reinforced concrete columns

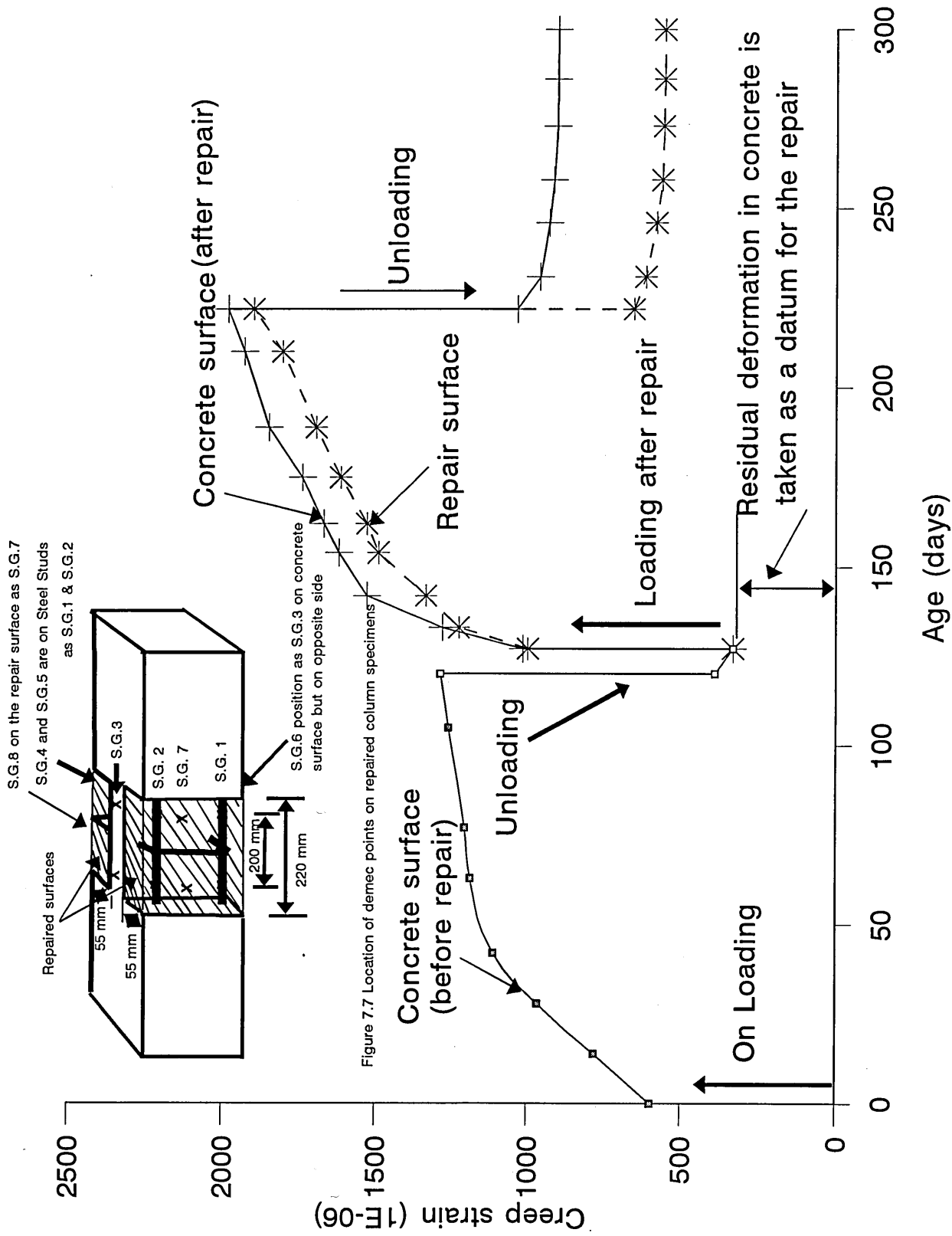


Figure 7.7 Location of demec points on repaired column specimens

Figure 7.19 Influence of patch repair (material B) on the creep of reinforced concrete columns

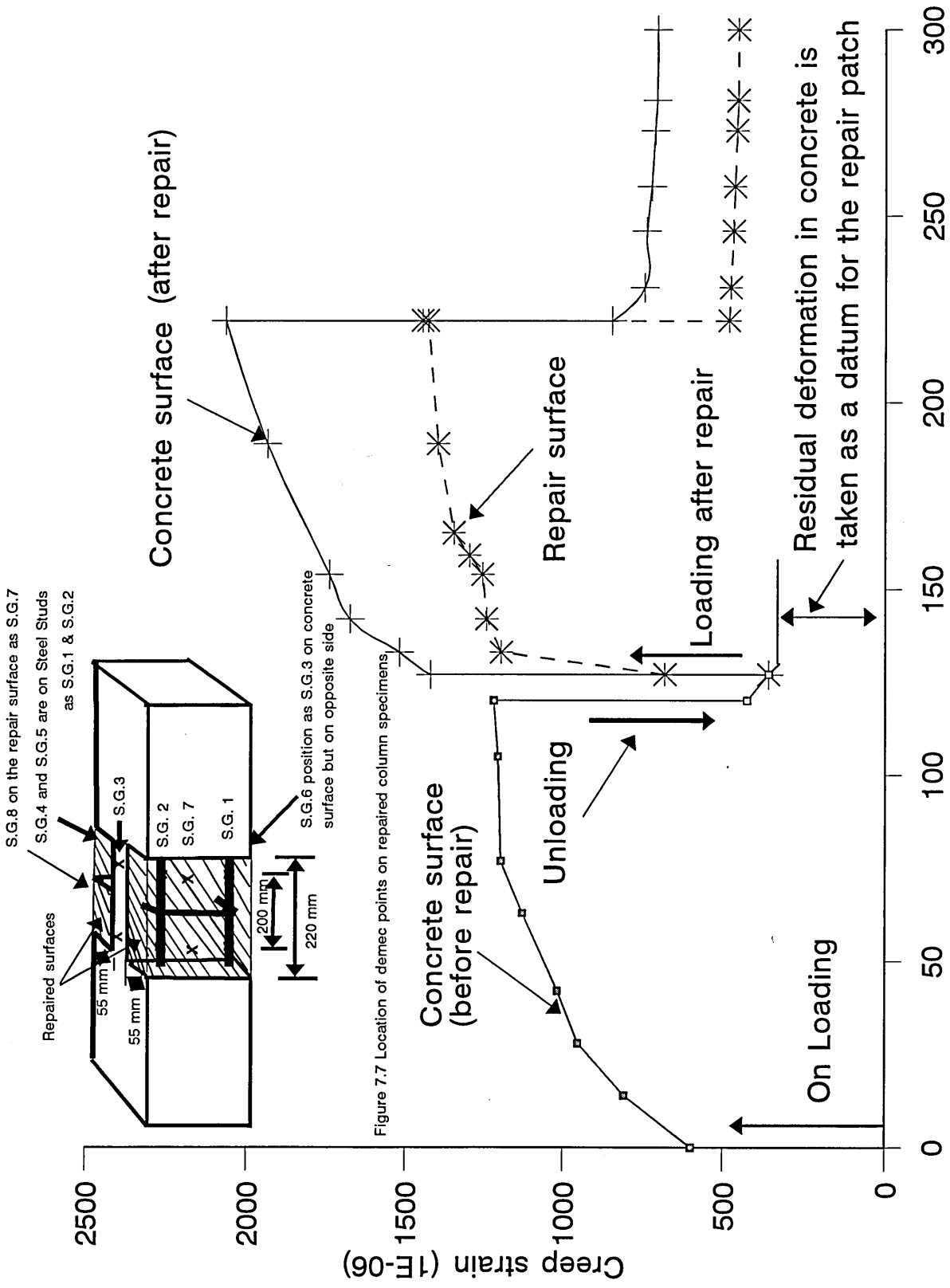


Figure 7.7 Location of demec points on repaired column specimens.

Figure 7.20 Influence of patch repair (material C) on the creep of reinforced concrete specimens

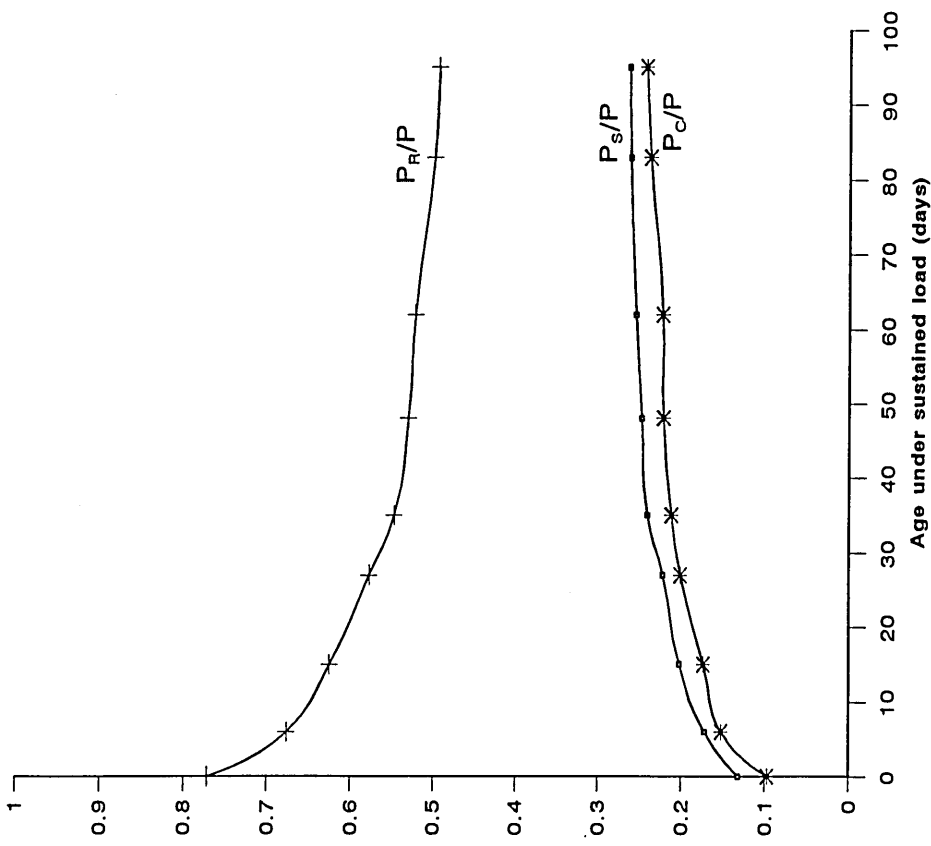


Figure 7.21
Load distribution in steel, repair and concrete phases of repaired reinforced concrete columns (average of three) under sustained load (repair material A)

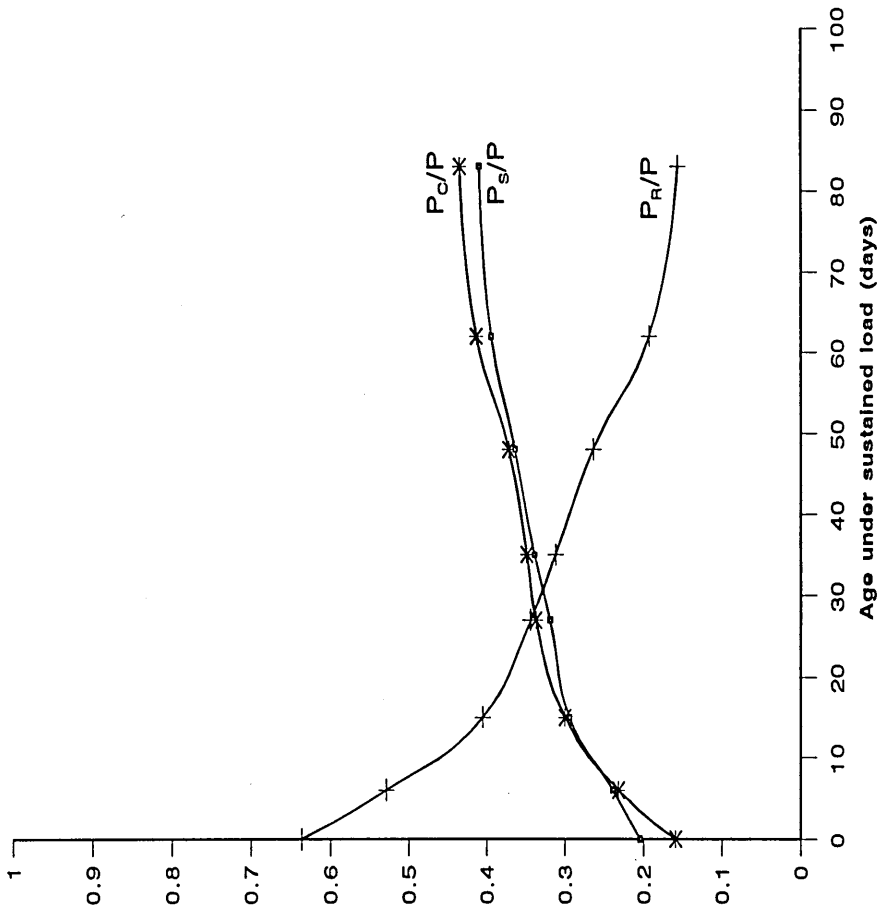


Figure 7.22
Load distribution in steel, repair and concrete phases of repaired reinforced concrete columns (average of three) under sustained load (repair material B)

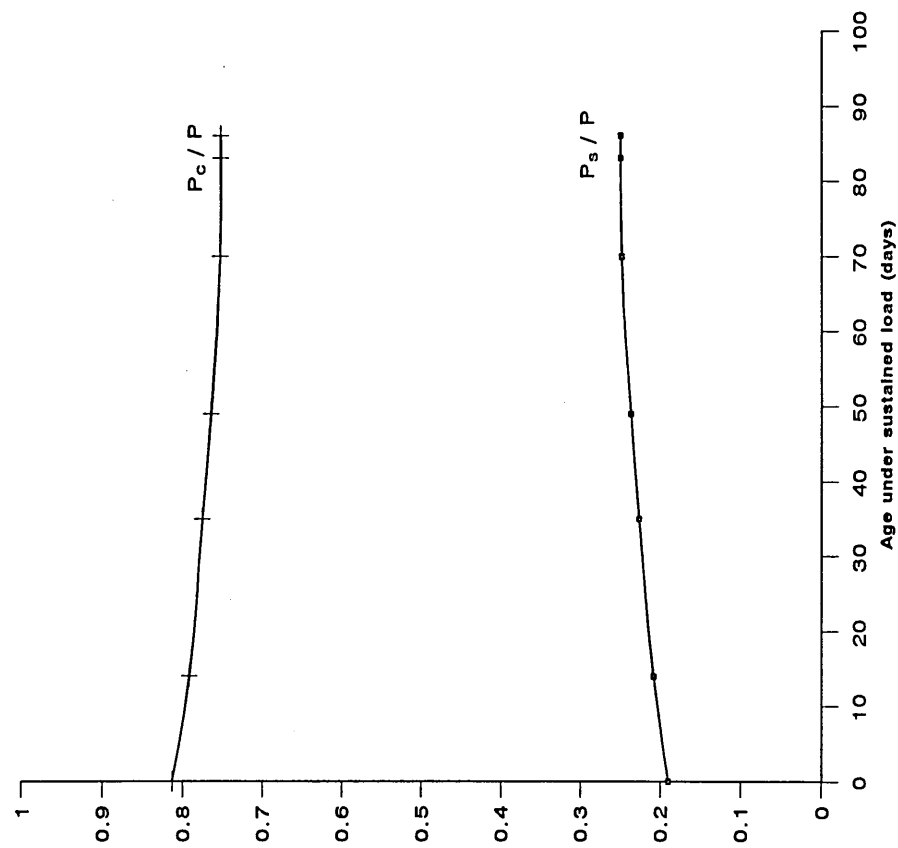


Figure 7.24
Load distribution under sustained load for control reinforced concrete columns
(average of three)

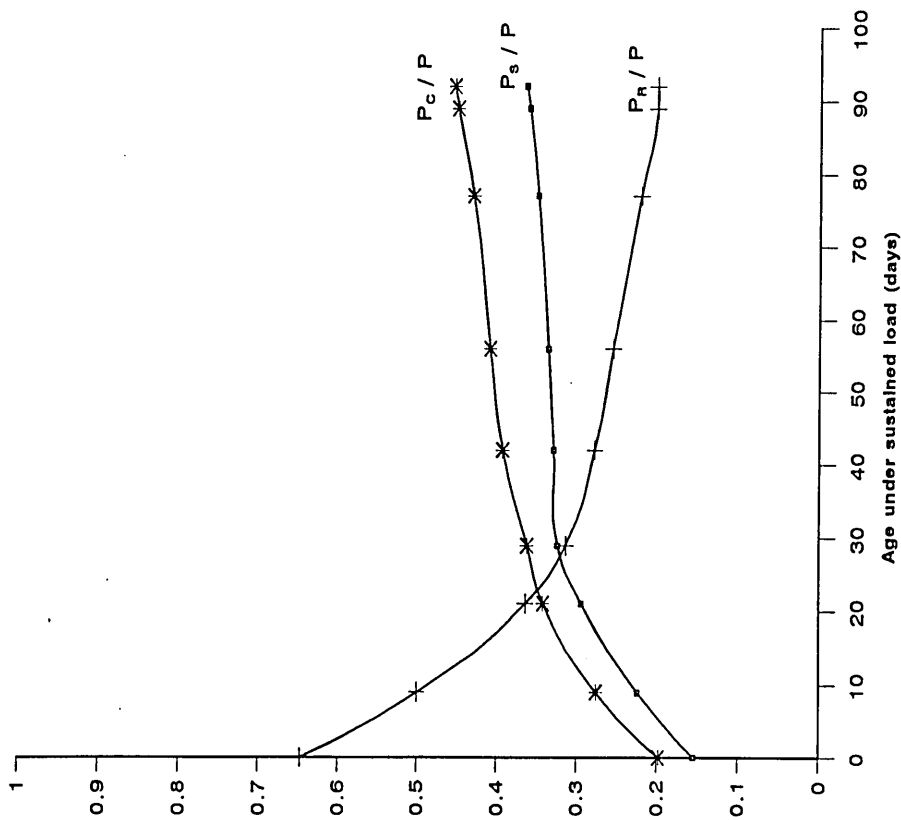


Figure 7.23
Load distribution in the steel, repair and concrete phases of repaired reinforced concrete
columns (average of three) under sustained load (repair material C)

7.5 A THEORY FOR THE CREEP OF REPAIRED REINFORCED CONCRETE COLUMNS UNDER COMPRESSION

7.5.1 Introduction

The preceding chapters have dealt with creep of different repair materials as a property of the material. A knowledge of this property is of importance in understanding the behaviour of such a material and its influence on the subsequent structural performance of a repaired member. The main interest lies in the application of repair materials and in determining the allowance which should be made for creep in design calculations.

The problems encountered are not easy, not only because of the complexity of the properties of a repair material itself, but also because repair is generally used in combination with reinforcing steel and substrate concrete. For this reason, it is the creep of repaired reinforced concrete and the effects of creep in relation to composite action in general that are of interest.

A simple mathematical expression to predict the total strain ratio (at repair cross-section) between the repair patch and substrate concrete at any time (t) is derived in this chapter. This mathematical analyses should form a useful guide in the selection of a repair material for efficient long-term structural interaction between a repair patch and the substrate concrete in compression members of reinforced concrete. A theory is derived in this section to determine the total strain ratio $(\epsilon_R/\epsilon_C)_t$:-

Where,

ϵ_R = total strain on repair patch,

ϵ_C = total strain on substrate concrete, at any time t in terms of the creep properties and modulus of elasticity of the materials, and the varying

sustained stress applied on the concrete and repair cross-section.

Experimental data using three generic repair materials is used to verify the validity of the proposed theory. The strain ratio, $(\epsilon_R / \epsilon_C)$, derived using this procedure shows good correlation with experimental data of this investigation.

7.5.2 Analysis of creep effects on repaired columns

An assumption is made that the rate of creep is constant at any time t , as shown in figure 7.25.

The elastic strain-plus- creep deformation under a unit stress is termed the creep function Φ , which is given by:

$$\Phi_{(t_0, t)} = \frac{1}{E_{(t_0)}} [1 + \phi_{(t_0, t)}] \quad (7.20)$$

Where,

- t_0 = age at first application of load,
- $E_{(t_0)}$ = modulus of elasticity at age t_0 , and
- $\phi(t_0, t)$ = creep coefficient.

where the creep coefficient is defined as the ratio of creep strain at observation time t to the elastic strain at time t_0 .

Given the ambient relative humidity, age at application of load, and volume/surface ratio the creep function can be calculated from equation (7.20) using the creep data and modulus of elasticity data available for repair materials and the substrate concrete mixes.

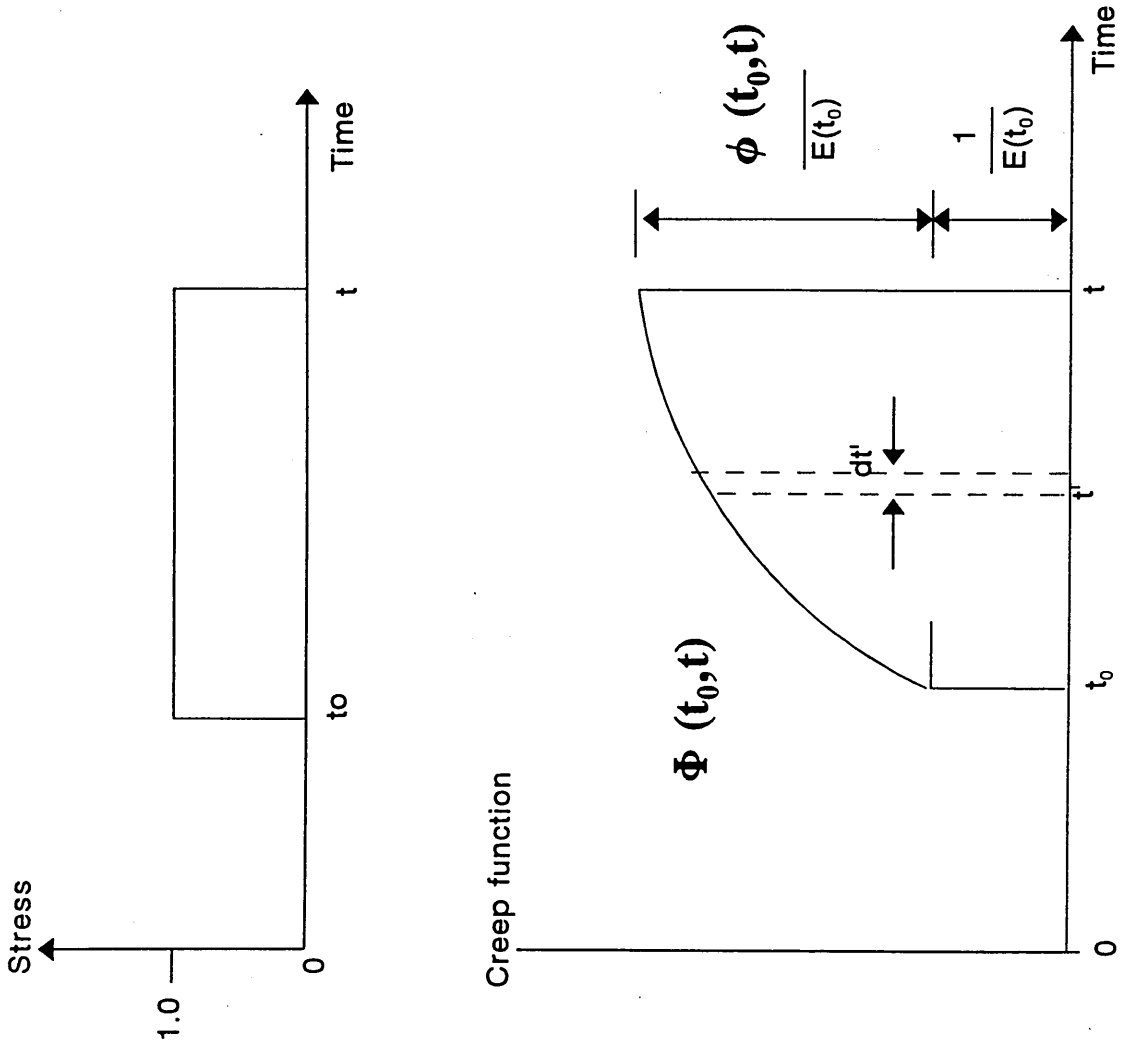


Figure 7.24
 Relation between strain and time for a unit stress applied during the period t_0 to t

Relation between strain and time for a unit stress applied during the period t_0 to t .

Derivation of the analytical expression in this section is based on the assumptions that;

- creep varies linearly with stress, and
- it obeys Boltzmann's principle of superposition, which was applied to concrete data by Dischinger [158] and Maslov [159].

In this investigation, the difference in creep of repair and substrate concrete leads to change in applied stress strength ratio continuous with age. Subsequently it results in strain deformation under a varying stress. In the following section equations for the total strain on repair patch and substrate concrete under varying stress/strength ratio was derived.

A practical method for directly computing the strain under a varying stress, or stress under a varying strain, was developed by Trost [161] and later improved by Bazant [160] who calls his method the 'Age Adjusted Effective Modulus Method'. This introduces the concept of an 'aging' coefficient.

The total strain resulting from an initial stress applied at age t_0 , $\sigma(t_0) = \sigma_0$, and from the subsequent continuously varying stress is given by :-

$$\varepsilon_{(t)} = \sigma_0 \Phi_{(t_0, t)} + \int_{t_0}^t \Phi_{(t', t)} \frac{\partial \sigma_{(t')}}{\partial t'} dt' \quad (7.21)$$

substituting for $\Phi(t_0, t)$ from equation (7.20) in equation (7.21) gives:

$$\varepsilon_{(t)} = \frac{\sigma_0}{E_{(t_0)}} [1 + \phi_{(t_0, t)}] + \int_{t_0}^t \frac{[1 + \phi_{(t', t)}]}{E_{(t')}} \frac{\partial \sigma_{(t')}}{\partial t'} dt' \quad (7.21 \text{ (a)})$$

Where,

$\Phi(t_0, t)$ is the creep function

σ_0 is the initial stress on application of load.

By evaluating the integral of equation 7.21 (a), for variation of stress ($\sigma(t), \sigma_0$) with time :-

$$\varepsilon(t) = \frac{\sigma_0}{E(t_0)} [1 + \Phi(t_0, t)] + \frac{\sigma(t) - \sigma_0}{E(t_0)} [1 + \chi(t_0, t) \Phi(t_0, t)] \quad (7.22)$$

In this equation, $\chi(t_0, t)$ is the aging coefficient which accounts for the effect of aging on the ultimate value of creep for stress increments or decrements occurring gradually after the application of the original load. The aging coefficient is defined by equating the last terms of equations (7.21 (a)) and (7.22), and rearranging as follows :

$$\frac{\sigma(t) - \sigma_0}{E(t_0)} [1 + \chi(t_0, t) \Phi(t_0, t)] = \int_{t_0}^t \frac{[1 + \Phi(t', t)]}{E(t')} \frac{\partial \sigma(t')}{\partial t'} dt' \quad (7.23)$$

$$\therefore \chi(t_0, t) = \frac{E(t_0)}{\Phi(t_0, t) [\sigma(t) - \sigma_0]} \int_{t_0}^t \frac{1 + \Phi(t', t)}{E(t')} \frac{\partial \sigma(t')}{\partial t'} dt' - \frac{1}{\Phi(t_0, t)} \quad (7.24)$$

For numerical evaluations:

$$\chi(t_0, t) = \frac{E(t_0)}{\Phi(t_0, t) [\sigma(t) - \sigma_0]} \sum_{t_0}^t \frac{\Delta \sigma(t')}{E(t')} [1 + \Phi(t', t)] - \frac{1}{\Phi(t_0, t)} \quad (7.25)$$

Thus, the value of the aging coefficient χ depends on t_0 , on the creep function, and on the variation of the stress or strain with time.

Using the aging coefficient and shrinkage property of material equation (7.22) can be arrange as follows:

$$\epsilon_{(t)} = \frac{\sigma_0}{E_{(t_0)}} [1 + \phi_{(t_0, t)}] + \frac{\sigma_{(t)} - \sigma_0}{E_{(t_0)}} [1 + \chi_{(t_0, t)} \phi_{(t_0, t)}] + \epsilon_{sh}(t_0, t) \quad (7.26)$$

Subsequently the total strain ratio of repair patch and substrate concrete, (ϵ_R/ϵ_C) , at any time t given by :-

$$\left(\frac{\epsilon_R}{\epsilon_C} \right)_t = \frac{\left[\left(\frac{\sigma_R}{E_R} \right)_{t_0} [1 + \phi_{R(t_0, t)}] + \frac{\sigma_{R(t)} - \sigma_{R(t_0)}}{E_{R(t_0)}} \right] \times [1 + \chi_{R(t_0, t)} \phi_{R(t_0, t)}] + K_1 \epsilon_{shR(t_0, t)}}{\left[\left(\frac{\sigma_C}{E_C} \right)_{t_0} [1 + \phi_{C(t_0, t)}] + \frac{\sigma_{C(t_0, t)} - \sigma_{C(t_0)}}{E_{C(t_0)}} \right] \times [1 + \chi_{C(t_0, t)} \phi_{C(t_0, t)}] + K_2 \epsilon_{shC(t_0, t)}} \quad (7.27)$$

Where,

K_1 and K_2 are the constants for volume/surface correction.

Equation 7.27 can be used to calculate total strain ratio at any time t , $(\epsilon_R/\epsilon_C)_t$, after loading using basic material properties such as modulus of elasticity on loading and shrinkage properties of materials, stress history and aging coefficient.

7.5.2.1 Determination of modulus of elasticity and stress on loading

In order to predict the total strain ratio, (ϵ_R/ϵ_c) , in repaired column specimens from equation (7.27) of the proposed theory, values of stress, modulus of elasticity on loading and creep coefficients have to be established first. This in turn requires the determination of the initial stress / strength ratio on the materials which is calculated by the following procedure :

From the condition of equilibrium (at repair cross-section):-

$$P = f_c A_c + f_s A_s + f_R A_R \quad (7.28)$$

Where,

P = applied axial load

f_c, f_s, f_R = compressive stress in the concrete, steel and repair patch respectively

A_c, A_s, A_R = cross-sectional area of concrete, steel and repair patch respectively.

Assuming full bond between the materials, then from the condition of compatibility of strains,

$$\frac{f_c}{E_c} = \frac{f_s}{E_s} = \frac{f_R}{E_R} \quad (7.29)$$

(Concrete Strain = Steel Strain = Repair Strain)

Where E_c, E_s and E_R are respectively the effective modulus of elasticity of the concrete, steel and repair material at the time of application of load.

From equations (7.28) and (7.29),

$$f_c = \frac{P - f_s A_s}{A_c + A_R \frac{E_R}{E_c}} \quad (7.30)$$

$$f_R = \frac{P - f_s A_s}{A_R + A_c \frac{E_c}{E_R}} \quad (7.31)$$

In the above equations, the quantity $(A_c + A_R E_R/E_c)$ represents the concrete area plus modular ratio times the repair area, and this is the same as the area of the transformed section in concrete.

In order to determine stress/strength ratio at application of load, stresses in concrete and repair material were divided by corresponding cube strength of each material at the time of loading. The experimental values of creep coefficients were determined by using materials properties under the same environment conditions.

7.5.2.2 Comparison of experimental and predicted total strains

The results in figures 7.26 to 7.29 show the comparison between the experimental and theoretical total strain (including elastic, creep and shrinkage strain) ratio of repair patch and substrate concrete at different ages. Generally all the predicted creep strain ratios are in close agreement with the experimental data obtained in this study. Therefore the derived mathematical model represents an accurate means of predicting creep strain ratio of repair patch and concrete surface. It is also clear that the stress on application of load and modulus of elasticity of materials at loading plays an important role in the strain distribution between repair patch and substrate concrete.

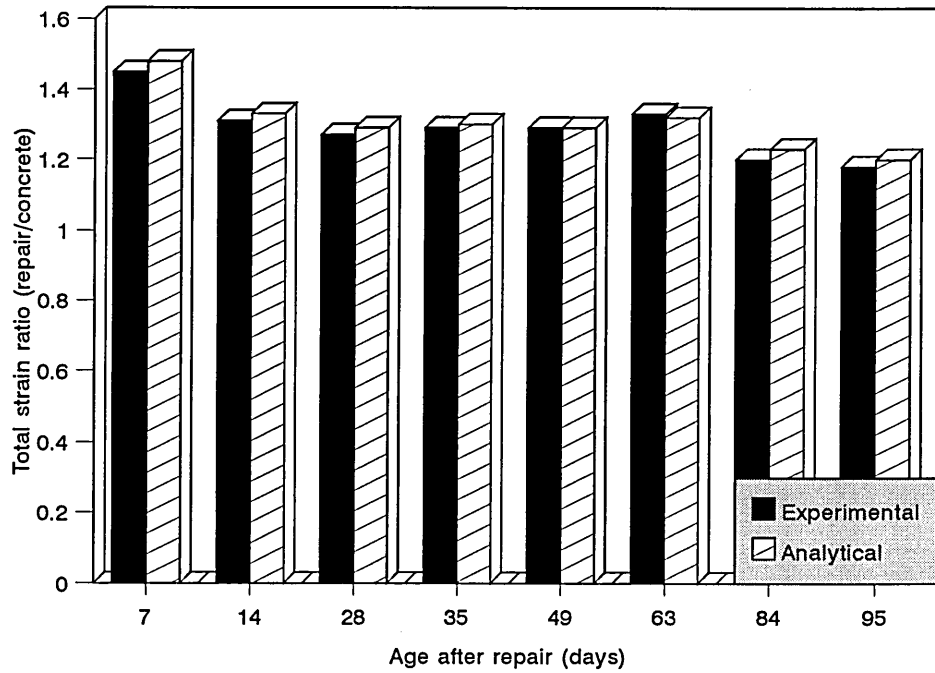


Figure 7.26
Comparison between the theoretical and experimental (average of three specimens) total strains at different ages, for reinforced concrete columns repaired with Material A

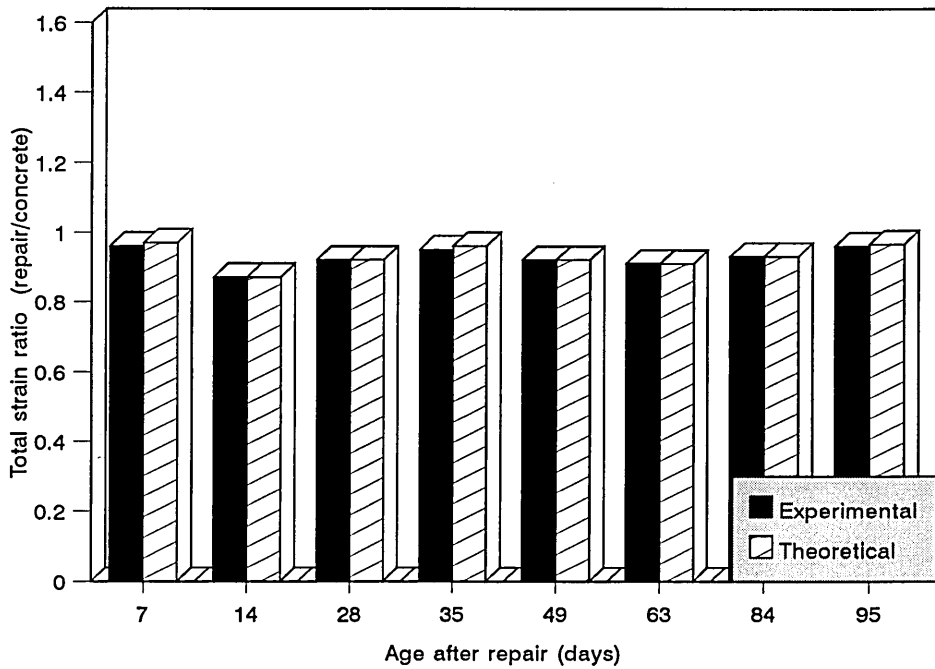


Figure 7.27
Comparison between the theoretical and experimental (average of three specimens) total strain ratios at different ages, for reinforced concrete columns repaired with Material B

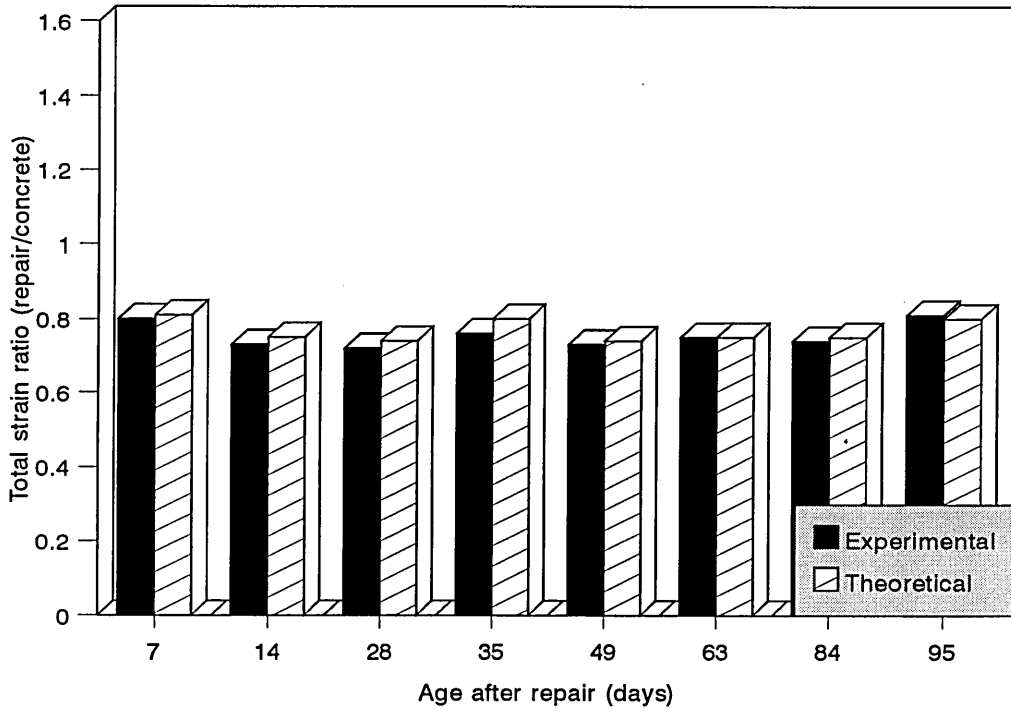


Figure 7.28
Comparison between the theoretical and experimental (average of three) total strain ratios at different ages, for reinforced concrete columns repaired with Material C

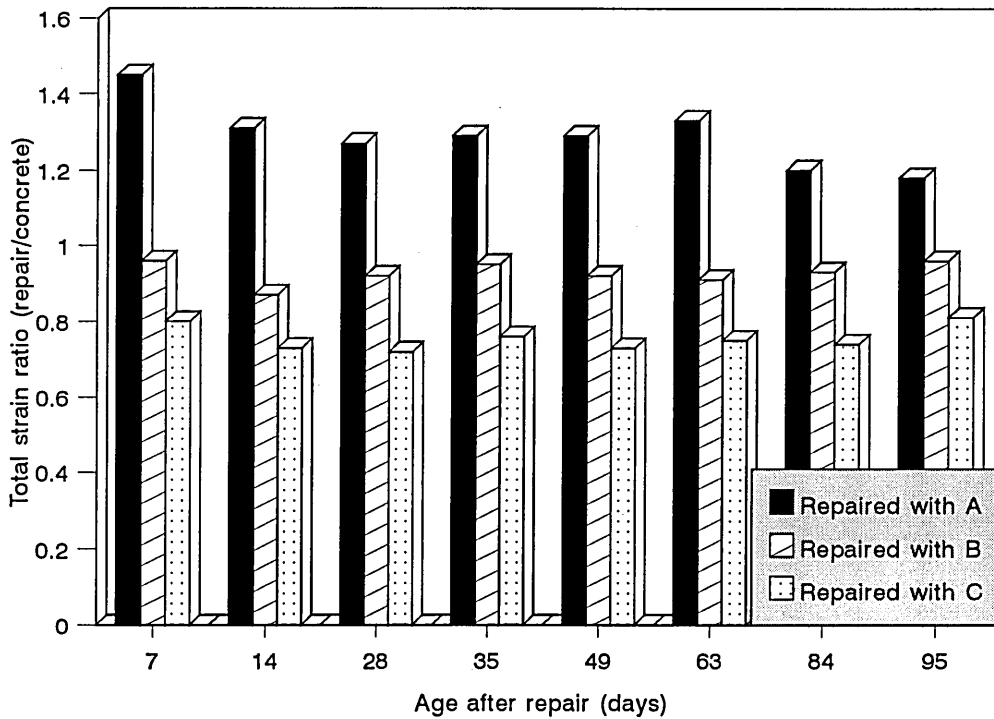


Figure 7.29
Comparison of total strain ratio for reinforced concrete columns (average of three) repaired with three different repair materials

Figure 7.29 compares the total strain ratio, $(\epsilon_R / \epsilon_c)_t$, for the reinforced column specimens repaired with three different repair materials. It is clear from this figure that a high strength and consequently high elastic modulus of the repair material A increases the load sharing capacity of the repair patch quite considerably compared to specimens repaired with material B and C.

7.6 CONCLUSIONS

The following conclusions are based on the results obtained in this chapter,

- The long-term cracking at the repair/substrate interface and the load sharing by the repair patch is primarily controlled by the shrinkage and creep characteristics of the repair materials. For efficient long-term structural interaction, these properties should not differ significantly from those of the substrate concrete.
- The elastic modulus is also an important property - a high strength and consequently high elastic modulus of the repair material increases the load sharing capacity of the repair patch, but also increases the possibility of cracking and failure.
- The presence of reinforcement reduces shrinkage to a greater extent than creep.
- Prediction of stress decrement in concrete made on the basis of an apparent effective modulus of elasticity (creep model) suggested by Samara [144] shows good agreement with the experimental data of this investigation.
- A mathematical expression to predict the creep strain ratio, of repair patch and concrete surface, $(\epsilon_R / \epsilon_c)$, at any time (t) after repair is derived in this study. Calculation of the strain ratios using this procedure shows good correlation with experiential data of this investigation.

CONCLUSIONS AND RECOMMENDATIONS FOR FUTURE RESEARCH

8.1 CONCLUSIONS

The following conclusions are based on the theoretical and experimental work reported in this thesis,

1. Compressive creep strains and drying shrinkage are greatest in the cementitious repair material which contains the styrene acrylic copolymer, despite the presence of some fibre additives in this material.
2. In all repair materials considered, most of the drying shrinkage occurs within the first 21 days and remains relatively stable beyond that age.
3. The shrinkage of specially formulated repair mortars, particularly those modified with polymer admixtures, is much more sensitive to the of relative humidity of the curing environment than plain concrete.
4. Coarse aggregate size particles in repair materials provide dimensional stability, ductility and higher stiffness.
5. Presence of a polymer admixture in a repair material reduces its water permeability. The highest water permeability coefficients were recorded for the mineral based material B. The mean values of permeability coefficient, K_{LD} (m/s), for material A

and C are 2.53×10^{-13} and 1.33×10^{-13} respectively, while for material B it is 5.62×10^{-11} , which shows more than an order of magnitude increase in permeability relative to the other materials.

6. For efficient long-term structural interaction with the substrate, the stiffness, shrinkage and creep deformation properties of repair materials should not differ significantly from those of the substrate concrete.
7. Under compression, plain concrete specimens and the two repair materials B and C failed in a relatively ductile manner whereas repair material A specimens failed in a brittle manner.
8. The chloride concentration profiles of repair materials, show a strong dependency on the initial curing conditions, especially during the early periods of exposure to chloride solution environment. But after a long period of exposure the effect of initial curing on chloride penetration is reduced.
9. Repair material A showed the lowest chloride penetration under all the initial curing conditions considered in this investigation, while cementitious repair material B showed the highest chloride uptake among all the materials.
10. The chloride diffusion coefficient decreases as the period of exposure to a chloride environment increases. The following formula was derived to predict long-term chloride concentration profiles,

$$C(x, t) = C_0 \left[1 - \operatorname{erf} \left(\frac{x}{K\sqrt{D_1 t^m}} \right) \right]$$

Where,

- $C(x,t)$ = chloride concentration as a function of distance x and time t
- x = distance (Cm)
- t = time (seconds)
- C_0 = Chloride concentration at the surface
- K & m = Constants which depends on the material property and initial curing conditions.

11. The equilibrium chloride concentration on the material surface, C_0 , and diffusion coefficient, D_e , are not related.
12. In repaired reinforced concrete column specimens under sustained axial load, the redistribution of stress (from substrate to repair patch) in specimens repaired with material C is significantly higher than in other repaired columns.
13. Shrinkage of a repair patch in a repaired reinforced concrete element is restrained by the substrate material. The substrate material itself shrinks due to the compressive stress induced by the differential shrinkage of the repair patch relative to the substrate material.

14. Selecting an appropriate material and predicting its shrinkage stress in the repaired structure for a specified situation is an important strategy for reducing the adverse effects due to restrained shrinkage.
15. The following mathematical expression has been derived for determining the long-term total strain distribution, $(\epsilon_R/\epsilon_C)_t$, in repaired reinforced concrete columns,

$$\left(\frac{\epsilon_R}{\epsilon_C}\right)_t = \frac{\left[\left(\frac{\sigma_R}{E_R}\right)_{t_0} [1 + \phi_R(t_0, t)] + \frac{\sigma_R(t) - \sigma_R(t_0)}{E_R(t_0)} \right] \times [1 + \chi_R(t_0, t) \phi_R(t_0, t)] + K_1 \epsilon_{shR}(t_0, t)}{\left[\left(\frac{\sigma_C}{E_C}\right)_{t_0} [1 + \phi_C(t_0, t)] + \frac{\sigma_C(t_0, t) - \sigma_C(t_0)}{E_C(t_0)} \right] \times [1 + \chi_C(t_0, t) \phi_C(t_0, t)] + K_2 \epsilon_{shC}(t_0, t)}$$

Where,

- t_0 = age at first application of load,
- σ_C, σ_R = Stress on substrate concrete and repair patch respectively,
- E_C, E_R = Modulus of elasticity of concrete and repair material,
- ϕ_C, ϕ_R = Creep coefficient of concrete and repair material,
- $\epsilon_{shC}, \epsilon_{shR}$ = Shrinkage on concrete surface and repair patch,
- χ_C, χ_R = aging coefficient for concrete surface and repair patch, and
- K_1 and K_2 = constants for volume/surface correction.

8.2 RECOMMENDATIONS FOR FURTHER WORK

The following may constitute important points for further research into the effect of generic repair materials on the performance of concrete repair:-

1. Evaluation of the long-term performance of damaged and repaired columns under variable or fatigue load.
2. Permeability of generic repair materials to chloride as well as water under practical curing conditions requires an indepth examination.
3. The variation of the equilibrium chloride concentration on the concrete surface with the duration of exposure to chloride environment need to be investigated further.

CHAPTER 9

REFERENCES

1. British Standard Institution
Portland Cement. BS 12; Part 2, London, 1971.
2. British Standard Institution
Specification for aggregates from natural sources for concrete. BS 882, London, 1965.
3. Elgarf, M. S. A.
The effect of reinforcement corrosion on the structural performance of concrete flexural members. Ph.D. Thesis, University of Aberdeen, 1994.
4. Swiss Bank Corporation (Stockbrokers).
Quarterly Building Bulletin, London, 26th Jan. 1989. pp 5-
5. Marosszeky, M. and Chew, M.
Site investigation of reinforcement placement on building and bridges. *Concr. Int.* 12 (4), 1990. pp 59-64
6. Coote, A. et al.
Repairs to reinforced concrete in marine conditions. *Construction repairs and maintenance*, 2, No.5, 1986. pp 18-22
7. Calder, A. J. and Thompson, D. M.
Repair of cracked reinforced concrete: assessment of corrosion protection. Transport and Road Research Laboratory, Crowthorne, TRRL research report 150, 1988.
8. Patterson, W. S. and Dill, M. J.
Further studies of the fatigue strength of reinforced concrete in seawater. Laing design and development centre, London, 1984.
9. Hewlett, P. C. and Hurley, S. A.
The consequences of polymer-cement mismatch. *Design life of buildings*, Thomas Telford, London, 1985. pp 179-196
10. Emberson, N. K. and Mays, G. C.
Polymer mortars for the repair of structural concrete: the significant of property mismatch", *Proc. ICPIC '87: 5th Int. Congress on polymers in concrete*. Brighton, Sept. 1987. pp 235-242

11. Plum, D. R.
Repair materials and repaired structures in varying environment. Proc. 3rd Int. Seminar on the life of structures- the role of physical testing. Brighton, 1989.
12. Wood, J. G. M. et al.,
Defining the properties of concrete repair materials for effective structural application. Proc. structural faults repairs'89, Vol. 2, London, 1989. pp 231-236
13. Emberson, N. K. and Mays, G. C.
Significance of property mismatch in the patch repair of structural concrete. part 1: properties of repair system, Magazine of Concrete Research, Vol. 42, No. 152, September 1990. pp 147-160
14. British Standard Institution
Methods of Testing Concrete. BS 1881 : Part 5, London, 1970. p 40
15. Callow, O. P.
An investigation into possible improvements to ISAT for site testing. Brunel university, Degree project, Materials Science and Technology, 1982/1983.
16. Figg, J. W.
Methods of measuring the air and water permeability of concrete. Magazine of Concrete Research. Vol. 25, Dec. 1973. pp 213-219
17. Green, J. K., Cookson, P. J. and Johnson, K. A. L.
The performance of pretensioned concrete beams that have cracked before transfer of prestress. The Structural Engineer, Vol. 62B, Dec. 1984. pp 79-84
18. Pihlajavaara, S. E. and Paroll, H.
On the correlation between permeability properties and strength of concrete. Cement and Concrete Research, Vol. 5, 1975. pp 321-327
19. Richards, P. W.
A laboratory investigation of the water permeability and crushing strength of concrete made with and without pfa, as affected by early curing temperature. Cement and Concrete Association, Advanced Concrete Technology Project 82/9, Slough, 1982.
20. Chantree, P. A.
A measurement of rates of water absorption of concretes. Appendix 5 in Harrison, W.H. and Teychune, Interim Report on long-term investigation at Nortwick park. BRE Report, HMSO, London, 1981. pp 58-61

21. Cather, R., Figg, J.W., Marsden, A.F. and O'Brien, T.P.
Improvement to the figg method for determining the air permeability of concrete. Magazine of Concrete Research, Vol. 36, Dec. 1984. pp 241-247
22. Kasai, Y., Matsui, I. and Nagano, M.
On site rapid air permeability test for concrete. In situ/non destructive testing of concrete, SP-82, American Concrete Institute, Detroit, 1984. pp 5543-554
23. Bamforthe, P. B.
The relationship between permeability coefficients for concrete obtained using Liquid and Gas. Magazine of Concrete Research, Vol. 39, No. 138, March 1987. pp 3-11
24. Kriz, L. B. and Lee, S. L.
Ultimate Strength of over Reinforced Beams. Proceedings of the American Society of Civil Engineers, Vol. 86, No EM3, June 1960. pp 95-105
25. Young, L. E.
Simplifying Ultimate Flexural Theory by Maximising the Moment of Stress Block. Journal of ACI, Vol. 32, No. 5, November 1960. pp 549-556
26. Carrerira, D. J. and Chu, K. H.
Stress-Strain Relationship for Plain Concrete in Compression. ACI Journal, Nov-Dec 1985. pp 797-804
27. Turner, P. W. and Barnard, P. R.
Stiff Constant Strain Rate Testing Machine. The Engineer, London, Vol. 214, no 5557, 1962. pp 146-148
28. Block, G.
Concrete Complete Stress-Strain Curves. Engineering, London, Vol. 193, No 5011, May 1962. p. 606
29. Barnard, P. R.
Research into the Complete Stress-Strain Curve for Concrete. Magazine of Concrete Research , Vol. 16, No 49, December 1964. pp 203-210
30. Sangha, C. M. and Dhir, R. K.
Relationships for Concrete Tested in uniaxial Compression under Different test Conditions. Materials and Structures/ Research and Testing (Paris). Vol. 5, no 30, Nov-Dec 1972. pp 361-370

31. Kosaka Y., Tanigawa Y., and Hatanaka, S.
Expression for Stress-Strain Curves of Concrete up to a Large Plastic Strain. Review of 34th General Meeting of Cement Association of Japan, Vol. 34, May 1980. pp 135-7
32. Popovics, S.
A Numerical Approach to the Complete Stress-Strain Curve of Concrete. Cement and Concrete Research, Vol. 3, No 5, Sept 1973. pp 583-599
33. Halabi, W. H.
High strength Concrete Corbels. PhD Thesis, University of Aberdeen, Department of Engineering, Dec 1991.
34. Desayi, P. and Krishnan, S.
Equation for the Stress - Strain Curve of Concrete. Journal of ACI , March 1964. pp 345-350
35. Saenz, L. P.
Discussion of Equation for Stress-Strain Curve of Concrete. By Prakesh Desayi and Krishnan S., ACI Journal Proceedings, Vol. 61, No 9, Sept 1964. pp 1229-1236
36. Smith, G. M. and Young, L. E.
Ultimate Flexural Analysis Based on Stress-Strain Curve of Cylinders. ACI Journal Proceedings, Vol. 53, No 6, Dec 1956. pp 597-609
37. Smith, G. M. and Young, L. E.
Ultimate Theory in Flexure by Exponential Function. ACI Journal Proceedings, Vol. 52, No 3, Nov 1955. pp 349-359
38. Wang P. T., Shah S. P and Naaman, A. E.
Stress-Strain Curve of Normal and Light Weight Concrete in Compression. Journal of ACI, Vol. 75, No 11, Nov 1978. pp 603-611
39. Wang P.Tsan, Surendra P. Shah and Antonie L. Naaman.
Complete Stress-Strain Curve of Concrete and its Effect on Ductility of Reinforced Concrete Members. Oct 1977. PhD Thesis
40. Liu, T. C. Y., Nilson, N. W. and Slate, F. O.
Stress-Strain Response and Fracture of Concrete in Uniaxial and Biaxial Compression. ACI Journal, May 1972. pp 291-295

41. Tsai, W. T.
Uniaxial Compressional Stress-Strain Relation of Concrete. ASCE, Vol. 44, No. 9, Sept. 1988. pp 2133-2136
42. Shah, S. P., Ulker, G. and Farhad, A.
An experimental Technique for Obtaining Complete Stress-Strain Curve of High Strength Concrete. The American Society for Testing and Materials, 1981. pp 21-27
43. Popovics, S.
The Fracture Mechanism in Concrete: How Much do We Know ? ASCE Proceedings, Vol. 95, No EM3, June 1969. pp 531-544
44. Gilkey, H. and Murphy, G.
Stress-Strain characteristics of Mortars and Concrete. ASTM Proceedings, Vol. 38, Part I, 1938. pp 318-326
45. Azari, M. M.
Fracture and Long Term Deformation Characteristics of Steel Fibre Reinforced Concrete Compression Member. PhD Thesis, University of Aberdeen, Department of Engineering, 1984
46. Hsu, T. C., Slate, F. O., Sturman, G. M. and Winter, G.
Micro Cracking of Plain Concrete and Shape of Stress-Strain Curve. Journal of ACI, Vol. 60, 1963. pp 209-224
47. Slate, F. O. and Olsefsky, S.
X-Ray for Study of Internal Structure of Micro Cracking of Concrete. Journal of ACI, Vol. 60, 1963. pp 575-588
48. Illston, J. M., Dinwoodie, J. M. and Smith, A. A.
Concrete, Timber and Metals, the Nature and Behaviour of Structural Materials. Van Nostrand Reinhold Company, 1979
49. Newman, K. and Newman, J. B.
Failure Theories and Design criteria for Plain Concrete. Proc. of Conference on Civil Eng. Materials, Wiley-Inter Science, 1971. pp 963-995
50. Dhir, R. K. and Sangha, C. M.
Development and Propagation of Microcracks in Plain Concrete. Materials and Structures, RILEM, Vol. 7, 1974. pp 17-23

51. Stroven, P.
Conference on "The Influence of Volume Change on the Design and Technology of Modern Building Structures". Karlovy Vary, CSR, 1971.
52. Shah, S. P. and Chandra, S.
Critical stress, Volume Change and Microcracking of Concrete. Journal of ACI, Volume 65, 1968. pp 770-781
53. Popov, L. N. and Ippolitov, E. N.
5th International Conference on Fracture. Cannes, 1981. pp 2287-2292
54. Zaitsev, T. V.
Deformation and Failure of Hardened Cement Paste and Concrete Subjected to Short Term Load. Cement and Concrete research, Vol. 1, NO 1, 1971. pp 123-137
55. Brandtzaeg, A.
Failure of Material Composed of Non-Isotropic Elements. Kong, Norske, Vid. Selsk. for Hand, No 2, 1927. pp 1-68
56. British Standard Institution
BS 1881, Testing Concrete : part 116 : Method for determination of compressive strength of concrete cubes. London, 1983.
57. British Standard Institution
BS 1881, Testing Concrete : part 118 : Method for determination of flexural strength. London, 1983.
58. Darcy, H. P. G.
Les Fontaines Publiques de la Ville de Dijon. Paris, V. Dalmont, 1856. pp 674
59. Shah, S. P., Naaman, A. E. and Moreno, J.
Effect of Confinement on the Ductility of Light Weight Concrete. The International Journal of Cement Composites and Light Weight Concrete, Vol. 5, No.1, Feb 1983. pp 15-25
60. David, A. Fanalla and Antoine, E. Naaman.
Stress-Strain Properties of Fibre Reinforced Mortar in Compression. ACI Journal, July-Aug 1985. pp 475-483
61. Gopalaratham, V. S. and Shah, S. P.
Softening Response of Plain Concrete in Direct Tension. ACI Journal, May-June 1985. pp 310-323

62. Swamy, R.N. and Lambert, G.H.
Mix Design and Properties of Concrete Made from PFA coarse Aggregates and Sand.
The International Journal of Cement Composites and Light Weight Concrete, Vol. 5,
No. 4, 1983. pp 263-275
63. Swamy, R. N. and Kameswara Rao, C. V. S.
Fracture Mechanics in Concrete Systems under Uniaxial Loading . Cement and
Concrete Research, Vol. 3, 1973. pp 413-427
64. Illston, J. M. and Pomeroy, C. D.
Recommendations for a standard creep test. Concrete, December 1975. pp 24-25
65. Lyse, I.
The shrinkage and creep of concrete. Magazine of Concrete Research, Vol. 54, No.
12, June 1958. pp 1111-1142
66. Neville, A. M.
Properties of Concrete. ELBS, 3rd Edition, 1983. pp 118-202
67. Lyse, I.
Shrinkage of Concrete. Proceedings of the American Society for Testing Materials,
Vol. 35, 1935. pp 383-398
68. Carlson, R. W.
Drying shrinkage of concrete as affected by many factors. Proceedings of the
American Society for Testing Materials, Part 2, Vol. 38, 1938. pp 419-437
69. Neville, A. M and Brooks, J. J.
Concrete Technology. English Language Book Society [ELBS] / Longman, 1987.
pp 237-250
70. Pickett, G.
Effect of Aggregate on Shrinkage of Concrete and Hypothesis Concerning Shrinkage.
Jnl. A.C.I., Vol. 52, 1956. pp 581-590
71. Neville, A. M.
Creep of Concrete-Plain, Reinforced and Prestressed. North Holland Publishing
Company, Amsterdam, 1970.
72. Illston, J. M.
The Components of Strain in Concrete Under Sustained Compressive Stress.
Magazine of Concrete Research. Vol. 17, No. 50, 1965. pp 21-28

73. Roll, F.
Long-Time Creep Recovery of Highly Stressed Concrete Cylinders, Creep of Concrete. Jnl. A.C.I. Publication SP9, Detroit, 1964. pp 95-114
74. Hsu, T. T. C.
Inelastic Behaviour of Concrete under Short-Time Loading. Colloquim on the Nature of Inelasticity of Concrete and its Structural Effects, Report No. 332, Cornell University, Ithaca, New York, Nov. 1965. pp 1-6
75. Lyse, I
The Shrinkage and Creep of Concrete. Magazine of Concrete Research, Vol. 11, Part 33, 1959. pp 143-150
76. Ross, A. D.
Concrete Creep Data. The Structural Engineer, Vol. 15, No. 8, 1937. pp 314 - 326
77. Pease, J.
The Enemy within. New Civ. Engr. roads supplement). September 1989. pp 69-73
78. Montague, S.
Glasgow's M8 bridge shows alarming faults. New Civ. Engr. May 1990. pp 8
79. Watson, R.
Spaghetti junction lifts off £400M repairs. New Civ. Engr. 28th June 1990. pp 7
80. Wallbank, E. J.
The Performance of Concrete in Bridges; a survey of 200 highway bridges. HMSO, London. 1989. pp 96
81. Mehta, P. K.
Effect of Cement Composition on Corrosion of Reinforcing Steel in Concrete. American Society of Testing and Materials, Special Technical Publications, STP 629, 4977. pp 12-19
82. Verbeck, G. J.
Mechanisms of Corrosion of Steel in Concrete. Corrosion of Metals in Concrete, ACI Publication, SP-49, 1975. pp 21-38
83. Tutti, K.
Service life of Structures with Regard to Corrosion of Embedded Steel. ACI Publication, SP-65, 1980. pp 223-236

84. Cavalier, P. G. and Vassie, P. R.
Investigation and Repair of Reinforced Corrosion in a Bridge Deck. Proceedings of ICE, Part 1, No. 70, August 1981. pp 461-480
85. Mansur, M. A. and Ong, K. C. G.
Epoxy Repaired Beams. Concrete International : Design and Construction. Vol. 7, No. 10, Oct. 1985. pp 46-50
86. Rasheeduzzafar; Dakhil, Fahd H. and Al-Gantani, A. S.
Deterioration of Concrete Structures in the environment of the Middle East. ACI Journal, Proceedings, Vol. 81, No. 1, Jan.-Feb. 1984. pp 13-20
87. Hausmann, D. A.
Steel Corrosion in Concrete, How Does it Occur ?. Materials protection. November 1967. pp 19-23
88. Dixon, W. J.
BMDP Statistical Software. University of California Press, 1985.
89. ACI Committee 222.
Corrosion of Metals in Concrete. ACI Journal, (ACI 222R-85), Detroit, No. 1, Proceedings, Vol. 82, January-February 1985. pp 3-32
90. Everett, L. H. and Treadaway, K. W. J.
Deterioration Due to Corrosion in Reinforced Concrete. BRE Information Paper, IP12/80, August 1980. pp 4
91. British Standards Institution
The Structural Use of Concrete. CP110, Part 1, 1972, London. Amendment No. 3, 31st May, 1977.
92. British Standards Institution
Structural Use of Concrete. BS 8110, Part 1, 1985. London
93. ACI Committee 201
Guide to Durable Concrete. American Concrete Institute, (ACI 201-2R-77), Detroit, 1977, (reaffirmed 1982), pp 37
94. Browne, R. D. and Geoghegan, M. P.
The Corrosion of Concrete Marine Structures - the Present Situation. Proceedings, Symposium on Corrosion of Steel Reinforcement in Concrete Construction, London. February 1978. pp 79-98

95. Stratful, R. F., Jurkowich, W. J. and Spellmann, D. L.
Corrosion Testing of Bridge Decks. Transportation Research Record No. 539, 1975.
pp 50-59
96. Clear, K. C.
Evaluation of Portland Cement for Permanent Bridge Deck Repair. Federal Highway Administration, Washington DC, 1974. Report FHWA-RA-74-5.
97. Sorensen, B. and Maahn, E.
Penetration of Chloride in Marine Concrete Structures. Nordic Concrete Research, Publication No. 1, Oslo, December 1982. Paper No. 24, pp 18
98. Tuuti, K.
Corrosion of Steel in Concrete. Swedish Cement and Concrete, Stockholom, 1982.
pp 469
99. Tritthart, J.
The Influence of the Hydraulic Concentration in the Pore Solution of Hardened Cement Paste on Chloride Binding- Chloride Binding in Cement I, Cement and Concrete Research. Vol.19, 1989. pp 683-691
100. Mangat, P. S. and Gurusamy, K.
Steel Fibre Reinforced Concrete for Marine Applications, Proceedings of 4th Int. Conf. on Behaviour of Offshore Structures, Delft, July 1985. pp 867-879
101. Mangat, P. S. and Gurusamy, K.
Is Steel Reinforced Concrete Durable?. 11th Conf. on World Concrete and Structure. Singapore, August 1986. pp 157-169
102. Mangat, P. S. and Gurusamy, K.
Chloride diffusion in Steel Fibre Reinforced Concrete. Cement and Concrete Research, Vol. 17, 1987. pp 385-396
103. Mangat, P. S. and Gurusamy, K.
Chloride Diffusion in Steel Fibre Reinforced Concrete Containing PFA. Cement and Concrete Research, Vol. 17, 1987. pp 640-650
104. Brown, R. D.
Design prediction of the Life for Reinforced Concrete in Marine and other Chloride Environment, Durability of Building Materials, 1982. pp 113-125

105. Goutley, J. T. and Bieniak, D. T.
Diffusion of Chloride into Reinforced Concrete Piles. Symposium on Concrete, Perth, October 1983. pp 41-45
106. Berke, N. S.
Resistance of Microsilica Concrete to Steel Corrosion, Erosion and Chemical Attack, Fly Ash, Silica Fume, Slag, and Natural Pozzolans in Concrete, Proc. 3rd Int. Conf., ACI SP-114, Editor, Malhotra, V. M., Vol. 2, Trondheim, Norway, 1989. pp 861-886
107. Decter, M. H., Short, R., Page, C. L. and Higgins, D. D.
Chloride ion Penetration into Blended Cement Pastes and Concrete, Fly Ash, Silica Fume, Slag and Natural Pozzolans in Concrete. Proc. 3rd Int. Conf., ACI SP-114, Editor, Malhotra, V.M., Vol. 2, Trondheim, Norway, 1989. pp 1399-1411
108. Uji, K., Matsuoka, Y. and Maruya, T.
Formulation of an Equation for Surface Chloride Content of Concrete due to Penetration of Chloride. Corrosion of Reinforcement in Concrete, Editors, Page, C.L., Treadaway, K.W.J. and Bamforth, P.B., SCI, May 1990. pp 258-267
109. The Standard Institution of Israel
Concrete Code, I.S. 466, Part 1:1987. pp 71
110. Jaegermann, C., Baum, H. and Carmel, D.
Effect of the Distance from the Sea on Amount of Chloride Penetrating into the Concrete, Interim Report, Building Research Station, Technion, Israel Institute of Technology, Haifa, Jan. 1987. pp 21
111. Cady, P. D. and Weyers, R. E.
Chloride Penetration and the Deterioration of Concrete Bridge Decks. Cement, Concrete and Aggregates, Vol. 5, Winter 1983. pp 81-87
112. West, R. E. and Hime, W. G.
Chloride Profiles in Salty Concrete. Materials Performance, Vol. 24, July 1985. pp 29-36
113. Crank, J.
The mathematics of Diffusion. 2nd Edition, Oxford Press, London. 1975
114. Browne, R. D.
Mechanisms of Corrosion of Steel in Concrete in Relation to Design, Inspection and

- Repair of Offshore and Costal Structures. ACI Publication, SP-65, 1980. pp 169-204
115. Killoh, D. C., Parrott, L. J., and patel R. G.
Influence of Curing at Different Relative Humidities on the Hydration and Porosity of Portland/Fly ash Cement paste, Fly Ash, Silica Fume, Slag, and Natural Pozzolans in Concrete. Proc. 3rd Int. Conf. ACI SP-114, Editors, Malhotra, V.M., Vol. 1, Norway, 1989, pp 157-174
116. Patel R. G., Parrott, L. J., Martin, J. A. and Killoh, D.C.
Gradients of Microstructure and Diffusion Properties in Cement Paste Caused by Drying, Cement and Concrete Research. Vol. 15, 1985. pp 343-356
117. Concrete Society
Non-Structural Cracks of Concrete. Concrete Society Materials Research Seminar, Serviceability of Concrete, Slough. July 1985
118. Byfors, K.
Influence of Silica fume and fly ash on Chloride Diffusion and pH values in Cement Pastes. Cement and Concrete Research, Vol. 17, 1987. pp 115-130
119. Ost, B. and Monfore, G. E.
Penetration of Chloride into Concrete. Materials Performance, June 1974. pp 21-24
120. Browne, R. D. and Geoghegan, M. P.
The Corrosion of Concrete Marine Structures- The Present Situation. Proceedings, Symposium on Corrosion of Steel Reinforcement in Concrete Construction, February 1978, London. pp 79-89
121. Vogel, I. A.
A text book of Quantitative Inorganic Analysis. 3rd Edition, Longmans, London, 1961. pp 258-259
122. Berman, H. A.
Determination of Chloride in Hardened Cement Paste, Mortar and Concrete. Journal of Materials, Vol. 7, 1972. pp 330-335
123. Gjorv, O. E. and Vennesland, O.
Diffusion of Chloride ions from Seawater into Concrete. Cement and Concrete Research, Vol. 9, 1979. pp 229-238
124. Midgley, H. G. and Illston, J. M.
The Penetration of Chloride into Hardened Cement Pastes. Cement and Concrete

- Research, Vol. 14, 1984. pp 546-558
125. El-Khatib, J. M.
Durability Related Properties of PFA, Slag and Silica Fume Concrete . Ph.D. Thesis, University of Aberdeen, 1991. pp 227-310
 126. Molloy, B. T.
Steel Fibre and Rebar Corrosion in Concrete under Marine Curing. Ph.D. Thesis, University of Aberdeen, 1990.
 127. Thomas, M.D.A., Matthews, J. D. and Haynes, C. A.
The Effect of Curing on the Strength and Permeability of PFA Concrete. Corrosion of Reinforcement in Concrete, Editors, Page, C. L., Treadaway, K.W.J. and Bamforth, P. B., SCI, May 1990. pp 198-212
 128. McCurrich, L.H., Keeley, C., Cheriton, L.W. and Turner, K.F.,
Mortar Repair Systems- Corrosion Protection for Damaged Reinforced Concrete. A Crane Editor, Corrosion of Reinforcement in Concrete Construction. Society of Chemical Industry, London. 1983.
 129. Murdock, L.J., Brook, K.M. and Dewar, J.D.
Concrete Materials and Practice. 6th Edition, Edward Arnold, London, 1991.
 130. Mays, G.
Durability of Concrete Structures: Investigation, Repair and Protection. E & FN Spon, 1992.
 131. Mindess, S., Odler, I. and Skalny, J.
Significance to Concrete Performance of Interfaces and Bond: Challenges of the Future. Proc. Rio Congress, Vol. I, 1986. pp 151-157
 132. Allen, R. T. and Forrester, J. A.
The Investigation and Repair of Damaged Reinforced Concrete Structures. A Crane Editor, Corrosion of Reinforcement in Concrete Construction, Society of Chemical Industry, London, 1983.
 133. Mangat, P.S. and Molloy, B. T.
Prediction of long-term chloride concentration in concrete. Materials and Structures, Vol. 27, No. 170, July 1994. pp 338-346
 134. Richart, F. E. and Stachle, G. C.
Column Tests at University of Illinois. Jnl. ACI, Vol. 27, No. 2, Feb.-March 1931.

- pp 731-761
135. Slater, W. A. and Lyse, I.
Column Tests at Lehigh University. Jnl. ACI, Vol. 27, No. 2, Feb-March 1931.
pp 159-317
 136. Kong, R. V. and Evans, R. H.
Reinforced and Prestressed Concrete. 3rd Edition, Van Nostrand Reinhold
(International), 1989.
 137. Lorman, W. R.
The Theory of Concrete Creep. Proceedings of ASTM, Vo. 40, 1940. pp 1082-1102
 138. Ferguson, P. M.
Reinforced Concrete Fundamentals with Emphasis on Ultimate Strength. Second
Edition, John Wiley and Sons, 1965.
 139. Evans, R. H.
Effect of rate of Loading on the Mechanical Properties of some materials. Journal
ICE, Vol. 18, June 1942. p. 296
 140. Evans, R. H.
Effect of rate of loading on some mechanical properties of concrete. Proceedings of
a Conference on Mechanical Properties of Non-Metallic Brittle Materials. Butterworths
Scientific Publications, London, 1958. pp 175-192
 141. Kong, F. K. and Evans, R. H.
Reinforced Concrete. Nelson, 1975. pp 45-51
 142. Conduct Becoming. New Civil Engineers, London. 21st Nov. 1991. pp 16-18
 143. Locke, C. E.
Corrosion of Steel in Concrete: Fundamental Studies. ASTM, STP 906, V. Chaker,
Editor, 1986. pp 5-14
 144. Raed M. Samra.
Creep Model for Reinforced Concrete Columns. ACI Structural Journal, January-
February 1989. pp 77-82
 145. Troxell, G. E., Raphael, J. M. and Davis, R. E.
Long-time creep and shrinkage tests of plain and reinforced concrete. Proc. ASTM,
58, 1958.

146. Lambotte, H., Van Nieuwenburg, D. and Cocquyt, F.
Influence of non-prestressed steel on shrinkage and creep deformations and on steel-concrete stress redistribution. *Partial Prestressing , from theory to practice (NATO ASI Series E: Applied Science, Vol. 2)*, ed. M.A. Cohn, Dordrecht, Martinus Nijhoff Publishers, 1983. pp 45-56
147. Okada, K., Kobayashi, K. and Hatamura, H.
Effects of supplementary reinforcement on flexural and long-term behaviours in unbounded prestressing concrete beams. Presented at the Symposia on Partial Prestressing and Practical Construction in Prestressed and Reinforced Concrete, Romanian Central Institute for Research, Design and Guidance in Building, Proceedings, Part 1, 1980.
148. Abeles, P. W.
The effect of non-tensioned steel in prestressed concrete. *Reinforced Concrete Review*, 5, June 1961. pp 635-642
149. Comité Euro-International du Béton (CEB): 'International recommendations for the design and construction of concrete structures, Principles and recommendations'. European Concrete Committee- International Federation of Prestressing (CEB_FIP), Cement and Concrete Association, London. 1970
150. Neville, A. M., Dilger, W. H., and Brooks, J. J.
Creep of Plain and Structural Concrete. Construction Press, 1983.
151. Branson, D. E.
Deformation of concrete structures. McGraw-Hill, 1977
152. Brooks, J. J., Gamble, A. E. and Chouman, M. M.
Assessment of methods of predicting time-dependent deformations of Plain and Reinforced concrete. *The Structural Engineer / Vol. 70/No.1/7 January 1992*. pp 8-13
153. Chouman, M. M.
The effect of additional reinforcement on time-dependent behaviour of partially prestressed concrete. PhD thesis, Department of Civil Engineering, University of Leeds, 1990.
154. Glanville, W. H. and Thomas, F. G.
Studies in reinforced concrete-IV, Further investigations on creep or flow of concrete under load. Building Research Technical Paper N0. 21, London, 1939. pp 44

155. Davis, R. E., Davis, H. E. and Brown, E. H.
Plastic flow and volume changes of concrete. Proceedings ASTM, 37, Part 2, 1937.
pp 317-330
156. Mamillan, M. A.
Study of the creep of concrete. RILEM Bulletin, Paris, NO. 3, July 1959. pp 15-31
157. Brooks, J. J. and Neville, A. M.
A comparison of creep, elasticity and strength of concrete in tension and in
compression. Magazine of Concrete Research, Vol. 29, No. 100, September 1977.
pp 131-141
158. Dischinger, F.
Untersuchungen über die Knicksicherheit, die elastische Verformung und das Kriechen
des Betons bei Bogenbrücken, Der Bouingenieur. 18, No. 33/34, 1937. pp 487-520;
No. 35/36, 1937. pp 539-552; No. 39/40, 1937. pp 595-621
159. Maslov. G. N.
Thermal stress state in concrete masses with account to creep of concrete. Izvestia
Nauchno-Issledovatelskogo Instituta VNII Gidrotekhniki, Gosener-goizdat, USSR, 28,
1940. pp 27-73
160. Bazant, Z. P.
Prediction of concrete creep effects using age-adjusted effective modulus method. ACI
Journal, 69, 1972. pp 212-217
161. Throst, H.
Auswirkungen des Superpositionsprinzips auf Kriech- und Relaxations-probleme bei
Beton und Spannbeton. Beton- und Stahlbetonbau, 62, No. 10, 1967. pp 230-238; No.
11, 1967. pp 261-269

LIST OF PUBLICATIONS

1. Mangat, P. S. and Limbachiya, M. K.
Repair material properties which influence long-term performance of concrete structures. *Construction and Building Materials*, Vol. 9, No. 2, pp. 81-90, 1995.
2. Mangat, P. S. and Limbachiya, M. K.
Long-term structural interaction between repair patch and substrate concrete in compression members, Under Publication
3. Mangat, P. S. and Limbachiya, M. K.
Stress-strain behaviour of repair materials under uniaxial compression, Under Publication